Ambient and intrinsic triangulations and topological methods in cosmology

Wintraecken, Mathijs

Ambient and intrinsic triangulations and topological methods in cosmology

Mathijs Wintraecken

Book cover: Cutting and pasting a genus g surface. Design: Niels Bos.

ISBN: 978-90-367-7972-2 (printed)
ISBN: 978-90-367-7971-5 (electronic)

Printed by Gildeprint

This work has been supported by the 7th Framework Programme for Research of the European Commission, under FET-Open grant number 255827 (CGL Computational Geometry Learning).

rijksuniversiteit
groningen

Ambient and intrinsic triangulations and topological methods in cosmology

Proefschrift

ter verkrijging van de graad van doctor aan de
Rijksuniversiteit Groningen
op gezag van de
Rector Magnificus prof. dr. E. Sterken,
en volgens besluit van het College voor Promoties.

De openbare verdediging zal plaatsvinden op

vrijdag 4 september 2015 om 16:15 uur

door

Mathijs Hubertus Maria Johannes Wintraecken

geboren op 18 januari 1985
te Zeist

Promotores
Prof. dr. G. Vegter
Prof. dr. M.A.M. van de Weijgaert

Beoordelingscommissie
Prof. dr. H.W. Broer
Prof. dr. J-M. Morvan
Prof. dr. J.M. Sullivan

ISBN: 978-90-367-7972-2 (printed)
ISBN: 978-90-367-7971-5 (electronic)

Contents

List of Figures

Part I

Triangulations

Chapter 1

Introduction

1.1 The two parts of this thesis

The research presented in this thesis has been conducted in the context of the 7th Framework Programme for Research of the European Commission, under FET-Open grant number 255827 (Computational Geometric Learning). The Rijksuniversiteit Groningen participated in two work packages within this project. One focussed on the approximation of embedded surfaces and manifolds and is represented in part one of this thesis. The other focussed on the topology of geometric patterns in cosmology and is represented in the second part of this thesis. This chapter provides an introduction to part one. For more information on the European project we refer to the appendix. For an introduction to the second part of the thesis we refer to Chapter 4.

A number of sections of this thesis have been published or have been accepted for publication. For a detailed overview we refer the reader to the appendix on publications.

1.2 The central question in part one

In part one of this thesis we consider the setting where a surface or some generalization (manifold) is given a priori and we want to subdivide this surface or manifold. For the subdivision we will restrict ourselves to triangulations. The central question we consider is the following: *How can one triangulate a manifold in a sensible manner?* There are two different ways in which the words triangulation and sensible can be interpreted that we will pursue:

- In the first interpretation we consider our surface or manifold as embed-

ded in Euclidean space and the triangulation is piecewise linear in Euclidean (it consists of straight rigid triangles, or more generally simplices, the d-dimensional versions of triangles). Sensible will mean that the triangulation is close to the original surface or manifold (in a manner we shall specify later) and using as small a number of triangles as possible. This interpretation is in line with applications in computer graphics; even though computers become more and more powerful the demands on and expectations of graphics increase as well, leaving a question for accurate approximations using few triangles. The triangulations in this setting are called *extrinsic triangulations*.

- The second interpretation considers the manifold as an entity per se, that is without referring to some ambient space. We also assume there is some specific distance defined on the manifold called a metric, to be precise it is a so-called Riemannian manifold. We define simplices on the Riemannian manifold based only on the Riemannian metric and study triangulations using these simplices. The triangulations in this setting are called *intrinsic triangulations*.

1.3 Triangulations of manifolds in Euclidean space

We will now go into the first interpretation of our central question. Here we assume that our manifold (in the two dimensional case a surface) is embedded in Euclidean space. The triangulation we consider is piecewise linear in the ambient Euclidean space, which means that the simplices are straight or (affinely) flat. We want our triangulation to be accurate. To specify what we mean by accuracy we need to introduce a distance between subsets in Euclidean space, in our case the triangulation and the manifold we want to triangulate. We will use the Hausdorff distance, but this choice is not unique. For example the Fréchet distance for curves is quite popular, various so-called L_p-norms are used in higher dimensions, usually for functions, and the symmetric difference is also used for full dimensional sets. We shall give a feel for the Hausdorff distance, but not for the others.

The Haussdorf distance, optimal triangulations and the Approximierbarkeit

The Hausdorff distance d_H is as said a distance between two embedded surfaces or manifolds. We shall always assume that these surfaces are embedded in Euclidean space. For a pictorial explanation of the Hausdorff distance we refer to Figure 1.1.

It will not surprise the reader that if we allow more vertices (and therefore more simplices) in our triangulation we can achieve greater accuracy in terms of the Hausdorff distance. For a given number of vertices we call a triangulation that achieves the smallest Hausdorff distance possible an *optimal triangulation*.

If we restrict ourselves to surfaces in three dimensional Euclidean space, it can be shown that for a sufficiently large number of vertices the Hausdorff distance of optimal triangulations is approximately inversely proportional to the number of vertices. The coefficient of this proportionality is called the '*Approximierbarkeit*', *approximation parameter*. It can be defined for arbitrary dimensions. The 'Approximierbarkeit' has been introduced by Fejes Tóth in two [FT48] (implicitly) and three [FT53] dimensions, mainly in the context of convex surfaces. Convex (hyper-) surfaces are positively curved everywhere, roughly speaking they are egg shaped.

Literature overview

The work of Fejes Tóth was later generalized by Schneider [Sch81] and Gruber [Gru93a, Gru93b] to convex hypersurfaces of arbitrary dimension.
Ludwig [Lud94, Lud98] studied the behaviour of higher order terms (with respect to the inverse number of vertices) in the asymptotic development of both the so-called symmetric difference and the Hausdorff distance for the approximation of convex curves in the plane. Higher order approximations of curves (that is by splines, which are piecewise polynomial curves) have been explored by Ghosh et al. [Gho10, GPV07] in two and three dimensions.

All references mentioned here, apart from [FT53] and [Gho10, GPV07], have focussed exclusively on convex (hyper-) surfaces. Similar questions, that is quantities like the Approximierbarkeit but based on different distances, have been considered for (hyper-) surfaces that are the graphs of functions. Naturally they still consider triangulations that are piecewise linear in the ambient Euclidean space. Desnogues and Devillers [DD95] consider the L_2-norm and Chen, Sun and Xu [CSX07] the more general L_p-norm. Pottmann, Krasauskas, Hamann, Joy and Seibold [PKH$^+$00] and Atariah [Ata14] study the maximum (supremum) of the vertical distance between the graph and the triangulation. D'Azevedo and Simpson [DS91] do not focus on a distance between two functions, but concentrate on a good approximation of the gradient of the function.

Clarkson [Cla06] has been a great source of inspiration because he studied upper bounds on the 'Approximierbarkeit', for non-convex hypersurfaces. See also De Laat [dL11], for a discussion of arbitrary co-dimension. Clarkson and De Laat study the behaviour of the Hausdorff distance for good, but not optimal triangulations. This gives an upper bound on the 'Approximierbarkeit'.

Boissonnat and Oudot [BO05] study, among others, the behaviour of the

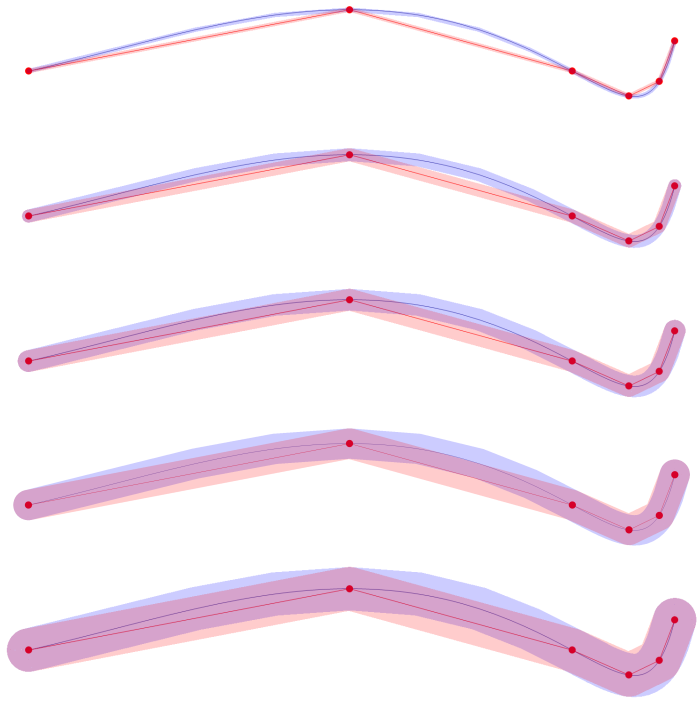

Figure 1.1: A smooth curve (blue) and a piecewise linear approximation (red) of the curve, with neighbourhoods of increasing size. We see that eventually (going from top to bottom) the blue neighbourhood encloses the piecewise linear curve and the red neighbourhood of the piecewise linear curve contains the blue curve. The Hausdorff distance is the smallest radius such that the neighbourhood of this radius of the smooth curve contains the piecewise linear curve and the neighbourhood of the same radius of the piecewise linear curve contains the smooth curve.

Hausdorff distance for triangulations constructed using so-called Delaunay triangulations. This work is also relevant for Chapter 3, see Section 3.1.4.

In the context of the triangulation of surfaces we should also mention meshes. It is important to note that the constituents of a mesh may include not only simplices, but more complicates objects. For an overview including explicit algorithms we refer to [BCSM$^+$06] and [CG06].

Results on extrinsic triangulations

In Chapter 2 we discuss the following:

- The relation between the 'Approximierbarkeit' of convex hypersurfaces for extrinsic triangulations whose vertices lie on the hypersurface and triangulations whose vertices are unrestricted. In particular we show that he 'Approximierbarkeit' in the two cases differ by a factor 2.

- The dependence of the 'Approximierbarkeit' on the intrinsic and extrinsic geometry of the embedded manifold.
  For convex surfaces (as was shown by Fejes Tóth and others) the 'Approximierbarkeit' can be expressed in term of the Gauss curvature. The Gauss curvature is an intrinsic geometric quantity, which means that it refers only to the manifold itself and not to its embedding in an ambient Euclidean space. It is remarkable that the 'Approximierbarkeit' which is defined for extrinsic triangulations can be expressed in intrinsic quantities.
  We show that the intrinsic nature of the expression for the 'Approximierbarkeit' is typical for low co-dimensions. In particular, we construct an explicit example that implies that for a sufficiently high co-dimension of the embedded manifold the 'Approximierbarkeit' is extrinsic in nature.
  We give a heuristic explanation of this result based on the Nash embedding theorem [Nas56].

- The extrinsic triangulation of the one-sheeted hyperboloid (with boundary) suggested by Fejes Tóth. The one-sheeted hyperboloid is an example of a negatively curved ruled surface.
  Fejes Tóth claimed that in this case the Hausdorff distance is inversely proportional to the *square* of the number of vertices. This would, among others, imply that the 'Approximierbarkeit' would be zero. This is incorrect. We prove that the Hausdorff distance is inversely proportional to the number of vertices or, to put it differently, the 'Approximierbarkeit' is nonzero.
  The example by Fejes Tóth begs the question: What is the 'Approximierbarkeit' for negatively curved surfaces? We study this question and are able to provide an answer for a large class of surfaces and discuss a method that could be employed to find a general answer.

1.4 Intrinsic simplices and triangulations

We will now turn our attention to the second interpretation of '*How can one triangulate a manifold in a sensible manner?*'.

Barycentric coordinates and Riemannian centres of mass

Suppose that we are given two points in Euclidean space. We shall think of these two as being ordered, that is there is an initial and a final point. We shall call them vertices. Any point on the line segment connecting the two vertices can be identified by the percentage of the total distance between the two points it is removed from the initial point. This identification by percentage of the distance can be generalized to barycentric coordinates, introduced by Möbius [Möb27].

The barycentric coordinates can be given as the point where an energy functional is minimized. This energy functional is given by the weighted sum of the squared distances to the vertices. The weights are identified as the barycentric coordinates.

One can generalize the energy functional on Euclidean space to an energy functional on a Riemannian manifold under conditions that will be made specific in Chapter 3. The generalized energy functional is called a Riemannian centre of mass or Karcher mean [Kar77], see also [Car29, Fré48, Ken90].

Intrinsic simplices

Riemannian centres of mass can be used to define simplices on a Riemannian manifold. See Figure 1.2 for an illustration. We shall call simplices defined in such a way *intrinsic simplices*, because they are defined in terms of intrinsic quantities.

It is not obvious that such an intrinsic simplex is homeomorphic to the standard (Euclidean) simplex (of the appropriate dimension). If it is we call it a non-degenerate simplex. In Chapter 3 we study conditions that guarantee that an intrinsic simplex is non-degenerate.

The relatively simple two dimensional case was studied by Rustamov [Rus10]. The same question has been addressed independently and simultaneously by Von Deylen [vDar], using somewhat different methods. The conditions we present are more explicit than Von Deylen's.

Intrinsic simplices have also been called geodesic finite elements within the field of numerical partial differential equations, see [San12, San13]. Degeneracy, however, plays no role in the study of geodesic finite elements.

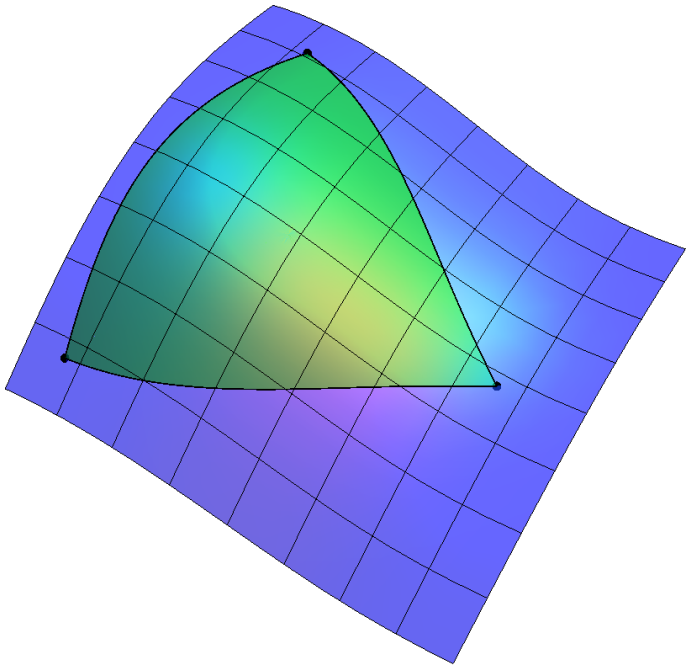

Figure 1.2: An intrinsic triangle on a surface.

Quality

In three dimensional Euclidean space a simplex with four vertices is degenerate if the vertices are coplanar. Quality measures can be used to indicate how close a simplex is to being degenerate. One such measure for quality is the normalized volume of a simplex, where the normalization uses the length of the longest edge of the simplex. This discussion extends to any dimension.

Intrinsic triangulations

In Chapter 3 we also consider triangulations of manifolds using intrinsic simplices.

The study of triangulations of manifolds is not new. A great deal of attention was given to the abstract triangulation of manifolds within the field of topology in the first half of the 20^{th} century. The efforts in this period left us with a number of proofs that every smooth manifold admits a triangulation, see for example [Cai34, Mun68]. These classical results were obtained by the use of charts

and/or embeddings for many of the constructions involved. Triangulations that are determined by the Riemannian metric are new.

The problem of constructing triangulations has been revisited in the computational geometry community, where the focus is on algorithms used to construct a triangulation. The one and two dimensional manifolds embedded in two and three dimensions have been extensively studied in the last decades, see [CDS13, Dey07] for introductions and overviews. Recently the higher dimensional settings have been studied [CDR05, BDG13a, BDG13b, BG14].

Results on intrinsic simplices and triangulations

The main contributions in Chapter 3 are:

- We give a new proof for the existence and uniqueness of Riemannian centres of mass (including negative weights).
- We give non-degeneracy criteria for intrinsic simplices. These criteria are formulated in terms of the quality of a (Euclidean) simplex to which we compare our intrinsic simplex. This simplex is found by taking the inverse image of all vertices under the inverse exponential map at one of the vertices.
- We formulate conditions on the density of vertices necessary to obtain a triangulation of a manifold using intrinsic simplices. These conditions involve local sectional curvatures and simplex quality. Such a triangulation is called an intrinsic triangulation. Conditions on the density of vertices are also known as sampling conditions in the computational geometry literature.
- Now suppose that we have constructed an intrinsic triangulation. We can now construct a geometric simplicial complex based on this intrinsic triangulation. By this we mean that for every intrinsic simplex we have a corresponding Euclidean simplex in the geometric simplicial complex whose edges have the same length as the edges of the intrinsic simplex. We derive a geometric distortion result, that is, show that the distances on the simplicial complex we thus construct are close to the distances on the original manifold.
- Finally we revisit the non-degeneracy criteria for individual simplices. We give sharper criteria (compared to the ones mentioned above, based on Euclidean simplices) for intrinsic simplices that lie on manifolds of which the curvature is almost constant.

1.5 Extrinsic triangulations versus intrinsic triangulations

We can also contrast the content of the final chapter of this part of this thesis with the content of the second. In Chapter 3 we give conditions on the density of vertices necessary to obtain a triangulation. For a fixed manifold this can be interpreted as an answer to the question:
What is the minimal number of vertices necessary to triangulate the manifold?
This contrasts with the setting of the second chapter where we let the number of vertices tend to infinity.

We can interpret Chapter 2 in a way that is seemingly more compatible with the interpretation of Chapter 3 we just gave. Namely the central question of Chapter 2 can be seen as:
What is the minimal number of vertices necessary to triangulate the manifold with a given accuracy?
However in a certain sense this emphasizes the difference between the two chapters even more, because in an intrinsic setting there is no accuracy, the concept does not make sense!

Chapter 2

Triangulations in Euclidean space

2.1 Introduction

In the seminal book 'Lagerungen in der Ebene, auf der Kugel und im Raum' [FT53] Fejes Tóth introduced inscribed and circumscribed triangulations approximating convex surfaces in $\mathbb{R}^3$ optimally and the 'Approximierbarkeit' (approximation parameter A_2). By a triangulation we shall in this chapter mean a geometric realization of a simplicial complex in Euclidean space homeomorphic to the surface, that is piecewise linear in ambient space. From now on, unless stated otherwise we take a simplicial complex to mean the geometric realization. All surfaces are assumed to be smooth (C^∞), unless stated otherwise.

Optimal triangulations with m vertices are triangulations or polytopes[1] which minimize[2] the Hausdorff distance between the surface and the polytope when this polytope ranges over the space of triangulations with m vertices. Depending on the setting these vertices lie on the surface (here the polytope is inscribed), the faces touch the surface (here the polytope is circumscribed), or the vertices are in general position. The Hausdorff distance between two subsets X and Y of the same Euclidean space is defined as:

$$d_H(X,Y) = \max\{\sup_{x\in X}\inf_{y\in Y}|x-y|, \sup_{y\in Y}\inf_{x\in X}|x-y|\},$$

[1] In the inscribed convex case there is no essential difference, because the boundary of the convex hull of the vertices is a polytope. It is clear that if more than d vertices are coplanar, where d is the dimension of the ambient space, we can subdivide the polytopes that make up the boundary into simplices.

[2] In Section 2.2.2 we shall see that this minimum is indeed attained.

where $|x-y|$ denotes the standard Euclidean distance of x and y. The one-sided Hausdorff distance from X to $Y$is given by

$$d_H^o(X,Y) = \sup_{x\in X} \inf_{y\in Y} |x-y|.$$

The inverse of the asymptotic value of the product of the number of vertices and the Hausdorff distance (or more generally for hypersurfaces the product of $m^{2/(d-1)}$ and the Hausdorff distance, where d is the dimension of the Euclidean space and thus $d-1$ the dimension of the hypersurface) is referred to as the *approximation parameter* A_2 (A_{d-1} in dimension d). The factor $m^{2/(d-1)}$ can be understood using the following two observations:

- The distance between m equally distributed points on a $d-1$ dimensional manifold is proportional to $m^{-1/(d-1)}$. This in turn can be seen as follows: Suppose that we are given a $d-1$-dimensional box whose sides are of unit length which contains $m = \tilde{m}^{d-1}$ points. We can distribute the points regularly and equally on a lattice. Let us assume that the basis vectors of this lattice points along the sides of the box. Clearly the length of the basis vectors of the lattice is $1/\tilde{m} = 1/m^{1/(d-1)}$. We may conclude that the distance between points is of the order $1/m^{1/(d-1)}$.

- Suppose we are given a circle whose curvature is k_i. A cord on the circle whose one-sided Hausdorff distance to the circle is η has a length proportional to $\sqrt{k_i\eta}$, for sufficiently small η. By one-sided Hausdorff η we mean that for each point on the cord there is a point on the circle that lies less than distance η from this point. This can be seen by considering the equation $\eta - \frac{1}{2}k_i x^2 \simeq 0$, describing the circle up to second order. We conclude that the Hausdorff distance is proportional to the square of the distance between points.

We should think of the k_i above as the principal curvatures of the surface. We therefore see that the two observations also indicate why A_{d-1} depends on the curvature. We will elaborate on this observation in Sections 2.1.1 and 2.3.

2.1.1 Fejes Tóth's bound on the approximation parameter.

Fejes Tóth gave a lower bound on the inverse of the approximation parameter for inscribed triangulations depending on the Gaussian curvature, which we shall now discuss. Our discussion is a slightly embellished version of the discussion in Chapter 5, Section 12 of [FT53]. The main goal is to give a lower bound on

$$\lim_{m\to\infty} d_H(\Sigma, T_m)m,$$

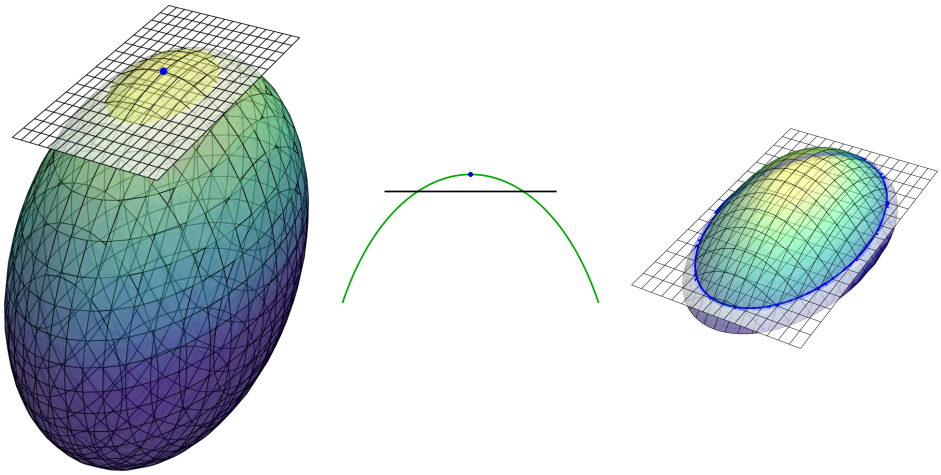

Figure 2.1: On the left, a general convex surface with a plane in which all triangles lie. The point in which the one-sided Hausdorff distance is attained, is indicated in blue. In the middle, the cross-section of the previous figure. On the right, a zoom-in of the first figure. In the zoom-in the ellipse is indicated in blue. The ellipse is the intersection of the surface and the plane.

where T_m is a triangulation of Σ with m vertices. We stress that Σ is a strictly convex surface in $\mathbb{R}^3$. Fejes Tóth also argued that this bound can be obtained.

As mentioned, we consider a strictly convex surface Σ, embedded in $\mathbb{R}^3$. This is equivalent with the fact that for every point on the surface both of the principal curvatures are positive. For every fixed point q of this convex surface and sufficiently small parameter $\eta > 0$, we consider all triangles that satisfy the following conditions:

- The vertices of the triangle lie on the surface Σ.
- The triangle has one-sided Hausdorff distance η to the surface, by which we mean that for each point on the triangle there is a point on the surface that lies less than distance η from the point on the triangle.
- The one-sided Hausdorff distance is attained in the point q.

These conditions imply that each triangle lies in the same plane, namely the plane parallel to the tangent plane of Σ at q and at distance η from this tangent plane. This is sketched in Figure 2.1.

Because the convex surface can locally be approximated by the Monge form $z = -\frac{1}{2}k_1x^2 - \frac{1}{2}k_2y^2$, where k_i are the principal curvatures, the intersection of

the plane introduced above and the convex surface is approximately an ellipse. Its semi-axes are $\sqrt{2\eta R_1}$ and $\sqrt{2\eta R_2}$, where the $R_i = k_i^{-1}$ are the principal radii (see Figure 2.1).

Because we are interested in a lower bound on

$$\lim_{n\to\infty} d_H(\Sigma, T_m)m,$$

we need to find a triangle with the greatest area that satisfies the three criteria given above. We look for the greatest area, because roughly speaking triangles with larger area lead to fewer vertices. Finding the triangle with the greatest area that satisfies the three criteria given above is equivalent to finding the largest triangle inscribed in the (approximate) ellipse. Using a linear transformation to reduce the problem to the circle, it is not very difficult to see that the inscribed triangle with greatest area satisfies

$$\text{Area}(t) = \frac{\sqrt{27}}{2}\eta\sqrt{R_1 R_2} + o(\eta),$$

where $\text{Area}(t)$ denotes the area of the triangle t, see Figure 2.2. Bringing η to the other side this gives

$$d_H^o = \eta \gtrsim \frac{2}{\sqrt{27}}\sqrt{K}\text{Area}(t), \tag{2.1}$$

for each triangle, where d_H^o denotes the one-sided Hausdorff distance from t to the surface and $\gtrsim$ is used to indicate $\geq$ up to leading order in η and $\frac{1}{R_1 R_2} = k_1 k_2 = K$ is the Gaussian curvature. To be entirely precise

$$\eta + o(\eta) \geq \frac{2}{\sqrt{27}}\sqrt{K}\text{Area}(t)$$

is denoted by

$$\eta \gtrsim \frac{2}{\sqrt{27}}\sqrt{K}\text{Area}(t).$$

Now we can consider a triangulation T of the surface. Applying the inequality (2.1) to every triangle in a triangulation we find

$$d_H(\Sigma, T_m)m_T \gtrsim \sum_{t\in T} \frac{2}{\sqrt{27}}\sqrt{K_t}\text{Area}(t),$$

where we specifically indicate the individual triangles in the triangulation by t and denote the number of triangles by m_T. For a triangle t, the Gaussian

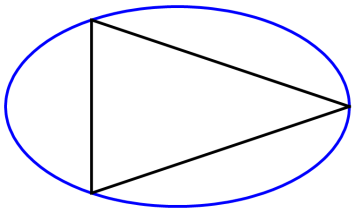

Figure 2.2: Sketch of the ellipse with semi-axis $\sqrt{2\eta R_1}$ and $\sqrt{2\eta R_2}$ and the inscribed triangle with the greatest possible surface area.

curvature K_t associated to t is the Gaussian curvature in the point on Σ closest to t whose tangent plane is parallel to t. Note that as the surface is convex we can replace the one-sided Hausdorff distance by the Hausdorff distance. As the number of triangles tends to infinity we may replace the summation with an integral, that is

$$\lim_{m_T\to\infty} d_H(\Sigma, T_m)m_T \geq \frac{2}{\sqrt{27}}\int \sqrt{K}\mathrm{d}A. \tag{2.2}$$

Traditionally, the number of vertices is used instead of the number of triangles in a triangulation. Following this, we rewrite this result using that for a compact surface $m_T \sim 2m$, with m number of vertices. This result is based on Euler's formula for triangulations of two dimensional topological spheres

$$m - m_e + m_T = \chi = 2,$$

with m_e the number of edges and the fact that each triangle has three edges and each edge is shared between two triangles. Because the number of vertices tends to infinity as the Hausdorff distance tends to zero this $\sim$ is compatible with $\gtrsim$. With this notation (2.2) reads

$$\lim_{m\to\infty} d_H(\Sigma, T_m)m \geq \frac{1}{\sqrt{27}}\int \sqrt{K}\mathrm{d}A. \tag{2.3}$$

We have provided a sketch in Figure 2.3.

Attaining the bound

Fejes Tóth argued (somewhat heuristically) that we can cover the entire surface with triangles for which

$$d_H^o \sim \frac{2}{\sqrt{27}}\sqrt{K}\mathrm{Area}(t),$$

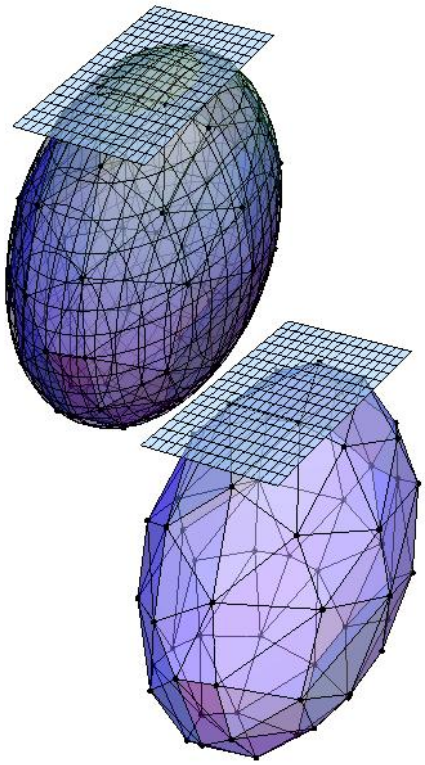

Figure 2.3: Sketch of the convex surface and a triangulation. The plane associated with one triangle is indicated.

where $\sim$ denotes equality up to leading order in the one-sided Hausdorff distance and d_H^o denotes the one-sided Hausdorff distance from the triangle to the surface. Schneider [Sch81] has improved on this reasoning. He gave a construction for a sequence of triangulations for a convex surface that asymptotically attain the bound. His construction is based on the observation that for a strictly convex surface the second fundamental form is in fact a metric. We now choose an optimal cover, with respect to this metric, with m points. An optimal cover of a compact Riemannian manifold with m points consists of the smallest possible radius and a distribution of the m points on the manifold such that the union of the geodesic balls with this radius and centred at the m points is the entire manifold. The convex hull of these points[3] is a polytope. The family of polytopes,

[3]Here we view the manifold as embedded in Euclidean space.

indexed by the number of vertices m, thus constructed asymptotically attains the bound given in (2.3) in the limit as m tends to infinity. It is indeed not hard to see that the triangles in this triangulation constructed in this manner locally converge to the triangle depicted in Figure 2.2.

Arbitrary dimension

The construction by Schneider [Sch81] works in arbitrary dimension. He used it to generalize the discussion of Fejes Tóth to convex hypersurfaces in Euclidean space of arbitrary dimension. In doing so Schneider gave a solid proof of the formula for the approximation parameter A_{d-1} of inscribed polytopes of convex C^3 hypersurfaces in any dimension. The formula for A_{d-1} reads

$$\frac{1}{A_{d-1}} = \lim_{m\to\infty} m^{2/(d-1)} d_H(\Sigma, T_m) = \frac{1}{2}\left(\frac{\theta_{d-1}}{\kappa_{d-1}}\int_\Sigma \sqrt{K(x)}\mathrm{dVol}\right)^{2/(d-1)}, \quad (2.4)$$

where $\kappa_d = \pi^{d/2}/\Gamma(1+d/2)$ is the volume of the d-dimensional unit ball, θ_d the covering density of the ball in d-dimensional space, dVol the volume form and K the Gaussian curvature. The covering density is defined as the infimum of the density over all coverings of, in this case, Euclidean space by the Euclidean unit ball, see for example [Rog64]. The density of a cover $U = \{U_i\}$ of a compact measurable space with volume form dVol by a finite number of sets U_i is defined as follows: Let f_U be the integer valued function whose value $f_U(x)$ at a point x is the number of sets U_i such that $x \in U_i$. The density for the covering U is

$$\frac{\int f_U \,\mathrm{dVol}}{\int \mathrm{dVol}}. \quad (2.5)$$

Lower differentiability class and the circumscribed case

Gruber [Gru93a, Gru93b] then extended the work by Schneider by considering hypersurfaces which are of lower differentiability class (C^2). Furthermore he discussed

$$\lim_{m\to\infty} d_H(\Sigma, T_m)m,$$

for optimal circumscribing polytopes. This resulted in the same value of the approximation parameter A_{d-1} as in (2.4). Circumscribing polytopes fell outside the scope of the article by Schneider.

2.1.2 Overview

Vertices in general position

Fejes Tóth also stated that the approximation parameter of optimal triangulations whose vertices are in general position, that is the polytope is neither inor circumscribed, is half of the approximation parameter in the inscribed setting. None of the previously mentioned papers gave a proof of this claim, although some (such as [Bro08]) mentioned it. In Section 2.2 we provide a proof of this statement for not strictly convex C^1 hypersurfaces with positive reach. The reach of an embedded manifold is the largest distance such that if a point p lies closer than this distance from the manifold, then there is a unique point q on the manifold for which q lies closest to p.

The extrinsic nature of A_{d-1}

Formula (2.4) is intrinsic in nature, as the Gaussian curvature is intrinsic. In fact it can be expressed in terms of the Riemann tensor, see Chapter 7 of [Spi75b].

In Section 2.3 we show that the intrinsic nature of the approximation parameter is particular to low co-dimension. This makes heuristically some sense because the rigidity of a manifold disappears if the co-dimension of the embedding is sufficiently high, as was noted by Nash in [Nas56]. In the setting of Nash, rigidity concerns metric preserving perturbations of the embedding. Nash proved that a compact n-manifold with a C^k Riemannian metric has a C^k isometric embedding in any small volume of Euclidean $(n/2)(3n+11)$-space, provided $3 < k \leq \infty$. So roughly speaking, one can squash a manifold in a small volume without affecting the intrinsic metric, but this would lead to wrinkles.

This is opposite to the results for surfaces in three dimensional Euclidean space (or generally manifolds embedded in codimension one.[4]) In codimension one rigidity is often interpreted in a global sense. By this we mean that we are not satisfied with metric preserving perturbations of the embedding but focus on uniqueness of the embedding up to Euclidean motions. Euclidean motions are generated by rotations and translations. A number of rigidity results in this global sense are available, see Spivak [Spi75a, Spi75c] for an overview. For us, the most relevant result is Theorem 1 of Chapter 12 of [Spi75c]. Let ν denote the Gauss map, $d\nu$ the Weingarten map and II the second fundamental form. With this notation Theorem 1 of Chapter 12 of [Spi75c] reads:

Theorem 2.1.1 *Let M and $\bar{M}$ be isometrically immersed hypersurfaces in $\mathbb{R}^{n+1}$ and let $\phi : M \to \bar{M}$ be an isometry. Suppose that $d\nu : T_pM \to T_pM$ has rank*

[4]Of course a great number of results also exists on rigid embeddings of more general low codimension, such as the result by Allendoerfer. This field still sees active research.

≥ 3. *Then* $(\phi^*\overline{\mathrm{II}})(p) = \pm\mathrm{II}(p)$. *[This equation makes sense even though* ν *and* $\bar{\nu}$ *may be defined only locally and then only up to sign.]*
Consequently, if M *and* $\bar{M}$ *are connected (not necessarily complete) hypersurfaces and* $d\nu : T_qM \to T_qM$ *has rank* ≥ 3 *for all* $q \in M$*, then* ϕ *is the restriction of a Euclidean motion.*

Our interest was raised by the upper bounds on

$$\lim_{m\to\infty} d_H(M, T_m^o)m^{n/2},$$

where M is an n-dimensional manifold embedded in Euclidean space and T_m^o denotes an optimal triangulation of M. As before, we mean by a optimal triangulation a triangulation of M with m vertices such that there is no triangulation $\tilde{T}_m$ such that $d_H(M, \tilde{T}_m) < d_H(M, T_m^o)$. These bounds have been discussed in the Master's thesis of David de Laat [dL11]. Similar upper bounds were the topic of, among others[5], Chen, Sun and Xu[CSX07]. These authors studied the L_p norm of the difference between a function and a linear approximation of this function. The bounds in [dL11] and [CSX07] are defined in terms of the Hessian and thus extrinsic in nature. Our result, Theorem 2.3.1, gives us that the extrinsic nature of the bounds is unavoidable.

The Fejes Tóth's triangulation of one-sheeted hyperboloid.

Fejes Tóth claimed that the approximation of ruled surfaces embedded in three dimensional Euclidean space would be entirely different from the approximation of convex surfaces. In Section 12 of Chapter 5 of [FT53] he states the following:[6]

> Let Σ be the one-sheeted hyperboloid bounded by two congruent circles A and B. We inscribe A and B by regular m-polygons $A_1 \dots A_m$ and $B_1 \dots B_m$ respectively, so that $A_1B_1, \dots, A_mB_m$ lie on the hyperboloid. The polyhedron-like surface T_{2m} is best described by its faces $A_1A_2B_1, \dots, A_mA_1B_m$ and $B_1B_2A_2, \dots, B_mB_1A_1$. The deviation $d_H(T_{2m}, \Sigma)$ is determined by the deviation of the m-polygon $A_1 \dots A_m$ from the circle A, this implies that the order of magnitude of the deviation is $1/m^2$ and not $1/m$.

Unfortunately this is incorrect, as we shall discuss in Section 2.4. In fact we shall show that the order of magnitude of $d_H(\Sigma, T_m)$ is $1/m$, like in the convex case. Moreover in this particular case we can explicitly calculate $d_H(\Sigma, T_m)$ and show that this triangulation is not optimal.

[5]The introduction of [CSX07] offers an extensive literature overview.

[6]Translation provided by the author. We have made the notation compatible with this introduction.

Fejes Tóth's triangulation and ruled surfaces

The fact that Fejes Tóth's claims regarding the triangulation of the one-sheeted hyperboloid with boundary are false raises the question if

$$\lim_{m\to\infty} d_H(\Sigma, T_m)m$$

depends on whether Σ is ruled or not. In case the surface contains no straight lines it is not difficult to prove that all edge lengths in a sequence of optimal triangulations indexed by their increasing number of vertices go to zero. If all lengths of the edges go to zero we can use local techniques to determine

$$\lim_{m\to\infty} d_H(T_m, \Sigma)m. \tag{2.6}$$

By local techniques we mean that we can do the analysis in the neighbourhood of a point. In particular one uses:

- The normal to the surface is approximately constant in a neighbourhood of a triangle.
- The surface is well approximated by the second order Taylor approximation of its Monge form.

If the local techniques can be applied it is not difficult to find an expression for (2.6) using arguments similar to those used in the convex case, see Section 2.1.1. Alternatively such an expression also follows from results by Pottmann et al. [PKH+00] and Atariah [Ata14]. These authors study triangulations of graphs of functions, where the relevant distance is the vertical distance between the triangulation (graph of a piecewise linear function) and the graph of the function. In this context we also need to mention Clarkson's roughly quadratic surfaces [Cla06].

However, if the surface contains a segment of a ruled surface it is not at all clear whether the local techniques still work. We have therefore not been able to find an expression for

$$\lim_{m\to\infty} d_H(\Sigma, T_m)m$$

if the surface contains a segment of a ruled surface. However, in Section 2.4.3 we do touch upon one possible approach to find such an expression.

The outcome of this search would not only be of theoretical interest. Let us explain this a bit further. The results for convex surfaces were instrumental in the development by Kamenev, see for example [Kam93], of algorithms for approximation of convex surfaces. Kamenev's algorithms are not really optimal in the sense that they achieve the best accuracy with a given number of vertices,

because finding optimal covers for a finite number of points is too difficult. Instead it makes use of a so-called greedy algorithm. Up to a multiplicative factor the result is satisfactory, by which we mean that using this method we find a sequence of triangulations for which

$$\lim_{m\to\infty} d_H(T_m, \Sigma)m$$

is finite but larger then the Approximierbarkeit.

In the non-convex case there are two possibilities: either the local techniques work or they fail. If the local techniques work one would expect that a relatively straightforward generalization of the work by Kamenev could be achieved, although this would require a significant amount of work. If they fail one would need to be very careful if a surface contains a segment of a ruled surface or even a segment that is close to a ruled surface in the Hausdorff sense. We do not pursue this problem in this thesis, but mention it because it indicates the practical importance of Section 2.4.3.

2.2 On the optimal triangulation of convex hypersurfaces, whose vertices lie in ambient space

Fejes Tóth also conjectured that the complexity of triangulations whose vertices are in general position, that is neither in- nor circumscribed, is half of the complexity in the inscribed setting. None of the previously mentioned papers gave a proof of this. Below we provide a proof of this statement for not strictly convex C^1 hypersurfaces with positive reach. Using the previously mentioned results this implies:

Theorem 2.2.1 *Let Σ be a strictly convex C^2 hypersurface embedded in $\mathbb{R}^d$ and for every m let S_m be an optimally approximating simplicial complex with m vertices having Hausdorff distance $d_H(S_m, \Sigma)$. Then we have*

$$\lim_{m\to\infty} m^{2/(d-1)} d_H(S_m, \Sigma) = \frac{1}{2A_d} = \frac{1}{4}\left(\frac{\theta_{d-1}}{\kappa_{d-1}}\int_\Sigma \sqrt{K(x)}\mathrm{d}\mu\right)^{2/(d-1)}.$$

2.2.1 The sphere

To illustrate the problem we first consider the standard circle S^1 in $\mathbb{R}^2$, with radius 1 and centred at the origin. We approximate the circle by a regular polygon with m vertices, P_m. Due to symmetry this is the optimal manner, because the Hausdorff distance must be attained in every edge. Suppose that for an optimal polygon the Hausdorff distance is not attained in one of the edges, then we can perturb one of its vertices so that the Hausdorff distance is not attained in this edge nor in its neighbours. Via induction we find that the polygon is not optimal. Naturally the centre of the regular polygon is the origin. The circumradius of the regular polygon will be denoted by R. A sketch is provided in figure 2.4. Clearly the points on the polygon furthest from or closest to the centre are the vertices and the centres of the edges. These points are the only points where the Hausdorff distance can be attained. The distance between the circle and the vertex or the centre of the edge is given by $R-1$ and $1-R\cos(\pi/m)$, respectively, which yields that the Hausdorff distance between the circle and the regular polygon is

$$\begin{aligned} d_H(P_m, S^1) &= \max\left\{R-1, 1-R(1-d_H(P_m^{\text{in}}, S^1))\right\} \\ &= \max\left\{R-1, 1-R\cos\left(\frac{\pi}{m}\right)\right\}, \end{aligned}$$

where P_m^{in} denotes the inscribed polygon, that is the polygon with $R=1$.

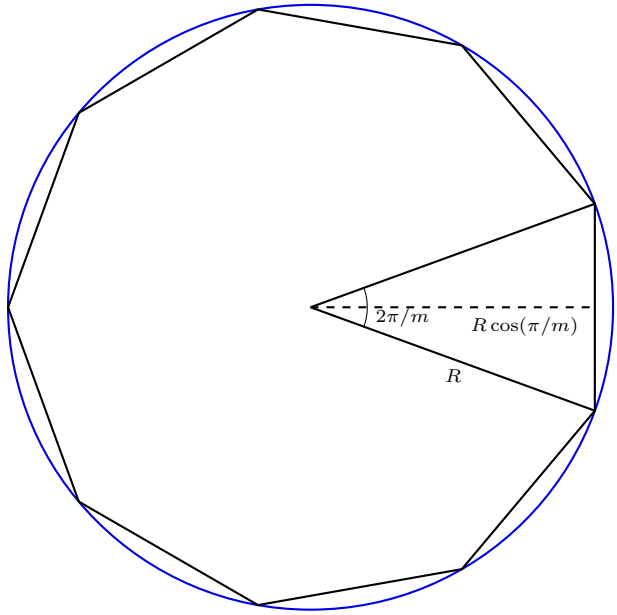

Figure 2.4: A polygon P_m and a circle, both with the same centre. R denotes the circumradius of P_m. We depict the inscribed case.

We can minimize $d_H(P_m, S^1)$ with respect to R by the following choice

$$R = \frac{2}{1+\cos\left(\frac{\pi}{m}\right)} = \frac{2}{2 - d_H(P_m^{\text{in}}, S^1)}.$$

So that

$$d_H(P_m, S^1) = \frac{2}{1+\cos\left(\frac{\pi}{m}\right)} - 1 = \frac{2}{2 - d_H(P_m^{\text{in}}, S^1)} - 1,$$

for sufficiently large m or rather sufficiently low $d_H(P_m^{\text{in}}, S^1)$ we can develop this expression

$$d_H(P_m, S^1) = \frac{2}{1+\cos\left(\frac{\pi}{m}\right)} - 1 = \frac{1}{4}\left(\frac{\pi}{m}\right)^2 + \mathcal{O}\left(\frac{1}{m^4}\right)$$
$$d_H(P_m, S^1) = \frac{2}{2 - d_H(P_m^{\text{in}}, S^1)} - 1 = \tfrac{1}{2} d_H(P_m^{\text{in}}, S^1) + \mathcal{O}((d_H(P_m^{\text{in}}, S^1)^2).$$

Remark 2.2.2 *One may wonder about the equivalent statement for the Banach-Mazur distance (δ^{BM}). The Banach-Mazur distance on convex bodies which are*

symmetric in the origin ($\mathcal{C}_0$), have been treated extensively by Gruber [Gru93a, Gru93b]. For two convex bodies $C, D \in \mathcal{C}_0$ the Banach-Mazur distance is defined [Gru93a] as

$$\delta^{BM}(C, D) = \inf\{\lambda > 1 : C \subset \ell(D) \subset \lambda C, \ell : \mathbb{R}^d \to \mathbb{R}^d \text{ linear}\}$$

In this setting it is again clear that the optimal approximating body of S^1 is a regular polygon P_m (in this case with its interior). Because the definition includes linear maps ℓ that work on P_m, rescaling P_m by R does not influence the result, that is $\delta^{BM}(S^1, P_m) = \delta^{BM}(S^1, RP_m)$, with the interiors having been left implicit.

For general S^d we are not able to give an explicit description of the inscribed polytope which approximates S^d optimally, as there are only so many Platonic solids. However, suppose that we are given such a polytope P_m^{in}, then by definition the vertices ($\{v_i\}$) of P_m^{in} lie on S^d and there are points ($\{q_i\}$) on the faces which attain a distance $d_H(P_m^{\text{in}}, S^d)$ to the sphere. We can now consider the polytope P_m^{in} rescaled by a factor R, denoted by $R\,P_m^{in}$. For $R\,P_m^{\text{in}}$, the points v_i, q_i, the vertices and the points where the maximum distance is attained in the inscribed setting, are the points closest to and furthest from the origin. This means that in these points the Hausdorff distance can be attained. Which in turn implies that

$$d_H(R\,P_m^{in}, S^d) = \max\left\{R - 1, 1 - R(1 - d_H(P_m^{\text{in}}, S^d))\right\},$$

which is minimized with respect to R by

$$R^* = \frac{2}{2 - d_H(P_m^{\text{in}}, S^d)}.$$

Therefore,

$$d_H(R^*\,P_m^{in}, S^d) = \frac{2}{2 - d_H(P_m^{\text{in}}, S^d)} - 1 = \frac{1}{2} d_H(P_m^{\text{in}}, S^d) + \mathcal{O}((d_H(P_m^{\text{in}}, S^d)^2).$$

In this manner we have constructed a simplicial complex ($R^*\,P_m^{in}$) such that the Hausdorff distance of this complex is half of the Hausdorff distance in the inscribed case, up to leading order. On the other hand let us now assume that we have a simplicial complex S_m with m vertices which minimizes $d_H(S_m, S^d)$, we can now make the following construction; we take the vertices v_i of S_m and project these on the sphere along the normal $\pi(v_i)$. The simplicial complex with these vertices and the simplexes corresponding to the original simplicial complex S_m we will denote by $\tilde{P}_m$. By the corresponding we mean that the convex hull of $v_{i_1}, \ldots, v_{i_l}$, denoted by s_j, lies in S_m, if and only if the convex hull of $\pi(v_{i_1}), \ldots, \pi(v_{i_l})$, denoted by s_j^π, lies in $\tilde{P}_m$. We have for individual simplexes in

the complex $d_H(s_i, s_i^\pi) \leq d_H(S_m, S^d)$, which is in this case not very hard to see, this will be proven in a general setting in lemma 2.2.6. From which we conclude that $d_H(S_m, \tilde{P}_m) \leq d_H(S_m, S^d)$. This in turn, in combination with the triangle inequality, yields

$$d_H(\tilde{P}_m, S^d) \leq d_H(S_m, \tilde{P}_m) + d_H(S_m, S^d) \leq 2d_H(S_m, S^d).$$

This means that we have proven theorem 2.2.1 in the case of the sphere, if we assume existence. In the next section we prove that there is indeed an inscribed polytope P_n^{in} which approximates S^d optimally.

2.2.2 The general case

In this section we first discuss the continuity of the Hausdorff distance and prove some results on existence of optimal triangulations. By an optimal triangulation we mean that that there is no complex with the same number of vertices (on the surface or in general position, depending on the context) that achieves a smaller Hausdorff distance. We then give one rather simple lemma that says that if we have an optimally approximating simplicial complex S_m with m vertices in ambient space of a hypersurface Σ, then the optimally approximating inscribed polytope P_m satisfies $d_H(P_m, \Sigma) \leq 2d_H(S_m, \Sigma)$. Subsequently, given an inscribed polytope P_m^{in}, we construct a simplicial complex S_m such that

$$d_H(S_m, \Sigma) \leq \frac{1}{2} d_H(P_m^{\text{in}}, \Sigma) + o(d_H(P_m^{\text{in}}, \Sigma)).$$

The proof consists of two steps. Roughly speaking, we first push every point on the polytope outwards by $\frac{1}{2}d_H(P_m^{\text{in}}, \Sigma)$ using the normal to the surface to create a new hypersurface. Note that this is no longer a simplicial complex. The second step considers the Hausdorff distance between this surface and the simplicial complex found by 'pushing the vertices outwards'.

Suppose that we are given a combinatorial simplicial structure on the set $\{1, \ldots, m\}$ and two (possibly degenerate) geometric realizations $S_m, \tilde{S}_m$ in $\mathbb{R}^d$ with (ordered) vertex sets $\{v_1, \ldots, v_m\} = V$ and $\{\tilde{v}_1, \ldots, \tilde{v}_m\} = \tilde{V}$. If we now interpret $V, \tilde{V}$ as elements in $(\mathbb{R}^d)^m$ and assume that $|V - \tilde{V}| \leq \delta$, then for each combinatorial simplex $\{i_1, \ldots, i_k\}$ we have

$$d_H(\text{CH}(v_{i_1}, \ldots, v_{i_k}), \text{CH}(\tilde{v}_{i_1}, \ldots, \tilde{v}_{i_k})) \leq \delta,$$

by linearity and, thus, $d_H(S_m, \tilde{S}_m) \leq \delta$, here CH denotes the convex hull.

Now we can prove that for a combinatorial simplicial complex and manifold Σ

$$d_H(\cdot, \Sigma) : (\mathbb{R}^d)^m \to \mathbb{R}_{\geq 0} : V \to d_H(V, \Sigma),$$

where we identify the vertices with the geometric realization of the complex, is continuous. Let $V, \tilde{V} \in (\mathbb{R}^d)^m$, with $\|V - \tilde{V}\| \leq \delta$, then the triangle inequality yields

$$d_H(V, \Sigma) - d_H(V, \tilde{V}) \leq d_H(\tilde{V}, \Sigma) \leq d_H(V, \Sigma) + d_H(V, \tilde{V}).$$

$|d_H(V, \Sigma) - d_H(\tilde{V}, \Sigma)| \leq \delta$, which shows continuity in the setting for a fixed simplicial structure. We now note that there are but a finite number of simplicial structures on a finite set. This together with the fact that the minimum of a finite number of continuous functions is again continuous gives us that $d_H(\cdot, \Sigma)$ is continuous for any set of simplicial structures, in particular those corresponding to topological $d-1$-manifolds or topological $d-1$-spheres. This means that we have continuity in a very broad setting.

In the following we shall sometimes refer to the reach. Let X be a hypersurface in $\mathbb{R}^d$. The reach $R(X)$ of X is the largest distance to X such that if the distance between a point in $\mathbb{R}^d$ and X is smaller than $R(X)$, there is a unique closest point on X. Federer [Fed59] has shown that a C^2 manifold has strictly positive reach. This result is not instrumental in the proofs of the following lemmas, but is used in Theorem 2.2.8.

Lemma 2.2.3 *For each m there exists an inscribed polytope P_m^{in} which approximates a given compact convex hypersurface Σ optimally, where we assume that the vertices of P_m^{in} lie on Σ. Here we specifically allow the vertices to coincide, so that we can use compactness arguments.*

Proof It suffices to note that $d_H(\cdot, \Sigma)$ is continuous if we restrict the domain to $\Sigma^m = \Sigma \times \cdots \times \Sigma$ and topological $d-1$ manifolds, using the same identifications as above. Because Σ and therefore Σ^m is compact and a continuous function attains its minimum on a compact set. Note that if we approximate a convex surface by a simplicial complex which is a topological $d-1$-manifold, then the optimally approximating triangulation is itself a convex surface, because any simplicial complex lies in the convex hull of its vertex set. This implies that the inward normal to the hypersurface intersects the convex hull first and then the simplicial complex, so that the Hausdorff distance to the convex surface is smaller. So P_m^{in} is indeed an inscribed polytope. □

A similar statement is true for triangulations whose vertices do not lie on the hypersurface.

Lemma 2.2.4 *Let Σ be a compact hypersurface. There exists a simplicial complex S_m, with m vertices which approximates Σ optimally.*

Proof Σ is compact, so it is bounded and thus contained in some ball $B(q, \rho)$ with radius ρ and centre q. Because $(B(q, 2\rho))^m$ is compact $d_H(\cdot, \Sigma)$ attains its

minimum on this set. This is also a global minimum because we have that $d_H(S_m, \Sigma) \leq d_H(S_1, \Sigma) \leq \rho$. □

Remark 2.2.5 *In the lemma above we use the obvious statement that for two optimal simplicial complexes (or polytopes) S_n and S_m, with n and m vertices respectively, where $n > m$ we have that $d_H(S_n, \Sigma) \leq d_H(S_m, \Sigma)$. However a strict inequality does not hold in the most general setting. An example of this is the following; consider the circle S^1 and its optimal approximating simplicial complexes for $m = 1$ and $m = 2$. These optimal approximating simplicial complexes are a point in the centre and any line segment which contains the centre and does not extend beyond twice the radius of the circle. It is easy to see that $d_H(S_1, S^1) = d_H(S_2, S^1)$.*

We now focus on the lemmas that discuss the relation between the Hausdorff distance of triangulations whose vertices are restricted to a given convex hypersurface and those that are not restricted to this hypersurface.

Lemma 2.2.6 *For a given m suppose that the simplicial complex S_m (in general, that is not necessarily inscribed) optimally approximates a compact convex hypersurface Σ, that is, there is no $\tilde{S}_m$ such that $d_H(\tilde{S}_m, \Sigma) < d_H(S_m, \Sigma)$. Then the optimally approximating inscribed polytope P_m with m vertices satisfies $d_H(P_m, \Sigma) \leq 2d_H(S_m, \Sigma)$.*

Proof For each vertex v_i of S_m choose a point v_i^{on} on Σ closest[7] to v_i. We define π to be the mapping $\pi : (v_1, \ldots, v_m) \mapsto (v_1^{\text{on}}, \ldots, v_m^{\text{on}})$. We endow $\{v_1^{\text{on}}, \ldots, v_m^{\text{on}}\}$ with the same simplicial structure as on $\{v_1, \ldots, v_m\}$. The resulting simplicial complex will be denoted by S_m^{on}. So π can be viewed as a simplicial map. Due to linearity we have that for every simplex $\{v_{i_1}, \ldots, v_{i_k}\}$, we have

$$d_H(\text{CH}(v_{i_1}, \ldots, v_{i_k}), \text{CH}(v_{i_1}^{\text{on}}, \ldots, v_{i_k}^{\text{on}})) \leq d_H(S_m, \Sigma)$$

and therefore $d_H(S_m, S_m^{\text{on}}) \leq d_H(S_m, \Sigma)$, which in turn, using the triangle inequality, yields

$$d_H(S_m^{\text{on}}, \Sigma) \leq d_H(S_m^{\text{on}}, S_m) + d_H(S_m, \Sigma) \leq 2d_H(S_m, \Sigma).$$

Note that by the argument we have given in lemma 2.2.3 the optimal approximating simplicial complex is indeed a polytope. So by definition of optimality on enclosed polytopes we have that $d_H(P_m, \Sigma) \leq d_H(S^{\text{on}}, \Sigma)$ which yields that $d_H(P_m, \Sigma) \leq 2d_H(S_m, \Sigma)$. □

[7] If $d_h(S_m, \Sigma) \leq R(\Sigma)$, with R the reach, the point is unique.

For the following lemma we need two observations: Let Σ be a convex (but not necessarily strictly convex) hypersurface and S_m a sequence of optimally approximating triangulations of Σ with m vertices. Suppose that $T_{m(i)}$ is a convergent (sub-) sequence of simplices with $T_{m(i)} \subset S_{m(i)}$ of which the lengths of the edges does not go to zero, then the sequence converges to a subset of a hyperplane that is also contained in Σ, because the Hausdorff distance between Σ and $S_{m(i)}$ tends to zero.

Secondly, if $\Sigma = \partial C$ is a convex C^1 hypersurface with C a convex body and L a line segment that is contained in Σ then the normal to Σ is constant along L. This can be seen by projecting the tangent spaces along L on a hyperplane orthogonal to L: If the normal is not constant then we can pick two points (p,q) where the normals are not the same. Let us denote by OL_p, OL_q the hyperplane that contain p and q respectively and are orthogonal to L. Let us write $C_p = OL_p \cap C$ and $C_q = OL_q \cap C$. We translate OL_q along L such that OL_p and OL_q coincide. If the normals are not the same there is a point r in the translated C_q that does not lie within the half space marked by the normal at p, which contradicts convexity, because the line that connects the (untranslated version) of that point r and p does not lie within C.

Lemma 2.2.7 *Let P_m^{in} be an optimally approximating inscribed polytope with Hausdorff distance $d_H(P_m^{in}, \Sigma)$ to a (not necessarily strictly) convex C^1 hypersurface with positive reach, such that $d_H(P_m^{in}, \Sigma)$ is smaller than reach of Σ. Then we can construct a simplicial complex S_m such that*

$$d_H(S_m, \Sigma) \leq \frac{1}{2} d_H(P_m^{in}, \Sigma) + o(d_H(P_m^{in}, \Sigma)).$$

Proof Let v_i be the vertices of P_m^{in} then we choose the vertices $\tilde{v}_i$ to be $v_i + \frac{1}{2} d_H(P_m^{\text{in}}, \Sigma)\nu(v_i)$, where ν denotes the normal to the hypersurface. We endow the vertex set $\{\tilde{v}_i\}$ with the same simplicial structure as $\{v_i\}$ has. The complex which arises will be denoted by S_m. This also corresponds to the boundary of the convex hull of $\{\tilde{v}\}$. We can see this as follows, P_m^{in} is the boundary of the convex hull of $\{v_i\}$. It suffices to prove that a $(d-1)$-dimensional simplex $v_{i_1}, \ldots, v_{i_d}$ in P_m^{in} corresponds to a simplex in $\partial(\text{CH}(\tilde{v}_1, \ldots, \tilde{v}_m))$. Suppose that is does not, then there exists a vertex $\tilde{v}_j$ which lies outside the plane spanned by $\tilde{v}_{i_1}, \ldots \tilde{v}_{i_d}$, this is impossible because the v_j does not lie on P_m. To see why the mapping defined above reduces the Hausdorff distance by half, up to higher order, we turn to the alternative definition of the Hausdorff distance, see for example Munkres [Mun00]:

$$d_H(X, Y) = \inf\{\epsilon | X \subset U(Y, \epsilon) \text{ and } Y \subset U(X, \epsilon)\},$$

where $U(X, \epsilon)$ denotes the ϵ-neighbourhood of X. Let C be the compact convex body such that $\Sigma = \partial C$. From this we see that P_m^{in} is contained in an inner rim

inside the convex hypersurface Σ that is

$$P_m^{\text{on}} \subset U(\Sigma, d_H(P_m^{\text{on}}, \Sigma)) \cap C.$$

We also have that

$$\Sigma \subset U(P_m^{\text{on}}, d_H(P_m^{\text{on}}, \Sigma)).$$

This yields that for every point $x \in P_m^{\text{on}}$ we have a unique point $y \in \Sigma$ which is closest to x, moreover the vector $(x - y)$ is normal to the hypersurface. We may now define the mapping Π by

$$\Pi : x \mapsto x + \frac{1}{2} d_H(P_m^{\text{on}}, \Sigma) \frac{x - y}{|x - y|}$$

and consider $\Pi(P_m^{\text{on}})$. By definition we have that

$$\Pi(P_m^{\text{on}}) \subset U(\Sigma, 1/2 d_H(P_m^{\text{on}}, \Sigma)).$$

We shall now show that

$$\Sigma \subset U(\Pi(P_m^{\text{on}}), \frac{1}{2} d_H(P_m^{\text{on}}, \Sigma)).$$

For every $y \in \Sigma$ there is a $x \in P_m^{\text{on}}$ such that $y - x$ is normal to Σ and $|y - x| \leq d_H(P_m^{\text{on}}, \Sigma)$. The first intersection point of $\{c - \lambda\nu(x) | \lambda \in \mathbb{R}\}$ and P_m^{on} will do, where by the first we mean the point with the smallest λ associated. Such an intersection point exists because of the following; suppose there exists a $y \in \Sigma$ such that

$$\{y - \lambda\nu(y) | \lambda \in \mathbb{R}\} \cap P_m^{\text{on}} = \emptyset,$$

then the line $\{y - \lambda\nu(y) | \lambda \in \mathbb{R}\}$ intersects Σ at some other point $\tilde{y} = y - \tilde{\lambda}\nu(y)$, without first intersecting P_m^{on}. This also means that there is a point $y_e = y - \tilde{\lambda}\nu(y)/2$, which has equal distance to y and $\tilde{y}$ so y_e lies further from Σ than the reach, but this contradicts the assumption that $d_H(P_m^{\text{on}}, \Sigma) \leq R(\Sigma)$. We will now show that $|y - x| \leq d_H(P_m^{\text{on}}, \Sigma)$. Suppose that there is a y' such that $|y' - x| \leq |y - x|$, then we can find a point along $y - x$ with equal distance to two points of Σ, namely y and y', again contradicting the assumption that $d_H(P_m^{\text{on}}, \Sigma) \leq R(\Sigma)$. Therefore y is the point on Σ which is closest to x and thus $|y - x| \leq d_H(P_m^{\text{in}}, \Sigma)$. Given the special role we have thrust on the normal ν it is clear that

$$\Sigma \subset U(\Pi(P_m^{\text{in}}), \frac{1}{2} d_H(P_m^{\text{in}}, \Sigma)).$$

This implies that

$$d_H(\Pi(P_m^{\text{in}}), \Sigma) \leq \frac{1}{2} d_H(P_m^{\text{in}}, \Sigma).$$

Finally we argue that $d_H(\Pi(P_m^{\text{in}}), S_m)$ tends to zero as m tends to infinity, faster than $d_H(P_m^{\text{in}}, \Sigma)$ tends to zero, that is $d_H(\Pi(P_m^{\text{in}}), S_m) = o(d_H(P_m^{\text{in}}, \Sigma))$. The normals $(x-y)/|x-y|$, where x is an element of T and y the point of Σ closest to x, line up with $\nu(v_i)$, where v_i is some vertex of T. Because the surface is continuously differentiable the normal is continuous, so if $T \subset S_m$ is an element of a convergent sequence of triangles and the edge lengths tend to zero $(x-y)/|x-y|$ converges trivially to the normal at any vertex because of continuity, if the edge lengths do not tend to zero we use the observation above that the normal along a line segment contained in the hypersurface is constant to conclude that the normals converge. This implies that $(x-y)/|x-y| - \nu(v_i)$ tends to zero so $d_H(P_m^{\text{in}}, \Sigma)((x-y)/|x-y| - \nu(v_i))$ tends to zero faster than $d_H(P_m^{\text{in}}, \Sigma)$. Because $d_H(P_m^{\text{on}}, \Sigma) \leq d_H(P_m^{\text{in}}, \Sigma)|(x - y/|x-y| - \nu(v_i)|$, by definition of the mapping Π, we have that

$$d_H(S_m, \Sigma) \leq d_H(\Pi(P_m^{\text{in}}), S_m) + d_H(\Pi(P_m^{\text{in}}), \Sigma) \leq \frac{1}{2} d_H(P_m^{\text{in}}, \Sigma) + o(d_H(P_m^{\text{in}}, \Sigma)).$$

We also used the triangle inequality for the first inequality. So S_m is a simplicial complex sufficiently close to Σ. □

We are now able by combining Lemmas 2.2.3, 2.2.4, 2.2.6 and 2.2.7 to prove Theorem 2.2.1, which we shall display in full.

Theorem 2.2.8 *Let Σ be a strictly convex C^2 hypersurface in $\mathbb{R}^d$. For every m let S_m be an optimally approximating simplicial complex with m vertices having Hausdorff distance $d_H(S_m, \Sigma)$ to the convex hypersurface Σ. Then we have*

$$\lim_{m\to\infty} m^{2/(d-1)} d_H(S_m, \Sigma) = \frac{1}{4} \left(\frac{\theta_{d-1}}{\kappa_{d-1}} \int_\Sigma \sqrt{K(x)} \mathrm{d}\mu \right)^{2/(d-1)},$$

where κ_d is the volume of the d-dimensional ball $\pi^{d/2}/\Gamma(1+d/2)$, θ_d is the covering density of the ball in d-dimensional space and K the Gaussian curvature.

Proof By Gruber and Schneider [Gru93a, Gru93b, Sch81] we have that

$$\lim_{m\to\infty} m^{2/(d-1)} d_H(P_m^{\text{in}}, \Sigma) = \frac{1}{2} \left(\frac{\theta_{d-1}}{\kappa_{d-1}} \int_\Sigma \sqrt{K(x)} \mathrm{d}\mu \right)^{2/(d-1)},$$

where P_m^{in} an optimally approximating inscribed polytope simplicial complex, which is automatically also a polytope. Lemmas 2.2.6 and 2.2.7 give us

$$\frac{1}{2}d_H(P_m,\Sigma) \leq d_H(S_m,\Sigma)$$

and the existence of a simplicial complex $\tilde{S}_m$, for sufficiently large m, satisfying

$$d_H(\tilde{S}_m,\Sigma) \leq \frac{1}{2}d_H(P_m^{\text{in}},\Sigma) + o(d_H(P_m^{\text{in}},\Sigma)).$$

By optimality the latter equation implies

$$d_H(S_m,\Sigma) \leq \frac{1}{2}d_H(P_m^{\text{in}},\Sigma) + o(d_H(P_m^{\text{in}},\Sigma)).$$

Furthermore, lemmas 2.2.3 and 2.2.4 give us the existence of the simplicial complexes involved. So that

$$\begin{aligned}\frac{1}{2}\lim_{m\to\infty} m^{2/(d-1)}d_H(P_m^{\text{in}},\Sigma) &\leq \lim_{m\to\infty} m^{2/(d-1)}d_H(S_m,\Sigma)\\ &\leq \lim_{m\to\infty} m^{2/(d-1)}\left(\frac{1}{2}d_H(P_m^{\text{in}},\Sigma) + o(d_H(P_m^{\text{in}},\Sigma))\right)\\ &= \frac{1}{2}\lim_{m\to\infty} m^{2/(d-1)}d_H(P_m^{\text{in}},\Sigma).\end{aligned}$$

Using the result of Gruber and Schneider yields

$$\lim_{m\to\infty} m^{2/(d-1)}d_H(S_m,\Sigma) = \frac{1}{4}\left(\frac{\theta_{d-1}}{\kappa_{d-1}}\int_\Sigma \sqrt{K(x)}\mathrm{d}\mu\right)^{2/(d-1)},$$

the desired result. □

The fact that the surface is convex is essential to our line of reasoning, because this insures that the simplices whose vertices lie on the surface do not intersect the surface. This is the reverse of the case of negative curvature, where in general the simplex and the surface will intersect.

2.3 The intrinsic and extrinsic properties of triangulations of Riemannian manifolds

The extrinsic nature of the asymptotic value of the product of the number of vertices and the Hausdorff distance of triangulations (piecewise linear in ambient space) of manifold embedded in Euclidean space higher codimensions is exhibited, by constructing an explicit family of isometric embeddings of the flat torus in Euclidean space.

Main result

We make the statement more precise, below we construct a family of isometric embeddings $E : S^1 \times S^1 \to \mathbb{R}^n$ of the flat torus, whose members are discriminated by the index $k \in \mathbb{Z}_{\geq 1}$. We write

$$\lim_{m\to\infty} d_H(E_k, T_m)m = c_{E_k},$$

where E_k indicates a member of the family of isometric embeddings of $S^1 \times S^1$, T_m is an optimal triangulation with m vertices that lie on E_k, d_H indicates the Hausdorff distance. By optimal triangulation with m vertices we mean that there is no other triangulation that attains a smaller the Hausdorff distance. c_{E_k} is a real number depending on E_k. For the family of embeddings we construct we have

$$\lim_{k\to\infty} c_{E_k} = \infty.$$

2.3.1 Higher order example

Before starting on the proof of the statement we note that although approximating surfaces by piecewise quadratic pieces (or more general pieces of an algebraic surface of higher order) is not so well understood[8], the dependence on the exact embedding is clearer than for a piecewise linear approximation. We exhibit this dependence for compact manifolds by giving two isometric embeddings of the flat torus (that is, the metric induced on the surface is in both cases that of the flat torus), namely:

$$E_0 = \{(x_1, x_2, x_3, x_4) \in \mathbb{R}^4 \mid x_1^2 + x_2^2 = 1, x_3^2 + x_4^2 = 1\}$$
$$E_1 = \{(x_1, x_2, x_3, x_4) \in \mathbb{R}^4 \mid (x_1/c)^2 + (x_2/c)^4 = 1, (x_3/c)^2 + (x_4/c)^4 = 1\},$$

[8]For piecewise quadratic approximations of convex surfaces satisfying some technical conditions the limit $\lim_{m\to\infty} m d_H(M, Q_m)^{2/3}$ exists but to date we have not been able to find an explicit expression of this limit in terms of geometric quantities.

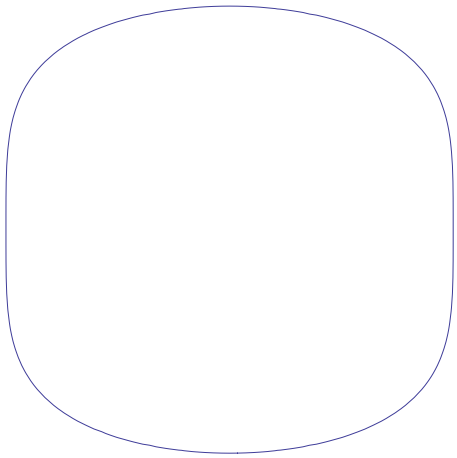

Figure 2.5: The set $\{(x_1, x_2) \in \mathbb{R}^2 \mid (x_1/c)^2 + (x_2/c)^4 = 1\}$.

where c is a constant such that the surface area of both embeddings are the same. That this condition is sufficient is easily seen in the following analogy; let us take a rectangular piece of paper and glue two opposite boundaries together. We thus get a cylinder ($S^1 \times [a, b]$), which we imagine to lie along the z-axis, so that S^1 lies in the xy-plane. However we may deform the circle in the xy-plane in whatever manner we like, so that $L \times [a, b]$ is isometric to $S^1 \times [a, b]$ as long as L is a loop without self-intersection having the same length. We depict $\{(x_1, x_2) \in \mathbb{R}^2 \mid (x_1/c)^2 + (x_2/c)^4 = 1\}$ in Figure 2.5.

The embedding E_0 results in an algebraic surface of order 2, so one piece of a quadratic surface, namely the surface itself, suffices to approximate the surface. This mean that we have

$$d_H(E_0, Q_1) = 0,$$

where Q_m is a piecewise quadratic surface with m patches which approximates the surface optimally. The embedding E_1 of the flat torus gives a quartic surface so there is no finite m such that

$$d_H(E_1, Q_m) = 0.$$

We are of course familiar with this result in three dimensions. If we again take the example of a rectangular sheet of paper and fold and glue it into a cylinder $\{(x_1, x_2) \in \mathbb{R}^2 \mid x_1^2 + x_2^2 = 1\} \times [a, b]$, with $a < b$. We can deform the cylinder by deforming the circle, thus changing the algebraic properties while the intrinsic geometry remains the same.

2.3.2 The construction

We could try and show the effect introduced above for the following family of embeddings of the flat torus which for the first two coordinates reads

$$\{(1+\cos(2k\theta)/20)(\cos\theta,\sin\theta)/r_k \mid \theta\in[0,2\pi]\},$$

where we have set the length of the topological circle to 2π by taking

$$r_k=\int_0^{2\pi}\frac{1}{40\sqrt{2}\pi}\sqrt{801+4k^2+80\cos(2k\theta)+(1-4k^2)\cos(4k\theta)}\mathrm{d}\theta.$$

The last two coordinates are defined in a similar manner. However since the extrinsic curvature of a member of this family is strongly dependent on the coordinate θ, which makes estimates of the Hausdorff distance very difficult and thus the example less clear, we shall not use this family of embeddings in $\mathbb{R}^4$ but focus on embeddings in $\mathbb{R}^8$. We shall study the family of embeddings of the flat torus E_k parameterized by $k\in\mathbb{Z}_{\geq 1}$, with a little abuse of notation

$$\begin{aligned}E_k(\theta,\varphi)=(&\cos(\theta),\sin(\theta),\cos(k\theta)/k,\sin(k\theta)/k,\\&\cos(\varphi),\sin(\varphi),\cos(k\varphi)/k,\sin(k\varphi)/k)\\E_k=\{&E_k(\theta,\varphi)\mid\theta\in[0,2\pi],\varphi\in[0,2\pi]\}.\end{aligned}$$

Firstly we note that since the surface contains no straight lines, for each (fixed) k, we have that the edge length of each edge in a triangulation T_m tends to zero as $d_H(T_m,E_k)$ tends to zero. This we can prove as follows: Suppose that there is a subsequence $T_{m(l)}$ for which the the length of edges $e_{m(l)}\in T_{m(l)}$ does not tend to zero. Without loss of generality we can assume (by chosing a convergent subsequence) that $e_{m(l)}$ converges to a limit line element whose length by assumption is not zero. Because we assume that the Hausdorff distance $d_H(T_m(l),E_k)$ tends to zero, this line element lies within E_k, which contradicts the fact that E_k contains no straight lines. Because of this we may locally approximate the surface. Moreover the tangent plane of the surface in the neighbourhood of a triangle is asymptotically well defined. Secondly, we may employ the natural group action of $(\mathrm{SO}(2))^4$ on the ambient space $\mathbb{R}^8$ to shift a given point on the torus to the origin. This means that we can approximate the surface locally by

$$(1-\theta^2/2,\theta,1-\theta^2/(2k),\theta,1-\varphi^2/2,\varphi,1-\varphi^2/(2k),\varphi),$$

where (θ,φ) are near the origin, and thus through a translation by

$$\Sigma_k(\theta,\varphi)\simeq(-\theta^2/2,\theta,-\theta^2/(2k),\theta,-\varphi^2/2,\varphi,-\varphi^2/(2k),\varphi).$$

Furthermore we may assume that the vertices of a triangle are $\Sigma_k(0,0) = 0 \in \mathbb{R}^8$, $\Sigma_k(\theta_1,\varphi_1)$, $\Sigma_k(\theta_2,\varphi_2)$. We shall employ techniques similar to the ones employed by Fejes Tóth [FT53] to find a a lower bound for

$$\lim_{m\to\infty} d_H(T_m, E_k)m.$$

The approach by Fejes Tóth is dicussed in Section 2.1.1. We shall also adopt his notation.

Because we are only interested in lower bounds it suffices to fix some lower bound on the Hausdorff distance and some upper bound on the area of the triangles satisfying this bound. To determine the Hausdorff distance we first determine for a given point $p = \Sigma_k(\theta_1,\varphi_1)\lambda_1 + \Sigma_k(\theta_2,\varphi_2)\lambda_2$ of the triangle under consideration, where $\lambda_1 \in [0,1]$ and $\lambda_2 \in [0, 1-\lambda_1]$, the point on the surface $\Sigma_k(\theta_c,\varphi_c)$ which is closest. We optimize in the usual manner, that is we impose

$$\begin{aligned}\partial_\theta |p - \Sigma_k(\theta,\varphi)|^2 &= 0\\ \partial_\varphi |p - \Sigma_k(\theta,\varphi)|^2 &= 0.\end{aligned}$$

It is not difficult to verify that $\theta_c \simeq \theta_1\lambda_1 + \theta_2\lambda_2$ and $\varphi_c \simeq \varphi_1\lambda_1 + \varphi_2\lambda_2$, where $\simeq$ denotes equality up to leading order in (θ_i,φ_i). This means that the distance between a point on the triangle and the surface is approximately given by

$$\begin{aligned}&\|\Sigma_k(\theta_1,\varphi_1)\lambda_1 + \Sigma_k(\theta_2,\varphi_2)\lambda_2 - \Sigma_k(\theta_1\lambda_1+\theta_2\lambda_2, \varphi_1\lambda_1+\varphi_2\lambda_2)\|\\ &\quad= \Big|\Big((\theta_1\lambda_1+\theta_2\lambda_2)^2/2 - \frac{\theta_1^2}{2}\lambda_1 - \frac{\theta_2^2}{2}\lambda_2, 0,\\ &\qquad k(\theta_1\lambda_1+\theta_2\lambda_2)^2/2 - k\frac{\theta_1^2}{2}\lambda_1 - k\frac{\theta_2^2}{2}\lambda_2, 0,\\ &\qquad (\varphi_1\lambda_1+\varphi_2\lambda_2)^2/2 - \frac{\varphi_1^2}{2}\lambda_1 - \frac{\varphi_2^2}{2}\lambda_2, 0,\\ &\qquad k(\varphi_1\lambda_1+\varphi_2\lambda_2)^2/2 - k\frac{\varphi_1^2}{2}\lambda_1 - k\frac{\varphi_2^2}{2}\lambda_2\Big)\Big|.\end{aligned}$$

For $\lambda_1 = 1/2$, $\lambda_2 = 0$ and $\lambda_1 = 0$, $\lambda_2 = 1/2$ this yields $\sqrt{1+k^2}\sqrt{\theta_1^4+\varphi_1^4}/8$ and $\sqrt{1+k^2}\sqrt{\theta_2^4+\varphi_2^4}/8$ respectively, so

$$d_H \geq \eta = \frac{1}{8}\sqrt{1+k^2}\max\Big\{\sqrt{\theta_1^4+\varphi_1^4},\ \sqrt{\theta_2^4+\varphi_2^4}\Big\}.$$

On the other hand the area of the triangle is approximately equal to

$$|\varphi_1\theta_2 - \theta_1\varphi_2|/2.$$

The area of a triangle on which a given η is attained is bounded from above by $c'\eta/\sqrt{1+k^2}$, with $c' > 8^2/2 = 32$ because $8\eta/\sqrt{1+k^2} \geq \theta_1, \theta_2, \varphi_1, \varphi_2$, see Section 2.1.1. Since furthermore the number of triangles $\tilde{m}$ in a triangulation is bounded from below by

$$\tilde{m} \gtrsim \frac{\text{Area}(E_k)}{\text{Area}(\triangle)},$$

where E_k denotes the embedding of the surface and $\triangle$ denotes the biggest triangle in the triangulation. These considerations give us

$$d_H m \gtrsim \eta\, m \gtrsim \eta \frac{\text{Area}(E_k)}{\text{Area}(\triangle)} \gtrsim \eta \frac{(4\pi)^2}{c'\eta/\sqrt{1+k^2}} = \frac{(4\pi)^2}{c'}\sqrt{1+k^2}$$

This implies that

$$\lim_{m\to\infty} d_H(T_m, E_k)m \geq \frac{(4\pi)^2}{c'}\sqrt{1+k^2}.$$

The result may be summarized in the following theorem

Theorem 2.3.1 *Let M be a Riemannian surface, then there is generally no function $f(g, \partial g, \ldots)$ which depends only on the metric and all its derivatives and a constant $\tilde{c}$ such that*

$$\lim_{m\to\infty} d_H(T_m, E(M))m \leq \tilde{c} \int_M f \mathrm{d}\mathit{Vol},$$

where $E(M)$ denotes the embedding of the manifold in Euclidean space and $\mathrm{d}\mathit{Vol}$ the volume form.

In this theorem we could have absorbed $\tilde{c}$ in $f(g)$. However, we have chosen this form to mimic the traditional form of the result of Fejes Tóth [FT53] and Schneider [Sch81]. The generalization of the above theorem to manifolds of arbitrary dimension is trivial.

2.3.3 Rigidity

It is clear that if the embedding of a manifold M is rigid then

$$\lim_{m\to\infty} m d_H(M, T_m)^{(n-1)/2},$$

where again T_m is optimal, must only depend on intrinsic quantities. What the converse statement should be is not so clear. For example the cylinder with

boundaries $S^1 \times [a, b]$ is non-rigid, while the limit of $md_H(M, T_m)$ is independent of embedding, albeit zero. This is why the exact relation between rigidity and the asymptotic behavior with respect to m of $d_H(M, T_m)$ occasions further research. Results in this direction could also provide a different perspective on combinatorial rigidity.

2.4 Fejes Tóth's triangulation of the hyperboloid and the triangulation of ruled surfaces

In 1953 Fejes Tóth [FT53] claimed that for some particular triangulation (with vertices on the surface) of the one-sheeted hyperboloid bounded by two congruent circles $d_H(T_m, \Sigma) \sim 1/m^2$, where $\sim$ denotes proportionality to the leading order in $1/m$, here m denotes the number of vertices. This claim is false.

In Section 2.4.1 we shall prove that $d_H(T_m, \Sigma) \sim 1/m$, and moreover that the triangulation suggested by Fejes Tóth is not optimal. By not optimal we mean that there are triangulations with the same number of vertices, such that the Hausdorff distance between the surface and the triangulation is smaller.

The intuition behind the claim of Fejes Tóth is clear, albeit wrong. Fejes Tóth's reasoning was that one could use the fact that the surface is ruled to snugly fit 'long' triangles to the surface. A ruled surface is a surface swept out by a straight line as it moves through space. The straight lines are known as rulings. These 'long' triangles would lie along the ruling. The only thing that one would need to worry about would be the boundary of the ruled surface, thus arriving at $d_H(T_m, \Sigma) \sim 1/m^2$.

In Section 2.4.2 we discuss the geometry of ruled surfaces. Assuming that the Gaussian curvature of the surface is non-zero we shall come to understand why 'long' triangles that lie along a ruling cannot lie close to the surface for the entire length of triangle. Instead the surface seems to rotate away from a 'long' triangle as we shall see in Corollary 2.4.5.

The presence of 'long' triangles such as the ones suggested for the triangulation of the one-sheeted hyperboloid prevent the use of local techniques to determine

$$\lim_{m\to\infty} d_H(T_m, \Sigma)m \tag{2.7}$$

for ruled surfaces and therefore for general non-convex surfaces. By local techniques we mean that we can do the analysis in the neighbourhood of a point, in particular one uses:

- The normal to the surface is approximately constant.
- The surface is well approximated by the second order Taylor approximation of its Monge form.

If the local techniques would work, one could prove that

$$\lim_{m\to\infty} d_H(T_m, \Sigma)m = \frac{1}{4\sqrt{5}} \int_\Sigma \sqrt{|K|}\mathrm{d}A, \tag{2.8}$$

for negatively curved surfaces, as we shall see in Section 2.4.3. This follows from arguments similar to those used in the convex case, see Section 2.1.1. Alternatively this also follows from results by Pottmann et al. [PKH$^+$00] and Atariah [Ata14]. These authors study triangulations of graphs of functions, where the relevant distance is the vertical distance between the triangulation (graph of a piecewise linear function) and the graph of the function.

In Section 2.4.2 we also prove that local techniques do work if the surface does not contain a segment of a ruled surface of positive measure. This means in particular that (2.8) holds.

In Section 2.4.3 we discuss a method to confront

$$\lim_{m\to\infty} d_H(T_m, \Sigma)m \tag{2.7}$$

for ruled surfaces. This method should lead to either one of the following alternatives:

- A proof that equation (2.8) holds for all negatively curved surfaces, that is including ruled surfaces
- A clear indication how to construct a sequence of triangulations of a ruled surface such that

$$\lim_{m\to\infty} d_H(T_m, \Sigma)m < \frac{1}{4\sqrt{5}} \int_\Sigma \sqrt{|K|}\mathrm{d}A.$$

We stress that if the second alternative holds, the normals of the triangles in a triangulation in such a sequence would not align with the normals of the surface as m tends to infinity.

The calculations involved the method to confront

$$\lim_{m\to\infty} d_H(T_m, \Sigma)m$$

seem however to be beyond the reach of an analytic approach.

2.4.1 The hyperboloid

In this section we first prove that for the triangulation of the one-sheeted hyperboloid (with two circles of equal size as boundary) suggested by Fejes Tóth we have $d_H(T_m, \Sigma) \sim 1/m$. In Section 2.4.2 we give some geometric intuition explaining this somewhat counter-intuitive result.

We parametrize the hyperboloid by

$$\sigma(u,t) = \frac{u}{\sqrt{2}} \begin{pmatrix} -\sin t \\ \cos t \\ 1 \end{pmatrix} + \begin{pmatrix} \cos t \\ \sin t \\ 0 \end{pmatrix}.$$

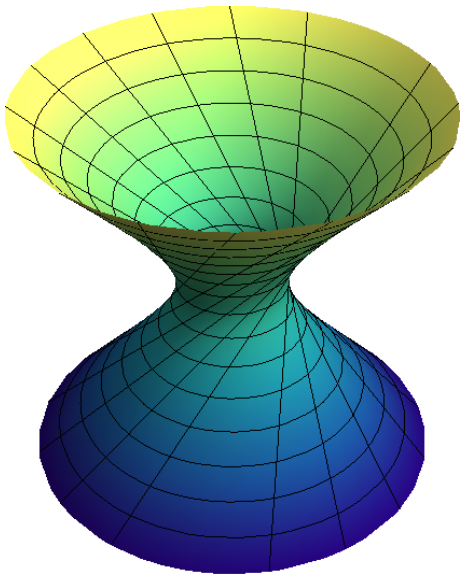

Figure 2.6: The one-sheeted hyperboloid.

This parametrization is compatible with the parametrization of ruled surfaces, that we introduce in Section 2.4.2. Note that the parametrization exhibits the ruling of the hyperboloid. We shall assume that $u \in [-u_{\max}, u_{\max}]$, so that the two circles that form the boundary lie at a distance $u_{\max}/\sqrt{2}$ above and below the xy-plane. In our parametrization we take $t \in [0, 2\pi]$.

The vertices of the triangulation discussed by Fejes Tóth are equally distributed along the lower and upper boundary and placed such that for every vertex on the lower boundary there is a vertex on the upper boundary that lies on the same ruling as the vertex on the lower boundary. By a ruling we mean a straight line (segment) on the surface. Fejes Tóth assumes that m is even. The triangulation is characterized by the fact that these rulings connecting the vertices are edges of the triangulation.

The edges of the triangles in the triangulation fall into three different categories:

- rulings that lie on the surface
- edges of a regular $m/2$-gon approximating the upper or lower boundary
- edges that connect vertices 'neighbouring' vertices on the upper and lower boundary.

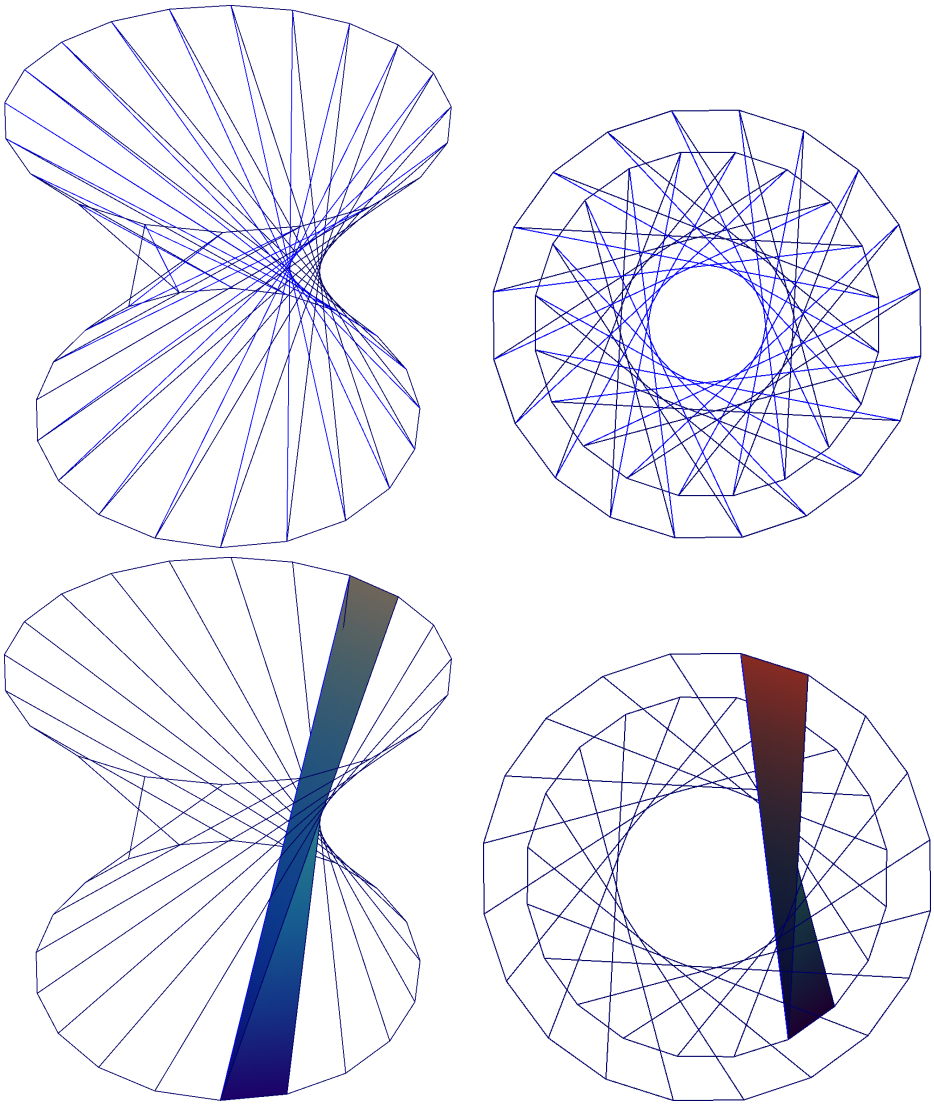

Figure 2.7: The one-sheeted hyperboloid with two of the triangles of the triangulation inserted.

Up to a rotation around the z-axis edges from the last category can be paramet-

rized by[9]

$$\lambda\sigma(u_{\max},0)+(1-\lambda)\sigma(-u_{\max},s), \tag{2.9}$$

with $s=4\pi/m$.

We now prove a lemma that refutes Fejes Tóth's claim that $d_H(T_m,\Sigma)\sim 1/m^2$ for the triangulations described above:

Lemma 2.4.1 *For the sequence of triangulations T_m of the one-sheeted hyperboloid Σ bounded by two congruent circles suggested by Fejes Tóth, as described above, we have*

$$\lim_{m\to\infty} d_H(\Sigma,T_m)m=\sqrt{2}\pi u_{max}.$$

Proof To determine $d_H(\Sigma,T_m)$ we first give an upper bound by considering the distance between the triangulation and the hyperboloid as restricted to a horizontal plane. This bound is found by considering the triangulation and the surface restricted to horizontal planes. The hyperboloid restricted to a horizontal plane is a circle. The restriction of the triangulation is a (somewhat complicated) polygon. This vertices of this polygon lie on the circle or are the restriction of an edge like (2.9). For each horizontal plane we can determine the Hausdorff distance between the polygon and circle. This is straightforward because it attained in the restriction of an edge like (2.9). The maximum of all these 'lower dimensional' Hausdorff distances bounds the Hausdorff distance between the hyperboloid and Fejes Tóth's triangulation. This maximum is attained for $z=0$, where the normal to the hyperboloid is horizontal so that here the 'lower dimensional' Hausdorff distance coincides with the Hausdorff distance between the hyperboloid and Fejes Tóth's triangulation.

To find the Hausdorff distance between the polygon and circle, it is convenient to introduce the pseudometric[10]

$$d_{\text{hor}}(v,w)=\sqrt{(v_1-w_1)^2+(v_2-w_2)^2},$$

where $v=(v_1,v_2,v_3)\in\mathbb{R}^3$ and $w=(w_1,w_2,w_3)\in\mathbb{R}^3$. We are now able to calculate

$$\begin{aligned} &d_{\text{hor}}(\lambda\sigma(u_{\max},0)+(1-\lambda)\sigma(-u_{\max},s),o)\\ &\qquad=\frac{\sqrt{2+(1-2\lambda)^2u_{\max}^2}}{\sqrt{2}}-\frac{2\lambda(\lambda-1)u_{\max}}{\sqrt{2+(1-2\lambda)^2u_{\max}^2}}s+\mathcal{O}(s^2), \end{aligned} \tag{2.10}$$

[9]Here we have picked a sign. We could have chosen

$$\lambda\sigma(-u_{\max},0)+(1-\lambda)\sigma(u_{\max},s).$$

The choice does not influence the outcome.

[10]The difference between a metric space and a pseudometric space is that in case of the latter $d(x,y)=0$ does not imply $x=y$.

where $o = (0, 0, 0)$. Note that $s = 4\pi/m$ and we are interested in the limit of m tending to infinity. On the other hand the z-coordinate of the edge parametrized by (2.9) is

$$\frac{(2\lambda - 1)u_{\max}}{\sqrt{2}},$$

so the hyperboloid restricted to the plane characterized by the coordinate is a circle with radius

$$\frac{\sqrt{2 + (1 - 2\lambda)^2 u_{\max}^2}}{\sqrt{2}},$$

this radius is exactly the constant term in (2.10). This gives that the supremum of remaining terms in (2.10) gives an upper bound on the Hausdorff distance

$$\sup_{\lambda \in [0,1]} \left| \frac{2\lambda(\lambda - 1)u_{\max}}{\sqrt{2 + (1 - 2\lambda)^2 u_{\max}^2}} s \right| + \mathcal{O}(s^2) = \frac{u_{\max}}{2\sqrt{2}} s + \mathcal{O}(s^2),$$

because the supremum is attained for $\lambda = \frac{1}{2}$, where $z = 0$ and the normal to the hyperboloid is horizontal for $z = 0$, this equals the Hausdorff distance. We therefore find that

$$\lim_{m \to \infty} d_H(\Sigma, T_m) m = \sqrt{2}\pi u_{\max}.$$

□

Lemma 2.4.1 contradicts the assertion of Fejes Tóth.

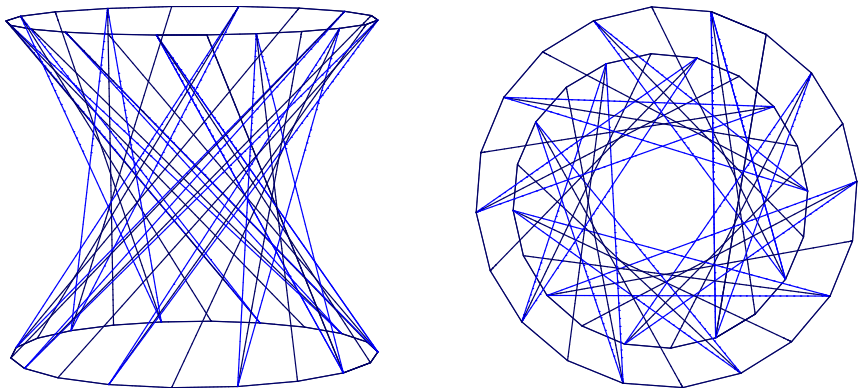

Figure 2.8: The one-sheeted hyperboloid with the edges of a more efficient triangulation indicated.

It is also easy to see that this triangulation is not optimal. We note that the Hausdorff distance is attained in but one of the edges of a triangle. This means that we can merge two such triangles as indicated in Figure 2.8 without increasing the Hausdorff distance.

Note that the surface area of the triangulations do not converge to the surface area of the surface in any case, see [HPW06] and [MT02].

2.4.2 Ruled surfaces

This section, that is Section 2.4.2, consists of three parts:

- First we discuss the parametrization of ruled surfaces and we shall see in Lemma 2.4.2 that ruled surfaces are the only surfaces that contain dense sets of straight lines.

- Based on the general discussion of ruled surfaces we are able to provide a general geometric context to Lemma 2.4.1. In particular Lemma 2.4.4 and Corollary 2.4.5 explain why a surface seems to rotate away from a long triangle.

- In the third part of this section we introduce the concept of asymptotically point-like and asymptotically line-like triangles. These are sequences of triangles in triangulations of surfaces for which the Hausdorff distance tends to zero. The lengths of the edges go to zero for asymptotically point-like triangles, but do not for asymptotically line-like triangles. We shall prove that if a surface contains no straight lines then all triangles are asymptotically point-like. If the surface is a segment of a ruled surface and has non-zero Gaussian curvature then a convergent asymptotically line-like triangle converges to a line segment on a ruling.

The results on the asymptotically point-like triangles will be used in Section 2.4.3 to find an expression for

$$\lim_{m\to\infty} d_H(T_m, \Sigma)m, \tag{2.7}$$

if the surface is negatively curved but does not contain a segment of a ruled surface. The results on the asymptotically line-like triangles imply that if the surface is ruled an expression for (2.7) can be found by studying a neighbourhood of a ruling.

The parametrization of ruled surfaces

A C^2 surface Σ embedded in $\mathbb{R}^3$ is called ruled[11] if for every point $p \in \Sigma$ there exists a (straight) line (segment) $L_p \subset \Sigma$ with $p \in L_p$. We first establish that, at least locally, we may parametrize such a surface in the standard manner, that is

$$\{r(t)u + p(t) | t \in U_1, u \in U_2\} = \Sigma, \tag{2.11}$$

where U_1 and U_2 are sufficiently small open intervals. We see this by considering a small neighbourhood U in Σ of a given point p_0 on some line (segment) L_0, we choose a C^2 curve $p : U_1 \to \Sigma : t \mapsto p(t)$ through p_0 whose tangent line at p_0 is not pointing in the direction of L_0. For every $p(t)$ there is a line (segment) that intersects $p(t)$, which lies in the surface Σ, that is we have

$$\{r(t)u + p(t) | t \in U_1, u \in U_2\} \subset \Sigma,$$

where U_1 and U_2 are sufficiently small open intervals. We can further assume that $r(t)$ is continuous. This can be argued as follows $u \mapsto r(t)u + p(t)$ is a line and hence an asymptotic curve, see for example [O'N06] or [Spi99] for a full definition. This implies that $r(t)$ points in an asymptotic direction (meaning that the normal curvature vanishes in that direction). There are only two such directions unless the Gaussian curvature is zero in some neighbourhood. Moreover the asymptotic directions are continuous for a C^2 surface. This implies that $r(t)$ can be assumed to be continuous and equal to one of the asymptotic directions along the curve p, if the Gaussian curvature is non-zero. If the Gaussian curvature is (locally) zero the surface is (locally) developable. Developable surfaces in three dimensions have been classified, see for example [Spi75a], and the the fact that we can parametrize according to (2.11) is obvious.

Having established the standard parametrization, we prove that if there is a dense subset of lines embedded in a surface then the surface is a ruled surface. To be precise:

Lemma 2.4.2 *Let Σ be a compact C^2 surface in $\mathbb{R}^3$ with a boundary and non-zero Gaussian curvature and let l_{min} be a strictly positive constant. If there is a set of line segments $L_i \subset \Sigma$ which is dense in Σ and $|L_i| \geq l_{min} > 0$ for every L_i, then Σ is a compact subset of a ruled surface. l_{min} is called the minimum length.*

Proof If the set L_i lies dense in Σ then for every $x \in \Sigma$ we can pick two sequences namely a sequence of line segments L_n and points x_n on those segments which converge to x. Due to compactness we can find a convergent subsequence of line segments. We shall call its limit L. Because L_i is a dense subset of Σ, the

[11] This is an alternative definition, we shall now see that it is equivalent to more common definition, namely: A ruled surface is a surface swept out by a straight line as it moves through space.

segment L must also lie on Σ. Furthermore because the length of each line segment is greater than the minimum length, L cannot shrink to a point, so x also lies on a line segment. Since the choice of x was arbitrary we find that for every point of Σ there is a line segment that lies on Σ and thus Σ is a compact subset of a ruled surface. □

From Lemma 2.4.2 we conclude that a surface with a dense set of line segments is a ruled surface and may be parametrized as follows:

$$\sigma(u,t) = u\, r(t) + p(t), \tag{2.12}$$

where we can consider $p(t)$ as a parametrization of a curve on the surface. We can reparameterize σ so that $\|r(t)\| = 1$ and $r' \cdot p' = 0$. Trivially, one also has $r \cdot r' = 0$. For a proof we refer to [DC76], page 190 onwards.

It is not difficult to verify that the normal ν of Σ satisfies

$$\nu = \frac{(ur' + p') \times r}{|(ur' + p') \times r|} = \frac{(ur' + p') \times r}{\sqrt{u^2 r^2 (r')^2 + (p' \times r)^2}} = \frac{(ur' + p') \times r}{\sqrt{u^2 (r')^2 + (p' \times r)^2}}.$$

For the Gaussian curvature we have

$$\begin{aligned} K = -\frac{\langle \nu, \partial_u \partial_t \sigma \rangle^2}{|(ur' + p') \times r|^2} &= -\left(\frac{r' \cdot (p' \times r)}{|(ur' + p') \times r|} \right)^2 \frac{1}{|(ur' + p') \times r|^2} \\ &= -\frac{|r'|^2 |p' \times r|^2}{(u^2 |r'|^2 + |p' \times r|^2)^2}. \end{aligned} \tag{2.13}$$

We can also easily deduce that the volume element is given by

$$\sqrt{u^2 |r|^2 |r'|^2 + |r \times p'|^2}\, \mathrm{d}u\mathrm{d}t$$

The geometric intuition for Section 2.4.1

We now focus on the following problem; how does the normal alter along a ruling, that is a straight line on the ruled surface. The result we derive is a corollary of lemma 2.4.4 but may also be seen as an extension of the following lemma (lemma 5.6.6 of [O'N06]):

Lemma 2.4.3 *A ruled surface Σ has Gaussian curvature $K \leq 0$. Furthermore, $K = 0$ if and only if the unit normal ν is parallel along each ruling of Σ.*

The following lemma uses the shape operator S. The shape operator is given by $S(v) = -\nabla_v \nu$ with ν the normal vector field of the surface. A full discussion of the shape operator can be found in [O'N06], [DC76] or [Spi99].

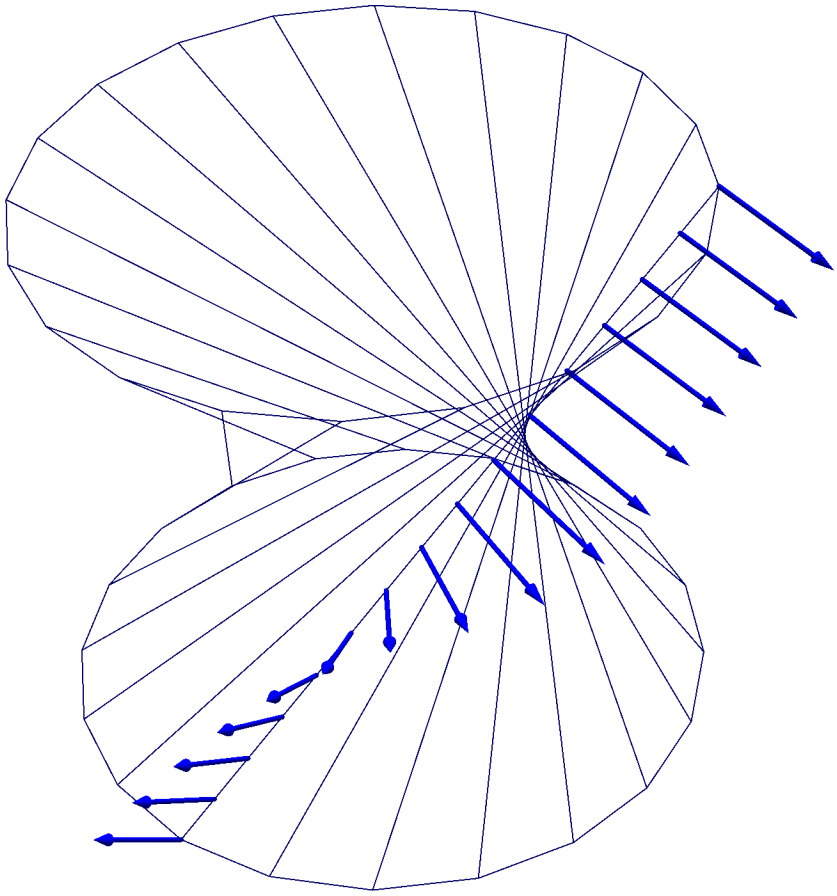

Figure 2.9: The normal along a ruling.

Lemma 2.4.4 *Let γ be an asymptotic curve, T its unit tangent and U the normal to the surface. Then the shape operator satisfies $S(T) = \pm\sqrt{|K|}U \times T$.*

Proof Consider the Darboux frame T, V, U of γ, where U equals ν the normal to the surface and $V = U \times T$. We have the Darboux equations

$$\begin{aligned} T' &= \quad gV + kU \\ V' &= -gT \quad + tU \\ U' &= -kT - tV, \end{aligned}$$

where $k = S(T) \cdot T$ is the normal curvature $k(T)$ in the T direction. g is called

the geodesic curvature and t the geodesic torsion. Because γ is assumed to be asymptotic $k = 0$. This implies that if we use the basis T, V the shape operator is of the form

$$S = \begin{pmatrix} 0 & * \\ t & * \end{pmatrix}.$$

Symmetry of the shape operator yields

$$S = \begin{pmatrix} 0 & t \\ t & * \end{pmatrix}.$$

This in turn yields that $K = -|K| = \det(S) = -t^2$. So that $S(T) = \pm\sqrt{|K|}V = \pm\sqrt{|K|}U \times T$. □

Lemma 2.4.4 also features as an exercise in [O'N06], albeit with a small error. We now immediately have

Corollary 2.4.5 *Let Σ be a ruled surface, parametrized by* (2.12)*. The derivative of the normal along the ruling ($\partial_u \nu$), usually identified with the image of r under the shape operator of Σ at $p(t)$ ($S(r)$), satisfies*

$$S(r) = \pm\sqrt{|K|}n,$$

where $n = \nu \times r$.

Proof Apply Lemma 2.4.4 to Σ, with $\gamma(u) = ur(t_0)$ for some fixed t_0. □

Corollary 2.4.5 explains why the triangulation suggested by Fejes Tóth does not have the nice properties claimed by him. The normal rotates along a ruling the triangles in the triangulation do not align with the surface but instead tend to go inwards or outwards. This is further illustrated in Figure 2.9.

Triangles in sequences of optimal triangulations

Having discussed the geometric context of Section 2.4.1 we now aim to prove that if a surface contains no straight lines the lengths of all edges in a family of triangulations tend to zero as the Hausdorff distance tends to zero. If the lengths of all edges tend to zero local analysis does suffice to find

$$\lim_{m\to\infty} d_H(T_m, \Sigma)m, \tag{2.7}$$

because in a neighbourhood of each triangle the surface is well approximated by its second order Taylor series and the normal is almost constant for that neighbourhood.

As we shall see in Section 2.4.3, the quantity (2.7) is expressed in terms of an integral. This, together with Lemma 2.4.2, implies that ruled surfaces are the only surfaces for which the fact that local analysis does not work obstructs the search for an expression for (2.7), because non-dense sets of straight line segments contained in a surface can be ignored because they have measure zero. We shall come back to this in more detail in Section 2.4.3.

We shall need the following consequence of the continuity of the Hausdorff distance, see Section 2.2.2:

Lemma 2.4.6 *Suppose that Σ is a compact connected smooth subset of a smooth ruled surface, containing no straight lines except for rulings. Further assume that E_n is a family of one dimensional simplices that satisfies*

$$\lim_{n\to\infty} d_H^o(E_n, \Sigma) = 0,$$

with $d_H^o(E_n, \Sigma)$ the one-sided Hausdorff distance from E_n to Σ and the simplices E_n converge to some line segment $E \subset \mathbb{R}^3$. Here we specifically allow the trivial case where E is a point. Under these conditions a ruling R of Σ exists such that

$$\lim_{n\to\infty} d_H^o(E_n, R) = 0.$$

Proof We first note that $d_H^o(E, \Sigma) = 0$ implies that $E \subset \Sigma$ and thus E is a segment of a ruling R. Continuity, in the sense of Cauchy, now implies that if

$$\lim_{n\to\infty} d_H^o(E_n, \Sigma) = 0,$$

then

$$\lim_{n\to\infty} d_H^o(E_n, R) = 0.$$

□

A result similar to that of Lemma 2.4.6 is true for triangles instead of one dimensional edges if one assumes that the ruled surface is not a subset of a plane:

Lemma 2.4.7 *Suppose that Σ is a compact connected smooth subset of a smooth ruled surface, containing no straight lines except for rulings and that is not the plane. Let t^i be a sequence of triangles, with vertices v_1^i, v_2^i, v_3^i, for which*

$$\lim_{i\to\infty} d_H^o(t^i, \Sigma) = 0,$$

then for every convergent subsequence t_c^i there exists a ruling R_c such that

$$\lim_{i\to\infty} d_H^o(t_c^i, R_c) = 0.$$

Such a convergent subsequence always exists because Σ is compact.

Proof Let us consider a convergent sequence t_c^i. Let us denote the edge connecting the vertices v_a^i and v_b^i of t_c^i by $v_a^i v_b^i$. Here we have $a, b \in \{1, 2, 3\}$. We can assume without loss of generality that $v_a^i v_b^i$ converges to some $v_a v_b$, because $v_a^i v_b^i$ are the edges of a convergent sequence of triangles. Moreover we have

$$\lim_{i\to\infty} d_H^o(v_a^i v_b^i, \Sigma) = 0,$$

because

$$\lim_{i\to\infty} d_H^o(t^i, \Sigma) = 0.$$

Lemma 2.4.6 yields that there is a ruling R_{ab} such that

$$\lim_{i\to\infty} d_H^o(v_a^i v_b^i, R_{ab}) = 0.$$

This holds for any choice of $a, b \in \{1, 2, 3\}$ and because we assumed that the ruled surface is not the plane R_{ab} should be independent of a, b. So we can denote the ruling by R_c and we have proven the result. □

Lemmas 2.4.6 and 2.4.7 lead us to the following definition:

Definition 2.4.8 *A sequence of triangles with*

$$\lim_{i\to\infty} d_H^o(t^i, \Sigma) = 0$$

is called asymptotically point-like *if the lengths of all edges tend to zero. It is called* asymptotically line-like *if they do not.*

The terminology asymptotically point-like has been chosen, because a convergent subsequence of a asymptotically point-like triangles converges to a point. If the ruled Σ has non-zero Gaussian curvature, then a convergent subsequence of a asymptotically line-like triangles converges to line segment in Σ, by Lemma 2.4.7. This explains terminology in the second case.

We are now able to state the following lemma:

Lemma 2.4.9 *Let Σ be a compact manifold (possibly with boundary), which contains no (non-trivial) straight line segments and let T_m be a sequence of optimal triangulations with m vertices. Moreover each T_m is assumed to be homeomorphic with Σ and the vertices of T_m are assumed to lie on Σ. Then every sequence t_m of triangles, with t_m a triangle in the triangulation T_m, is asymptotically point-like.*

Proof Suppose there is a sequence t_m which is not asymptotically point-like. Then consider the edges E_i^m, $i = 1, 2, 3$, of t_m and choose a convergent subsequence $E_{i(m)}^m$ that tends to E, a line segment whose length is strictly greater than zero. This is possible because t_m is assumed to be asymptotically line-like and Σ compact. Because T_m is an optimal triangulation we have that

$$\lim_{m\to\infty} d_H^o(E_m^{i(m)}, \Sigma) = 0$$

and thus $E \subset \Sigma$. So Σ contains a straight line segment, a contradiction with the hypothesis that it did not. □

2.4.3 Outlook on the approximation parameter for ruled surfaces

In the previous subsection we remarked that if a surface does not contain straight lines every sequence of triangles whose one-sided Hausdorff distance to the surface tends to zero is asymptotically point-like. This means that for a convergent sequence of triangles whose Hausdorff distance to the surface tends to zero it suffices to study the surface locally. This implies that a non-convex surface is adequately described by its local Monge form:

$$z \simeq \frac{k_1}{2}x^2 + \frac{k_2}{2}y^2,$$

where $\simeq$ denotes equality up to third order in the variables x, y. In Section 2.1.1 we have seen this in the convex case, that is with the same signs for k_1 and k_2. Note also that because the sequence of triangles is symptotically point-like we can take the normal of the surface to be the normal in the origin, that is the vertical vector.

One can prove, similar to the convex case we have discussed in Section 2.1.1, that for any triangle t

$$d_H^o(t, \Sigma) \gtrsim \frac{\sqrt{|k_1 k_2|}}{2\sqrt{5}}\text{Area}(t), \tag{2.14}$$

where Σ denotes the surface $d_H^o(t, \Sigma)$ the one-sided Hausdorff distance of the triangle to the surface, Area(t) denotes the area of the triangle and $\gtrsim$ should be interpreted in the same manner as in (2.1). For a proof of (2.14) we refer to [Ata14, PKH$^+$00].

Using arguments similar to those of Fejes Tóth, again as sketched in Section 2.1.1, we see that for any triangulation T_m with m vertices we have that

$$\lim_{m\to\infty} d_H(T_m, \Sigma)m \geq \int_\Sigma \frac{\sqrt{|K|}}{4\sqrt{5}}\mathrm{d}A, \tag{2.15}$$

for a triangulation with only point-like triangles.

The bound in (2.14) can in fact be attained in the limit for point-like triangles. In general one can use reflected and translated copies of a triangle to triangulate a plane. This has been illustrated in Section 3.5.2 of [Ata14] in the case of the surface $z = x^2 - y^2$. As Fejes Tóth [FT53] argued in the convex case, this gives us that the bound in (2.15) can be attained. It would be interesting to see if we can provide a constructive proof similar to the proof by Schneider [Sch81] in the convex case and along the lines of [Cla06].

The inequality (2.15) also holds if Σ contains a non-dense set of straight lines. Because in this case we can remove an arbitrarily small neighbourhood of the closure of the set of straight lines from the surface and for what remains of the surfaces (2.15) holds. As we have seen in Lemma 2.4.2 that if set of straight lines lies dense in a segment of a surface, this segment is ruled. We now have the following:

Theorem 2.4.10 *Let Σ be negatively curved a surface in $\mathbb{R}^3$ with boundary, that does not contain a segment of a ruled surface. Then for any triangulation T_m with m vertices*

$$\lim_{m\to\infty} d_H(T_m, \Sigma)m \geq \int_\Sigma \frac{\sqrt{|K|}}{4\sqrt{5}}\mathrm{d}A. \tag{2.15}$$

Moreover this bound can be attained.

This however leaves open the question: Can one do better then (2.15)? By this we mean that if Σ is a segment of a ruled surface does there exist a sequence of triangulations T_m with m vertices such that

$$\lim_{m\to\infty} d_H(T_m, \Sigma)m < \int_\Sigma \frac{\sqrt{|K|}}{4\sqrt{5}}\mathrm{d}A.$$

We therefore propose the following question: Does the following equation also hold for ruled surfaces

$$\frac{1}{4\sqrt{5}}\int_{t_\Sigma} \sqrt{|K|}\mathrm{d}A \lesssim \frac{1}{2}d_H^o(t, \Sigma), \tag{2.16}$$

with t a triangle whose vertices lie on Σ, t_Σ the triangle on the surface associated to t whose boundary consists of the geodesics[12] connecting the vertices of t?[13] Due to Lemma 2.4.7 we know that in this case (if the surface is not a subset of a plane) we can further reduce our investigations to a neighbourhood of a ruling.

[12] Simplices like t_Σ will be the topic of Chapter 3.

[13] Alternatively we could also consider t_Σ to be the projection of t on the surface via the normal, although in this case greater care should be taken of boundary effects.

Ignoring the boundary of the ruled surface this would imply that

$$\lim_{m\to\infty} d_H(T_m,\Sigma)m = \int_\Sigma \frac{\sqrt{|K|}}{4\sqrt{5}}\mathrm{d}A, \tag{2.17}$$

for an optimal triangulation of a negatively curved surface. The implication follows by

$$\begin{aligned}\frac{1}{4\sqrt{5}}\int_\Sigma \sqrt{|K|}\mathrm{d}A &\leq \frac{1}{4\sqrt{5}}\sum_{t\in T_m}\int_{t_\Sigma}\sqrt{|K|}\mathrm{d}A\\ &\lesssim \sum_{t\in T_m}\frac{1}{2}d_H^o(t,\Sigma)\\ &\lesssim m\sup_{t\in T_m} d_H^o(t,\Sigma)\\ &\leq m d_H(T_m,\Sigma),\end{aligned} \tag{2.18}$$

with T_m the triangulation. The first line of (2.18) follows from the fact that T_m is a triangulation, the second is the hypothesis (2.16), the third follows because the number of triangles behaves[14] like $2m$ as m tends to infinity, with m the number of vertices.

[14]Here we use that the alternating sum of the number of simplices is the Euler characteristic and (ignoring the boundary) every triangle has three edges and every edge is shared between between two triangles.

Chapter 3

Riemannian simplices and triangulations

3.1 Introduction

3.1.1 Motivation

In this chapter we study a natural definition of geometric simplices in Riemannian manifolds of arbitrary finite dimension. By a natural definition we mean an intrinsic one; the simplex is defined by the positions of its vertices in the manifold, which need not be embedded in an ambient space.

The construction of an intrinsic simplex is not entirely trivial. This is difficult because the standard construction using convex hulls in Euclidean space does not generalize to Riemannian manifolds. So-called Riemannian centres of mass or Karcher means do allow us to map the standard simplex on a manifold in an intrinsic manner. We shall make this more precise below.

The map from the standard simplex to the manifold is not automatically a homeomorphism to its image. If the map is a homeomorphism the intrinsic simplex on the manifold that is the image of the map is called *non-degenerate*. Our first goal in this chapter is to give conditions that guarantee that an intrinsic simplex is non-degenerate. The conditions are formulated in term of quality.

Having given conditions on individual triangles we want to use these triangles to triangulate an entire manifold. This will involve conditions on all simplices in a small neighbourhood, to be precise all simplices that have a vertex in common a so-called star.

We stress that it is the intrinsic nature of the triangles and triangulations and the explicit condition on the vertex set, that set this chapter apart.

3.1.2 Defining simplices; from Euclidean space to Riemannian manifolds

We will now explain how the convex hull construction we use in Euclidean space fails on Riemannian manifolds. We shall then sketch the construction of intrinsic simplices, using Riemannian centres of mass or Karcher means. We denote manifolds by M and the dimension of the manifold by n, unless explicitly stated otherwise.

Complications using the convex hull

The standard definition of a Euclidean simplex as the convex hull of its vertices is not useful for defining simplices in general Riemannian manifolds. A set on a Riemannian manifold is called convex if any two points in the set are connected by a unique minimizing geodesic contained in the set. The convex hull of a set of points is the smallest convex set that contains these points.

There are two main obstructions to the use of convex hulls:

- Convex hulls are difficult to compute. Almost nothing is known about the convex hull of three distinct points in a manifold of dimension three or higher, see for example [Ber03, §6.1.3]. The standing conjecture (according to Berger) is that the convex hull of three points is not closed in all but a number of special cases.

- The convex hulls of a number (smaller then the dimension plus one) of points can not be used as building blocks for triangulations. By this we mean that they cannot be used to define geometric simplicial complexes. This is because if two full dimensional convex simplices share a boundary facet, that facet must itself be convex. This constrains the facet to lie on a totally geodesic submanifold (i.e., minimising geodesics between points on the facet must lie in the facet), and when the sectional curvature is not constant such submanifolds cannot be expected to exist (see [Ber03, Thm 58] or [Che00, §11]). By the same reasoning we see that the convex hull of three points in a three or higher dimensional manifold is generally not two dimensional.

Riemannian centres of mass

Given the vertices, a geometric Euclidean simplex can also be defined as the domain on which the barycentric coordinate functions are non-negative. This definition *does* extend to general Riemannian manifolds in a natural way. The construction is based on the fact that the barycentric coordinate functions can be defined by a 'centre of mass' construction. Suppose $\{v_0, \ldots, v_n\} \subset \mathbb{R}^n$, and

$(\lambda_i)_{0\leq i\leq n}$ is a set of non-negative weights that sum to 1. If u is the point that minimises the function

$$y \mapsto \sum_{i=0}^{n} \lambda_i d_{\mathbb{R}^n}(y, v_i)^2, \tag{3.1}$$

where $d_{\mathbb{R}^n}(x, y) = |x - y|$ is the Euclidean distance, then $u = \sum \lambda_i v_i$, and λ_i are the barycentric coordinates of u in the simplex $[v_0, \ldots, v_n]$. Here $[v_0, \ldots, v_n]$ denotes the usual geometric simplex in $\mathbb{R}^n$ with vertices $v_0, \ldots, v_n$.

We can view a given set of barycentric coordinates $\lambda = (\lambda_0, \lambda_1, \ldots, \lambda_n)$ as a point in $\mathbb{R}^{n+1}$. The set $\mathbf{\Delta}^n$ of all points in $\mathbb{R}^{n+1}$ with non-negative coefficients that sum to 1 is called the *standard Euclidean n-simplex*. Thus the minimisation of the function (3.1) defines a map from the standard Euclidean simplex to the Euclidean simplex $[v_0, \ldots, v_n] \subset \mathbb{R}^n$.

If instead the points $v_0, \ldots, v_n$ lie in a convex set W in a Riemannian manifold M, then, by using the metric of the manifold instead of $d_{\mathbb{R}^n}$ in Equation (3.1), we obtain a function $\mathcal{E}_\lambda : W \to \mathbb{R}$ that has a unique minimum $x \in W$, provided W is sufficiently small (See Section 3.2.1). In this way we obtain a mapping $\lambda \mapsto x$ from $\mathbf{\Delta}^n$ to W. We call the image of this map an *intrinsic simplex*, or a *Riemannian simplex*.

3.1.3 Quality and non-degeneracy

Quality

When we speak about the quality of a Euclidean simplex, we are referring to a function that parametrises how close the simplex is to being degenerate. A common quality measure for an n-simplex is the ratio of the volume to the n^{th} power of the longest edge length. Another useful quality measure is the ratio of the smallest altitude to the longest edge length. A Euclidean simplex is degenerate if and only if its quality measure vanishes.

Non-degeneracy

In this chapter we shed light on the relationship between the local curvature in the manifold, and the size and quality of the simplices involved in a triangulation. We articulate explicit criteria that are sufficient to guarantee that a simplicial complex with vertices on the manifold is homeomorphic to the manifold. The intrinsic simplices defined by the centre of mass construction provide a convenient tool for this purpose.

Although the idea of Riemannian simplices defined in this way has been in the mathematical community for some time (see Berger [Ber03, 6.1.5]), we are

not aware of any published work exploiting the notion (of simplices in particular) prior to that of Rustamov [Rus10] and Sander [San12]. For our purposes we need to establish a property that Sander did not consider. We need to ensure that the map from the Euclidean simplex to the manifold is a smooth embedding (i.e., the map extends to a smooth map from an open neighbourhood of the Euclidean simplex). This ensures that the barycentric coordinates mapped to the manifold do in fact provide a local system of coordinates. If the map is not a smooth embedding, we call the Riemannian simplex *degenerate*.

A Euclidean simplex is non-degenerate if and only if its vertices are affinely independent. We show that a Riemannian simplex is non-degenerate if and only if for every point in the simplex the vertices are affinely independent when they are lifted by the inverse of the exponential map to the tangent space of that point.

Surfaces and trivial quality

In a two dimensional manifold this condition is satisfied for a triangle as long as the vertices do not lie on a common geodesic. Similar to the Euclidean case, such a configuration can be avoided by applying an arbitrarily small perturbation to the vertices.

Non-trivial quality in higher dimensions

However, when the dimension is greater than two, a non-trivial constraint on simplex quality is required. In dimension two a sampling density for triangulation can be specified in terms of the convexity radius [Lei99, DZM08] (maximal radius for which a geodesic ball is convex, see Section 3.2.1), and depends only on an upper bound on the sectional curvatures (Lemma 3.2.1).

In dimension higher than two, we require the simplex size (maximum edge length) to also be constrained by a lower bound on the sectional curvatures (the upper bound on the edge lengths is inversely proportional to the square root of an upper bound on the absolute value of the sectional curvatures), so we cannot express the sampling density requirements in terms of a convexity radius alone.

Quality of a simplex found by lifting to the tangent space

We define a quality measure for a Riemannian simplex by considering the quality of the Euclidean simplex obtained by lifting the vertices to the tangent space at one of the vertices. For our purposes we require a lower bound on the smallest such quality measure when each of the vertices is considered.

Method for establishing quality bounds

The quality of the Riemannian simplex that is required to ensure that it is non-degenerate depends on the maximum edge length, as well as on the magnitude of the sectional curvatures in the neighbourhood. We discuss two ways to establish such a relationship:

- Using the Rauch comparison theorem, which provides an estimate on the differences in edge lengths of Euclidean simplices obtained by lifting the vertices of the Riemannian simplex to different tangent spaces. By exploiting previously established bounds on the degradation of the quality of a Euclidean simplex under perturbations of the edge lengths [BDG13a], we establish conditions that guarantee that the Riemannian simplex is non-degenerate. This method yields quality conditions in terms of the height of a simplex.
- Using the Topogonov comparison theorem and determinant bounds by Friedland [Fri82]. This method yields quality conditions in terms of the volume of a simplex.

To triangulations

We use this result to establish conditions that guarantee that a simplicial complex is homeomorphic to the manifold. Finding these conditions is the primary motivation for this chapter. Given an abstract simplicial complex whose vertex set is identified with points on the manifold, we are ensured that it triangulates the manifold if certain conditions are met, the principal one being a relationship between the size and quality of the Riemannian simplices.

Sampling conditions

The conditions on the density and distribution of the vertices that guarantee that one is able to construct a triangulation of a manifold are known in the computational geometry community as sampling conditions. The density alone is referred to as sampling density in this context.

3.1.4 Previous work

The history of Riemannian centres of mass or Karcher means

The minimum of the function Equation (3.1) defines a point with given barycentric coordinates as a weighted centre of mass. These centres of mass have a rich history:

- Centres of mass were introduced in 1929 for Riemannian manifolds with negative curvature by Cartan [Car29] for a finite number of points [Ber03, §6.1].
- Fréchet also studied the minima of functions like Equation (3.1) for metric spaces in 1948 [Fré48].
- Karcher [Kar77] gave an extensive treatment particular to the Riemannian setting. Averages defined in this way on smooth Riemannian manifolds are often referred to as 'Karcher means'.

Riemannian centres of mass and global results

Karcher's exposition [Kar77] is the standard reference for Karcher means. However, for our purposes a particularly good resource is the work by Buser and Karcher [BK81, §6, §8]. This work was exploited by Peters [Pet84], where Karcher means are used to interpolate between locally defined diffeomorphisms between manifolds in order to construct a global diffeomorphism in a proof of Cheeger's finiteness theorem. This result has particularly inspirational because it showed the global use of Karcher means. Just as we shall use intrinsic simplices to study global triangulations. Chavel [Cha06, Ch. IX] gives a detailed exposition of Peters's argument. Kendal [Ken90] is another important reference for Karcher means. Riemannian simplices are not explicitly considered in any of these works.

Intrinsic simplices

More recently, Rustamov [Rus10] introduced barycentric coordinates on a surface via Karcher means. Sander [San12] used the method in arbitrary dimensions to define Riemannian simplices as described above. He called them *geodesic finite elements*, reflecting the application setting in numerical solutions to partial differential equations involving functions which take values in a manifold. Independently, von Deylen [vDar] has treated the question of degeneracy of Riemannian simplices. His work, based on a method by [Kau76], includes a detailed analysis of the geometry of the barycentric coordinate map, and several applications. He does not address the problem of sampling criteria for triangulation.

Sampling

This chapter is motivated by a desire to develop sampling requirements for representing a compact smooth Riemannian manifold with a simplicial complex.

By this we mean that we seek conditions on a finite set $\mathcal{P} \subset M$ that guarantee that $\mathcal{P}$ can be the vertex set of an (abstract) simplicial complex that is homeomorphic to M. We are particularly interested in manifolds of dimension greater than 2. For 2-dimensional manifolds a triangulation is guaranteed to exist when $\mathcal{P}$ meets density requirements. These density requirements can be specified either in terms of:

- extrinsic criteria (the distance to the medial axis), for surfaces embedded in Euclidean space [BO05, ACDL00]
- in terms of intrinsic criteria [Lei99, DZM08].

In higher dimensions it is well known that a smooth manifold admits a triangulation. However, to the best of our knowledge explicit sampling conditions sufficient to guarantee the existence of a triangulation have yet to be described.

Classical results on triangulations

For arbitrary finite dimension, Cairns [Cai34] first demonstrated that a smooth compact manifold admits a triangulation. Cairns' proof consisted of two steps:

- He embedded Euclidean complexes into the manifold using coordinate charts.
- He showed that if the complexes were sufficiently refined (while maintaining a constant lower bound on the simplex quality) the embedding maps could be perturbed so that they remain embeddings and the images of simplices coincide where the coordinate patches overlap. This gives a global embedding of a complex.

Whitehead [Whi40] refined the technique into a general approximation theory which is described in detail by Munkres [Mun68] and is not restricted to compact manifolds. Whitney [Whi57] used his result[1] that a manifold can be embedded into Euclidean space to triangulate the manifold. The triangulation was constructed by intersecting the manifold with a fine Cartesian grid in the ambient space. Lower bounds on the quality were also essential for Whitney.

Triangulations and sampling in Computational geometry

The problem has been revisited more recently in the computational geometry community, where the focus is on algorithms used to construct a triangulation when a compact submanifold is known only through a finite set of sample points. The computational geometry community relies heavily on Voronoi diagrams and Delaunay complexes for constructing triangulations.

[1] Now most commonly known as the Whitney embedding theorem.

Voronoi diagrams and Delaunay complexes A *Voronoi cell* $V(u)$ of a point u in a locally finite set of points S in $\mathbb{R}^n$ is the set

$$V(u) = \{x \in \mathbb{R}^n \mid |x-u| \leq |x-v| \text{ for all } v \in S\}.$$

A *Voronoi diagram* consists of all such cells. The cells are convex polyhedra. When the Euclidean distances in the definition of a Voronoi cell are be replaced by the weighted square distance function $\pi_u(x) = |x-u|^2 - w_u^2$, we have the *weighted Voronoi diagram*. The Voronoi cells defined in this way are still convex polyhedra.

The Voronoi diagram $\{V(u)\}_{u \in S}$ is a cover of $\mathbb{R}^n$. The *nerve of a cover* is a simplicial complex K, where a simplex $\sigma = \{u_0, \ldots, u_j\} \subset S$ belongs to K if

$$\bigcap_{u \in \sigma} V(u) \neq \emptyset.$$

The *Delaunay complex* of $S \subset \mathbb{R}^n$ is the nerve of the Voronoi diagram of S. Delaunay [Del34] showed that if the Voronoi cells are bounded (i.e., every open half-space contains a point of S), then under a mild genericity assumption the Delaunay complex defines a triangulation of $\mathbb{R}^n$. The Delaunay complex is then called the *Delaunay triangulation*.

Given a submanifold $M \subseteq \mathbb{R}^n$, the *restricted Voronoi diagram* is the collection of the restricted Voronoi cells $V_M(u) = V(u) \cap M$. The *restricted Delaunay complex* is the nerve of the restricted Voronoi diagram.

Submanifold reconstruction algorithms Edelsbrunner and Shah [ES97] proved that if the restricted Voronoi diagram of a submanifold $M \subset \mathbb{R}^n$ has the so-called closed ball property, then the restricted Delaunay complex is homeomorphic to M, and therefore defines a triangulation. We define the restricted *Voronoi face* $V_M(\sigma)$ associated to a resticted Delaunay simplex σ as the intersection of the relevant restricted Voronoi cells: $V_M(\sigma) = \cap_{u \in \sigma} V_M(u)$. The restricted Voronoi diagram of a k-manifold $M \subset \mathbb{R}^n$ has *the closed ball property* if every Voronoi face $V_M(\sigma)$ is homeomorphic to a closed ball with dimension $k - \dim \sigma \geq 0$.

Cheng et al. [CDR05] used this generic triangulation result of Edelsbrunner and Shah to argue that a weighted Delaunay complex will triangulate a submanifold of $\mathbb{R}^n$. The work by Boissonnat and Ghosh [BG14] adapted Whitney's argument to give a construction of a triangulation by a Delaunay-based complex whose computation does not involve the ambient dimension.

Quantifying quality conditions

Both these and the classical works used a metric on the manifold to compute the triangulation. However, for all of these results there is no explicit expression

to describe the sampling density sufficient to guarantee a triangulation. There is only the assurance that if the maximum distance between adjacent vertices is small enough, a triangulation can be obtained.

In fact, in all of these results, the required sampling density depends not only on the geometric properties of the manifold[2], but also on the geometric properties of the simplices that are involved in the construction. By geometric properties of the simplices we specifically mean their quality. Some measure of simplex quality is introduced, and a lower bound on this quality measure is an essential component of the construction. This dependence on simplex quality is also present in our results, but we actually quantify what bound on the edge lengths is small enough to ensure a triangulation, given a bound on the quality of the simplices.

3.1.5 Outline and main results

We will now discuss the content of the individual sections. We present some of the main definitions and main results. Here it may happen that we touch on the same subjects we also discussed in the introduction above.

Section 3.2; definitions and notation

In Section 3.2 we present the framework for centre of mass constructions, and introduce the barycentric coordinate map and Riemannian simplices. Riemannian simplices are defined (Definition 3.2.4) as the image of the barycentric coordinate map, so they are "filled in" geometric simplices. A Riemannian simplex $\boldsymbol{\sigma}_M$ is defined by its vertices $\sigma = \{p_0, \ldots, p_n\} \subset M$, which are constrained to lie in a convex neighbourhood $B_\rho \subset M$. For any $x \in B_\rho$ we define a Euclidean simplex $\sigma(x) \subset T_xM$ by $\sigma(x) = \{v_0(x), \ldots, v_n(x)\}$, where $v_i(x) = \exp_x^{-1}(p_i)$. In general we use a boldface symbol when we are referring to a simplex as a set of non-negative barycentric coordinates, and normal type refers to the finite vertex set; the convex hull of $\sigma(x)$ is $\boldsymbol{\sigma}_{\mathbb{E}}(x)$.

We give a characterisation of non-degenerate Riemannian simplices in terms of affine independence. We show that $\boldsymbol{\sigma}_M$ is non-degenerate if and only if $\sigma(x)$ is non-degenerate for every $x \in \boldsymbol{\sigma}_M$.

[2]Here we mean the sectional curvatures in our setting, but in the computational geometry literature often the local feature size is used. For a smooth surface in three dimensional Euclidean space the local feature size is the distance to the medial axis. The medial axis is defined as the set of points that have more than one closest point on the surface.

Section 3.3; the Toponogov comparison theorem

In Section 3.3 we briefly discuss the Topogonov comparison theorem, which we shall use in sections 3.4, 3.6 and 3.10.

Section 3.4; Riemannian centres of mass

In Section 3.4 we give an alternative proof for the existence and uniqueness of Riemannian centres of mass. As mentioned Riemannian centres of mass are used in our definition of Riemannian simplices. The proof is based on the Toponogov comparison theorem and Morse theoretical arguments. We also discuss conditions for the existence and uniqueness of Riemannian centres of mass if we allow negative weights.

Section 3.5; Rauch based non-degeneracy conditions

In Section 3.5 we establish criteria to ensure that a Riemannian simplex is non-degenerate. We first review properties of Euclidean simplices, including *thickness*, the quality measure we employ. The thickness is essentially the ratio of the smallest altitude to the longest edge length of the simplex. If the edge lengths in a Euclidean simplex change by a small amount, we can quantify the change in the thickness. In particular, if $F : \mathbb{R}^n \to \mathbb{R}^n$ is a bi-Lipschitz map, we can quantify a bound on the thickness, $t(\sigma)$, of a simplex σ relative to the metric distortion (i.e., the bi-Lipschitz constant) that establishes when the Euclidean simplex $F(\sigma)$ is non-degenerate.

The Rauch theorem establishes bounds on the norm of the differential of the exponential map, relative to the sectional curvatures. Using this we obtain a bound on the metric distortion of the transition function

$$\exp_x^{-1} \circ \exp_p : T_pM \to T_xM \tag{3.2}$$

which maps $\sigma(p)$ to $\sigma(x)$, and so we are able to establish conditions ensuring that $\sigma(x)$ is non-degenerate, based on quality assumptions on $\sigma(p)$.

An open *geodesic ball* of radius r centred at $x \in M$ is the set $B_M(x; r)$ of all points in M whose geodesic distance from x is less than r. The *injectivity radius at* x, denoted $\iota(x)$, is the supremum of the radii r for which $\exp_x$ restricts to a diffeomorphism between the Euclidean ball of radius r centred at $0 \in T_xM$, and $B_M(x; r)$. The injectivity radius of M is the infimum of $\iota(x)$ over all $x \in M$, and is denoted ι_M.

Theorem 3.1 (Non-degeneracy criteria) *Suppose M is a Riemannian manifold with sectional curvatures K bounded by $|K| \leq \Lambda$, and $\boldsymbol{\sigma}_M$ is a Riemannian*

simplex, with $\boldsymbol{\sigma}_M \subset B_\rho \subset M$, where B_ρ is an open geodesic ball of radius ρ with

$$\rho < \rho_0 = \min\left\{\frac{\iota_M}{2}, \frac{\pi}{4\sqrt{\Lambda}}\right\}. \tag{3.3}$$

Then $\boldsymbol{\sigma}_M$ is non-degenerate if there is a point $p \in B_\rho$ such that the lifted Euclidean simplex $\sigma(p)$ has thickness satisfying

$$t(\sigma(p)) > 10\sqrt{\Lambda}L(\boldsymbol{\sigma}_M), \tag{3.4}$$

where $L(\boldsymbol{\sigma}_M)$ is the geodesic length of the longest edge in $\boldsymbol{\sigma}_M$.

Section 3.6; Topogonov based non-degeneracy conditions

In Section 3.6 an alternate approach to non-degenerate Riemannian simplices is presented. This approach is based on bounding angles and edge lengths in geodesic triangles via the Toponogov comparison theorem.

Section 3.7; Intrinsic triangulations

In Section 3.7 we develop our sampling criteria for triangulating manifolds. We establish properties of maps whose differentials are bounded close to a fixed linear isometry, and use these properties to reveal conditions under which a complex will be embedded into a manifold. We then exploit a refinement of the Rauch theorem, and other estimates established by Buser and Karcher [BK81], to bound the differential of the barycentric coordinate map in this way.

If p is a vertex in an abstract simplicial complex $\mathcal{A}$, we define the *star of* p to be the subcomplex $\underline{\mathrm{St}}(p)$ of $\mathcal{A}$ consisting of all simplices that contain p, together with the faces of these simplices. The underlying topological space (or *carrier*) of a complex $\mathcal{A}$ is denoted $|\mathcal{A}|$. We say that $\underline{\mathrm{St}}(p)$ is a *full star* if $|\underline{\mathrm{St}}(p)|$ is a closed topological ball of dimension n with p in its interior, and $\mathcal{A}$ contains no simplices of dimension greater than n. We have:

Theorem 3.2 (Triangulation criteria) *Suppose M is a compact n-dimensional Riemannian manifold with sectional curvatures K bounded by $|K| \leq \Lambda$, and $\mathcal{A}$ is an abstract simplicial complex with finite vertex set $\mathcal{P} \subset M$. Define a quality parameter $t_0 > 0$, and let*

$$h = \min\left\{\frac{\iota_M}{4}, \frac{\sqrt{n}t_0}{6\sqrt{\Lambda}}\right\}. \tag{3.5}$$

If

1. *For every $p \in \mathcal{P}$, the vertices of $\underline{\mathrm{St}}(p)$ are contained in $B_M(p;h)$, and the balls $\{B_M(p;h)\}_{p\in\mathcal{P}}$ cover M.*

2. *For every $p \in \mathcal{P}$, the restriction of the inverse of the exponential map $\exp_p^{-1}$ to the vertices of $\underline{\mathrm{St}}(p) \subset \mathcal{A}$ defines a piecewise linear embedding of $|\underline{\mathrm{St}}(p)|$ into T_pM, realising $\underline{\mathrm{St}}(p)$ as a full star such that every simplex $\sigma(p)$ has thickness $t(\sigma(p)) \geq t_0$.*

then $\mathcal{A}$ triangulates M, and the triangulation is given by the barycentric coordinate map on each simplex.

The techniques employed to obtain Theorem 3.2 exploit stronger bounds on the differential of the exponential map, and provide a slightly better bound for non-degeneracy than the one stated in Theorem 3.1, but at the expense of a stronger constraint on the allowed diameter of the simplex. This is the reason Equation (3.4) appears as a stronger constraint on the thickness than the curvature controlled part of Equation (3.5).

We refer to the criteria of Theorem 3.2 as sampling criteria, even though they require a simplicial complex for their definition. Although there is no explicit constraint on the minimal distance between points of $\mathcal{P}$, one is implicitly imposed by the quality constraint on the Riemannian simplices. The required sampling density depends on the quality of the Riemannian simplices, which leaves open the question of what kind of quality of simplices can we hope to attain. Recent work [BDG13a] constructs a Delaunay complex conforming to the requirements of Theorem 3.2 with the thickness t_0 bounded by $\Omega(2^{-n^3})$. It would be interesting to see this improved.

Section 3.8; metric distortion

The complex $\mathcal{A}$ in Theorem 3.2 naturally admits a piecewise linear metric by assigning edge lengths to the simplices given by the geodesic distance in M between the endpoints. In Section 3.8 we observe that in order to ensure that this does in fact define a piecewise-flat metric, we need to employ slightly stronger constraints on the scale parameter h. In this case, the complex $\mathcal{A}$ becomes a good geometric approximation of the original manifold, and we find:

Theorem 3.3 (Metric distortion) *If the requirements of Theorem 3.2, are satisfied with the scale parameter* (3.5) *replaced by*

$$h = \min\left\{\frac{\iota_M}{4}, \frac{t_0}{6\sqrt{\Lambda}}\right\},$$

then $\mathcal{A}$ is naturally equipped with a piecewise flat metric $d_{\mathcal{A}}$ defined by assigning to each edge the geodesic distance in M between its endpoints.

If $H : |\mathcal{A}| \to M$ is the triangulation defined by the barycentric coordinate map in this case, then the metric distortion induced by H is quantified as

$$|d_M(H(x), H(y)) - d_{\mathcal{A}}(x, y)| \leq \frac{50\Lambda h^2}{t_0^2} d_{\mathcal{A}}(x, y),$$

for all $x, y \in |\mathcal{A}|$.

Section 3.9; comparison of quality measures

The criteria of these three theorems can also be formulated in terms of the thickness of the Euclidean simplices defined by the geodesic edge lengths of the Riemannian simplices, rather than the Euclidean simplices we find in the tangent spaces. In Section 3.9 we briefly mention this alternative formulation of our results. We also compare the thickness quality measure for simplices with a commonly used volumetric quality measure which we call fatness.

Section 3.10; simplices modelled on spaces of constant curvature

In Section 3.10 we revisit Section 3.6 with the important distinction that now we focus on manifolds whose sectional curvatures are nearly constant and large. For these simplices we give conditions for non-degeneracy similar to Theorem 3.2.

To be precise we are interested in Riemannian simplices on manifolds whose sectional curvatures are very close to constant, meaning that the sectional curvature K satisfies $\Lambda_- \leq K \leq \Lambda_+$ with $|\Lambda_- - \Lambda_+|$ small relative to $|\Lambda_-|$. This means that we always suppose that $0 < \Lambda_-$ or $\Lambda_+ < 0$. The case where Λ_- and Λ_+ are nearly zero is uninteresting, or rather this has been adequately treated in Sections 3.5 and 3.6. Because the sectional curvatures are very close to constant comparing the manifold to Euclidean space is unnatural. Instead we compare to spaces of constant curvature Λ_{mid}, whose sectional curvature lies in the interval $[\Lambda_-, \Lambda_+]$. For these spaces of constant curvature we introduce new quality measures for simplices on spaces of constant curvature.

The non-degeneracy conditions will be in terms of the quality of the simplex $\sigma_{\mathbb{H}(\Lambda_{\text{mid}})}(v_r)$ with vertices

$$\exp_{\mathbb{H}(\Lambda_{\text{mid}})} \circ \exp_{v_r, M}^{-1}(v_i),$$

where $\exp_{v_r, M}$ denotes the exponential function of M at v_r. Here $\mathbb{H}(\Lambda_{\text{mid}})$ denotes a space with constant sectional curvature.

3.2 Riemannian simplices

In this section we summarise the results of the theory of Riemannian centres of mass that we need in order to define Riemannian simplices. We then give an explicit description of the barycentric coordinate map that is used to define these simplices. We take the view that if the barycentric coordinate map is well defined, then the simplex is well defined, but it may be degenerate. The geodesic finite elements employed by Sander [San12] are Riemannian simplices without a requirement of non-degeneracy. In Section 3.2.3 we demonstrate that non-degeneracy of a Riemannian simplex $\boldsymbol{\sigma}_M$ is characterised by the affine independence of the vertices when lifted to the tangent space of any point in $\boldsymbol{\sigma}_M$.

3.2.1 Riemannian centre of mass

We work with an n-dimensional Riemannian manifold M. The centre of mass construction developed by Karcher [Kar77] hinges on the notion of convexity in a Riemannian manifold. A set $B \subseteq M$ is *convex* if any two points $x, y \in B$ are connected by a minimising geodesic γ_{xy} that is unique in M, and contained in B. For $c \in M$, the geodesic ball of radius r is the set $B_M(c;r)$ of points in M whose distance from c is less than r, and we denote its closure by $\overline{B}_M(c;r)$. If r is small enough, $\overline{B}_M(c;r)$ will be convex; the following lemma quantifies "small enough".

In order to obtain non-degeneracy criteria for Riemannian simplices we require both an upper and a lower bound on the sectional curvatures, so it is convenient to work with a bound Λ on the absolute value of the sectional curvatures, $|K| \leq \Lambda$. However, the *definition* of Riemannian simplices only requires an upper bound on the sectional curvatures. In order to emphasise this we introduce distinct symbols for the upper and lower bounds on the sectional curvatures. Thus $\Lambda_- \leq K \leq \Lambda_+$, and $\Lambda = \max\{\Lambda_+, -\Lambda_-\}$.

We have [Cha06, Thm. IX.6.1]:

Lemma 3.2.1 *Suppose the sectional curvatures of M are bounded by $K \leq \Lambda_+$, and ι_M is the injectivity radius. If*

$$r < \min\left\{\frac{\iota_M}{2}, \frac{\pi}{2\sqrt{\Lambda_+}}\right\},$$

then $\overline{B}_M(x;r)$ is convex. (If $\Lambda_+ \leq 0$, we take $1/\sqrt{\Lambda_+}$ to be infinite.)

Remark 3.2.2 *Lemma 3.2.1 is stated in terms of global bounds on the injectivity radii and sectional curvatures (on a non-compact manifold, these may be useless), but really we only need these bounds in a neighbourhood of x. Let $K(x)$*

be an upper bound on the sectional curvatures at x, and denote the injectivity radius at x by $\iota(x)$. Now define $I(x)$ and $\Lambda_+(x)$ to be the infimum and supremum respectively of $\iota(y)$ and $K(y)$, where y ranges over the ball $B_M(x;R)$ of radius

$$R = \min\left\{\frac{\iota(x)}{2}, \frac{\pi}{2\sqrt{K(x)}}\right\}.$$

Then Lemma 3.2.1 holds if ι_M and Λ_+ are replaced by $I(x)$ and $\Lambda_+(x)$ respectively in the bound on r. For simplicity, we will continue to refer to global bounds, but everywhere they occur a similar remark applies.

Also, in all cases where an upper bound on the sectional curvatures is employed, this bound is only relevant when it is positive. If M has non-positive curvature, then $1/\sqrt{\Lambda_+}$ may be assumed to be infinite.

In our context, we are interested in finding a weighted centre of mass of a finite set $\{p_0, \ldots, p_j\} \subset B \subset M$, where the containing set B is open, and its closure $\overline{B}$ is convex. The centre of mass construction is based on minimising the function $\mathcal{E}_\lambda : \overline{B} \to \mathbb{R}$ defined by

$$\mathcal{E}_\lambda(x) = \frac{1}{2}\sum_i \lambda_i d_M(x, p_i)^2, \tag{3.6}$$

where the $\lambda_i \geq 0$ are non-negative weights that sum to 1, and d_M is the geodesic distance function on M. Karcher's first simple observation is that the minima of $\mathcal{E}_\lambda$ must lie in the interior of $\overline{B}$, i.e., in B itself. This follows from considering the gradient of $\mathcal{E}_\lambda$:

$$\operatorname{grad}\mathcal{E}_\lambda(x) = -\sum_i \lambda_i \exp_x^{-1}(p_i). \tag{3.7}$$

At any point x on the boundary of $\overline{B}$, the gradient vector lies in a cone of outward pointing vectors. It follows that the minima of $\mathcal{E}_\lambda$ lie in B. The more difficult result that the minimum is unique, Karcher showed by demonstrating that $\mathcal{E}_\lambda$ is convex. If $B \subseteq M$ is a convex set, a function $f : B \to \mathbb{R}$ is *convex* if for any geodesic $\gamma : I \to B$, the function $f \circ \gamma$ is convex (here $I \subseteq \mathbb{R}$ is an open interval). If f has a minimum in B, it must be unique. By Equation (3.7), it is the point x where

$$\sum_i \lambda_i \exp_x^{-1}(p_i) = 0.$$

We have the following result [Kar77, Thm 1.2]:

Lemma 3.2.3 (Unique centre of mass) *If $\{p_0, \ldots, p_j\} \subset B_\rho \subset M$, and B_ρ is an open ball of radius ρ with*

$$\rho < \rho_0 = \min\left\{\frac{\iota_M}{2}, \frac{\pi}{4\sqrt{\Lambda_+}}\right\},$$

then on any geodesic $\gamma : I \to B_\rho$, we have

$$\frac{\mathrm{d}^2}{\mathrm{d}t^2}\mathcal{E}_\lambda(\gamma(t)) \geq C(\Lambda_+, \rho) > 0, \tag{3.8}$$

where $C(\Lambda_+, \rho)$ is a positive constant depending only on Λ_+ and ρ. In particular, $\mathcal{E}_\lambda$ is convex and has a unique minimum in B_ρ.

Karcher gives an explicit expression for $C(\Lambda_+, \rho)$, but we will not need to refer to it here. Also, Karcher expresses the centre of mass concept in more generality by using an integral over a set whose measure is 1, rather than a weighted sum over a finite set as we have used.

3.2.2 The barycentric coordinate map

Let $\boldsymbol{\Delta}^j$ denote the standard Euclidean j-simplex. This can be realised as the set of points $\lambda \in \mathbb{R}^{j+1}$ whose components are non-negative, $\lambda_i \geq 0$, and sum to one: $\sum_i \lambda_i = 1$. We index the coordinates starting from zero: these are the *barycentric coordinates* on the standard simplex.

Definition 3.2.4 (Riemannian simplex) *If a finite set $\sigma^j = \{p_0, \ldots, p_j\} \subset M$ in an n-manifold is contained in an open geodesic ball B_ρ whose radius, ρ, satisfies Equation* (3.3)*, then σ^j is the set of vertices of a geometric* Riemannian simplex*, denoted $\boldsymbol{\sigma}^j_M$, and defined to be the image of the map*

$$\begin{aligned}\mathcal{B}_{\sigma^j} :&\boldsymbol{\Delta}^j \to M\\ &\lambda \mapsto \operatorname*{argmin}_{x \in \overline{B}_\rho} \mathcal{E}_\lambda(x).\end{aligned}$$

We say that $\boldsymbol{\sigma}^j_M$ is non-degenerate *if $\mathcal{B}_{\sigma^j}$ is a smooth embedding; otherwise it is* degenerate*.*

Define an i-face of $\boldsymbol{\sigma}^j_M$ to be the image of an i-face of $\boldsymbol{\Delta}^j$. Since an i-face of $\boldsymbol{\Delta}^j$ may be identified with $\boldsymbol{\Delta}^i$ (e.g., by an order preserving map of the vertex indices), the i-faces of $\boldsymbol{\sigma}^j_M$ are themselves Riemannian i-simplices. In particular, if τ and μ are the vertices of Riemannian simplices $\boldsymbol{\tau}_M$ and $\boldsymbol{\mu}_M$, and $\sigma^i = \tau \cap \mu$,

then the Riemannian i-simplex $\boldsymbol{\sigma}_M^i$ is a face of both $\boldsymbol{\tau}_M$ and $\boldsymbol{\mu}_M$. The *edges* of a Riemannian simplex are the Riemannian 1-faces. We observe that these are geodesic segments. We will focus on full dimensional simplices, i.e., unless otherwise specified, $\boldsymbol{\sigma}_M$ will refer to a Riemannian simplex defined by a set σ of $n+1$ vertices in our n-dimensional manifold M.

Remarks The barycentric coordinate map $\mathcal{B}_\sigma$ is differentiable. This follows from the implicit function theorem, as is shown by Buser and Karcher [BK81, §8.3.3], for example. They work in local coordinates on the tangent bundle, and use the connection to split the derivative of $\operatorname{grad}\mathcal{E}_\lambda : M \to TM$ into horizontal and vertical components. The strict convexity condition (3.8) implies that the vertical component of the derivative is full rank, and permits the use of the implicit function theorem.

The argument of Buser and Karcher assumes that the map is defined on an open domain. We observe that $\mathcal{B}_\sigma$ is well defined if we allow negative barycentric coordinates of small magnitude. For a sufficiently small $\epsilon > 0$, Lemma 3.2.3 holds if the barycentric coordinates λ_i satisfy $\sum \lambda_i = 1$ and $\lambda_i > -\epsilon$ for all $i \in \{0, \ldots, n\}$, albeit with $C(\Lambda_+, \rho)$ replaced with a smaller positive constant. This follows from the observation that $\frac{d^2}{dt^2}\mathcal{E}_\lambda$ is continuous in the barycentric coordinates, thus since it is strictly positive on the boundary of $\boldsymbol{\Delta}^n$, it can be extended to an open neighbourhood. This means that $\mathcal{B}_\sigma$ is smooth on the closed domain $\boldsymbol{\Delta}^n$, as defined in Section 3.7.1.

Karcher himself mentioned that his result can accommodate signed measures [Kar77, Remark 1.8], and Sander has demonstrated this in some detail [San13]. However, for our current purposes we are only claiming that we can accommodate arbitrarily small negative barycentric coordinates assuming the stated bound on ρ_0 (Equation (3.3)).

A Riemannian simplex is not convex in general, but as Karcher [Kar77] observed, being the image of the barycentric coordinate map, it will be contained in any convex set that contains the vertices of the simplex. Thus the Riemannian simplex is contained in the intersection of such sets.

Equation (3.3) gives an upper bound on the size of a Riemannian simplex that depends only on the injectivity radius and an *upper* bound on the sectional curvature. For example, in a non-positively curved manifold, the size of a well defined Riemannian simplex is constrained only by the injectivity radius. However, if the dimension n of the manifold is greater than 2, we will require also a *lower* bound on the sectional curvatures in order to ensure that the simplex is non-degenerate.

Lemma 3.2.3 demands that a Riemannian simplex be contained in a ball whose radius is constrained by ρ_0. Thus Riemannian simplices always have edge lengths less than $2\rho_0$. If the longest edge length, $L(\boldsymbol{\sigma}_M)$, of $\boldsymbol{\sigma}_M$ is less than

ρ_0, then $\boldsymbol{\sigma}_M$ must be contained in the closed ball of radius $L(\boldsymbol{\sigma}_M)$ centred at a vertex. Indeed, any open ball centred at a vertex whose radius is larger than $L(\boldsymbol{\sigma}_M)$, but smaller than ρ_0, must contain the vertices and have a convex closure. The simplex is thus contained in the intersection of these balls. If $L(\boldsymbol{\sigma}_M) \geq \rho_0$, then a ball of radius $L(\boldsymbol{\sigma}_M)$ need not be convex. In this case we claim only that $\boldsymbol{\sigma}_M$ is contained in a ball of radius $2\rho_0$ centred at any vertex.

3.2.3 The affine independence criterion for non-degeneracy

In this subsection we show that a Riemannian simplex $\boldsymbol{\sigma}_M$ is non-degenerate if, and only if, for any $x \in \boldsymbol{\sigma}_M$, the lift of the vertices by the inverse exponential map yields a non-degenerate Euclidean simplex. We first introduce some notation and terminology to better articulate this statement.

Notation

A Euclidean simplex σ of dimension k is defined by a set of $k+1$ points in Euclidean space $\sigma = \{v_0, \ldots, v_k\} \subset \mathbb{R}^n$. In general we work with abstract simplices, even though we attribute geometric properties to the simplex, inherited from the embedding of the vertices in the ambient space (see Section 3.5.1). When we wish to make the dimension explicit, we write it as a superscript, thus σ^k is a k-simplex. Traditional "filled in" geometric simplices are denoted by boldface symbols; $\boldsymbol{\sigma}_{\mathbb{E}} = \mathrm{conv}(\sigma)$ is the convex hull of σ. If such a simplex is specified by a vertex list, we employ square brackets: $\boldsymbol{\sigma}_{\mathbb{E}} = [v_0, \ldots, v_k]$.

The *barycentric coordinate functions* $\{\lambda_i\}$ associated to σ are affine functions $\mathbb{R}^n \to \mathbb{R}$ that satisfy $\lambda_i(v_j) = \delta_{ij}$ and $\sum_{i=0}^n \lambda_i = 1$. It is often convenient to choose one of the vertices, v_0 say, of σ to be the origin. We let P be the $n \times k$ matrix whose i^{th} column is $v_i - v_0$. Then the barycentric coordinate functions $\{\lambda_i\}$ are linear functions for $i > 0$, and they are dual to the basis defined by the columns of P. This means that if we represent the function λ_i as a row vector, then the matrix Q whose i^{th} *row* is λ_i satisfies $QP = I_{k\times k}$.

A full dimensional Euclidean simplex σ is non-degenerate, if and only if the corresponding matrix P is non-degenerate. In particular, if σ is full dimensional (i.e., $k = n$), then $Q = P^{-1}$. Suppose $\sigma \subset \mathbb{R}^n$ is an n-simplex. If $\xi \in \mathbb{R}^n$, let $\lambda(\xi) = (\lambda_1(\xi), \ldots, \lambda_n(\xi))^{\mathsf{T}}$. Then $\lambda(\xi)$ is the vector of coefficients of $\xi - v_0$ in the basis defined by the columns of P. I.e., $\xi - v_0 = P\lambda(\xi)$.

We will be interested in Euclidean simplices that are defined by the vertices of a Riemannian simplex: If $\sigma = \{p_0, \ldots, p_n\} \subset B_\rho \subset M$ is the set of vertices of $\boldsymbol{\sigma}_M$, it is convenient to introduce the notation $v_i(x) = \exp_x^{-1}(p_i)$, and $\sigma(x) = \exp_x^{-1}(\sigma)$. Thus $\sigma(x) = \{v_0(x), \ldots, v_n(x)\}$ is a Euclidean simplex in T_xM.

The norm of a vector v in a Euclidean space is denoted $|v|$. For example, if $v \in T_pM$, then $|v| = g(v,v)^{\frac{1}{2}}$, where g is the Riemannian metric tensor on M, and if $v \in \mathbb{R}^n$, then $|v| = (v \cdot v)^{\frac{1}{2}}$. The differential of a map $F : M \to \bar{M}$ is denoted by dF; so $dF_x : T_xM \to T_{F(x)}\bar{M}$ is a linear map whose operator norm is $\|dF_x\|$. All differentiable maps, operators, and manifolds are assumed to be C^∞.

An expression for the differential

The expression for the differential obtained in Equation (3.10) below is obtained as a particular case of an argument presented by Buser and Karcher [BK81, §8.3]. The argument was later exploited by Peters [Pet84] to sharpen bounds on Cheeger's finiteness theorem [Che70]. A thorough exposition appears also in Chavel [Cha06, IX.8].

We work in a domain $U \subset \mathbb{R}^n$ defined by a chart $\phi : M \supset W \to U$ such that $B_\rho \subset W$. Let $\tilde{\sigma} = \phi(\sigma)$ be the image of the vertices of a Riemannian n-simplex $\boldsymbol{\sigma}_M \subset B_\rho$. Label the vertices of $\tilde{\sigma} = \{v_0, \ldots, v_n\}$ such that $v_i = \phi(p_i)$, and assume v_0 is at the origin. The affine functions $\lambda_i : u \mapsto \lambda_i(u)$ are the barycentric coordinate functions of $\tilde{\sigma}$. We consider $\operatorname{grad} \mathcal{E}_\lambda$, introduced in Equation (3.7), now to be a vector field that depends on both $u \in U$ and $x \in B_\rho$. Specifically, we consider the vector field $\nu : U \times B_\rho \to TM$ defined by

$$\nu(u,x) = -\sum_{i=0}^{n} \lambda_i(u) v_i(x). \tag{3.9}$$

Let $b : \tilde{\boldsymbol{\sigma}}_{\mathbb{E}} \to \boldsymbol{\sigma}_M$ be defined by $b = \mathcal{B}_\sigma \circ \mathcal{L}$, where $\mathcal{L}$ is the canonical linear isomorphism that takes the vertices of $\tilde{\sigma}$ to those of $\boldsymbol{\Delta}^n$, and $\mathcal{B}_\sigma$ is the barycentric coordinate map introduced in Definition 3.2.4. This map is differentiable, by the arguments presented by Buser and Karcher, and $\nu(u, b(u)) = 0$ for all $u \in \tilde{\boldsymbol{\sigma}}_{\mathbb{E}}$. Regarded as a vector field along b, the covariant differential $\nabla \nu_{(u,b(u))} = 0$ may be expanded as

$$\partial_u \nu + \left(\nabla^M \nu\right) db = 0,$$

where $\partial_u \nu$ denotes the differential of $\nu(u,x)$ with x fixed, i.e.,

$$\partial_u \nu_{(u,x)} : T_u\mathbb{R}^n \to T_xM$$
$$\left(\partial_u \nu_{(u,x)}\right) \dot{u}(0) = \frac{d}{dt} \nu(u(t), x)\Big|_{t=0},$$

with $\dot{u}(0)$ denoting the tangent vector at 0 to some curve $t \mapsto u(t)$ in $U \subset \mathbb{R}^n$. Similarly $\nabla^M \nu$ is the covariant differential when u is fixed:

$$\nabla^M \nu_{(u,x)} : T_xM \to T_xM$$
$$\left(\nabla^M \nu_{(u,x)}\right) \dot{x}(0) = D_t \nu(u, x(t))\big|_{t=0},$$

where $D_t\nu$ is the covariant derivative along the curve $x(t)$. Finally $db : T_u\mathbb{R}^n \to T_xM$ is the differential of b, our barycentric coordinate map onto the Riemannian simplex $\boldsymbol{\sigma}_M$.

Our objective is to exhibit conditions that ensure that db is non-degenerate. It follows from the strict convexity conditon (3.8) of Lemma 3.2.3 that the map $\nabla^M\nu$ is non-degenerate. Indeed, if $v \in T_xM$ for some $x \in B_\rho$, there is a geodesic $\gamma : I \to B_\rho$ with $\gamma'(0) = v$, and $\frac{d^2}{dt^2}\mathcal{E}_\lambda(\gamma(t))\big|_{t=0} = g(\nabla^M_v\nu, v) > 0$. Therefore, we have that

$$db = -\left(\nabla^M\nu\right)^{-1}\partial_u\nu, \tag{3.10}$$

and thus db has full rank if and only if $\partial_u\nu$ has full rank.

The differential as a matrix

Recalling Equation (3.9), notice that when x is fixed, ν is an affine map $\mathbb{R}^n \supset U \to T_xM$, and so $(\partial_u\nu)_v = (\partial_u\nu)_w$ for all $v, w \in U$. We see that

$$\partial_u\nu = -\sum_{i=0}^{n} v_i(x)\, d\lambda_i.$$

Since $\sum_{i=0}^n \lambda_i = 1$, we have that $\sum_{i=0}^n d\lambda_i = 0$. We may thus write $d\lambda_0 = -\sum_{i=1}^n d\lambda_i$, and so for $\xi \in T_uU$, we have

$$(\partial_u\nu)\,\xi = -\sum_{i=1}^{n}\big(v_i(x) - v_0(x)\big)d\lambda_i(\xi)\,. \tag{3.11}$$

Now, since the domain of the barycentric coordinates is U, and the origin of $U \subset \mathbb{R}^n$ coincides with v_0, the functions λ_i for $i \in \{1, \ldots, n\}$ are *linear* functions, and we use the canonical identification of tangent spaces in $\mathbb{R}^n$ to conclude that $d\lambda_i(\xi) = \lambda_i(\xi)$, where in the right hand side we view ξ as an element of $\mathbb{R}^n$, rather than an element of $T_u\mathbb{R}^n$. As discussed above, we have $\lambda(\xi) = P^{-1}\xi$, where $\lambda(\xi) = (\lambda_1(\xi), \ldots, \lambda_n(\xi))^{\mathsf{T}}$, and P is the matrix whose i^{th} column is v_i. Thus, using an arbitrary linear isometry to get a coordinate system for T_xM, and letting $\tilde{P}$ be the matrix whose i^{th} column is $(v_i(x) - v_0(x))$, we may rewrite Equation (3.11) as

$$(\partial_u\nu)\,\xi = -\tilde{P}\lambda(\xi) = -\tilde{P}P^{-1}\xi. \tag{3.12}$$

From Equation (3.12) we conclude that $\partial_u\nu$ is full rank if and only if $\tilde{P}$ is of full rank, and this is the case if and only if $\sigma(x)$ is a non-degenerate Euclidean simplex, i.e., its vertices $\{v_i(x)\}$ are affinely independent.

We observe that if db is non-degenerate on $\boldsymbol{\sigma}_M$, then b must be injective. Indeed, if $x = b(u)$, then $\{\lambda_i(u)\}$, the barycentric coordinates of u with respect

to $\tilde{\sigma}$, are also the barycentric coordinates of the origin in T_xM, with respect to the simplex $\sigma(x)$. Thus if $b(u) = x = b(\tilde{u})$, then $\lambda_i(u) = \lambda_i(\tilde{u})$, and we must have $\tilde{u} = u$ by the uniqueness of the barycentric coordinates.

In summary, we have

Proposition 3.2.5 *A Riemannian simplex $\boldsymbol{\sigma}_M \subset M$ is non-degenerate if and only if $\sigma(x) \subset T_xM$ is non-degenerate for every $x \in \boldsymbol{\sigma}_M$.*

3.3 The Toponogov Comparison Theorem

In this section we shall introduce the Toponogov Comparison Theorem and the definitions which go with it. This result will be intrumental for Sections 3.4, 3.6 and 3.10. Our exposition will follow Karcher [Kar89]. Then we give the cosine rules in spaces of constant curvature.

We shall use the notation $\mathbb{H}^n(K_c)$ for the simply connected space of dimension n with constant sectional curvature K_c. We write K_c to emphasize that on a space of constant sectional curvature the section curvature K is constant. If we do not wish to emphasize the dimension we simply write $\mathbb{H}(K_c)$. A simply connected space with constant sectional curvature is also called a space form. Often when we mention a space of constant curvature we shall tacitly assume that it is simply connected and thus a space form.

Definition 3.3.1 *A* geodesic triangle T *in a Riemannian manifold consists of three minimizing geodesics connecting three points, sometimes also referred to as vertices. We stress that a geodesic triangle does not include an interior. Assume lower curvature bounds $\Lambda_- \leq K$ (or upper bounds $K \leq \Lambda_+$). A triangle with the same edge lengths as T in $\mathbb{H}^n(\Lambda_-)$ (or $\mathbb{H}^n(\Lambda_+)$), is called an* Alexandrov triangle T_{Λ_-} *(or T_{Λ_+}) associated with T, named after Alexandrov who used these in his study of convex surfaces [Kar89]. Two edges of a geodesic triangle and the enclosed angle form a* hinge*; a* Rauch hinge *in $\mathbb{H}^n(\Lambda_-)$ (or $\mathbb{H}^n(\Lambda_+)$) of a given hinge, consists of two geodesics emanating from a single point with the same lengths and enclosed angles as the original hinge. The edge closing the Rauch hinge in $\mathbb{H}^n(\Lambda_-)$ (or $\mathbb{H}^n(\Lambda_+)$), that is the minimizing geodesic connecting the two endpoint of the geodesics emanating from a single point with the same lengths and enclosed angles as the hinge in a space of arbitrary curvature, will be called the* Rauch edge *of the hinge.*

Note that because spaces of constant curvature are homogeneous, the Alexandrov triangles and Rauch hinges are uniquely defined, up to isometry of $\mathbb{H}(\Lambda_\pm)$.

The Toponogov Comparison Theorem or Triangle Comparison Theorem reads

Theorem 3.3.2 (Toponogov Comparison Theorem) *Let T be a geodesic triangle in M that lies within every geodesic ball of radius less than the injectivity radius centred at one of the vertices and assume that the sectional curvatures K of M satisfy the bounds $\Lambda_- \leq K \leq \Lambda_+$. If $\Lambda_+ > 0$, assume also that the triangle circumference is less then $2\pi {\Lambda_+}^{-1/2}$. Then Alexandrov triangles T_{Λ_-} and T_{Λ_+} exist. Moreover, any angle α of T satisfies*

$$\alpha_{\Lambda_-} \leq \alpha \leq \alpha_{\Lambda_+},$$

where α_{Λ_-} and α_{Λ_+} are the corresponding angles in T_{Λ_-} and T_{Λ_+} respectively. The length c of the third edge closing a hinge is bounded in length by the lengths of the Rauch edges, c_{Λ_-} and c_{Λ_+}, closing the Rauch hinges on $\mathbb{H}(\Lambda_-)$ and $\mathbb{H}(\Lambda_+)$ respectively:

$$c_{\Lambda_-} \geq c \geq c_{\Lambda_+}.$$

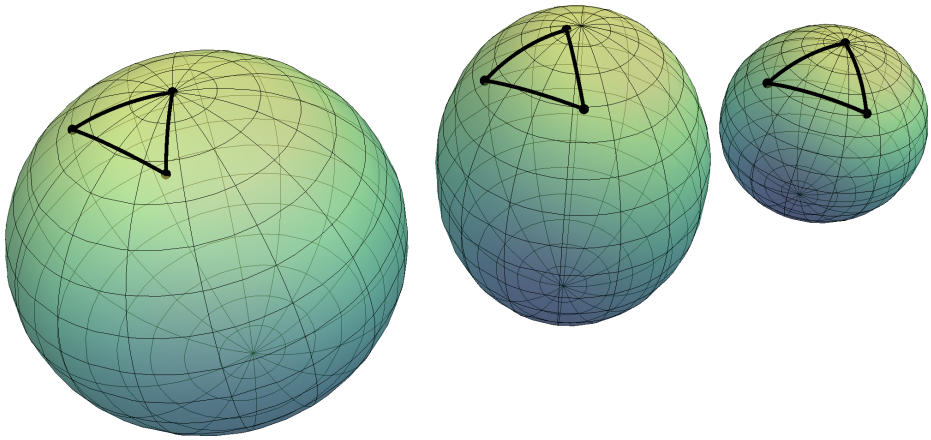

Figure 3.1: An ellipsoid (centre) with a hinge with closing geodesic and corresponding Rauch hinges with closing geodesic on the spaces of constant curvatures (left and right), in this case both elliptic spheres.

We also give the cosine rule which is of use in explicit calculations involving the Toponogov comparison theorem.

The cosine rule for elliptic spaces, that is positively curved spaces of constant curvature, is given in Section 18.6 of Berger [Ber87b] and Section 12.7 of Coxeter [Cox98] and reads

$$\cos\frac{a}{k} = \cos\frac{b}{k}\cos\frac{c}{k} + \sin\frac{b}{k}\sin\frac{c}{k}\cos\alpha, \tag{3.13}$$

in a space of sectional curvature (or Gaussian curvature in two dimensions) $1/k^2$, here $k > 0$.

The cosine rule for hyperbolic spaces, that is negatively curved spaces of constant curvature, is given in Section 19.3 of Berger [Ber87b] and Section 12.9 of Coxeter [Cox98] to be

$$\cosh\frac{a}{k} = \cosh\frac{b}{k}\cosh\frac{c}{k} - \sinh\frac{b}{k}\sinh\frac{c}{k}\cos\alpha, \tag{3.14}$$

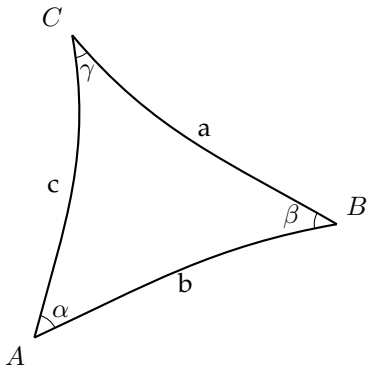

Figure 3.2: Triangle with the standard symbols for angles and lengths

in a space of sectional curvature $-1/k^2$, here $k > 0$. See Figure 3.2 for a figure with the edge lenths and angles indicated.

3.4 Existence and uniqueness of Riemannian centres of mass

3.4.1 Results and methods

Riemannian centres of mass, or Karcher means, generalize the concept of centres of mass which we are familiar with in a Euclidean setting to Riemannian manifolds. In this context the centre of mass in a sufficiently small convex ball is defined to be the minimum of the average squared distance to the mass in our distribution. It is not obvious that such a minimum exists and, assuming that it exists, is unique. It has been proven that the Riemannian centre of mass of a mass distribution in a sufficiently small convex ball exists and is unique for a positive mass distribution. If we allow negative weights existence and uniqueness has been shown under extra conditions.

Contribution

Our proof of the existence and uniqueness of Riemannian centres of mass uses Morse theoretical arguments and the Topogonov comparison theorem. In particular we do the following:

- We use the Topogonov comparison theorem to prove that every critical point is a local minimum.
- We use Morse theory to conclude that there is only one critical point.

Unlike the already existing proofs it requires little background in differential geometry, apart from working knowledge of the Topogonov comparison theorem. The conditions we provide for the negative weight case are also more explicit than the conditions available.

Results

We arrive at the following:

Theorem 3.4.2 *Let M be a manifold whose sectional curvature K is bounded, that is $\Lambda_- \leq K \leq \Lambda_+$. Let P_M the function on B_ρ defined by*

$$P_M(x) = \frac{1}{2} \int d_M(x,p)^2 \mathrm{d}\mu(p), \tag{3.15}$$

where $\mathrm{d}\mu$ is a positive measure and the support of $\mathrm{d}\mu$ is contained in B_ρ. We now give two conditions on ρ:

- *ρ is less than half the injectivity radius,*
- *if $\Lambda_+ > 0$ then*

$$\rho < \frac{\pi}{2\sqrt{\Lambda_+}}.$$

If these conditions are met then P_M has a unique critical point in B_ρ, which is a minimum.

Theorem 3.4.9 *Let M be a manifold whose sectional curvature K is bounded, that is $\Lambda_- \leq K \leq \Lambda_+$. Let P_M the function on $B_\rho(c)$, a geodesic ball of radius ρ centred on c, defined by*

$$P_M(x) = \frac{1}{2}\int d_M(x,p)^2 \mathrm{d}\mu(p), \tag{3.15}$$

where the support of μ is contained in $B_r(c)$ and we write $R + r = \rho$. Using the notation

$$\mathrm{d}\mu_+ = 1_{\{\mu>0\}}\mathrm{d}\mu, \qquad |\mu_+| = \left|\int \mathrm{d}\mu_+\right|$$
$$\mathrm{d}\mu_- = 1_{\{\mu<0\}}\mathrm{d}\mu, \qquad |\mu_-| = \left|\int \mathrm{d}\mu_-\right|,$$

and

$$k_l = \frac{1}{\sqrt{|\Lambda_-|}} \qquad k_u = \frac{1}{\sqrt{|\Lambda_+|}},$$

we are now able give conditions on ρ depending on the curvature bounds Λ_- and Λ_+:

- *ρ is less than half the injectivity radius,*
- *if $0 < \Lambda_- \leq \Lambda_+$*

$$\frac{\frac{2\rho}{k_l}}{\tan\frac{2\rho}{k_l}}|\mu_+| - |\mu_-| > 0,$$

- *if $\Lambda_- \leq 0 \leq \Lambda_+$*

$$\frac{\frac{2\rho}{k_l}}{\tan\frac{2\rho}{k_l}}|\mu_+| - \frac{\frac{2\rho}{k_u}}{\tanh\frac{2\rho}{k_u}}|\mu_-| > 0,$$

- *if* $\Lambda_- \leq \Lambda_+ \leq 0$

$$|\mu_+| - \frac{\frac{2\rho}{k_u}}{\tanh \frac{2\rho}{k_u}}|\mu_-| > 0,$$

-

$$R|\mu_+| - (2r + R)|\mu_-| > 0$$

If these conditions are met then P_M *has a unique minimum in* B_ρ*.*

Previous work

There are two proofs for the existence and uniqueness of Riemannian centres of mass available. A first one by Karcher [Kar77] and a later one by Kendall [Ken90]. Karcher used comparison theorems of Rauch type to prove that the function

$$P_M(x) = \frac{1}{2} \int d_M(x, p)^2 \mathrm{d}\mu(p) \tag{3.15}$$

is convex on a sufficiently small convex ball, where as before, d_M denotes the distance on the manifold M and $\mathrm{d}\mu$ denotes the mass distribution, whose support is contained in the convex ball. Below we shall make the conditions on the convex ball and the mass distribution more precise.

Comparison theorems of Rauch type compare the behaviour of vector fields on spaces of arbitrary curvature to the behaviour of vector fields on spaces of constant curvature, like the Topogonov comparison theorem does for geodesic triangles. These comparison theorems are also used in Sections 3.5.2 and 3.7.2.

The proof by Kendall [Ken90] is based on the concept of 'convex geometry' which arose from work by Emery on Dirichlet problems. The definition of 'convex geometry' used in the context of Dirichlet problems is quite unlike the definition of convexity:

Definition 3.4.1 ('convex geometry' [Ken90]) *Let* $\mathcal{B}$ *be a compact submanifold (with boundary) of a complete Riemannian manifold* M*, with* $\dim \mathcal{B} = \dim M$*. The domain* $\mathcal{B}$ *is said to have convex geometry if there is a continuous non-negative bounded convex function*[3]

$$\Psi : \mathcal{B} \times \mathcal{B} \to [0, \infty)$$

vanishing precisely on the diagonal

$$\{(x, x) | x \in \mathcal{B}\}.$$

[3]The function is geodesically convex with respect to Riemannian structure.

If a geodesic ball $\mathcal{B}$ has 'convex geometry' then one can prove the uniqueness of the Riemannian centre of mass in $\mathcal{B}$. The proof is presented in Section 7 of [Ken90] and is relatively short. The fact that a so-called regular geodesic ball has 'convex geometry' is not entirely straightforward and the proof of this occupies most of Sections 2 and 4 of [Ken90].

Karcher [Kar77] noted that his proof can be extended to mass distributions with negative weights but positive total weight. This has been studied in detail by Sander [San13], see also [San12]. Sander gave conditions that guarantee the existence and uniqueness of Riemannian centres of mass for mass distributions that allow negative weights.

Overview of our 'Morse theoretical' proof

We shall present alternative proofs for the existence and uniqueness of Riemannian centres of mass for both the original setting (all weights are positive) and the setting where we allow negative weights. Note that for Riemannian centres of mass to make sense the total mass needs to be positive. In fact we shall follow Karcher [Kar77] and Kendall [Ken90] and assume that the total mass is one.

The proof we give is inspired by Morse theory and relies heavily on the Topogonov comparison theorem. For a review of Morse theory we refer to Section 4.3.3. The proof of existence is straightforward for the positive weights case. The idea of the proof of uniqueness in the same setting consists, roughly speaking, of four steps:

- We consider two points x and y on a space of constant curvature. We parametrize a small neighbourhood of x by vectors v in the tangent space at x using the exponential map. We then calculate the squared distance between a point near x parametrized by v and y on the space of constant curvature. These squared distances can be approximated by its Taylor series, where we take the length of v to be our small parameter. We find that the quadratic terms in the Taylor series are positive.

- We now consider two points x and y on a manifold M. Again we parametrize a small neighbourhood of x by vectors v in the tangent space at x using the exponential map. Now we use the Topogonov comparison theorem to conclude that the quadratic terms of the Taylor series in $|v|$ of the squared distance between $\exp_x(v)$ and y are positive.

- The previous step implies that the critical points of P_M are local minima for manifolds of arbitrary but bounded sectional curvature.

- We use the Morse inequalities to conclude that there is only one critical point.

In the case where we allow negative weights the steps are more or less the same but extra conditions need to be met.

Unless mentioned otherwise we assume that every manifold is smooth (C^∞) and simply connected.

3.4.2 Reminder of definitions and (re-)introduction of notation

As we mentioned in Section 3.3 we call a space of constant negative sectional curvature a hyperbolic space. We refer to a setting where a space of constant negative curvature is involved as the hyperbolic case. In particular if we compare a geodesic triangle on a manifold to a geodesic triangle on a space of constant negative curvature, this is referred to as the hyperbolic case.

Likewise a space of positive constant curvature is called elliptic space. We refer to a setting where a space of constant positive curvature is involved as the elliptic case. In particular if we compare a geodesic triangle on a manifold to a geodesic triangle on a space of constant positive curvature, this is referred to as the elliptic case.

If the space of constant sectional curvature has zero curvature it is (locally) Euclidean space. As for the spaces of non-zero curvature we refer to a setting where the space is Euclidean as the Euclidean case.

We shall use the notation $\mathbb{H}^n(K_c)$ for the space of dimension n with constant sectional curvature K_c. If we do not wish to emphasize the dimension we simply write $\mathbb{H}(K_c)$. In this section we write K_c to emphasize that the sectional curvature is constant. We specifically allow $K_c = 0$ for $\mathbb{H}(K_c)$. However we shall not write $\mathbb{H}(0)$ if we specifically focus on a space of zero sectional curvature[4], but emphasize that it is Euclidean space by writing $\mathbb{E}$. If we concentrate on a surface we use Gaussian curvature interchangeably with sectional curvature, for they are the same. As before we define $k = 1/\sqrt{|K_c|}$, provided $K_c \neq 0$.

If we need to distinguish the elliptic and hyperbolic cases we write K_c^- to indicate negative constant curvature and K_c^+ to indicate positive constant curvature. This means that the spaces of constant curvature are denoted by $\mathbb{H}(K_c^+)$, $\mathbb{E}$ and $\mathbb{H}(K_c^-)$.

We shall not write $\mathbb{H}(\pm 1/k^2)$, because using that notation makes it unnecessarily difficult to accommodate Euclidean space and we specifically wish to include this case. The notation $\mathbb{H}(\pm 1/k^2)$ will be used in Section 3.10.

In the Topogonov comparison theorem, Theorem 3.3.2, we used the notation Λ_- and Λ_+ to indicate bounds on the sectional curvature K of a manifold M, that is $\Lambda_- \leq K \leq \Lambda_+$. Depending on the manifold M the bounds Λ_- and Λ_+

[4]Of course the flat torus also has zero sectional curvature, but this is ignored because as long as one does not cross the injectivity radius one does not see a difference between Euclidean space and the flat torus.

may both be positive or negative. They should not be confused with K_c^- or K_c^+, the symbols for negative and positive constant curvature. In particular, by definition we have $K_c^- < 0$ and $K_c^+ > 0$. Because Λ_- and Λ_+ may both be positive or negative $\mathbb{H}(\Lambda_-)$ and $\mathbb{H}(\Lambda_+)$ may both be hyperbolic or elliptic. In fact the cases where Λ_- and Λ_+ have the same sign are of great importance in Section 3.4.4.

As we have seen before in Section 3.2 d_N denotes the geodesic distance on the manifold N. Here we specifically allow that N is a space of constant sectional curvature. The length of a vector v in Euclidean space with the usual norm is denoted by $|v|$.

The tangent space T_xM at a point x of a Riemannian manifold M is endowed with an inner product. The tangent space T_xM can be identified with Euclidean space. We also write $|\cdot|$ to denote the norm induced by the Riemannian inner product on the tangent space. The exponential map $\exp$ at a point x on a manifold N will be denoted by $\exp_{x,N}$. Here we again specifically allow N to be a space of constant curvature.

As in Section 3.3, we denote the lengths of the edges of a (geodesic) triangle by a, b and c.

3.4.3 Positive weights

In this subsection we give an alternative proof of the existence and uniqueness of Riemannian centres of mass or Karcher means.

The function P_M

Before we can prove the existence and uniqueness of Riemannian centres of mass we first have to give some definitions. Here we follow Karcher [Kar77]:

Let $\mathrm{d}\mu$ be a non-negative measure, whose support is contained within B_ρ, a convex ball of finite radius ρ as referred to in Lemma 3.2.1. If we want to specify at which point we consider the measure we write $\mathrm{d}\mu(p)$. Let us illustrate this by an example: If f is a function from $B_\rho \times \mathbb{R}$ to $\mathbb{R}$ we write

$$\int f(p,x)\mathrm{d}\mu(p)$$

to make it clear that p is the variable over which we integrate. We shall further assume that the measure $\mathrm{d}\mu$ has volume 1, that is

$$\int_M \mathrm{d}\mu = \int_{B_\rho} \mathrm{d}\mu = 1.$$

We can make this assumption without loss of generality because we can always normalize. We shall call $\mathrm{d}\mu$ a 'mass distribution' on B_ρ.

We define the function

$$P_M : \bar{B}_\rho \to \mathbb{R},$$

by

$$P_M(x) = \frac{1}{2} \int d_M(x,p)^2 \mathrm{d}\mu(p). \tag{3.15}$$

If the domain of an integral is not specified we shall assume that we integrate over the support of $\mathrm{d}\mu$, which is equivalent to integrating over B_ρ or M.

The function P_M reduces to

$$\mathcal{E}_\lambda(x) = \frac{1}{2} \sum_i \lambda_i d_M(x,p_i)^2, \tag{3.6}$$

if the support of the measure μ consists of the points p_i and the weight for p_i is λ_i for every i.

A comparison of proof strategies

As Karcher [Kar77] also remarked, the gradient vector field of P_M is given by

$$\mathrm{grad} P_M(x) = -\int \exp_{x,M}^{-1}(p) \mathrm{d}\mu(p). \tag{3.16}$$

Note that $\exp_{x,M}^{-1}(p) \in T_xM$ and thus, roughly speaking, the measure $\mathrm{d}\mu(p)$ in equation (3.16) attaches weights to vectors is T_xM. Because the support of $\mathrm{d}\mu$ is contained in a convex ball the exponential map is a diffeomorphism.

Equation (3.16) implies in particular that at boundary points $x \in \partial B_\rho$ the gradient $\mathrm{grad} P_M(x)$ is an average over outward pointing vectors. This yields that P_M has only interior minima on the compact ball $\bar{B}_\rho$.

Karcher then proves that

$$\frac{d^2}{dt^2} P_M(\gamma(t)) > 0, \tag{3.17}$$

for any geodesic γ in $\bar{B}_\rho$. The inequality (3.17) proves that the minimum is unique. The proof of (3.17) is as mentioned based on comparison theorems of Rauch type.

We too shall prove that P_M has a unique minimum. However we do not prove (3.17) in our approach, nor do we use estimates on vector fields, as Karcher

did. Instead we perform some straightforward calculations on spaces of constant curvature. Combining these calculations with the Topogonov comparison theorem we conclude that every critical point of P_M is a local minimum. As already noticed by Karcher, the gradient of P_M is pointing inward on the boundary of a convex ball, that contains the support of the measure μ. This observation follows directly from the definition of convexity. This implies that P_M has a unique minimum, by the Morse inequalities.

Main theorem

The result can be summarised in the following theorem.

Theorem 3.4.2 *Let M be a manifold whose sectional curvature K is bounded, that is $\Lambda_- \leq K \leq \Lambda_+$. Let P_M the function on B_ρ defined by*

$$P_M(x) = \frac{1}{2} \int d_M(x,p)^2 \mathrm{d}\mu(p), \tag{3.15}$$

where $\mathrm{d}\mu$ is a positive measure and the support of $\mathrm{d}\mu$ is contained in B_ρ. We now give two conditions on ρ:

- *ρ is less than half the injectivity radius,*
- *if $\Lambda_+ > 0$ then*

$$\rho < \frac{\pi}{2\sqrt{\Lambda_+}}.$$

If these conditions are met then P_M has a unique critical point in B_ρ, which is a minimum.

Spaces of constant curvature

We start with one of these straightforward calculations in spaces of constant curvature. Our observation concerns geodesic triangles of which one of the edges (we have chosen b) is very short compared to the other edges, see Figure 3.3. We shall compare these geodesic triangles in spaces of constant curvature to triangles in Euclidean space.

In Lemma 3.4.4 we shall use the following notation:

Definition 3.4.3 *Let N be a Riemannian manifold. Here we specifically allow N to be a space of constant sectional curvature, in particular N is allowed to be Euclidean space. As usual $|\cdot|$ denotes the norm induced by the Riemannian*

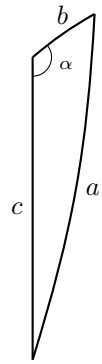

Figure 3.3: A sketch of a triangle with short edge. The depiction is made 'using' Riemann normal coordinates. It is supposed to be a sketch of a triangle on an arbitrary manifold, but especially in Lemma 3.4.4 the manifold is a space of constant curvature.

metric on T_xN. Let $x, y \in N$ separated by a distance smaller then the injectivity radius. We introduce the notation

$$d_{T_xN}(v, \exp_{x,N}^{-1}(y))^2 = |\exp_{x,N}^{-1}(y)|^2 - 2|\exp_{x,N}^{-1}(y)|(\cos\alpha)|v| + |v|^2,$$

with α the angle between $\exp_{x,N}^{-1}(y)$ and v in T_xN, where the angle is determined by the Riemannian metric.

We shall now prove the following regarding spaces of constant curvature:

Lemma 3.4.4 *Let $x, y \in \mathbb{H}(K_c^+), \mathbb{E}, \mathbb{H}(K_c^-)$ and $v \in T_x\mathbb{H}(K_c^+), T_x\mathbb{E}, T_x\mathbb{H}(K_c^-)$. Here we use K_c^+, $\mathbb{E}$ and K_c^- to distinguish the positive, zero and negative curvature cases. For K_c^+ we add the condition that $2d_{\mathbb{H}(K_c^+)}(x, y) < \frac{\pi}{\sqrt{K_c^+}}$. The quadratic terms in the Taylor approximation of $d_{\mathbb{H}(K_c^+)}(\exp_{x,\mathbb{H}(K_c^+)}(v), y)^2$, $d_{\mathbb{E}}(\exp_{x,\mathbb{E}}(v), y)^2$ and $d_{\mathbb{H}(K_c^-)}(\exp_{x,\mathbb{H}(K_c^-)}(v), y)^2$ with respect to $|v|$ are positive, moreover they are equal up to first order, that is*

$$\begin{aligned} d_{T_x\mathbb{H}(K_c^-)}(v, \exp_{x,\mathbb{H}(K_c^-)}^{-1}(y))^2 &= d_{\mathbb{H}(K_c^-)}(\exp_{x,\mathbb{H}(K_c^-)}(v), y)^2 + \mathcal{O}(|v|^2) \\ d_{T_x\mathbb{E}}(v, \exp_{x,\mathbb{E}}^{-1}(y))^2 &= d_{\mathbb{E}}(\exp_{x,\mathbb{E}}(v), y)^2 \\ d_{T_x\mathbb{H}(K_c^+)}(v, \exp_{x,\mathbb{H}(K_c^+)}^{-1}(y))^2 &= d_{\mathbb{H}(K_c^+)}(\exp_{x,\mathbb{H}(K_c^+)}(v), y)^2 + \mathcal{O}(|v|^2). \end{aligned}$$

Here we emphasize that the length of v (denoted by $|v|$)is the length of a vector in $T_x\mathbb{H}(K_c)$, with respect to the inner product induced by the Riemannian metric.

Note that we may even assume that $\mathbb{H}(K_c^+), \mathbb{E}, \mathbb{H}(K_c^-)$ are two dimensional in Lemma 3.4.4.

Proof The result of the lemma follows by approximating the cosine rule for triangles as sketched in Figure 3.4 using Taylor's theorem. We start with the cosine rules in spaces of constant curvature (where a, b and c denote the lengths of edges). As we have seen in Section 3.3, the cosine rules read

$$\begin{aligned}
\cos\frac{a}{k} &= \cos\frac{b}{k}\cos\frac{c}{k} + \sin\frac{b}{k}\sin\frac{c}{k}\cos\alpha, && \text{(elliptic)}\\
a^2 &= b^2 + c^2 - 2bc\cos\alpha && \text{(Euclidean)}\\
\cosh\frac{a}{k} &= \cosh\frac{b}{k}\cosh\frac{c}{k} - \sinh\frac{b}{k}\sinh\frac{c}{k}\cos\alpha, && \text{(hyperbolic)}
\end{aligned} \tag{3.18}$$

for spaces of positive, zero and negative constant curvature respectively. We write (elliptic) to indicate that the space has positive constant curvature, (Euclidean) to indicate that the space has zero curvature, and (hyperbolic) to indicate that the space has negative constant curvature. Here we used that $k = 1/\sqrt{|K_c|}$, with K_c the value of the sectional curvature K. As mentioned, we write K_c to emphasize that the sectional curvature of a space of constant sectional curvature is constant.

With the cosine rules we do the following:

- We take the $\arccos$, square root and $\operatorname{arccosh}$ respectively, of both sides of (3.18) that is,
- bring k where necessary (if the curvature is non-zero) to the other side,
- square all terms (on both sides),
- use Taylor's theorem with respect to b (on the right hand side),

this yields:

$$\begin{aligned}
a^2 &= c^2 - 2bc\cos\alpha + \left(\cos^2\alpha + \sin^2\alpha\frac{\frac{c}{k}}{\tan\frac{c}{k}}\right)b^2 + \mathcal{O}(b^3) && \text{(elliptic)}\\
a^2 &= c^2 - 2bc\cos\alpha + b^2 && \text{(Euclidean)}\\
a^2 &= c^2 - 2bc\cos\alpha + \left(\cos^2\alpha + \sin^2\alpha\frac{\frac{c}{k}}{\tanh\frac{c}{k}}\right)b^2 + \mathcal{O}(b^3) && \text{(hyperbolic),}
\end{aligned} \tag{3.19}$$

where for the elliptic case we assume that we do not cross the injectivity radius, that is $\frac{\pi k}{2} > c$. We note that because $x/\tan x > 0$, for $0 < x < \pi/2$, and $x/\tanh x > 0$ the quadratic terms are strictly positive.

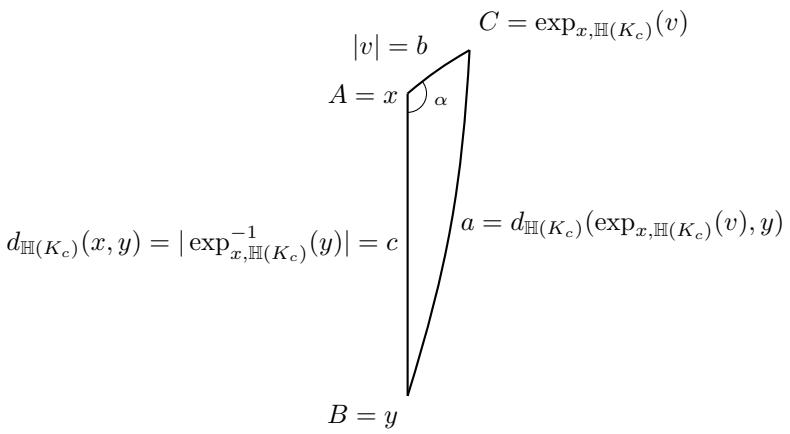

Figure 3.4: A sketch of a geodesic triangle with short edge. Here we assume that the space has constant sectional curvature. The depiction is made 'using' Riemann normal coordinates.

We now choose the vertices of the triangle to be given by $A = x$, $B = y$ and $C = \exp_{x,H(K_c)}(v)$, as indicated in Figure 3.4. With these choices we have

$$a = d_{\mathbb{H}(K_c)}(\exp_{x,\mathbb{H}(K_c)}(v), y), \quad b = |v|, \quad c = |\exp^{-1}_{x,\mathbb{H}(K_c)}(y)| = d_{\mathbb{H}(K_c)}(x, y),$$

where K_c can be either positive, zero or negative and thus $\mathbb{H}(K_c)$ denotes either elliptic space (if the constant sectional curvature K_c is positive), Euclidean space (if the constant sectional curvature K_c is zero) or hyperbolic space (if the constant sectional curvature K_c is negative). We repeat that $\mathbb{H}(K_c)$ may be Euclidean space if K_c is zero, but the notation $\mathbb{E}$ is used to stress this if necessary and not in a general context.

With the vertices and therefore lengths of edges we have given in the previ-

ous paragraph (also see the sketch in Figure 3.4) equation (3.19) now reads

$$\begin{aligned} d_{\mathbb{H}(K_c^+)}(\exp_{x,\mathbb{H}(K_c^+)}(v),y)^2 =& |\exp^{-1}_{x,\mathbb{H}(K_c^+)}(y)|^2 - 2|\exp^{-1}_{x,\mathbb{H}(K_c^+)}(y)|(\cos\alpha)|v| \\ &+ \left(\cos^2(\alpha) + \sin^2(\alpha)\frac{\vartheta_+}{\tan\vartheta_+}\right)|v|^2 + \mathcal{O}(|v|^3) \\ d_{\mathbb{E}}(\exp_{x,\mathbb{E}}(v),y)^2 =& |\exp^{-1}_{x,\mathbb{E}}(y)|^2 - 2|\exp^{-1}_{x,\mathbb{E}}(y)|(\cos\alpha)|v| + |v|^2 \\ d_{\mathbb{H}(K_c^-)}(\exp_{x,\mathbb{H}(K_c^-)}(v),y)^2 =& |\exp^{-1}_{x,\mathbb{H}(K_c^-)}(y)|^2 - 2|\exp^{-1}_{x,\mathbb{H}(K_c^-)}(y)|(\cos\alpha)|v| \\ &+ \left(\cos^2(\alpha) + \sin^2(\alpha)\frac{\vartheta_-}{\tanh\vartheta_-}\right)|v|^2 + \mathcal{O}(|v|^3), \end{aligned} \tag{3.20}$$

with

$$\begin{aligned} \vartheta_+ &= \frac{\left|\exp^{-1}_{x,\mathbb{H}(K_c^+)}(y)\right|}{k^+} \\ \vartheta_- &= \frac{\left|\exp^{-1}_{x,\mathbb{H}(K_c^-)}(y)\right|}{k^-}, \end{aligned} \tag{3.21}$$

where we use K_+, $\mathbb{E}$ and K_- to distinguish the positive, zero and negative curvature cases, $k^+ = 1/\sqrt{K_c^+}$ and $k^- = 1/\sqrt{|K_c^-|}$. As we noted above the expressions are the same up to first order in $|v|$, that is

$$\begin{aligned} d_{T_x\mathbb{H}(K_c^-)}(v, \exp^{-1}_{x,\mathbb{H}(K_c^-)}(y))^2 &= d_{\mathbb{H}(K_c^-)}(\exp_{x,\mathbb{H}(K_c^-)}(v),y)^2 + \mathcal{O}(|v|^2) \\ d_{T_x\mathbb{E}}(v, \exp^{-1}_{x,\mathbb{E}}(y))^2 &= d_{\mathbb{E}}(\exp_{x,\mathbb{E}}(v),y)^2 \\ d_{T_x\mathbb{H}(K_c^+)}(v, \exp^{-1}_{x,\mathbb{H}(K_c^+)}(y))^2 &= d_{\mathbb{H}(K_c^+)}(\exp_{x,\mathbb{H}(K_c^+)}(v),y)^2 + \mathcal{O}(|v|^2). \end{aligned}$$

□

From spaces of constant curvature to manifolds of arbitrary sectional curvature

We can now combine Lemma 3.4.4 with the Toponogov comparison theorem, see Section 3.3. Suppose that the sectional curvatures K of a manifold M satisfy the bound $\Lambda_- \leq K \leq \Lambda_+$. Note that Λ_- and Λ_+ may both be positive or negative. When we use Lemma 3.4.4 we therefore may use the result for hyperbolic of elliptic spaces twice.

To be able to use the Topogonov comparison theorem (Theorem 3.3.2) we assume that the points x and y lie within a convex geodesic ball B_ρ in M. We shall assume that the following two conditions on ρ are satisfied:

- ρ is less than half the injectivity radius,
- should moreover $\Lambda_+ > 0$ then

$$\rho < \frac{\pi}{2\sqrt{\Lambda_+}}.$$

Let us identify x with a point in $\mathbb{H}(\Lambda_-)$ and a point in $\mathbb{H}(\Lambda_+)$. We can now also identify the tangent spaces of the different spaces at x.[5] With these definitions the Topogonov comparison theorem yields

$$\begin{aligned} &d_{\mathbb{H}(\Lambda_-)}(\exp_{x,\mathbb{H}(\Lambda_-)}(v), \exp_{x,\mathbb{H}(\Lambda_-)} \circ \exp_{x,M}^{-1}(y))^2 \\ &\qquad \geq d_M(\exp_{x,M}(v), y)^2 \\ &\qquad \geq d_{\mathbb{H}(\Lambda_+)}(\exp_{x,\mathbb{H}(\Lambda_+)}(v), \exp_{x,\mathbb{H}(\Lambda_+)} \circ \exp_{x,M}^{-1}(y))^2. \end{aligned} \tag{3.22}$$

Lemma 3.4.4 then implies that the upper and lower bounds in (3.22) are the same up to linear order in $|v|$, to be precise

$$\begin{aligned} &d_{\mathbb{H}(\Lambda_-)}(\exp_{x,\mathbb{H}(\Lambda_-)}(v), \exp_{x,\mathbb{H}(\Lambda_-)} \circ \exp_{x,M}^{-1}(y))^2 = \\ &\qquad |\exp_{x,M}^{-1}(y)|^2 - 2|\exp_{x,M}^{-1}(y)|(\cos\alpha)|v| + \mathcal{O}(|v|^2) \\ &d_{\mathbb{H}(\Lambda_+)}(\exp_{x,\mathbb{H}(\Lambda_+)}(v), \exp_{x,\mathbb{H}(\Lambda_+)} \circ \exp_{x,M}^{-1}(y))^2 = \\ &\qquad |\exp_{x,M}^{-1}(y)|^2 - 2|\exp_{x,M}^{-1}(y)|(\cos\alpha)|v| + \mathcal{O}(|v|^2). \end{aligned} \tag{3.23}$$

Note that these expressions do not depend on the signs of Λ_- and Λ_+, in particular both the upper and the lower bound may have the same sign. Because the upper and lower bounds in (3.22) (as given in (3.23)) are the same up to first order we can conclude

$$\begin{aligned} P_M(\exp_{x,M}(v)) &= \int d_M(\exp_{x,M}(v), p)^2 \mathrm{d}\mu(p) \\ &= \int |v - \exp_{x,M}^{-1}(p)|^2 \mathrm{d}\mu(p) + \mathcal{O}(|v|^2). \end{aligned} \tag{3.24}$$

Equation (3.24) implies that critical points x of P_M are characterized by

$$\int \exp_{x,M}^{-1}(p) \mathrm{d}\mu(p) = 0, \tag{3.25}$$

as we have seen in (3.16).

[5] Here it is crucial that all manifolds, that is including the spaces of constant curvature have the same dimension.

Lemma 3.4.4 also gives us that the quadratic terms in the Taylor series of

$$d_{\mathbb{H}(\Lambda_-)}(\exp_{x,\mathbb{H}(\Lambda_-)}(v), \exp_{x,\mathbb{H}(\Lambda_-)} \circ \exp_{x,M}^{-1}(y))^2$$

and

$$d_{\mathbb{H}(\Lambda_+)}(\exp_{x,\mathbb{H}(\Lambda_+)}(v), \exp_{x,\mathbb{H}(\Lambda_+)} \circ \exp_{x,M}^{-1}(y))^2$$

in $|v|$ are positive. With the Topogonov comparison theorem this implies that the quadratic terms in the Taylor series of $d_M(\exp_{x,M}(v), y)^2$ are positive. From this we may conclude that the quadratic terms in the series development of

$$P_M(\exp_{x,M}(v)) = \int d_M(\exp_{x,M}(v), y)^2 \mathrm{d}\mu(y)$$

at x are positive. This in turn implies that every critical point of P_M is a local minimum. We can further conclude that P_M is Morse, because of the quadratic nature of the critical points.

Uniqueness using Morse type arguments

To be able to conclude that every critical point is a local minimum and that the gradient is pointing outwards on the boundary $\partial \bar{B}_\rho$, where $\bar{B}_\rho$ is a convex ball, together imply that there is a unique minimum inside $\bar{B}_\rho$ we now prove the following lemma

Lemma 3.4.5 *Let f be a positive Morse function on the n-dimensional ball $\bar{B}^n(0,1)$ of radius 1 centred at the origin in Euclidean space such that the gradient of f is pointing outwards on $\partial \bar{B}^n(0,1)$. Then there exists a Morse function $\tilde{f}$ on $\bar{B}^n(0,1)$ that has the same critical points as f and $\tilde{f}|_{\partial \bar{B}^n(0,1)}$ is constant.*

Proof First note that because ∇f is pointing outward on $\partial \bar{B}^n(0,1)$ there is some $\epsilon_0 > 0$ such that ∇f is pointing outward on all $\partial \bar{B}^n(0, 1-\epsilon)$ for all $\epsilon \in [0, \epsilon_0]$. This is a consequence of the fact that ∇f is continuous.

Because the gradient is linear and reads

$$\nabla f(r, \theta) = \frac{\partial f}{\partial r} e_r + \ldots,$$

where the dots indicate terms orthogonal to the radial direction, with r the radial coordinate and $\theta \in S^{n-1}$, it suffices to construct a smooth function g satisfying:

- g is zero on $\bar{B}^n(0, 1-\epsilon_0)$
- $g|_{\partial \bar{B}^n(0,1)} = (C - f)|_{\partial \bar{B}^n(0,1)}$, where $C = \max_{S^{n-1}} f|_{\partial \bar{B}^n(0,1)} + 1$

- $\partial_r g > 0$ on $\bar{B}^n(0,1) \setminus \bar{B}^n(0,1-\epsilon_0)$

So that we can take $\tilde{f} = f + g$. We use factorization to simplify the search and define g to be $(C - f(1,\theta))\psi(r)$ with $\theta \in S^{n-1}$ and r the usual radial coordinate, with $\psi : \mathbb{R} \to \mathbb{R}$ any function that satisfies

- $\psi(r) = 0$, for $r \in [0, 1-\epsilon_0]$
- $\psi(1) = 1$
- $\psi'(r) > 0$ for $r \in (1-\epsilon_0, 1]$.

It is clear that such a function exists, for example

$$\psi(r) = \begin{cases} e^{-\frac{1}{(r-(1-\epsilon_0))^2} + \frac{1}{\epsilon_0^2}}, & \text{if } r \in (1-\epsilon_0, 1] \\ 0, & r \in [0, 1-\epsilon_0] \end{cases}$$

will do. □

Karcher already noted in [Kar77] that if B_ρ is any convex geodesic ball that contains the support of μ and μ is a positive measure, the gradient of P_M is pointing outwards on $\partial\bar{B}_\rho$ because it is the average of outward pointing vectors. We observed above that all critical points of P_M are local minima and moreover P_M is Morse. By going to Riemann normal coordinates and rescaling we can apply Lemma 3.4.5, to conclude that there is another Morse function $\tilde{P}_M$ with the same critical points as P_M and of the same type, but for which the boundary of the ball is a level set. Because all critical points of $P_M$are local minima the Morse inequalities imply that the number of critical points equals the number of connected components of the sublevelset. This in turn gives that there must be a unique minimum. This concludes the proof of Theorem 3.4.2.

Remark 3.4.6 *We could also use Lemma 3.4.4 and the Topogonov comparison to give an argument like Karcher, see* (3.17)*. However we have chosen this approach in the hope to eventually extend this method to a more general setting, including pseudo-Riemannian manifolds.*

3.4.4 Negative weights

In this subsection we shall give conditions to ensure that P_M has a unique minimum if we allow our mass distribution μ to have negative weights, while still imposing that $\int \mathrm{d}\mu(p) = 1$. We shall use the same approach as above, that is with only positive weights. This means that we must address two points:

- find conditions such that every critical point is a local minimum

- find a geodesic ball such that the gradient of $P_M(x)$ is pointing outward on the boundary of the geodesic ball.

The distinction between the positive and negative weight parts will be very important, so we define

$$\begin{aligned} \mathrm{d}\mu_+ &= 1_{\{\mu>0\}}\mathrm{d}\mu, & |\mu_+| &= \left|\int \mathrm{d}\mu_+\right| \\ \mathrm{d}\mu_- &= 1_{\{\mu<0\}}\mathrm{d}\mu, & |\mu_-| &= \left|\int \mathrm{d}\mu_-\right|, \end{aligned}$$

with 1_B the indicator function for the set B.

Criteria such that every critical point is a local minimum

We shall start by examining conditions such that every critical point is a local minimum. Because μ is allowed to have negative weights we shall need both the upper and lower bounds of (3.22) and more precise bounds on (3.20) than the observation that all quadratic parts are positive.

Further bounds on the quadratic part of the Taylor series of $d_{\mathbb{H}(K_c)}(\exp_{x,\mathbb{H}(k_c)}, y)$ with respect to $|v|$. We are now going to expand on Lemma 3.4.4. We stress that we work in a space form (space of constant curvature). In particular we are going to give bounds on the quadratic terms in the Taylor approximation of $d_{\mathbb{H}(K_c^+)}(\exp_{x,\mathbb{H}(K_c^+)}(v), y)^2$ and $d_{\mathbb{H}(K_c^-)}(\exp_{x,\mathbb{H}(K_c^-)}(v), y)^2$ with respect to $|v|$. We shall not explicitly go into the (trivial) case where the space of constant curvature is Euclidean space, that is $d_{\mathbb{E}}(\exp_{x,\mathbb{E}}(v), y)^2$.

These exact bounds are necessary because of the negative weights there is a negative contribution to the quadratic terms in the Taylor series[6] of

$$P_M(\exp_{x,M}(v)) = \int d_M(\exp_{x,M}(v), p)^2 \mathrm{d}\mu(p)$$

in $|v|$ given by the quadratic terms in the Taylor series of

$$P_M(\exp_{x,M}(v)) = \int d_M(\exp_{x,M}(v), p)^2 \mathrm{d}\mu_-(p).$$

To give bounds on the quadratic terms in the Taylor approximation of $d_{\mathbb{H}(K_c^+)}(\exp_{x,\mathbb{H}(K_c^+)}(v), y)^2$ and $d_{\mathbb{H}(K_c^-)}(\exp_{x,\mathbb{H}(K_c^-)}(v), y)^2$ with respect to $|v|$, we

[6]Here we explain the role our calculations play in the formulation of conditions that guarantee existence and uniqueness, M is therefore a manifold of arbitrary non-constant, but bounded curvature.

need to introduce an extra assumption, that was not used in Lemma 3.4.4. This extra assumption is

$$d_{\mathbb{H}(K_c)}(x,y) = |\exp^{-1}_{x,\mathbb{H}(K_c)}(y)| < 2\tilde{\rho}.$$

As in Lemma 3.4.4 we add[7] the condition for K_c^+ that $2d_{\mathbb{H}(K_c^+)}(x,y) < \frac{\pi}{\sqrt{K_c^+}}$.

Bounds on the quadratic parts of

$$\begin{aligned} d_{\mathbb{H}(K_c^+)}(\exp_{x,\mathbb{H}(K_c^+)}(v),y)^2 =& |\exp^{-1}_{x,\mathbb{H}(K_c^+)}(y)|^2 - 2|\exp^{-1}_{x,\mathbb{H}(K_c^+)}(y)|(\cos\alpha)|v| \\ &+ \left(\cos^2(\alpha) + \sin^2(\alpha)\frac{\vartheta_+}{\tan\vartheta_+}\right)|v|^2 + \mathcal{O}(|v|^3) \\ d_{\mathbb{H}(K_c^-)}(\exp_{x,\mathbb{H}(K_c^-)}(v),y)^2 =& |\exp^{-1}_{x,\mathbb{H}(K_c^-)}(y)|^2 - 2|\exp^{-1}_{x,\mathbb{H}(K_c^-)}(y)|(\cos\alpha)|v| \\ &+ \left(\cos^2(\alpha) + \sin^2(\alpha)\frac{\vartheta_-}{\tanh\vartheta_-}\right)|v|^2 + \mathcal{O}(|v|^3), \end{aligned} \tag{3.20}$$

where

$$\begin{aligned} \vartheta_+ &= \frac{\left|\exp^{-1}_{x,\mathbb{H}(K_c^+)}(y)\right|}{k^+} \\ \vartheta_- &= \frac{\left|\exp^{-1}_{x,\mathbb{H}(K_c^-)}(y)\right|}{k^-}, \end{aligned} \tag{3.21}$$

are easy to determine if one observes that $x/\tan(x)$ and $x/\tanh(x)$ are monotone decreasing and increasing respectively. With this observation we see that

$$\begin{aligned} \frac{\frac{2\tilde{\rho}}{k^+}}{\tan\frac{2\tilde{\rho}}{k^+}} \leq \frac{\vartheta_+}{\tan\vartheta_+} \leq 1 \\ 1 \leq \frac{\vartheta_-}{\tanh\vartheta_-} \leq \frac{\frac{2\tilde{\rho}}{k^-}}{\tanh\frac{2\tilde{\rho}}{k^-}}. \end{aligned} \tag{3.26}$$

[7] It turns out that we need to impose stronger conditions below so we shall not encounter this condition explicitly in Theorem 3.4.9.

The bounds in (3.26) give us

$$\begin{aligned}
&|\exp^{-1}_{x,\mathbb{H}(K_c^+)}(y)|^2 - 2|\exp^{-1}_{x,\mathbb{H}(K_c^+)}(y)|(\cos\alpha)|v| + \frac{\frac{2\tilde{\rho}}{k^+}}{\tan\frac{2\tilde{\rho}}{k^+}}|v|^2 + \mathcal{O}(|v|^3)\\
&\leq d_{\mathbb{H}(K_c^+)}(\exp_{x,\mathbb{H}(K_c^+)}(v), y)^2\\
&= |\exp^{-1}_{x,\mathbb{H}(K_c^+)}(y)|^2 - 2|\exp^{-1}_{x,\mathbb{H}(K_c^+)}(y)|(\cos\alpha)|v|\\
&+ \left(\cos^2\alpha + \sin^2\alpha\frac{\vartheta_+}{\tan\vartheta_+}\right)|v|^2 + \mathcal{O}(|v|^3)\\
&\leq |\exp^{-1}_{x,\mathbb{H}(K_c^+)}(y)|^2 - 2|\exp^{-1}_{x,\mathbb{H}(K_c^+)}(y)|(\cos\alpha)|v| + |v|^2 + \mathcal{O}(|v|^3) \qquad (3.27)
\end{aligned}$$

and

$$\begin{aligned}
&|\exp^{-1}_{x,\mathbb{H}(K_c^-)}(y)|^2 - 2|\exp^{-1}_{x,\mathbb{H}(K_c^-)}(y)|(\cos\alpha)|v| + |v|^2 + \mathcal{O}(|v|^3)\\
&\leq d_{\mathbb{H}(K_c^-)}(\exp_{x,\mathbb{H}(K_c^-)}(v), y)^2\\
&= |\exp^{-1}_{x,\mathbb{H}(K_c^-)}(y)|^2 - 2|\exp^{-1}_{x,\mathbb{H}(K_c^-)}(y)|(\cos\alpha)|v|\\
&+ \left(\cos^2\alpha + \sin^2\alpha\frac{\vartheta_-}{\tanh\vartheta_-}\right)|v|^2 + \mathcal{O}(|v|^3),\\
&\leq |\exp^{-1}_{x,\mathbb{H}(K_c^-)}(y)|^2 - 2|\exp^{-1}_{x,\mathbb{H}(K_c^-)}(y)|(\cos\alpha)|v| + \frac{\frac{2\tilde{\rho}}{k^-}}{\tanh\frac{2\tilde{\rho}}{k^-}}|v|^2 + \mathcal{O}(|v|^3).
\end{aligned} \qquad (3.28)$$

With these expressions we can give conditions on the positive and negative weights so that every critical point of P_M is a local minimum.

The Taylor series of $d_{\mathbb{H}(K_c)}(\exp_{x,\mathbb{H}(K_c)}, y)$ and the Topogonov comparison theorem. We can now combine these new bounds with the Toponogov comparison theorem, see Section 3.3. Suppose that the sectional curvatures K of a manifold M satisfy the bound $\Lambda_- \leq K \leq \Lambda_+$. Note that Λ_- and Λ_+ may both positive or negative.

To be able to use the Topogonov comparison theorem (Theorem 3.3.2) as before we assume that the points x and y lie within a convex geodesic ball B_ρ in M. We shall assume that the following two conditions on ρ are satisfied:

- ρ is less than half the injectivity radius,
- if $\Lambda_+ > 0$ then
$$\rho < \frac{\pi}{2\sqrt{\Lambda_+}}.$$

As for the positive weight case, let us identify x with a point in $\mathbb{H}(\Lambda_-)$ and a point in $\mathbb{H}(\Lambda_+)$. We can now also identify the tangent spaces of the different spaces at x.[8] With these definitions the Topogonov comparison theorem yields

$$\begin{aligned} &d_{\mathbb{H}(\Lambda_-)}(\exp_{x,\mathbb{H}(\Lambda_-)}(v), \exp_{x,\mathbb{H}(\Lambda_-)} \circ \exp_{x,M}^{-1}(y))^2 \\ &\quad \geq d_M(\exp_{x,M}(v), y)^2 \\ &\quad \geq d_{\mathbb{H}(\Lambda_+)}(\exp_{x,\mathbb{H}(\Lambda_+)}(v), \exp_{x,\mathbb{H}(\Lambda_+)} \circ \exp_{x,M}^{-1}(y))^2. \end{aligned} \tag{3.22}$$

We are now ready to give condition that ensure that the quadratic terms in the Taylor series of

$$P_M(\exp_{x,M}(v)) = \int d_M(\exp_{x,M}(v), p)^2 \mathrm{d}\mu(p)$$

in $|v|$ are positive. This is equivalent to every critical point of P_M is a local minimum.

Conditions We have to distinguish several cases based on the sign of Λ_- and Λ_+. To this end we introduce the notation

$$k_l = \frac{1}{\sqrt{|\Lambda_-|}} \qquad\qquad k_u = \frac{1}{\sqrt{|\Lambda_+|}}.$$

Note that critical points are characterised by (3.25), just as they were when the weights were exclusively positive.

The conditions are as follows:

- We shall first assume that $0 < \Lambda_- \leq \Lambda_+$. In this case we have for every critical point x

$$P_M(\exp_{x,M}(v)) \geq c_\mu + \left(\frac{\frac{2\rho}{k_l}}{\tan \frac{2\rho}{k_l}} |\mu_+| - |\mu_-| \right) |v|^2 + \mathcal{O}(|v|^3),$$

  where $c_\mu = P_M(x)$. Here we have split P_M up

$$\begin{aligned} P_M(\exp_{x,M}(v)) &= \int d_M(\exp_{x,M}(v), p)^2 \mathrm{d}\mu(p) \\ &= \int d_M(\exp_{x,M}(v), p)^2 \mathrm{d}\mu_+(p) + \int d_M(\exp_{x,M}(v), p)^2 \mathrm{d}\mu_-(p) \end{aligned}$$

[8] Here it is crucial that all manifolds, that is including the spaces of constant curvature have the same dimension.

and then used (3.22), (3.27) and (3.28). This means that every critical point is a local minimum if

$$\frac{\frac{2\rho}{k_l}}{\tan\frac{2\rho}{k_l}}|\mu_+| - |\mu_-| > 0.$$

- If $\Lambda_- \leq 0 \leq \Lambda_+$, we have for every critical point x

$$P_M(\exp_{x,M}(v)) \geq c_\mu + \left(\frac{\frac{2\rho}{k_l}}{\tan\frac{2\rho}{k_l}}|\mu_+| - \frac{\frac{2\rho}{k_u}}{\tanh\frac{2\rho}{k_u}}|\mu_-|\right)|v|^2 + \mathcal{O}(|v|^3).$$

In this setting we have that every critical point is a local minimum if

$$\frac{\frac{2\rho}{k_l}}{\tan\frac{2\rho}{k_l}}|\mu_+| - \frac{\frac{2\rho}{k_u}}{\tanh\frac{2\rho}{k_u}}|\mu_-| > 0.$$

- If $\Lambda_- \leq \Lambda_+ \leq 0$, we have for every critical point x

$$P_M(\exp_{x,M}(v)) \geq c_\mu + \left(|\mu_+| - \frac{\frac{2\rho}{k_u}}{\tanh\frac{2\rho}{k_u}}|\mu_-|\right)|v|^2 + \mathcal{O}(|v|^3).$$

This gives us the condition

$$|\mu_+| - \frac{\frac{2\rho}{k_u}}{\tanh\frac{2\rho}{k_u}}|\mu_-| > 0,$$

for critical points to be local minima.

Remark 3.4.7 *We have used $|\mu_+|$ and $|\mu_-|$ in our conditions, because we want to emphasize thee contributions of the positive and negative weights. However, note that*

$$|\mu_+| - |\mu_-| = 1$$

because of the normalization assumption on $\mathrm{d}\mu$.

This completes our discussion of the conditions for the critical points being local minima in the case of negative weights.

A geodesic ball such that the gradient of P_M is pointing outward on the boundary of the geodesic ball

We are now ready to address the second point, finding conditions such that there exists a geodesic ball containing the support of μ such that the gradient of P_M is pointing outward on the boundary of the ball. Like in the positive weights case, we shall assume that the support of μ is contained in a convex geodesic ball $B(p_c, r)$. We have specifically chosen r and not ρ as the radius because ρ will be the radius for which the gradient of P_M at $\partial B(p_c, \rho)$ is pointing outwards. We find it convenient to write $r + R = \rho$. So let us consider the gradient of P_M on the boundary of the geodesic ball $B(p_c, r + R)$, with $R > 0$. We have that

$$\text{grad}P_M(x) = -\int \exp_{x,M}^{-1}(y)\mathrm{d}\mu(y).$$

Because we assume that $R > 0$ the inward pointing part of the gradient

$$-\int \exp_{x,M}^{-1}(y)\mathrm{d}\mu_-(y).$$

may be bounded in the radial direction from above by $(2r+R)|\mu_-|$, because any given point in $B(p_c, r)$ lies at most $2r + R$ from a point on $\partial B(p_c, r + R)$.

The outward pointing part of the gradient

$$-\int \exp_{x,M}^{-1}(y)\mathrm{d}\mu_+(y).$$

in radial direction may be bounded from below by $R|\mu_+|$. This bound is not as easy to prove as the bound on the inward pointing part of the gradient. Let us now assume that $x \in \partial B(p_c, r + R)$. Assume that $z \in \partial B(p_c, r)$ is the point on $\partial B(p_c, r)$ that is closest to x. Let $S = \exp_{x,M}^{-1}(\partial B(p_c, r))$. We view its tangent space $T_{\exp_{x,M}^{-1}(z)}S$ as an affine subspace of T_xM. We shall prove that $\exp_{x,M}^{-1}(B(p_c, r))$ lies in a half space of T_xM defined by the tangent space $T_{\exp_{x,M}^{-1}(z)}S$. To prove that $\exp_{x,M}^{-1}(B(p_c, r))$ lies in the half space we show the following: The only geodesic triangle with edge lengths r, $r + R$, b, angle θ, vertices p_c and x as in figure 3.5 and $b \leq R/\cos\theta$ is the trivial triangle with $\theta = 0$.

In our proof we shall need the following inequality

$$\sin(as) \leq a \sin s$$

for $a \geq 1$ and $\pi/2 \geq as \geq 0$, which is strict if $s > 0$ and $a > 1$. This inequality follows from the fact that $\cos as \leq \cos s$ under the same conditions. With this observation we have

$$\frac{\sin as}{a} = \int_0^s \cos(at)\mathrm{d}t \leq \int_0^s \cos(t)\mathrm{d}t = \sin s.$$

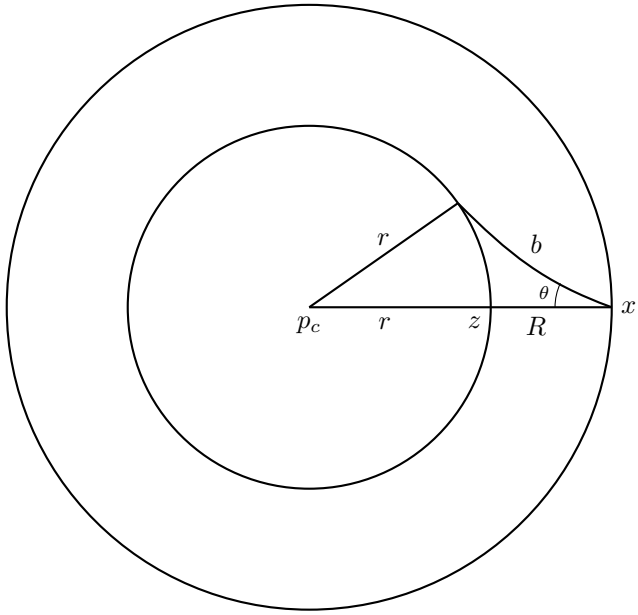

Figure 3.5: Sketch of two geodesic balls and θ, here we have chosen Riemann normal coordinates whose origin coincides with the centre of both geodesic balls.

We can now focus on the geodesic triangle. By the Toponogov comparison theorem we know that $\cos\theta$ is bounded from below by $\cos\theta_{\Lambda_+}$, where θ_{Λ_+} denotes the angle corresponding to θ for the Alexandrov triangle in the space of curvature Λ_+. Without loss of generality we can assume that Λ_+ is positive.[9]

We now consider the Alexandrov triangle with edge lengths r, $r+R$, b, angle θ_{Λ_+} and $b \leq R/\cos\theta_{\Lambda_+}$. Note that because of the triangle inequality we have that $b \geq R$. The cosine rule for spaces of positive curvature now yields

$$\begin{aligned}
\cos r &= \cos(r+R)\cos(b) + \sin(r+R)\sin(b)\cos\theta_{\Lambda_+} \\
&\leq \cos(r+R)\cos(b) + \sin(r+R)\sin(R/\cos\theta_{\Lambda_+})\cos\theta_{\Lambda_+} \\
&\leq \cos(r+R)\cos(b) + \sin(r+R)\sin(R) \\
&\leq \cos(r+R)\cos(R) + \sin(r+R)\sin(R) \\
&= \cos r,
\end{aligned} \tag{3.29}$$

with strict inequalities unless $\theta_{\Lambda_+} = 0$.

[9] Clearly if $\Lambda_+ < 0$ then $\Lambda_+ < 1$ and 1 can serve as Λ_+.

With the Topogonov comparison theorem this implies that there is but a single point of $\exp_{x,M}^{-1}(\partial B(p_c, r))$ on $T_{\exp_{x,M}^{-1}(z)}(S)$, namely $\exp_{x,M}^{-1}(z)$ itself. This then yields that the outward pointing part of the gradient in the radial direction may be bounded from below by $R|\mu_+|$.

We can now combine the bounds on the outward and inward pointing contributions to the gradient in this lemma

Lemma 3.4.8 *The gradient of P_M is pointing outward on the boundary of the geodesic ball $B(p_c, r + R)$, if*

$$R|\mu_+| - (2r + R)|\mu_-| > 0.$$

Combining the results

We can now state the result of our investigations in one theorem:

Theorem 3.4.9 *Let M be a manifold whose sectional curvature K is bounded, that is $\Lambda_- \leq K \leq \Lambda_+$. Let P_M the function on $B_\rho(c)$, a geodesic ball of radius ρ centred on c, defined by*

$$P_M(x) = \frac{1}{2} \int d_M(x, p)^2 \mathrm{d}\mu(p), \tag{3.15}$$

where the support of μ is contained in $B_r(c)$ and we write $R + r = \rho$. Using the notation

$$\mathrm{d}\mu_+ = 1_{\{\mu>0\}}\mathrm{d}\mu, \qquad |\mu_+| = \left| \int \mathrm{d}\mu_+ \right|$$
$$\mathrm{d}\mu_- = 1_{\{\mu<0\}}\mathrm{d}\mu, \qquad |\mu_-| = \left| \int \mathrm{d}\mu_- \right|,$$

we are now able give conditions on ρ depending on the curvature bounds Λ_- and Λ_+:

- *ρ is less than half the injectivity radius,*
- *if* $0 < \Lambda_- \leq \Lambda_+$

$$\frac{\frac{2\rho}{k_l}}{\tan \frac{2\rho}{k_l}} |\mu_+| - |\mu_-| > 0,$$

- *if* $\Lambda_- \leq 0 \leq \Lambda_+$

$$\frac{\frac{2\rho}{k_l}}{\tan \frac{2\rho}{k_l}} |\mu_+| - \frac{\frac{2\rho}{k_u}}{\tanh \frac{2\rho}{k_u}} |\mu_-| > 0,$$

- *if* $\Lambda_- \leq \Lambda_+ \leq 0$

$$|\mu_+| - \frac{\frac{2\rho}{k_u}}{\tanh \frac{2\rho}{k_u}} |\mu_-| > 0,$$

-

$$R|\mu_+| - (2r + R)|\mu_-| > 0$$

If these conditions are met then P_M *has a unique minimum in* B_ρ.

3.5 Non-degeneracy criteria

In this section we exploit Proposition 3.2.5 to establish geometric criteria that ensure that a Riemannian simplex is non-degenerate. In Section 3.2.3 we worked in an arbitrary coordinate chart $\phi : M \supset W \to \mathbb{R}^n$, where the convex ball B_ρ containing $\boldsymbol{\sigma}_M$ is contained in W. Now we will choose ϕ to be the inverse of the exponential map at some point $p \in B_\rho$. Specifically, we set $\phi = u \circ \exp_p^{-1} : W \to \mathbb{R}^m$, where $u : T_pM \to \mathbb{R}^n$ is an arbitrary linear isometry. The coordinate function u serves to represent a generic point in $U = \phi(W)$. The Euclidean simplex $\tilde{\sigma}$ in the coordinate domain can now be identified with $\sigma(p)$, and we observe that $\exp_x \circ \exp_p^{-1}$ maps $\sigma(p)$ to $\sigma(x)$.

In Section 3.5.1 we review some properties of Euclidean simplices, including *thickness*, the quality measure that we use, and recall a lemma that bounds the difference in thickness between two simplices whose corresponding edge lengths are almost the same. Thus given an assumed thickness of $\sigma(p)$, the question of whether or not $\boldsymbol{\sigma}_M$ is degenerate becomes a question of how much the exponential transition function (3.2) distorts distances. In order to address this question, we exploit the Rauch comparison theorem, which we discuss in Section 3.5.2. We put these observations together in Section 3.5.3 to obtain explicit bounds on the required quality of $\sigma(p)$, relative to its size (longest edge length) and the sectional curvatures in B_ρ.

3.5.1 The stability of Euclidean simplex quality

A Euclidean simplex $\sigma = \{v_0, \ldots, v_k\} \subset \mathbb{R}^n$ has a number of geometric attributes. An i-face of σ is a subset of $i+1$ vertices, and a $(k-1)$ face of a k-simplex is a *facet*. The facet of σ that does not have v_i as a vertex is denoted σ_{v_i}. The *altitude* of $v_i \in \sigma$ is the distance from v_i to the affine hull of σ_{v_i}, denoted $a_{v_i}(\sigma)$, and the longest edge length is denoted $L(\sigma)$. When there is no risk of confusion, we will simply write L, and a_i.

The simplex quality measure that we will use is the *thickness* of a k-simplex σ, defined as

$$t(\sigma) = \begin{cases} 1 & \text{if } k = 0 \\ \min_{v \in \sigma} \dfrac{a_v}{kL} & \text{otherwise.} \end{cases} \tag{3.30}$$

If $t(\sigma) = 0$, then σ is *degenerate*. We say that σ is t_0-thick, if $t(\sigma) \geq t_0$. If σ is t_0-thick, then so are all of its faces. We write t for the thickness if the simplex in question is clear.

As discussed in Section 3.2.3, we can associate a matrix P to a Euclidean simplex. The quality of a simplex σ is closely related to the quality of P, which can be quantified by means of its *singular values*. In fact, we are only interested

in the smallest and largest singular values. The smallest singular value, $s_k(P) = \inf_{|x|=1} |Px|$, vanishes if and only if the matrix P does not have full rank. The largest singular value is the same as the operator norm of P, i.e., $s_1(P) = \|P\| = \sup_{|x|=1} |Px|$. We have the following result [BDG13b, Lem. 2.4] relating the thickness of σ to the smallest singular value of P:

Lemma 3.5.1 (Thickness and singular value) *Let $\sigma = \{v_0, \dots, v_k\}$ be a non-degenerate k-simplex in $\mathbb{R}^n$, with $k > 0$, and let P be the $n \times k$ matrix whose i^{th} column is $v_i - v_0$. Then the i^{th} row of the pseudo-inverse $P^{-1}_{\text{left}} = (P^\mathsf{T} P)^{-1} P^\mathsf{T}$ is given by w_i^T, where w_i is orthogonal to $\mathrm{aff}(\sigma_{v_i})$, and*

$$|w_i| = a_i^{-1}.$$

We have the following bound on the smallest singular value of P:

$$s_k(P) \geq \sqrt{k} t L.$$

The appearance of the dimension k in the denominator in the definition of thickness is a convention introduced so that t provides a clean bound on the condition number of P: Since the columns of P have norm bounded by L, we have that $s_1(P) \leq \sqrt{k} L$, and thus Lemma 3.5.1 implies $\frac{s_1(P)}{s_k(P)} \leq t^{-1}$. Although we adhere to definition (3.30) in this work, we acknowledge that this normalisation convention may obscure the relationship between simplex quality and dimension. We frequently make use of the fact that for a k-simplex σ, we have $kt(\sigma) \leq 1$.

The crucial property of thickness for our purposes is its stability. If two Euclidean simplicies with corresponding vertices have edge lengths that are almost the same, then their thicknesses will be almost the same. This allows us to quantify a bound on the smallest singular value of the matrix associated with one of the simplices, given a bound on the other. To be precise, we have the following consequence of the more general Lemma 3.8.3 demonstrated in Section 3.8.1:

Lemma 3.5.2 (Thickness under distortion) *Suppose that $\sigma = \{v_0, \dots, v_k\}$ and $\tilde{\sigma} = \{\tilde{v}_0, \dots, \tilde{v}_k\}$ are two k-simplices in $\mathbb{R}^n$ such that*

$$||v_i - v_j| - |\tilde{v}_i - \tilde{v}_j|| \leq C_0 L(\sigma)$$

for all $0 \leq i < j \leq k$. Let P be the matrix whose i^{th} column is $v_i - v_0$, and define $\tilde{P}$ similarly.

If

$$C_0 = \frac{\eta t(\sigma)^2}{4} \qquad \text{with} \quad 0 \leq \eta \leq 1,$$

then

$$s_k(\tilde{P}) \geq (1 - \eta) s_k(P).$$

and

$$t(\tilde{\sigma}) \geq \frac{4}{5\sqrt{k}}(1-\eta)t(\sigma).$$

3.5.2 The Rauch Comparison Theorem

The Rauch comparison theorem gives us bounds on the norm of the differential of the exponential map. This in turn implies a bound on how much the exponential map can distort distances. It is called a comparison theorem because it is implicitly comparing the exponential map on the given manifold to that on a space of constant sectional curvatures. In this context we encounter the functions

$$\mathbf{S}_\kappa(r) = \begin{cases} (1/\sqrt{\kappa})\sin\sqrt{\kappa}r & \kappa > 0 \\ r & \kappa = 0 \\ (1/\sqrt{-\kappa})\sinh\sqrt{-\kappa}r & \kappa < 0, \end{cases}$$

parameterised by κ, which can be thought of as representing a constant sectional curvature.

The Rauch theorem can be found in Buser and Karcher [BK81, §6.4] or in Chavel [Cha06, Thm. IX.2.3], for example. In the statement of the theorem we implicitly use the identification between the tangent spaces of a tangent space and the tangent space itself.

Lemma 3.5.3 (Rauch theorem) *Radially the exponential map* $\exp_p : T_pM \to M$ *is an isometry:*

$$\left|(d\exp_p)_v v\right| = |v|.$$

Assume the sectional curvatures, K*, are bounded by* $\Lambda_- \leq K \leq \Lambda_+$*. Taking* $|v| = 1$*, one has for any* w *perpendicular to* v

$$\frac{\mathbf{S}_{\Lambda_+}(r)}{r}|w| \leq \left|(d\exp_p)_{rv} w\right| \leq \frac{\mathbf{S}_{\Lambda_-}(r)}{r}|w|.$$

The inequalities hold when $r < 2\rho_0$ *(defined in Equation* (3.3)*). Also, if* $\Lambda_- < 0$*, then the right inequality is valid for all* r*, and if* $\Lambda_+ > 0$*, then the left inequality is valid for all* r*.*

For convenience, we will use a bound on the absolute value of the sectional curvatures, rather than separate upper and lower bounds. Thus $|K| \leq \Lambda$, where $\Lambda = \max\{\Lambda_+, -\Lambda_-\}$. We use Taylor's theorem to obtain

$$\mathbf{S}_{-\Lambda}(r) \leq r + \frac{\Lambda r^3}{2} \qquad \text{when } 0 \leq r < \frac{\pi}{2\sqrt{\Lambda}}$$

$$\mathbf{S}_{\Lambda}(r) \geq r - \frac{\Lambda r^3}{6} \qquad \text{for all } r \geq 0.$$

We can restate the Rauch theorem in a weaker, but more convenient form:

Lemma 3.5.4 *Suppose the sectional curvatures in M are bounded by $|K| \leq \Lambda$. If $v \in T_pM$ satisfies $|v| = r < \frac{\pi}{2\sqrt{\Lambda}}$, then for any vector $w \in T_v(T_pM) \cong T_pM$, we have*

$$\left(1 - \frac{\Lambda r^2}{6}\right)|w| \leq \left|(d\exp_p)_v w\right| \leq \left(1 + \frac{\Lambda r^2}{2}\right)|w|.$$

3.5.3 Non-degenerate Riemannian simplices

Our goal now is to estimate the metric distortion incurred when we map a simplex from one tangent space to another via the exponential maps

$$\exp_x^{-1} \circ \exp_p : T_pM \to T_xM,$$

and this is accomplished by the bounds on the differential. Specifically, if $F : \mathbb{R}^n \to \mathbb{R}^n$ satisfies $\|dF\| \leq \eta$, then the length of the image of the line segment between x and y provides an upper bound on the distance between $F(x)$ and $F(y)$:

$$|F(y) - F(x)| \leq \int_0^1 \left|dF_{x+s(y-x)}(y-x)\right| \, ds \leq \eta\,|y-x|. \tag{3.31}$$

If $x, p, y \in B_\rho$, with $y = \exp_p(v)$, then $|v| < 2\rho$, and $\left|\exp_x^{-1}(y)\right| < 2\rho$. Then, if $\rho < \rho_0$ given in Equation (3.3), Lemma 3.5.4 tells us that

$$\begin{aligned}\left\|d\left(\exp_x^{-1} \circ \exp_p\right)_v\right\| &\leq \left\|\left(d\exp_x^{-1}\right)_y\right\| \left\|\left(d\exp_p\right)_v\right\| \\ &\leq \left(1 + \frac{\Lambda(2\rho)^2}{3}\right)\left(1 + \frac{\Lambda(2\rho)^2}{2}\right) \\ &\leq 1 + 5\Lambda\rho^2.\end{aligned}$$

Therefore (3.31) yields

$$|v_i(x) - v_j(x)| \leq (1 + 5\Lambda\rho^2)\,|v_i(p) - v_j(p)|.$$

We can do the same argument the other way, so

$$|v_i(p) - v_j(p)| \leq (1 + 5\Lambda\rho^2)\,|v_i(x) - v_j(x)|,$$

and we find

$$\begin{aligned}\big|\,|v_i(x) - v_j(x)| - |v_i(p) - v_j(p)|\,\big| &\leq 5\Lambda\rho^2(1 + 5\Lambda\rho^2)\,|v_i(p) - v_j(p)| \\ &\leq 21\Lambda\rho^2\,|v_i(p) - v_j(p)| \qquad \text{when } \rho < \rho_0.\end{aligned} \tag{3.32}$$

Letting P be the matrix associated with $\sigma(p)$, and using $C_0 = 21\Lambda\rho^2$, in Lemma 3.5.2, we find that the matrix $\tilde{P}$ associated with $\sigma(x)$ in Proposition 3.2.5 is non-degenerate if $\sigma(p)$ satisfies a thickness bound of $t_0 > 10\sqrt{\Lambda}\rho$, and we have:

Theorem 3.1 *Suppose M is a Riemannian manifold with sectional curvatures K bounded by $|K| \leq \Lambda$, and $\boldsymbol{\sigma}_M$ is a Riemannian simplex, with $\boldsymbol{\sigma}_M \subset B_\rho \subset M$, where B_ρ is an open geodesic ball of radius ρ with*

$$\rho < \rho_0 = \min\left\{\frac{\iota_M}{2}, \frac{\pi}{4\sqrt{\Lambda}}\right\}.$$

Then $\boldsymbol{\sigma}_M$ is non-degenerate if there is a point $p \in B_\rho$ such that the lifted Euclidean simplex $\sigma(p)$ has thickness satisfying

$$t(\sigma(p)) > 10\sqrt{\Lambda}\rho.$$

The ball B_ρ may be chosen so that this inequality is necessarily satisfied if

$$t(\sigma(p)) > 10\sqrt{\Lambda}L(\boldsymbol{\sigma}_M),$$

where $L(\boldsymbol{\sigma}_M)$ is the geodesic length of the longest edge in $\boldsymbol{\sigma}_M$.

The last assertion follows from the remark at the end of Section 3.2.2: If $L(\boldsymbol{\sigma}_M) < \rho_0$, then $\boldsymbol{\sigma}_M$ is contained in a closed ball of radius $L(\boldsymbol{\sigma}_M)$ centred at one of the vertices.

Remark 3.5.5 *Using Proposition 3.7.7 and Lemma 3.7.1 of Section 3.7, we can replace Equation* (3.32) *with*

$$\big|\,|v_i(x) - v_j(x)| - |v_i(p) - v_j(p)|\,\big| \leq 6\Lambda\rho^2\,|v_i(p) - v_j(p)| \qquad \text{when } \rho < \frac{1}{2}\rho_0,$$

and we find, that the Riemannian simplex $\boldsymbol{\sigma}_M$ of Theorem 3.1 is non-degenerate if

$$t(\sigma(p)) > 5\sqrt{\Lambda}\rho,$$

but with the caveat that ρ must now satisfy $\rho \leq \frac{1}{2}\rho_0$.

Orientation In Euclidean space $\mathbb{E}^n$ we can define an orientation as an equivalence class of frames, two frames being equivalent if the linear transformation between them has a positive determinant. We can likewise associate an orientation to a (non-degenerate) Euclidean n-simplex $\sigma = \{v_0, \ldots, v_n\}$: it is the orientation associated with the basis $\{(v_i - v_0)\}_{i\in\{1,\ldots,n\}}$. The orientation depends on

how we have indexed the points. Any even permutation of the indices yields the same orientation.

In a manifold, we can assign an orientation locally, in a neighbourhood $U \subset M$ on which the tangent bundle admits a local trivialisation, for example. Then we can define an orientation by defining an orientation on T_pM for some $p \in U$. If $\sigma = \{p_0, \ldots, p_n\} \subset U$ defines a non-degenerate Riemannian simplex, then we can associate an orientation to that simplex: it is the orientation of $\sigma(p_0) \subset T_{p_0}M$. Again, we will get agreement on the orientation if we perform any even permutation of the vertex indices. The reason is that our non-degeneracy assumption implies that the orientation of $\sigma(p_i)$ will agree with the orientation of $\sigma(p_j)$ for any $i, j \in \{0, \ldots, n\}$.

In the particular case discussed in this section, where $\phi = u \circ \exp_p^{-1}$, for $p \in B_\rho$, the barycentric map $b : \boldsymbol{\sigma}_{\mathbb{E}}(p) \to \boldsymbol{\sigma}_M$ is orientation preserving. Since $\exp_x^{-1} \circ \exp_y$ is orientation preserving for any $x, y \in B_\rho$, it is enough to consider the case where $p = p_0 \in \sigma$. Consider Equation (3.10):

$$(db)_{v_0(p_0)} = -\left(\nabla_x \nu\right)^{-1} \partial_u \nu_{v_0(p_0)}.$$

By Equation (3.12), we have $(\partial_u \nu)_{v_0(p_0)} = -\operatorname{Id}$. Also, it follows from Lemma 3.2.3 that $\nabla^M \nu$ has positive determinant. (Buser and Karcher [BK81, p.132] show that $\nabla^M \nu$ is bounded near the identity), and thus so must db everywhere, since it does not vanish on its domain.

3.6 The Toponogov point of view

In this section we discuss an approach for finding conditions that guarantee that a Riemannian simplex is non-degenerate, that is diffeomorphic to the standard simplex. It is based on the Toponogov comparison theorem, instead of Rauch's theorem (which used in Section 3.5).

The Toponogov comparison theorem, discussed in Section 3.3, says the following: Let M be an n-dimensional manifold, whose sectional curvature K is bounded from above by Λ_+ and from below by Λ_-, that is $\Lambda_- \leq K \leq \Lambda_+$. We now have to distinguish two settings:

- Suppose there is a geodesic triangle in M of which we know the lengths of the three geodesics, then the angles of the triangle are bounded by the angles for a geodesic triangle in a simply connected space of constant curvature Λ_- or Λ_+ whose geodesics have the same lengths.
- Suppose we are given lengths of two geodesics edges and the enclosed angle in a geodesic triangle in M, then the length of the third geodesic is bounded by the lengths of the third geodesic in a geodesic triangle with the same lengths for two geodesics and the same enclosed angle in a simply connected space of constant curvature Λ_- or Λ_+.

Remark 3.6.1 *Note that in this section we shall assume $\Lambda_+ = \Lambda$ and $\Lambda_- = -\Lambda$, with $\Lambda > 0$ to simplify the proof. More precise estimates that do not use this simplification are treated in Section 3.10.*

With the Toponogov comparison theorem we can prove the following statement:

Theorem 3.6.6 *Let $v_0, \ldots, v_n$ be a set of vertices lying in a Riemannian manifold M, whose sectional curvatures are bounded in absolute value by Λ, within a convex geodesic ball of radius D centred at any one of the vertices (v_r) and such that $\sqrt{\Lambda}D < 1/2$. If $\sigma^{\mathbb{E}}(v_r)$, the convex hull of $(\exp_{v_r}^{-1}(v_i))_{i=0}^n = (v_i(v_r))_{i=0}^n$ in $T_{v_r}M$, satisfies*

$$\left(\frac{n!\mathrm{vol}(\sigma^{\mathbb{E}}(v_r))}{(n+1)(2D)^n}\right)^2 > \tfrac{25}{24} n\Lambda D^2, \tag{3.43}$$

then the Riemannian simplex with vertices $v_0, \ldots, v_n$ is non-degenerate, that is diffeomorphic to the standard n-simplex.

The fraction

$$\frac{\mathrm{vol}(\sigma^{\mathbb{E}}(v_r))}{(D)^n}$$

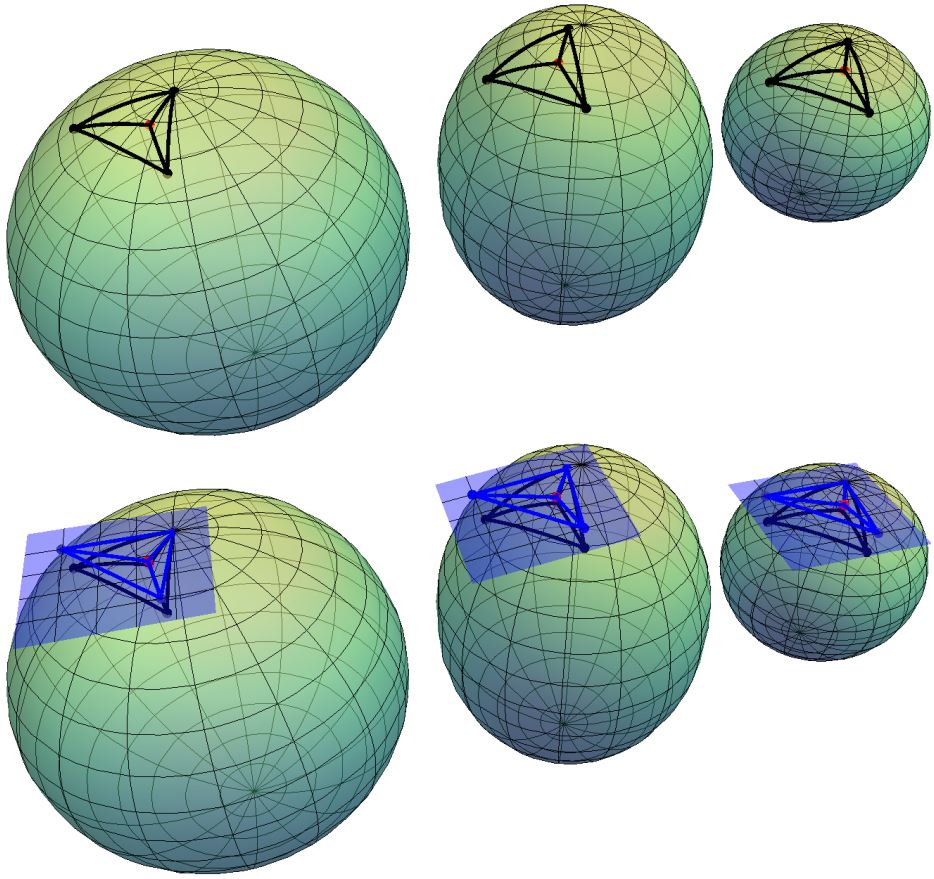

Figure 3.6: Pictorial overview of our approach: Given any point (red) and some vertices (black) we can first compare the angles between the geodesics at the red point on a surface of arbitrary bounded curvature (the ellipsoid in the middle) to the angles in the space of constant curvature. In these spaces of constant curvature, study the simplex by lifting to the tangent space at one of the vertices by the exponential map (bottom figure).

is also referred to as the thickness of $\sigma^{\mathbb{E}}(v_r)$. The thickness is a quality measure that indicates how close the (Euclidean) simplex $\sigma^{\mathbb{E}}(v_r)$ is to degeneracy.

The proof of Theorem 3.6.6 relies the following observation: If for all x within a convex geodesic ball of radius D centred at one of the vertices there are n tangents to geodesics emanating from x to some subset of the vertices (the choice

of subset does depend on x) that are linearly independent, then the Riemannian simplex is non-degenerate. This statement is proven in Section 3.6.2.

The linear independence of n tangent vectors to geodesics emanating from x is equivalent with $n+1$ tangent vectors being affinely independent. This is a direct consequence of the following; for a point x in a Riemannian simplex with barycentric coordinates λ_i we have $\sum \lambda_i v_i(x) = 0$, with $\sum \lambda_i = 1$. Remember that we write $v_i(x) = \exp_x^{-1}(v_i)$.

Establishing linear independence is more involved. The steps we use we shall outline now.

Overview of the proof of Theorem 3.6.6

As stated in Theorem 3.6.6 we assume that a set of points $\{v_0, \ldots, v_n\}$ in a convex ball centred on v_r in M is given. The sectional curvatures K of M are bounded, that is $|K| \leq \Lambda$. We think of the points $v_0, \ldots, v_n$ as vertices of the Riemannian simplex. The point x is an arbitrary point in the convex ball that contains the vertices. It is quality of the simplex ($\sigma^{\mathbb{E}}(v_r)$) found by taking the convex hull of the image of $v_0, \ldots, v_n$ under the inverse exponential map $\exp_{v_r}^{-1}$ that is used in the conditions for non-degeneracy of the Riemannian simplex.

To give the conditions in Theorem 3.6.6 we started with $\exp_{v_r}^{-1}(x), \exp_{v_r}^{-1}(v_0), \ldots, \exp_{v_r}^{-1}(v_n)$ and use the following steps:

1. Use the Toponogov comparison theorem to bound the difference between the lengths of the geodesics connecting vertices v_i and v_j and the lengths of the geodesics connecting vertices x and v_i on the one hand and the corresponding (via the map $\exp_{\mathbb{H}(\pm\Lambda)} \circ \exp_{v_r}^{-1}$) lengths of geodesics on spaces of constant curvature $\mathbb{H}(\pm\Lambda)$ on the other.

2. Prove that the lengths of these geodesics are not far from what one would expect in the Euclidean case (via the map $\exp_M^{-1}$) if the vertices and x lie close together relative to the bounds on the sectional curvature on M.

3. Given these approximate lengths of the geodesics we again use the Toponogov comparison theorem and explicit calculations on spaces of constant curvature to give estimates on the difference between the inner products between tangents to the geodesics from x to the vertices and the expectation in the Euclidean case.

4. $n \times n$ of these inner products between the tangents of geodesics from x to the vertices are put into a single Gram matrix. The determinant of this matrix is non-zero if and only if the tangents to the geodesics emanating from x are linearly independent. A result by Friedland describes the behaviour of the determinant under perturbations of the entries. This means

that the determinant of the Gram matrix is close to the determinant of the Gram matrix one expects in the Euclidean case, to be precise the matrix with entries $(\exp_{v_r}^{-1}(v_i) - \exp_{v_r}^{-1}(x)) \cdot (\exp_{v_r}^{-1}(v_l) - \exp_{v_r}^{-1}(x))$. This allows us to give conditions that guarantee that there are n tangents to the geodesics emanating from x that are linearly independent, based on the quality of the simplex you would expect in the Euclidean case ($\sigma^{\mathbb{E}}(v_r)$).

5. If for every x in a sufficiently large convex neighbourhood some n tangents to the geodesics emanating from x and going to the vertices are linearly independent the simplex is non-degenerate.

This approach puts the emphasis on the geodesics as apposed to barycentric coordinate functions, which provides us with a very concrete geometric picture, as given in Figure 3.6.

3.6.1 Preliminaries

The second step described in the introduction will use the Toponogov Comparison Theorem 3.3.2. In particular, we use this result and some calculations on spaces of constant curvature to provide bounds on the inner product between the vectors tangent to geodesics emanating from a point $x \in \sigma_M$ to n (that is all but one) of the vertices of σ_M. These bounds are then used to show that the Gram matrix associated with these vectors is non-singular. Here we discuss Gram matrices, bounds on determinants and do some calculations concerning geodesic triangles on spaces of constant curvature.

Gram matrices

Gram matrices can be applied to general finite dimensional inner product spaces with inner product G. We shall denote the inner product space by $\mathbb{R}^n_G$. If the inner product is the Euclidean inner product on the standard basis $G_{ij} = \delta_{ij}$, where δ_{ij} denotes the Kronecker delta, we shall write $\mathbb{R}^n_{\delta_{ij}} = \mathbb{E}^n$. Below these inner product space will be the tangent spaces (T_xM) of Riemannian manifolds with inner product $g(x)$. For a space with inner product G and with regard to any basis we have

$$\det(\langle w_i, w_j \rangle_G) = \det(G) \det(w_1, \ldots, w_n)^2,$$

where $w_1, \ldots, w_n \in \mathbb{R}^n_G$, and $(w_1, \ldots, w_n)$ denotes the matrix with w_i as columns. Note that the Gram determinant in any metric is nonzero if and only if $\{w_1, \ldots, w_n\}$ is a linearly independent system. One can already think of the vectors w_i as the

tangent vectors $w_i = v_i(x) = \exp_x^{-1}(v_i)$ discussed in the introduction. This can be seen by taking the determinant of

$$(\langle w_i, w_j \rangle_G) = (w_1, \ldots, w_n)^t (G)(w_1, \ldots, w_n).$$

Bounds on determinants

The following result by Friedland [Fri82], see also Bhatia and Friedland [BF81], Ipsen and Rehman [IR08] and Bhatia [Bha97] problem I.1.6, will be essential to some estimates below:

$$|\det(A+E) - \det(A)| \leq n \max\{\|A\|_p, \|A+E\|_p\}^{n-1} \|E\|_p \tag{3.33}$$

where A and E are $n \times n$-matrices and $\|\cdot\|_p$ is the p-norm, with $1 \leq p \leq \infty$, for linear operators:

$$\|A\|_p = \max_{x \in \mathbb{R}^n} \frac{|Ax|_p}{|x|_p},$$

with $|\cdot|_p$ the p-norm on $\mathbb{R}^n$. In our context A will be the reduced Gram matrix for the Euclidean case and E the matrix with the small angle deviations from the Euclidean case (or rather the deviations of their cosines) due to the local geometry, of which each entry is bounded by some ϵ.
From (3.33) we see that in this particular context

$$\begin{aligned} |\det(A+E)| &\geq |\det A| - n(\max\{\|A\|_\infty, \|A+E\|_\infty\})^{n-1} \|E\|_\infty \\ &\geq |\det(A)| - n\epsilon, \end{aligned} \tag{3.34}$$

where we use that every entry of A and $A+E$ is bounded in absolute value by 1 because they are reduced Gram matrices, a matrices of cosines.

Geodesic triangles on spaces of constant curvature

We now prove two lemmas for geodesic triangles in a space of constant curvature. In the following we use the notation $c^{\mathbb{E}}$ to denote the length of the (Rauch) edge closing a hinge with lengths a and b and enclosed angle γ in Euclidean space. This means that

$$(c^{\mathbb{E}})^2 = a^2 + b^2 - 2ab\cos\gamma.$$

In general we will use the superscript $\mathbb{E}$ to indicate (comparisons to) Euclidean space.

Lemma 3.6.2 *Let M be a space of constant (sectional) curvature K. As in Section 3.3 we write $k = 1/\sqrt{|K|}$. Suppose that a and b are two of the edge-lengths of a hinge in M satisfying:*

$$a, b \leq d_{max}/2 \qquad\qquad d_{max}/k < 1/2. \tag{3.35}$$

Here d_{max} is a bound on the lengths of the geodesics in the space of constant curvature. Under these conditions the length of the (Rauch) edge of the hinge c satisfies

$$c^2 = (c^{\mathbb{E}})^2 + E', \tag{3.36}$$

with $|E'| \leq 5d_{max}^4/(3k^2)$. The geometric interpretation of E' is a measure for the deviation from the Euclidean case. Alternatively, (3.36) *with said bound on $|E'|$ holds if the condition* (3.35) *is substituted by*

$$a, b, c \leq d_{max} \qquad\qquad d_{max}/k < 1/2.$$

Proof Taylor's theorem implies

$$\sin(\phi) = \phi(1 + \tilde{E}_s(\phi)) \qquad \cos(\phi) = 1 - \frac{1}{2}\phi^2 + E_c(\phi)$$
$$\sinh(\phi) = \phi(1 + \tilde{E}_{sh}(\phi)) \qquad \cosh(\phi) = 1 + \frac{1}{2}\phi^2 + E_{ch}(\phi),$$

here E stands for the error. The subscripts s, sh, c and ch refer to the $\sin$, $\sinh$, $\cos$ and $\cosh$ functions. The 'errors' are bounded; if we assume that $\phi \leq \phi_m < 1$ we have

$$|\tilde{E}_s(\phi)| \leq \frac{1}{3!}\phi_m^2 \qquad |E_c(\phi)| \leq \frac{1}{4!}\phi_m^4$$
$$|\tilde{E}_{sh}(\phi)| \leq \frac{1}{3!}\frac{8}{7}\phi_m^2 \qquad |E_{ch}(\phi)| \leq \frac{1}{4!}\frac{8}{7}\phi_m^4.$$

Trivially these bounds can be weakened to

$$|\tilde{E}_s(\phi)| \leq \frac{1}{3!}\frac{8}{7}\phi_m^2 \qquad |E_c(\phi)| \leq \frac{1}{4!}\frac{8}{7}\phi_m^4$$
$$|\tilde{E}_{sh}(\phi)| \leq \frac{1}{3!}\frac{8}{7}\phi_m^2 \qquad |E_{ch}(\phi)| \leq \frac{1}{4!}\frac{8}{7}\phi_m^4.$$

It is convenient to use these weaker bounds as this affords a universal approach. We therefore drop the subscript from $E_c(\phi)$ and $E_{ch}(\phi)$ and $\tilde{E}_s(\phi)$ and $\tilde{E}_{sh}(\phi)$ and write $E(\phi)$ and $\tilde{E}(\phi)$ respectively. So for example $E(\phi)$ can mean either $E_c(\phi)$ or $E_{ch}(\phi)$, but the choice does not matter because we use the weaker bounds.

We define

$$\phi_1 = a/k \qquad \phi_2 = b/k \qquad \phi_3 = c/k \qquad \phi_m = d_{\max}/k.$$

Using these the cosine rules, see Section 3.3 in particular (3.13) and (3.14), read

$$\begin{aligned} \cos\phi_3 &= \cos\phi_1\cos\phi_2 + \sin\phi_1\sin\phi_2\cos\gamma && \text{(elliptic)} \\ \cosh\phi_3 &= \cosh\phi_1\cosh\phi_2 - \sinh\phi_1\sinh\phi_2\cos\gamma && \text{(hyperbolic).} \end{aligned}$$

We shall now bound ϕ_3, assuming ϕ_1, ϕ_2 and γ given. Because $\phi_1, \phi_2 \leq \phi_m/2 < 1/4$ we have that $\phi_3 \leq \phi_m$ by the triangle inequality. We find

$$\begin{aligned} \frac{1}{2}\phi_3^2 + E(\phi_3) = \frac{1}{2}\phi_1^2 + \frac{1}{2}\phi_2^2 + \frac{1}{4}\phi_1^2\phi_2^2 + E(\phi_1) + E(\phi_2) + \frac{1}{2}E(\phi_1)\phi_2^2 + \frac{1}{2}E(\phi_2)\phi_1^2 \\ + E(\phi_1)E(\phi_2) - \phi_1\phi_2\cos\gamma - \phi_1\phi_2\cos\gamma(\tilde{E}(\phi_1) + \tilde{E}(\phi_2) + \tilde{E}(\phi_1)\tilde{E}(\phi_2)) \end{aligned}$$

and thus

$$\begin{aligned} E'(\phi_1,\phi_2,\phi_3) =& \phi_3^2 - \left(\phi_1^2 + \phi_2^2 - 2\phi_1\phi_2\cos\gamma\right) \\ =& + \frac{1}{2}\phi_1^2\phi_2^2 + 2E(\phi_1) + 2E(\phi_2) + E(\phi_1)\phi_2^2 + E(\phi_2)\phi_1^2 \\ & + 2E(\phi_1)E(\phi_2) - 2\phi_1\phi_2\cos\gamma(\tilde{E}(\phi_1) \\ & + \tilde{E}(\phi_2) + \tilde{E}(\phi_1)\tilde{E}(\phi_2)) - E(\phi_3) \end{aligned} \tag{3.37}$$

satisfies

$$\begin{aligned} |E'(\phi_1,\phi_2,\phi_3)| \leq& |\tfrac{1}{2}\phi_1^2\phi_2^2 + 2E(\phi_1) + 2E(\phi_2) + E(\phi_1)\phi_2^2 + E(\phi_2)\phi_1^2 \\ & + 2E(\phi_1)E(\phi_2) - 2\phi_1\phi_2\cos\gamma(\tilde{E}(\phi_1) + \tilde{E}(\phi_2) \\ & + \tilde{E}(\phi_1)\tilde{E}(\phi_2)) - E(\phi_3)| \\ \leq& |\tfrac{1}{2}\phi_1^2\phi_2^2| + 2|E(\phi_1)| + 2|E(\phi_2)| + \tfrac{1}{2^2}|E(\phi_1)| + \tfrac{1}{2^2}|E(\phi_2)| \\ & + \tfrac{8}{7}\tfrac{1}{4!}\tfrac{1}{2^4}|E(\phi_1)| + 2|\phi_1\phi_2||\tilde{E}(\phi_1)| + 2|\phi_1\phi_2||\tilde{E}(\phi_2)| \\ & + 2\tfrac{8}{7}\tfrac{1}{3!}\tfrac{1}{2^2}|\phi_1\phi_2||\tilde{E}(\phi_2)| + |E(\phi_3)| \\ =& |\tfrac{1}{2}\phi_1^2\phi_2^2| + \left(2 + \tfrac{1}{4} + \tfrac{8}{7}\tfrac{1}{4!}\tfrac{1}{2^4}\right)|E(\phi_1)| + \left(2 + \tfrac{1}{4}\right)|E(\phi_2)| \\ & + 2|\phi_1\phi_2||\tilde{E}(\phi_1)| + 2\tfrac{8}{7}\tfrac{1}{3!}\tfrac{1}{2^2}|\phi_1\phi_2||\tilde{E}(\phi_2)| \\ & + 2|\phi_1\phi_2||\tilde{E}(\phi_2)| + |E(\phi_3)| \\ \leq& \tfrac{1}{2}\phi_m^4 + \left(5 + \tfrac{1}{2} + \tfrac{8}{7}\tfrac{1}{4!}\tfrac{1}{2^4}\right)\tfrac{8}{7}\tfrac{1}{4!}\phi_m^4 + \tfrac{8}{7}\tfrac{1}{3!}\left(4 + 2\tfrac{8}{7}\tfrac{1}{3!}\tfrac{1}{2^2}\right)\phi_m^4 \\ =& \tfrac{1209}{784}\phi_m^4 \\ \leq& \tfrac{5}{3}\phi_m^4. \end{aligned} \tag{3.38}$$

So we see that

$$\left|\frac{c^2}{k^2} - \left(\frac{a^2}{k^2} + \frac{b^2}{k^2} - 2\frac{ab}{k^2}\cos\gamma\right)\right| = \left|\frac{c^2}{k^2} - \frac{(c^{\mathbb{E}})^2}{k^2}\right| \leq \tfrac{5}{3}\frac{d_{\max}^4}{k^4}.$$

□

We now study a geodesic triangle in a simply connected space of constant curvature for which we have some estimates on the edge-lengths. To be precise we assume that the edges of the geodesic triangle are themselves the closing (Rauch) edges of some hinges. If we use the same notation as in Lemma 3.6.2 for the edge lengths, that is a, b and c, then all these lengths are assumed to be close to $a^{\mathbb{E}}$, $b^{\mathbb{E}}$ and $c^{\mathbb{E}}$. We shall think of $a^{\mathbb{E}}$, $b^{\mathbb{E}}$ and $c^{\mathbb{E}}$ as coming from a comparison to a Euclidean setting.

We shall also assume that the conditions of Lemma 3.6.2 are satisfied on the geodesic triangle with edge lengths a, b and c. We now shall prove that the angles of the geodesic triangle with edge lengths a, b and c in the space of constant curvature are close to the angles of the triangle with edge lengths $a^{\mathbb{E}}$, $b^{\mathbb{E}}$ and $c^{\mathbb{E}}$ in Euclidean space. To help make this precise we define for any lengths $a^{\mathbb{E}}$, $b^{\mathbb{E}}$ and $c^{\mathbb{E}}$ that satisfy the triangle inequality , the angle $\alpha^{\mathbb{E}}$ by

$$\cos\alpha^{\mathbb{E}} = \frac{(b^{\mathbb{E}})^2 + (c^{\mathbb{E}})^2 - (a^{\mathbb{E}})^2}{2b^{\mathbb{E}}c^{\mathbb{E}}}.$$

Lemma 3.6.3 *If M is a space of constant sectional curvature and the edge-lengths (a, b, c) of a geodesic triangle in M satisfy*

$$(a/k)^2 = (a^{\mathbb{E}}/k)^2 + E_1, \quad (b/k)^2 = (b^{\mathbb{E}}/k)^2 + E_2, \quad (c/k)^2 = (c^{\mathbb{E}}/k)^2 + E_3, \tag{3.39}$$

with $E_1, E_2, E_3 \leq 5d_{max}^4/(3k^4)$, and

$$a, b, c < d_{max}, \tag{3.40}$$

then

$$|bc\cos\alpha - b^{\mathbb{E}}c^{\mathbb{E}}\cos\alpha^{\mathbb{E}}| \leq \frac{25}{6}\frac{d_{max}^4}{k^2}. \tag{3.41}$$

Proof To avoid having to drag along the $1/k$ we shall write $\phi_1 = a/k$, $\phi_1^{\mathbb{E}} = a^{\mathbb{E}}/k$ et cetera. Using the Lemma 3.6.2 we see that ϕ_1, ϕ_2, ϕ_3 satisfy

$$(\phi_1)^2 = (\phi_2)^2 + (\phi_3)^2 - 2\phi_2\phi_3\cos\alpha + E_4,$$

with $|E_4| \leq 5d_{\max}^4/(3k^2)$. Performing a calculation similar to the one in Lemma 3.6.2 we find that

$$\begin{aligned}
|\phi_2\phi_3\cos\alpha - \phi_2^{\mathbb{E}}\phi_3^{\mathbb{E}}\cos\alpha^{\mathbb{E}}| &= |\phi_2\phi_3\cos\alpha - \tfrac{1}{2}((\phi_2^{\mathbb{E}})^2 + (\phi_3^{\mathbb{E}})^2 - (\phi_1^{\mathbb{E}})^2)| \\
&= \tfrac{1}{2}|\phi_2^2 + \phi_3^2 - \phi_1^2 - (\phi_2^{\mathbb{E}})^2 - (\phi_3^{\mathbb{E}})^2 + (\phi_1^{\mathbb{E}})^2 + 2E_4| \\
&= \tfrac{1}{2}|E_1 + E_2 + E_3 + 2E_4| \\
&\leq \tfrac{1}{2}(|E_1| + |E_2| + |E_3| + 2|E_4|) \\
&\leq \tfrac{25}{6}\phi_m^4
\end{aligned}$$

So we see that

$$\left|\frac{bc}{k^2}\cos\alpha - \frac{b^{\mathbb{E}}c^{\mathbb{E}}}{k^2}\cos\alpha^{\mathbb{E}}\right| \leq \frac{25}{6}\frac{d_{\max}^4}{k^4}.$$

□

3.6.2 Relation with linear independence

A Euclidean simplex is non-degenerate if and only if for any point x in Euclidean space we can find n vertices such that the vectors from x to the vertices are linearly independent. Linear independence likewise plays an important role in the definition of a non-degenerate Riemannian simplex. We remind ourselves, see Section 3.2.2, that a Riemannian simplex σ_M is *non-degenerate* if the barycentric coordinate map $\mathbf{\Delta}^n \to \sigma_M$ is a smooth embedding.

Lemma 3.6.4 *If for any x in the image of the map given in Definition 3.2.4 (σ_M) there are n tangents to geodesics connecting this point x to some subset of the vertices $v_0, \ldots, v_{j-1}, v_{j+1}, \ldots, v_n$ (this choice does depend on x) that are linearly independent then*

- *The map $\mathbf{\Delta}^n \to \sigma_M$ is bijective*
- *The inverse of $\mathbf{\Delta}^n \to \sigma_M$ is smooth*

In the proof we shall need the following observation: Within any ball smaller than the injectivity radius containing v_i, the vector field $v_i(x) = \exp_x^{-1}(v_i)$ depends smoothly on the point x for all $x \neq v_i$. This is obvious if we consider Riemannian normal coordinates at v_i. The geodesic between x and origin (v_i) is a straight line, that depends smoothly on x. The same holds for the tangent to the geodesic at x, this is precisely $v_i(x) = \exp_x^{-1}(v_i)$.

Proof We now prove the first of our claims by contradiction. Let us assume that

$$\sum \lambda_i v_i(x) = \sum \tilde{\lambda}_i v_i(x) = 0$$

for some $\lambda, \tilde{\lambda} \in \mathbf{\Delta}^n$, $\lambda \neq \tilde{\lambda}$. Because $v_0(x), \ldots, v_{j-1}(x), v_{j+1}(x), \ldots, v_n(x)$ are assumed to be linearly independent we have $\lambda_j \neq 0, \tilde{\lambda}_j \neq 0$. This means that we can solve for v_j in both cases, so

$$\begin{aligned}\frac{\lambda_0}{\lambda_j} v_0(x) + \ldots + \frac{\lambda_{j-1}}{\lambda_j} v_{j-1}(x) + \frac{\lambda_{j+1}}{\lambda_j} v_{j+1}(x) + \ldots + \frac{\lambda_n}{\lambda_j} v_n(x) = \\ \frac{\tilde{\lambda}_0}{\tilde{\lambda}_j} v_0(x) + \ldots + \frac{\tilde{\lambda}_{j-1}}{\tilde{\lambda}_j} v_{j-1}(x) + \frac{\tilde{\lambda}_{j+1}}{\tilde{\lambda}_j} v_{j+1}(x) + \ldots + \frac{\tilde{\lambda}_n}{\tilde{\lambda}_j} v_n(x).\end{aligned}$$

This contradicts the assumption of linear independence. This establishes injectivity.

We can use a similar argument to show that the inverse of $\mathbf{\Delta}^n \to \sigma_M$ is smooth. As we have seen linear independence implies that $\lambda_j \neq 0$, which means that we have

$$\lambda_0 v_0(x) + \ldots + \lambda_{j-1} v_{j-1}(x) + \lambda_{j+1} v_{j+1}(x) + \ldots + \lambda_n v_n(x) = -\lambda_j v_j(x).$$

We can now regard the left hand side as the product of the matrix with columns $(v_i(x))_{i \neq j}$ with the vector $(\lambda_i)_{i \neq j}$. We can divide by $-\lambda_j$ and bring the matrix to the right hand side by inverting, because $\{v_i(x)\}_{i \neq j}$ is a linear independent set this is possible. We now find

$$(v_0(x), \ldots, v_{j-1}(x), v_{j+1}(x), \ldots v_n(x))^{-1} v_j(x) = \frac{1}{\lambda_j}(\lambda_0, \ldots, \lambda_{j-1}, \lambda_{j+1}, \ldots, \lambda_n)^t,$$

which is smooth because $v_i(x)$ is smooth and $\{v_i(x)\}_{i \neq j}$ are linear independent by assumption. □

In Lemma 3.6.4 we refer to points lying in σ_M, because σ_M is not so easy to determine a priori, we will need to determine a neighbourhood that contains σ_M where we can determine linear independence. To this end we observe the following:

Remark 3.6.5 *σ_M lies within a ball centred at any of the vertices v_r of radius D, where $D = \max d_M(v_i, v_r)$, provided D is smaller than the injectivity radius and the ball is convex.*

Karcher [Kar77] (see also Section 3.4) noted that the centre of mass of any mass distribution is contained in any convex set that contains the support of the mass distribution, so in particular this ball.

3.6.3 Determining linear independence

In the previous subsection we established that if for any point $x \in \sigma_M$ there are n tangents to geodesics connecting this point to some subset of the vertices $v_0, \ldots, v_{j-1}, v_{j+1}, \ldots, v_n$ (depending on x) are linearly independent, then the simplex σ_M is well defined. In this subsection we shall formulate conditions on the vertex set $v_0, \ldots, v_n$ such that we can guarantee linear independence. These conditions are simple for surfaces. For higher dimensional manifolds we shall need bounds on the quality of the simplex found by taking the convex hull of the image of the inverse exponential map at one of the vertices. The quality of the simplex is considered good if the ratio between the volume of the simplex and the n^{th} power of the largest edge length is large, which we shall make precise in Theorem 3.6.6, see also [Whi57, BDG13a].

As mentioned, linear dependence for surfaces is easy to determine. Let us suppose $v_0(x) = \exp_x^{-1}(v_0)$, $v_1(x)$, $v_2(x)$ do not span T_xM. Because M is a surface it follows that $v_0(x)$, $v_1(x)$, $v_2(x)$ are co-linear. This is in turn equivalent to v_0, v_1 and v_2 lying on a geodesic. Using lemma 3.6.4 we find that σ_M is diffeomorphic to the standard simplex if all three vertices do not lie on a geodesic. In the two dimensional setting bijection has been argued previously by Rustamov [Rus10].

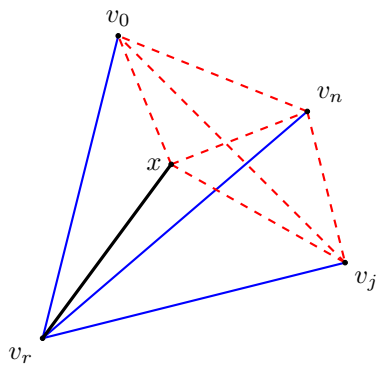

Figure 3.7: A schematic depiction of $\sigma^{\mathbb{E}}(v_r)$, where we use red dashed lines to indicate that these lengths of these edges are not equal to the lengths of the corresponding edges in σ_M.

Returning to manifolds of arbitraty dimension, we discuss conditions such that for any point x in a ball of radius D centred at the vertex v_r, the vectors $v_i(x)$ in the tangent space at x form an affinely independent set. Because of Remark 3.6.5 this is the neighbourhood of interest, because it suffices to show independ-

ence here. Assume that the sectional curvatures K of M are bounded in absolute value: $|K| \leq \Lambda$. Define $\sigma^{\mathbb{E}}(v_r)$ to be the convex hull of $(v_i(v_r))_{i=0}^n$ in $T_{v_r}M$. It will be on $\sigma^{\mathbb{E}}(v_r)$ that we impose conditions to ensure that the Riemannian simplex σ_M in non-degenerate. Note that given $\sigma^{\mathbb{E}}(v_r)$ we in particular have the lengths of all geodesics from v_r to v_i and the angles between their tangents. Using the Toponogov comparison theorem, we bound $d_M(x, v_i)$ for each i by means of Rauch hinges in $\mathbb{H}^n(\Lambda)$ and $\mathbb{H}^n(-\Lambda)$ the lengths of the closing edges of the hinges are denoted by $d_{\mathbb{H}^n(\Lambda)}(x^{\mathbb{H}^n(\Lambda)}, v_i^{\mathbb{H}^n(\Lambda)})$ and $d_{\mathbb{H}^n(-\Lambda)}(x^{\mathbb{H}^n(-\Lambda)}, v_i^{\mathbb{H}^n(-\Lambda)})$, where $y^{\mathbb{H}^n(\pm\Lambda)}$ is the point corresponding (via $\exp_{\mathbb{H}^n(\pm\Lambda)} \circ \exp_{v_r,M}^{-1}$) to y on the space constant curvature. Lemma 3.6.2 implies that

$$(d_{\mathbb{H}^n(\pm\Lambda)}(x^{\mathbb{H}^n(\pm\Lambda)}, v_i^{\mathbb{H}^n(\pm\Lambda)}))^2 = |x(v_r) - v_i(v_r)|^2 + E_{(x,v_i),\pm\Lambda},$$

with $\exp_{v_r}^{-1}(x) = x(v_r)$ as usual, $E_{(x,v_i),\pm\Lambda}$ an error term satisfying the bound $|E_{(x,v_i),\pm\Lambda}| < \frac{5}{3}\Lambda(2D)^4$, provided

$$|v_i(v_r)|, |x(v_r)| \leq D \qquad \text{and} \qquad \sqrt{\Lambda}D < \frac{1}{2}.$$

Here the radius of the geodesic ball D is the maximum distance $d_{\max}$ in the spaces of constant curvature $\mathbb{H}^n(\pm\Lambda)$, introduced in Lemmas 3.6.2 and 3.6.3. Because $|E_{(x,v_i),\pm\Lambda}| < \frac{5}{3}\Lambda(2D)^4$ we conclude that

$$\begin{aligned} d_M(x, v_i)^2 &= |x(v_r) - v_i(v_r)|^2 + E_{(x,v_i)}. \\ d_M(v_l, v_k)^2 &= |v_l(v_r) - v_k(v_r)|^2 + E_{(v_l,v_k)}, \end{aligned} \tag{3.42}$$

with $|E_{(v_l,v_k)}|, |E_{(x,v_i)}| < \frac{5}{3}\Lambda(2D)^4$.

At this point we know all the lengths of the geodesics between the points $x, v_0, \ldots, v_n$ in the manifold up to a small and explicit deviation term, where the deviation is from the Euclidean space or $T_{v_r}M$ in which $x(v_r)$ and $\sigma^{\mathbb{E}}(v_r)$ lie. Any three points from the set $\{x, v_0, \ldots, v_n\}$ together with the geodesics connecting them can be regarded as a geodesic triangle. For a geodesic triangle of which we know all edge lengths the Toponogov comparison theorem gives bounds on the angles in terms of the Alexandrov triangles in the spaces $\mathbb{H}^n(\Lambda)$ and $\mathbb{H}^n(-\Lambda)$. Let us denote by $\theta_{il}^{\mathbb{H}^n(\pm\Lambda)}$ the angle $\angle v_i^{\mathbb{H}^n(\pm\Lambda)} x^{\mathbb{H}^n(\pm\Lambda)} v_l^{\mathbb{H}^n(\pm\Lambda)}$ between the geodesics in $\mathbb{H}^n(\pm\Lambda)$ and let $\theta_{il}^{\mathbb{E}}$ denote the angle $\angle v_i(v_r)x(v_r)v_l(v_r)$ in $T_{v_r}M$, which we may regard as Euclidean space. Lemma 3.6.3 in turn gives us bounds on the angles or rather inner products in $\mathbb{H}^n(\Lambda)$ and $\mathbb{H}^n(-\Lambda)$ compared to the corresponding angles or inner products in Euclidean space. To be precise we have

$$\begin{aligned} |d_{\mathbb{H}^n(\pm\Lambda)}(v_i^{\mathbb{H}^n(\pm\Lambda)}, x^{\mathbb{H}^n(\pm\Lambda)}) d_{\mathbb{H}^n(\pm\Lambda)}(v_l^{\mathbb{H}^n(\pm\Lambda)}, x^{\mathbb{H}^n(\pm\Lambda)}) \cos\theta_{il}^{\mathbb{H}^n(\pm\Lambda)} \\ -|v_i(v_r) - x(v_r)||v_l(v_r) - x(v_r)| \cos\theta_{il}^{\mathbb{E}}| \leq \tfrac{25}{6}\Lambda d_{\max}^4. \end{aligned}$$

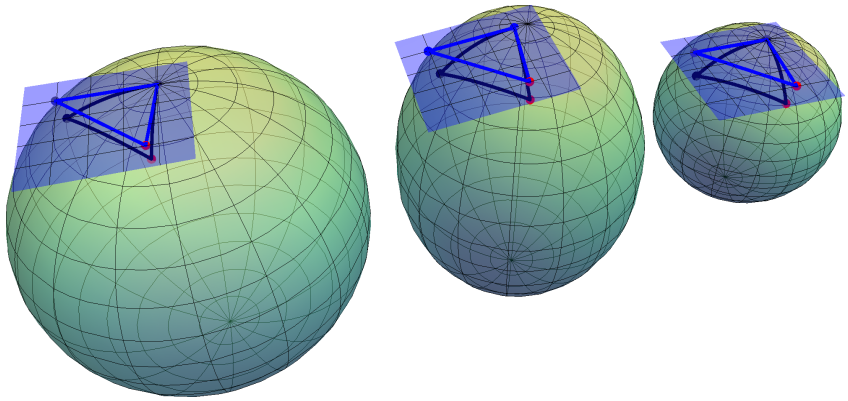

Figure 3.8: A symbolic sketch of the procedure: the lengths of edges and angles between geodesics in a manifold of arbitrary curvature (symbolized by the ellipsiod in the centre) are approximated by those in the spaces of constant curvature (the two spheres). Here in turn the triangles are approximated by the Euclidean simplex in 'the tangent space'.

With the Toponogov comparison theorem we see that

$$\begin{aligned} d_{\mathbb{H}^n(-\Lambda)}(v_i^{\mathbb{H}^n(-\Lambda)}, x^{\mathbb{H}^n(-\Lambda)}) \geq & d_M(v_i, x) \geq d_{\mathbb{H}^n(\Lambda)}(v_i^{\mathbb{H}^n(\Lambda)}, x^{\mathbb{H}^n(\Lambda)}) \\ \cos\theta_{il}^{\mathbb{H}^n(-\Lambda)} \geq & \cos\theta_{il}^{\mathbb{E}} \geq \cos\theta_{il}^{\mathbb{H}^n(\Lambda)} \end{aligned}$$

so that

$$|d_M(v_i, x)d_M(v_l, x)\cos\theta_{il} - |v_i(v_r) - x(v_r)||v_l(v_r) - x(v_r)|\cos\theta_{il}^{\mathbb{E}}| \leq \tfrac{25}{6}\Lambda d_{\max}^4.$$

Using Gram matrices and the estimates by Friedland we now see:

$$\begin{aligned} & |\det((2D)^{-2}d_M(v_i, x)d_M(v_l, x)\cos\theta_{il})_j| \\ \geq & |\det((2D)^{-2}|v_i(v_r) - x(v_r)||v_l(v_r) - x(v_r)|\cos\theta_{il}^{\mathbb{E}})_j| - \tfrac{25}{4\cdot 6}n\Lambda D^2, \end{aligned}$$

with $(\cos\theta_{il})_j$ and $(\cos\theta_{il}^{\mathbb{E}})_j$ the matrix cosines of angles between the tangents of geodesics emanating from x to $v_0, \ldots, v_{j-1}, v_{j+1}, \ldots, v_n$ and corresponding cosines for $\sigma^{\mathbb{E}}(v_r)$, which is equivalent to,

$$\begin{aligned} & (2D)^{-2n}|\det(d_M(v_i, x)d_M(v_l, x)\cos\theta_{il})_j| \\ \geq & (2D)^{-2n}\det(v_0(v_r) - x(v_r), \ldots, v_{j-1}(v_r) - x(v_r), \\ & \qquad v_{j+1}(v_r) - x(v_r), \ldots, v_n(v_r) - x(v_r))^2 \\ & \qquad - \tfrac{25}{24}n\Lambda D^2, \end{aligned}$$

Lemma 3.6.4 states that we have non-degeneracy of the simplex if for any x in $B(v_r, D)$ we have that $|\det(d_M(v_i, x)d_M(v_l, x)\cos\theta_{il})_j| > 0$ for some j, this means that if

$$\begin{aligned}\min_{x\in B(v_r,D)}\max_{j\in\{0,\ldots,n\}}(2D)^{-2n}\det(v_0(v_r)-x(v_r),\ldots,v_{j-1}(v_r)-x(v_r),\\ v_{j+1}(v_r)-x(v_r),\ldots,v_n(v_r)-x(v_r))^2\\ >\tfrac{25}{24}n\Lambda D^2,\end{aligned}$$

non-degeneracy is established. This can be simplified by remarking that the mimimum of

$$\begin{aligned}\max_{j\in\{0,\ldots,n\}}\det(v_0(v_r)-x(v_r),\ldots,v_{j-1}(v_r)-x(v_r),\\ v_{j+1}(v_r)-x(v_r),\ldots,v_n(v_r)-x(v_r))\end{aligned}$$

is attained in the barycenter and equals $\frac{n!}{n+1}\text{vol}(\sigma^{\mathbb{E}}(v_r))$.

This means that we now have the condition for non-degeneracy

$$\left(\frac{n!\text{vol}(\sigma^{\mathbb{E}}(v_r))}{(n+1)(2D)^n}\right)^2 > \tfrac{25}{24}n\Lambda D^2. \tag{3.43}$$

We can now summarize

Theorem 3.6.6 *Let $v_0,\ldots,v_n$ be a set of vertices lying in a Riemannian manifold M, whose sectional curvatures are bounded in absolute value by Λ, within a convex geodesic ball of radius D centred at one of the vertices (v_r) and such that $\sqrt{\Lambda}D < 1/2$. If $\sigma^{\mathbb{E}}(v_r)$, the convex hull of $(\exp_{v_r}^{-1}(v_i))_{i=0}^n = (v_i(v_r))_{i=0}^n$, satisfies*

$$\left(\frac{n!\textit{vol}(\sigma^{\mathbb{E}}(v_r))}{(n+1)(2D)^n}\right)^2 > \tfrac{25}{24}n\Lambda D^2. \tag{3.43}$$

then the Riemannian simplex with vertices $v_0,\ldots,v_n$ is non-degenerate, that is diffeomorphic to the standard n-simplex.

3.7 Triangulation criteria

We are interested in the following scenario. Suppose we have a finite set of points $\mathcal{P} \subset M$ in a compact Riemannian manifold, and an (abstract) simplicial complex $\mathcal{A}$ whose vertex set is $\mathcal{P}$, and such that every simplex in $\mathcal{A}$ defines a non-degenerate Riemannian simplex. When can we be sure that $\mathcal{A}$ triangulates M? Consider a convex ball B_ρ centred at $p \in \mathcal{P}$. We require that, when lifted to T_pM, the simplices near p triangulate a neighbourhood of the origin. If we require that the simplices be small relative to ρ, and triangulate a region extending to near the boundary of the lifted ball, then Riemannian simplices outside of B_ρ cannot have points in common with the simplices near the centre of the ball, and it is relatively easy to establish a triangulation.

Instead, we aim for finer local control of the geometry. We establish geometric conditions (Lemma 3.7.4) that ensure that the complex consisting of simplices incident to p, (i.e., the star of p) is embedded by a given map into the manifold. In order to achieve this result we require a strong constraint on the differential of the map in question. Since we work locally, in a coordinate chart, we consider maps $F : \mathbb{R}^n \supseteq U \to \mathbb{R}^n$. We demand that for some linear isometry $T : \mathbb{R}^n \to \mathbb{R}^n$ we have

$$\|dF_u - T\| \leq \eta, \tag{3.44}$$

for some $0 \leq \eta \leq 1$, and all $u \in U$. This is stronger than the kind of bounds found, for example, in the Rauch theorem (Lemma 3.5.4), which have the form

$$(1 - \eta)\,|w| \leq |dF_u w| \leq (1 + \eta)\,|w|\,. \tag{3.45}$$

Whereas (3.45) implies that dF_u is close to a linear isometry at every $u \in U$, Equation (3.44) means that dF_u is close to *the same* linear isometry for all $u \in U$.

Using a local constraint of the form (3.44) to establish the embedding of vertex stars, we demonstrate, in Section 3.7.1, generic criteria which ensure that a map from a simplicial complex to a Riemannian manifold is a homeomorphism. We then turn our attention to the specific case where the map in question is the barycentric coordinate map on each simplex.

Using a refinement of the Rauch theorem established by Buser and Karcher [BK81] we show, in Section 3.7.2, that transition functions arising from the exponential map (Equation (3.2)) are subject to bounds of the form (3.44). Then in Section 3.7.3 we observe that the barycentric coordinate map is also subjected to such bounds, and thus yield Theorem 3.2 as a particular case of the generic triangulation criteria.

3.7.1 Generic triangulation criteria

We say that a map $F : \mathbb{R}^m \to \mathbb{R}^n$ is *smooth* if it is of class C^∞. If $A \subset \mathbb{R}^m$, then $F : A \to \mathbb{R}^n$ is *smooth* on A if F can be extended to a function that is smooth in an open neighbourhood of A, i.e., there exists an open neighbourhood $U \in \mathbb{R}^m$ and a smooth map $\tilde{F} : U \to \mathbb{R}^n$ such that $A \subseteq U$, and $\tilde{F}|_A = F$. This definition is independent of the ambient space $\mathbb{R}^m$ containing A. In particular, if $A \subseteq \mathbb{R}^k \subseteq \mathbb{R}^m$, then the smoothness of F does not depend on whether we consider A to be a subset of $\mathbb{R}^k$ or of $\mathbb{R}^m$. In the case that A is the closure of a non-empty open set, continuity of the partial derivatives implies that they are well defined on all of A and independent of the chosen extension. See Munkres [Mun68, §1] for more details.

For our purposes, we are interested in smooth maps from non-degenerate closed Euclidean simplices of dimension n into an n-dimensional manifold M. We will work within coordinate charts, so our primary focus will be on maps of the form

$$F : \boldsymbol{\sigma}^n_{\mathbb{E}} \to \mathbb{R}^n,$$

such that Equation (3.44) is satisfied for all $u \in \boldsymbol{\sigma}^n_{\mathbb{E}}$. As an example of how we can exploit this bound, we observe that a map satisfying Equation (3.44) is necessarily an embedding with bounded metric distortion if its domain is convex:

Lemma 3.7.1 *Suppose $A \subset \mathbb{R}^n$ is convex, and $F : A \to \mathbb{R}^n$ is a smooth map such that, for some non-negative $\eta < 1$,*

$$\|dF_u - T\| \leq \eta,$$

for all $u \in A$, and some linear isometry $T : \mathbb{R}^n \to \mathbb{R}^n$. Then

$$|\,|F(u) - F(v)| - |u - v|\,| \leq \eta\,|u - v| \quad \text{for all } u, v \in A.$$

Proof We observe that it is sufficient to consider the case $T = \mathrm{Id}$, because if $\tilde{F} = T^{-1} \circ F$, then $\left\|d\tilde{F} - \mathrm{Id}\right\| = \|dF - T\|$, and $\left|\tilde{F}(u) - \tilde{F}(v)\right| = |F(u) - F(v)|$.

Assume $u \neq v$. For the lower bound we consider the unit vector $\hat{u} = \frac{u-v}{|u-v|}$, and observe that

$$dF(u - v) \cdot \hat{u} \geq (1 - \eta)\,|u - v| > 0,$$

so, by integrating along the segment $[u, v]$, we find

$$|F(u) - F(v)| \geq \big(F(u) - F(v)\big) \cdot \hat{u} \geq (1 - \eta)\,|u - v|\,.$$

For the upper bound we employ the unit vector $\hat{w} = \frac{F(u)-F(v)}{|F(u)-F(v)|}$:

$$\big(F(u) - F(v)\big) \cdot \hat{w} = |F(u) - F(v)| \leq (1 + \eta)(u - v) \cdot \hat{w} \leq (1 + \eta)\,|u - v|\,.$$

□

For our purposes we will be free to choose a coordinate system so that F keeps a vertex fixed. We will have use for the following observation, which can be demonstrated with an argument similar to the proof of Lemma 3.7.1:

Lemma 3.7.2 *If $A \subseteq \mathbb{R}^n$ is a convex set and $F : A \to \mathbb{R}^n$ is a smooth map with a fixed point $p \in A$ and*

$$\|dF_u - \mathrm{Id}\| \leq \eta, \qquad \text{for all } u \in A,$$

then

$$|F(u) - u| \leq \eta |u - p| \qquad \text{for all } u \in A.$$

Embedding complexes In preparation for considering triangulations we first consider the problem of mappings of complexes into $\mathbb{R}^n$.

A simplicial complex $\mathcal{C}$ is a set of abstract simplices such that if $\sigma \in \mathcal{C}$, then $\tau \in \mathcal{C}$ for every face $\tau \subset \sigma$. We will only consider finite simplicial complexes. A subcomplex of $\mathcal{C}$ is a subset that is also a simplicial complex. The *star* of a simplex $\sigma \in \mathcal{C}$ is the smallest subcomplex of $\mathcal{C}$ consisting of all simplices that have σ as a face, and is denoted $\underline{\mathrm{St}}(\sigma)$. In particular, if p is a vertex of $\mathcal{C}$, then $\underline{\mathrm{St}}(p)$ is the set of simplices that contain p, together with the faces of these simplices.

The *carrier* ("geometric realisation") of $\mathcal{C}$ is denoted $|\mathcal{C}|$. We are interested in complexes endowed with a *piecewise flat metric*. This is a metric on $|\mathcal{C}|$ that can be realised by assigning lengths to the edges in $\mathcal{C}$ such that each simplex $\sigma \in \mathcal{C}$ is associated with a Euclidean simplex $\boldsymbol{\sigma}_{\mathbb{E}} \subset |\mathcal{C}|$ that has the prescribed edge lengths. Certain constraints on the edge lengths must be met in order to define a valid piecewise flat metric, but for our current purposes we will have a metric inherited from an embedding in Euclidean space.

We say that $\mathcal{C}$ is *embedded* in $\mathbb{R}^n$ if the vertices lie in $\mathbb{R}^n$ and the convex hulls of the simplices in $\mathcal{C}$ define a geometric simplicial complex. In other words, to each $\sigma, \tau \in \mathcal{C}$ we associate $\boldsymbol{\sigma}_{\mathbb{E}} = \mathrm{conv}(\sigma)$, $\boldsymbol{\tau}_{\mathbb{E}} = \mathrm{conv}(\tau)$, and we have $\boldsymbol{\sigma}_{\mathbb{E}} \cap \boldsymbol{\tau}_{\mathbb{E}} = \mathrm{conv}(\sigma \cap \tau)$. The topological boundary of a set $B \subset \mathbb{R}^n$ is denoted by ∂B, and its topological interior by $\mathrm{int}(B)$. If $\mathcal{C}$ is embedded in $\mathbb{R}^n$, and p is a vertex of $\mathcal{C}$, we say that $\underline{\mathrm{St}}(p)$ is a *full star* if $p \in \mathrm{int}(|\underline{\mathrm{St}}(p)|)$.

The *scale* of $\mathcal{C}$ is an upper bound on the length of the longest edge in $\mathcal{C}$, and is denoted by h. We say that $\mathcal{C}$ is t_0-thick if each simplex in $\mathcal{C}$ has thickness greater than t_0. The *dimension* of $\mathcal{C}$ is the largest dimension of the simplices in $\mathcal{C}$. We call a complex of dimension n an *n-complex*. If every simplex in $\mathcal{C}$ is the face of an n-simplex, then $\mathcal{C}$ is a *pure n-complex*.

A map $F : |\mathcal{C}| \to \mathbb{R}^n$ is *smooth on $\mathcal{C}$* if for each $\sigma \in \mathcal{C}$ the restriction $F\big|_{\boldsymbol{\sigma}_{\mathbb{E}}}$ is smooth. This means that $d(F\big|_{\boldsymbol{\sigma}_{\mathbb{E}}})$ is well defined, and even though dF is not well defined, we will use this symbol when the particular restriction employed

is either evident or unimportant. When the underlying complex on which F is smooth is unimportant, we simply say that F is *piecewise smooth*.

F is *piecewise linear* if its restriction to each simplex is an affine map. The *secant map* of F is the piecewise linear map defined by the restriction of F to the vertices of $\mathcal{C}$.

We are interested in conditions that ensure that $F : |\mathcal{C}| \to \mathbb{R}^n$ is a topological embedding. Our primary concern is with the behaviour of the boundary. The reason for this is captured by the following variation of a lemma by Whitney [Whi57, Lem AII.15a]:

Lemma 3.7.3 (Whitney) *Let $\mathcal{C}$ be a (finite) simplicial complex embedded in $\mathbb{R}^n$ such that $\mathrm{int}(|\mathcal{C}|)$ is non-empty and connected, and $\partial|\mathcal{C}|$ is a compact $(n-1)$-manifold. Suppose $F : |\mathcal{C}| \to \mathbb{R}^n$ is smooth on $\mathcal{C}$ and such that $\det d(F\big|_{\boldsymbol{\sigma}_{\mathbb{E}}}) > 0$ for each n-simplex $\sigma \in \mathcal{C}$. If the restriction of F to $\partial|\mathcal{C}|$ is an embedding, then F is a topological embedding.*

Proof The assumptions on $\mathrm{int}(|\mathcal{C}|)$ and $\partial|\mathcal{C}|$ imply that $\mathcal{C}$ is a pure n-complex, and that each $(n-1)$ simplex is either a boundary simplex, or the face of exactly two n-simplices. Whitney showed [Whi57, Lem AII.15a] that any $x \in \mathrm{int}(|\mathcal{C}|)$ admits an open neighbourhood $U \subset \mathrm{int}(|\mathcal{C}|)$ such that the restriction of F to U is a homeomorphism. In particular, $F(\mathrm{int}(|\mathcal{C}|))$ is open.

By the Jordan-Brouwer separation theorem [OR09, §IV.7], $\mathbb{R}^n \setminus F(\partial|\mathcal{C}|)$ consists of two open components, one of which is bounded. Since $F(|\mathcal{C}|)$ is compact, $F(\mathrm{int}(|\mathcal{C}|))$ must coincide with the bounded component, and in particular $F(\mathrm{int}(|\mathcal{C}|)) \cap F(\partial|\mathcal{C}|) = \emptyset$, so $F(\mathrm{int}(|\mathcal{C}|))$ is a single connected component.

We need to show that F is injective. First we observe that the set of points in $F(\mathrm{int}(|\mathcal{C}|))$ that have exaclty one point in the preimage is non-empty. It suffices to look in a neigbhourhood of a point $y \in F(\partial|\mathcal{C}|)$. Choose $y = F(x)$, where x is in the relative interior of $\boldsymbol{\sigma}^{n-1}_{\mathbb{E}} \subset \partial|\mathcal{C}|$. Then there is a neighbourhood V of y such that V does not intersect the image of any other simplex of dimension less than or equal to $n-1$. Let σ^n be the unique n-simplex that has σ^{n-1} as a face. Then $F^{-1}(V \cap F(|\mathcal{C}|) \subset \boldsymbol{\sigma}^n_{\mathbb{E}}$, and it follows that every point in $V \cap \mathrm{int}(|\mathcal{C}|)$ has a unique point in its image.

Now the injectivity of F follows from the fact that the number of points in the preimage is locally constant on $F(\mathrm{int}(|\mathcal{C}|)) \setminus F(\partial|\mathcal{C}|)$, which in our case is connected. This is a standard argument in degree theory [OR09, Prop. IV.1.2]: A point $a \in F(\mathrm{int}(|\mathcal{C}|)) \setminus F(\partial|\mathcal{C}|)$ has k points $\{x_1, \ldots, x_k\}$ in its preimage. There is a neighbourood V of a and disjoint neighbourhoods U_i of x_i such that $F|_{U_i} : U_i \to V$ is a homeomorphism for each $i \in \{1, \ldots, k\}$. It follows that the number of points in the preimage is k for every point in the open neighbourhood of a defined as

$$W = V \setminus F(|\mathcal{C}| \setminus \bigcup_i U_i).$$

□

Lemma 3.7.4 (Embedding a star) *Suppose $\mathcal{C} = \underline{\mathrm{St}}(p)$ is a t_0-thick, pure n-complex embedded in $\mathbb{R}^n$ such that all of the n-simplices are incident to a single vertex, p, and $p \in \mathrm{int}(|\mathcal{C}|)$ (i.e., $\underline{\mathrm{St}}(p)$ is a full star). If $F : |\mathcal{C}| \to \mathbb{R}^n$ is smooth on $\mathcal{C}$, and satisfies*

$$\|dF - \mathrm{Id}\| < nt_0 \tag{3.46}$$

on each n-simplex of $\mathcal{C}$, then F is an embedding.

Proof If $|\mathcal{C}|$ is convex, then the claim follows immediately from Lemma 3.7.1.

From the definition of thickness, we observe that $nt_0 \leq 1$, and therefore $\|dF\| > 0$. By Lemma 3.7.3, it suffices to consider points $x, y \in \partial|\mathcal{C}|$. Rather than integrating the differential of a direction, as we did implicitly in the proof of Lemma 3.7.1, we will integrate the differential of an angle.

Let Q be the 2-dimensional plane defined by p, x, and y. We define the angle function $\phi : \mathbb{R}^n \to \mathbb{R}$ as follows: For $z \in \mathbb{R}^n$, let $\check{z}$ be the orthogonal projection of z into Q. Then $\phi(z)$ is the angle that $\check{z} - p$ makes with $x - p$, where the orientation is chosen so that $\phi(y) < \pi$. (We can assume that x and y are not colinear with p, since in that case $[x, y]$ must be contained in $|\mathcal{C}|$, and the arguments of Lemma 3.7.1 ensure that we would not have $F(x) = F(y)$.)

Let α be the piecewise linear curve obtained by projecting the segment $[x, y] \subset Q$ onto $\partial|\mathcal{C}|$ via the radial rays emanating from p. Parameterise α by the angle ϕ, i.e., by the arc between $\frac{x-p}{|x-p|}$ and $\frac{y-p}{|y-p|}$ on the unit circle in Q. Then $d\phi(\alpha') = 1$, and we have

$$\phi(F(y)) - \phi(F(x)) = \int_{F(\alpha)} d\phi = \int_0^{\phi(y)} d\phi(dF\alpha'(s))\, ds.$$

We will show that $d\phi(dF\alpha'(s)) > 0$; it follows that $\phi(F(y)) > \phi(F(x))$ and hence $F(y) \neq F(x)$.

We need an observation about thick simplices: Suppose that p is a vertex of a t_0-thick n-simplex $\boldsymbol{\sigma}_{\mathbb{E}}$, and $\boldsymbol{\tau}_{\mathbb{E}}$ is the facet opposite p. Then a line r through p and $\boldsymbol{\tau}_{\mathbb{E}}$ makes an angle θ with $\boldsymbol{\tau}_{\mathbb{E}}$ that is bounded by

$$\sin\theta \geq nt_0.$$

Indeed, the altitude of p satisfies $a_p \geq nt_0 L$ by the definition of thickness, and the distance between p and the point of intersection of r with $\boldsymbol{\tau}_{\mathbb{E}}$ is less than L.

If $\alpha(s)$ is the point of intersection of r with $\boldsymbol{\tau}_{\mathbb{E}}$, we observe that $d\phi(\alpha'(s)) = |\alpha'(s)| \sin\theta$, i.e., the magnitude of the component of $\alpha'(s)$ orthogonal to r. By the hypothesis (3.46), the angle β between $dF\alpha'(s)$ and $\alpha'(s)$ satisfies $\sin\beta < nt_0$.

Therefore

$$\begin{aligned} d\phi(dF\alpha'(s)) &\geq |dF\alpha'(s)|\,(\sin\theta - \sin\beta) \\ &> 0. \end{aligned}$$

□

Triangulations For our purposes a *manifold* is always compact and without boundary. A simplicial complex $\mathcal{A}$ is a *manifold simplicial complex* if $|\mathcal{A}|$ is a topological manifold. A *triangulation* of a manifold M is a homeomorphism $H : |\mathcal{A}| \to M$, where $\mathcal{A}$ is a simplicial complex. If M is a differentiable manifold, then H is a *smooth triangulation* if it is smooth on $\mathcal{A}$, i.e., the restriction of H to any simplex in $\mathcal{A}$ is smooth. We are concerned with smooth triangulations of compact Riemannian manifolds.

Our homeomorphism argument is based on the following observation:

Lemma 3.7.5 *Let $\mathcal{A}$ be a manifold simplicial complex of dimension n with finite vertex set $\mathcal{P}$, and let M be a compact n-manifold. Suppose $H : |\mathcal{A}| \to M$ is such that for each $p \in \mathcal{P}$, $H\big|_{|\underline{\mathrm{St}}(p)|} : |\underline{\mathrm{St}}(p)| \to M$ is an embedding. If for each connected component M_i of M there is a point $y \in M_i$ such that $h^{-1}(y)$ contains exactly one point in $|\mathcal{A}|$, then H is a homeomorphism.*

Proof The requirement that the star of each vertex be embedded means that H is locally a homeomorphism, so it suffices to observe that it is bijective. It is surjective by Brouwer's invariance of domain; thus H is a covering map. The requirement that each component of M has a point with a single point in its pre-image implies that $H : |\mathcal{A}| \to M$ is a single-sheeted covering, and therefore a homeomorphism. □

The following proposition generically models the situation we will work with when we describe a triangulation by Riemannian simplices:

Proposition 3.7.6 (Triangulation) *Let $\mathcal{A}$ be a manifold simplicial n-complex with finite vertex set $\mathcal{P}$, and M a compact Riemannian manifold with an atlas $\{(W_p, \phi_p)\}_{p\in\mathcal{P}}$ indexed by $\mathcal{P}$. Suppose*

$$H : |\mathcal{A}| \to M$$

satisfies:

1. *For each $p \in \mathcal{P}$ the secant map of $\phi_p \circ H$ restricted to $|\underline{\mathrm{St}}(p)|$ is a piecewise linear embedding $\mathcal{L}_p : |\underline{\mathrm{St}}(p)| \to \mathbb{R}^n$ such that each simplex $\sigma \in \mathcal{C}_p = \mathcal{L}_p(\underline{\mathrm{St}}(p))$ is t_0-thick, and $|\mathcal{C}_p| \subset B_{\mathbb{R}^n}(\mathcal{L}_p(p); h)$, with $\mathcal{L}_p(p) \in \mathrm{int}(|\mathcal{C}_p|)$. The scale parameter h must satisfy $h < \frac{\iota_M}{4}$, where ι_M is the injectivity radius of M.*

2. *For each $p \in \mathcal{P}$, $\phi_p : W_p \xrightarrow{\cong} U_p \subset \mathbb{R}^n$ is such that $\overline{B} = \overline{B}_{\mathbb{R}^n}(\mathcal{L}_p(p); \frac{3}{2}h) \subseteq U_p$, and $\left\|(d\phi_p^{-1})_u\right\| \leq \frac{4}{3}$, for every $u \in \overline{B}$.*

3. *The map*
$$F_p = \phi_p \circ H \circ \mathcal{L}_p^{-1} : |\mathcal{C}_p| \to \mathbb{R}^n$$
satisfies
$$\|(dF_p)_u - \mathrm{Id}\| \leq \frac{nt_0}{2}$$
on each n-simplex $\sigma \in \mathcal{C}_p$, and every $u \in \boldsymbol{\sigma}_{\mathbb{E}}$.

Then H is a smooth triangulation of M.

Proof By Lemma 3.7.4, F_p is a homeomorphism onto its image. It follows then that $H\big|_{|\underline{\mathrm{St}}(p)|}$ is an embedding for every $p \in \mathcal{P}$. Therefore, since $|\mathcal{A}|$ is compact, $H : |\mathcal{A}| \to M$ is a covering map.

Given $x \in |\mathcal{A}|$, with $x \in \boldsymbol{\sigma}_{\mathbb{E}}$, and p a vertex of $\boldsymbol{\sigma}_{\mathbb{E}}$, let $\tilde{x} = \mathcal{L}_p(x) \in |\mathcal{C}_p|$. Then the bound on dF implies that $|F_p(\tilde{x}) - \mathcal{L}_p(p)| \leq \left(1 + \frac{nt_0}{2}\right) h \leq \frac{3}{2}h$, so $F_p(\tilde{x}) \in \overline{B}$. Since $\phi_p^{-1} \circ F_p(\tilde{x}) = H(x)$, and

$$\left|(d\phi_p^{-1})_{F(u)}(dF_p)_u\right| \leq \frac{4}{3}\left(1 + \frac{nt_0}{2}\right) \leq 2$$

for any $u \in \boldsymbol{\sigma}_{\mathbb{E}} \subset |\mathcal{C}_p|$, we have that $d_M(H(p), H(x)) \leq 2h$.

Suppose $y \in |\mathcal{A}|$ with $H(y) = H(x)$. Let $\tau \in \mathcal{A}$ with $y \in \boldsymbol{\tau}_{\mathbb{E}}$, and $q \in \tau$ a vertex. Then $d_M(H(p), H(q)) \leq 4h < \iota_M$. Thus there is a path γ from $H(x)$ to $H(p)$ to $H(q)$ to $H(y) = H(x)$ that is contained in the topological ball $B_M(H(p); \iota_M)$, and is therefore null-homotopic. Since H is a covering map, this implies that $x = y$. Thus H is injective, and therefore defines a smooth triangulation. □

3.7.2 The differential of exponential transitions

If there is a unique minimising geodesic from x to y, we denote the parallel translation along this geodesic by T_{yx}. As a preliminary step towards exploiting Proposition 3.7.6 in the context of Riemannian simplices, we show here that the estimates of Buser and Karcher [BK81, §6] imply

Proposition 3.7.7 (Strong exponential transition bound) *Suppose the sectional curvatures on M satisfy $|K| \leq \Lambda$. Let $v \in T_pM$, with $y = \exp_p(v)$. If $x, y \in B_M(p; \rho)$, with*
$$\rho < \frac{1}{2}\rho_0 = \frac{1}{2}\min\left\{\frac{\iota_M}{2}, \frac{\pi}{4\sqrt{\Lambda}}\right\},$$
then
$$\left\|d(\exp_x^{-1} \circ \exp_p)_v - T_{xp}\right\| \leq 6\Lambda\rho^2.$$

The primary technical result that we use in the demonstration of Proposition 3.7.7 is a refinement of the Rauch theorem demonstrated by Buser and Karcher [BK81, §6.4]. We make use of a simplified particular case of their general result:

Lemma 3.7.8 (Strong Rauch theorem) *Assume the sectional curvatures on M satisfy $|K| \leq \Lambda$, and suppose there is a unique minimising geodesic between x and p. If $v = \exp_p^{-1}(x)$, and*

$$|v| = d_M(p, x) = r \leq \frac{\pi}{2\sqrt{\Lambda}},$$

then

$$\left\|(d\exp_p)_v - T_{xp}\right\| \leq \frac{\Lambda r^2}{2}.$$

Proof Given distinct upper and lower bounds on the sectional curvatures, $\Lambda_- \leq K \leq \Lambda_+$, the result of Buser and Karcher [BK81, §6.4.2] is stated as

$$\left|(d\exp_p)_v w - T_{xp}\left(\frac{\mathbf{S}_\kappa(r)w}{r}\right)\right| \leq |w|\left(\frac{\mathbf{S}_{\kappa-\lambda}(r) - \mathbf{S}_\kappa(r)}{r}\right),$$

for any vector w perpendicular to v, and as long as $\mathbf{S}_\kappa$ is nonnegative. Here κ is arbitrary, and $\lambda = \max\{\Lambda_+ - \kappa, \kappa - \Lambda_-\}$.

We take $\Lambda = \max\{\Lambda_+, -\Lambda_-\}$, and $\kappa = 0$. The stated bound results since now $\mathbf{S}_\kappa(r) = \mathbf{S}_0(r) = r$, and the constraint $r \leq \frac{\pi}{2\sqrt{\Lambda}}$ ensures that

$$\frac{\mathbf{S}_{-\Lambda}(r) - r}{r} \leq \frac{\Lambda r^2}{2},$$

as observed in Section 3.5.2. The result applies to all vectors since the exponential preserves lengths in the radial direction. □

We obtain a bound on the differential of the inverse of the exponential map from Lemma 3.7.8 and the following observation:

Lemma 3.7.9 *Suppose $A : \mathbb{R}^n \to \mathbb{R}^n$ is a linear operator that satisfies*

$$\|A - T\| \leq \eta,$$

for some linear isometry $T : \mathbb{R}^n \to \mathbb{R}^n$. If $\eta \leq \frac{1}{2}$, then

$$\left\|A^{-1} - T^{-1}\right\| \leq 2\eta.$$

Proof We first bound $\left\|A^{-1}\right\| = s_n(A)^{-1}$, the inverse of the smallest singular value. Since $s_n(A) = s_n(T^{-1}A)$, and $\left\|T^{-1}A - \mathrm{Id}\right\| \leq \eta$, we have $|s_n(A) - 1| \leq \eta$. Thus $s_n(A)^{-1} \leq (1-\eta)^{-1} \leq 1 + 2\eta$.

Now write $A = T + \eta E$, where $\|E\| \leq 1$. The trick [GVL96, p. 50] is to observe that

$$\begin{aligned} A^{-1} &= T^{-1} - A^{-1}(A - T)T^{-1} \\ &= T^{-1} - \eta A^{-1} E T^{-1}, \end{aligned}$$

and the stated bound follows. □

Lemma 3.7.10 *Suppose the sectional curvatures on M satisfy $|K| \leq \Lambda$. Let $v \in T_pM$, with $y = \exp_p(v)$. If $x, y \in B_M(p;\rho)$, with*

$$\rho \leq \min\left\{\frac{\iota_M}{2}, \frac{1}{2\sqrt{\Lambda}}\right\},$$

then

$$\left\|d(\exp_x^{-1} \circ \exp_p)_v - T_{xy}T_{yp}\right\| \leq 5\Lambda\rho^2.$$

Proof By Lemma 3.2.1, $B_M(p;\rho)$ is convex. Since $d_M(x,y) < 2\rho$, Lemma 3.7.8 yields $\|(d\exp_x)_w - T_{yx}\| < 2\Lambda\rho^2 \leq \frac{1}{2}$, where $w = \exp_x^{-1}(y)$. Since $T_{xy} = T_{yx}^{-1}$, we may use Lemma 3.7.9 to write

$$(d\exp_x^{-1})_y = T_{xy} + \left(4\Lambda\rho^2\right) E,$$

where E satisfies $\|E\| \leq 1$. We obtain the result by composing this with

$$(d\exp_p)_v = T_{yp} + \left(\frac{\Lambda\rho^2}{2}\right)\tilde{E},$$

where $\left\|\tilde{E}\right\| \leq 1$. □

In order to compare T_{xp} with $T_{xy}T_{yp}$ we exploit further estimates demonstrated by Buser and Karcher. If $\alpha : [0,1] \to M$ is a curve, let $T_{\alpha(t)} : T_{\alpha(0)}M \to T_{\alpha(t)}M$ denote the parallel translation operator (we do not require that α be a minimising geodesic). Buser and Karcher [BK81, §6.1, §6.2] bound the difference in the parallel translation operators between two homotopic curves:

Lemma 3.7.11 (Parallel translation comparison) *Let $c_i : [0,1] \to M$ be piecewise smooth curves from p to q, and let*

$$c : [1,2] \times [0,1] \to M$$

be a piecewise smooth homotopy between c_1 and c_2, i.e., $c(1,t) = c_1(t)$, and $c(2,t) = c_2(t)$. Let $\mathfrak{a} = \int \det dc_{(s,t)}\, dsdt$ be the area of the homotopy. If the sectional curvatures are bounded by $|K| \leq \Lambda$, then

$$\left\| T_{c_2(1)} - T_{c_1(1)} \right\| \leq \frac{4}{3}\Lambda\mathfrak{a}.$$

In our case the two curves of interest form the edges of a geodesic triangle. A *geodesic triangle* in M is a set of three points (vertices) such that each pair is connected by a unique minimising geodesic, together with these three minimising geodesics (edges). Any three points in a convex set are the vertices of a geodesic triangle. Buser and Karcher [BK81, §6.7] demonstrate an estimate of A. D. Aleksandrow that says that the edges of a small geodesic triangle are the boundary of a topological disk whose area admits a natural bound:

Lemma 3.7.12 (Small triangle area) *Let $p, x, y \in M$ be the edges of a geodesic triangle whose edge lengths, $\ell_{px}, \ell_{xy}, \ell_{yp}$ satisfy*

$$\ell_{px} + \ell_{xy} + \ell_{yp} \leq \min\left\{ \iota_M, \frac{2\pi}{\sqrt{\Lambda_+}} \right\},$$

where Λ_+ is an upper bound on the sectional curvatures of M, and ι_M is the injectivity radius. Then the edges of triangle pxy form the boundary of an immersed topological disk whose area $\mathfrak{a}$ satisfies

$$\mathfrak{a} \leq \mathfrak{a}_{\Lambda_+},$$

where $\mathfrak{a}_{\Lambda_+}$ is the area of a triangle with the same edge lengths in the sphere of radius $\frac{1}{\sqrt{\Lambda_+}}$.

Consider $x, y \in B_M(p;\rho)$, where $\rho < \frac{1}{2}\rho_0$ and as usual Λ is a bound on the absolute values of the sectional curvatures. In this case, Buser and Karcher [BK81, §6.7.1] observe that the area of the triangle in the sphere of radius $\frac{1}{\sqrt{\Lambda}}$ that has the same edge lengths as pxy satisfies

$$\mathfrak{a}_\Lambda \leq \frac{5}{8}\rho^2.$$

It follows then, from Lemma 3.7.11, that

$$\|T_{xp} - T_{xy}T_{yp}\| \leq \frac{5}{6}\Lambda\rho^2.$$

This, together with Lemma 3.7.10, yields

$$\left\| d(\exp_x^{-1} \circ \exp_p)_v - T_{xp} \right\| \leq 5\Lambda\rho^2 + \frac{5}{6}\Lambda\rho^2 \leq 6\Lambda\rho^2,$$

and we obtain Proposition 3.7.7.

3.7.3 Triangulations with Riemannian simplices

We now exploit Proposition 3.7.7 to demonstrate that a bound of the form (3.44) is satisfied by the differential (3.10) of the barycentric coordinate map defining a Riemannian simplex $\boldsymbol{\sigma}_M$

$$db = -\left(\nabla^M \nu\right)^{-1} \partial_u \nu,$$

and find a bound on the scale that allows us to exploit Proposition 3.7.6.

Choose a vertex p_0 of $\boldsymbol{\sigma}_M$, and an arbitrary linear isometry $u : T_{p_0}M \to \mathbb{R}^n$ to establish a coordinate system on $T_{p_0}M$ so that $v_0(p_0)$ remains the origin. Let P be the matrix whose i^{th} column is $v_i(p_0)$. For $x \in B_\rho$, rather than placing an arbitrary coordinate system on T_xM, we identify $T_{p_0}M$ and T_xM by the parallel translation operator T_{p_0x}, i.e., use $u \circ T_{p_0x}$ for coordinates. Let $\tilde{P}$ be the matrix whose i^{th} column is $v_i(x) - v_0(x)$.

Now the map

$$F : v \mapsto \exp_x^{-1} \circ \exp_{p_0}(v) - v_0(x)$$

can be considered as a map $\mathbb{R}^n \supset U \to \mathbb{R}^n$, and the matrix whose i^{th} column is $F(v_i(p_0))$ is $\tilde{P}$. It follows from Proposition 3.7.7 that if $h < \frac{1}{2}\rho_0$, then for any $u \in B_{\mathbb{R}^n}(0;h)$, we have $\|(dF)_u - \mathrm{Id}\| \leq \eta$, with $\eta = 6\Lambda h^2$.

Lemma 3.7.2 implies a bound on the difference of the column vectors of P and $\tilde{P}$:

$$|v_i(p_0) - (v_i(x) - v_0(x))| \leq \eta\, |v_i(p_0)| \leq \eta L(\sigma(p_0)).$$

It follows that $\left\|P - \tilde{P}\right\| \leq \sqrt{n}\eta L(\sigma(p_0))$. Assume also that $t(\sigma(p_0)) \geq t_0$. Then, recalling Equation (3.12), and recognising that T_{xp_0} is represented by the identity matrix in our coordinate systems, we have

$$\begin{aligned}
\|-(\partial_u \nu) - T_{xp_0}\| &= \left\|\tilde{P}P^{-1} - PP^{-1}\right\| \\
&= \left\|\left(\tilde{P} - P\right)P^{-1}\right\| \\
&\leq \sqrt{n}6\Lambda h^2 L(\sigma(p_0))\left\|P^{-1}\right\| \\
&\leq \frac{\sqrt{n}6\Lambda h^2 L(\sigma(p_0))}{\sqrt{n}t_0 L(\sigma(p_0))} \qquad \text{by Lemma 3.5.1} \\
&\leq \frac{6\Lambda h^2}{t_0}.
\end{aligned}$$

Buser and Karcher show [BK81, §8.1.3] that for any $x \in B_M(p;h)$, with $h < \rho_0$, we have

$$\left\|(\nabla^M \nu)_x - \mathrm{Id}\right\| \leq 2\Lambda h^2.$$

When $h < \frac{1}{2}\rho_0$, we have $2\Lambda h^2 < \frac{1}{2}$, and Lemma 3.7.9 yields

$$\left\|(\nabla^M \nu)^{-1} - \mathrm{Id}\right\| \leq 4\Lambda h^2.$$

Therefore we have, when $b(u) = x$

$$\begin{aligned} \|db_u - T_{xp_0}\| &= \left\| - \left(\nabla^M \nu\right)^{-1} \partial_u \nu - T_{xp_0} \right\| \\ &\leq 4\Lambda h^2 + \frac{6\Lambda h^2}{t_0} + 4\Lambda h^2 \left(\frac{6\Lambda h^2}{t_0}\right) \\ &\leq \frac{14\Lambda h^2}{t_0}, \end{aligned} \tag{3.47}$$

using $h < \frac{\pi}{8\sqrt{\Lambda}}$.

Finally, in order to employ Proposition 3.7.6 we consider the composition $\exp_{p_0}^{-1} \circ b$. From Lemma 3.7.8 and Lemma 3.7.9 we have that

$$\left\|(d\exp_{p_0}^{-1})_x - T_{p_0 x}\right\| \leq \Lambda h^2.$$

Therefore, since $T_{p_0 x} = T_{xp_0}^{-1}$ we have

$$\begin{aligned} \left\|d(\exp_{p_0}^{-1} \circ b)_u - \mathrm{Id}\right\| &\leq \Lambda h^2 + \frac{14\Lambda h^2}{t_0} + \Lambda h^2 \left(\frac{14\Lambda h^2}{t_0}\right) \\ &\leq \frac{18\Lambda h^2}{t_0}. \end{aligned}$$

In order to meet the conditions of Proposition 3.7.6, we require

$$\frac{18\Lambda h^2}{t_0} \leq \frac{1}{2} n t_0,$$

or

$$h \leq \frac{\sqrt{n} t_0}{6\sqrt{\Lambda}}.$$

We obtain

Theorem 3.2 *Suppose M is a compact n-dimensional Riemannian manifold with sectional curvatures K bounded by $|K| \leq \Lambda$, and $\mathcal{A}$ is an abstract simplicial complex with finite vertex set $\mathcal{P} \subset M$. Define a quality parameter $t_0 > 0$, and let*

$$h = \min\left\{\frac{\iota_M}{4}, \frac{\sqrt{n} t_0}{6\sqrt{\Lambda}}\right\}.$$

If

1. *For every $p \in \mathcal{P}$, the vertices of $\underline{\mathrm{St}}(p)$ are contained in $B_M(p;h)$, and the balls $\{B_M(p;h)\}_{p\in\mathcal{P}}$ cover M.*

2. *For every $p \in \mathcal{P}$, the restriction of the inverse of the exponential map $\exp_p^{-1}$ to the vertices of $\underline{\mathrm{St}}(p) \subset \mathcal{A}$ defines a piecewise linear embedding of $|\underline{\mathrm{St}}(p)|$ into T_pM, realising $\underline{\mathrm{St}}(p)$ as a full star such that every simplex $\sigma(p)$ has thickness $t(\sigma(p)) \geq t_0$.*

then $\mathcal{A}$ triangulates M, and the triangulation is given by the barycentric coordinate map on each simplex.

3.8 The piecewise flat metric

The complex $\mathcal{A}$ described in Theorem 3.2 naturally inherits a piecewise flat metric from the construction. The length assigned to an edge $\{p, q\} \in \mathcal{A}$ is the geodesic distance in M between its endpoints: $\ell_{pq} = d_M(p, q)$. We first examine, in Section 3.8.1, conditions which ensure that this assignment of edge lengths does indeed make each $\sigma \in \mathcal{A}$ isometric to a Euclidean simplex. With this piecewise flat metric on $\mathcal{A}$, the barycentric coordinate map is a bi-Lipschitz map between metric spaces $H : |\mathcal{A}| \to M$. In Section 3.8.2 we estimate the metric distortion of this map.

Several of the lemmas in this section are generalisations of lemmas that appeared in [BDG13a, §A.1]. The arguments are essentially the same, but we have included the proofs here for convenience.

3.8.1 Euclidean simplices defined by edge lengths

If G is a symmetric positive definite $n \times n$ matrix, then it can be written as a Gram matrix, $G = P^{\mathsf{T}}P$ for some $n \times n$ matrix P. Then P describes a Euclidean simplex with one vertex at the origin, and the other vertices defined by the column vectors. The matrix P is not unique, but if $G = Q^{\mathsf{T}}Q$, then $Q = OP$ for some linear isometry O. Thus a symmetric positive definite matrix defines a Euclidean simplex, up to isometry.

If $\sigma = \{p_0, \dots, p_n\} \subset B_\rho$, is the vertex set of a Riemannian simplex $\boldsymbol{\sigma}_M$, we define the numbers $\ell_{ij} = d_M(p_i, p_j)$. These are the edge lengths of a Euclidean simplex $\boldsymbol{\sigma}_{\mathbb{E}}$ if and only if the matrix G defined by

$$G_{ij} = \frac{1}{2}(\ell_{0i}^2 + \ell_{0j}^2 - \ell_{ij}^2) \tag{3.48}$$

is positive definite.

We would like to use the smallest eigenvalue of G to estimate the thickness of $\boldsymbol{\sigma}_{\mathbb{E}}$, however, an unfortunate choice of vertex labels can prevent us from doing this easily. We make use of the following observation:

Lemma 3.8.1 *Suppose $\sigma = \{v_0, \dots, v_k\} \subset \mathbb{R}^n$ is a Euclidean k-simplex, and let P be the $n \times k$ matrix whose i^{th} column is $v_i - v_0$. If for some $i \neq 0$, an altitude at least as small as a_0 is realised, i.e, $a_i \leq a_0$, then*

$$t(\sigma) \geq \frac{s_k(P)}{kL(\sigma)}.$$

Proof We assume that σ is non-degenerate, since otherwise the bound is trivial. If v_i is a vertex of minimal altitude, then by Lemma 3.5.1, the i^{th} row of the

pseudo-inverse P_{left}^{-1} is given by ${w_i}^{\mathsf{T}}$, where

$$|w_i| = a_i^{-1} = (ktL)^{-1}.$$

It follows then that $s_1(P_{\text{left}}^{-1}) \geq (ktL)^{-1}$, and therefore $s_k(P) \leq ktL$, yielding the stated bound. □

If G is positive definite, then we may write $G = P^{\mathsf{T}}P$, where P is a matrix describing $\boldsymbol{\sigma}_{\mathbb{E}} = [v_0, \ldots, v_k]$, with the edge lengths $\{\ell_{ij}\}$ dictating the vertex labelling. If $\mu_k(G) = s_k(P)^2$ is the smallest eigenvalue of G, then *provided some vertex other than v_0 realises the smallest altitude in $\boldsymbol{\sigma}_{\mathbb{E}}$*, Lemma 3.8.1 yields

$$t(\boldsymbol{\sigma}_{\mathbb{E}}) \geq \frac{\sqrt{\mu_k(G)}}{kL(\sigma)}. \tag{3.49}$$

For our current purposes, we can ensure the existence, and bound the thickness of $\boldsymbol{\sigma}_{\mathbb{E}}$ by comparing it with a related simplex such as $\sigma(p_0)$. To this end we employ the following observation (where $\tilde{\sigma}$ plays the role of $\sigma(p_0)$):

Lemma 3.8.2 *Suppose $\tilde{\sigma} = \{\tilde{v}_0, \ldots, \tilde{v}_k\}$ is a Euclidean k-simplex, and $\{\ell_{ij}\}$ is a set of positive numbers defined for all $0 \leq i \neq j \leq k$ such that $\ell_{ij} = \ell_{ji}$, and*

$$||\tilde{v}_i - \tilde{v}_j| - \ell_{ij}| \leq C_0 L(\tilde{\sigma}).$$

Let $\tilde{P}$ be the matrix whose i^{th} column is $\tilde{v}_i - \tilde{v}_0$, and define the matrix G by

$$G_{ij} = \frac{1}{2}(\ell_{0i}^2 + \ell_{0j}^2 - \ell_{ij}^2).$$

Let E be the matrix that records the difference between G and the Gram matrix $\tilde{P}^{\mathsf{T}}\tilde{P}$:

$$G = \tilde{P}^{\mathsf{T}}\tilde{P} + E.$$

If $C_0 \leq \frac{2}{3}$, then the entries of E are bounded by $|E_{ij}| \leq 4C_0 L(\tilde{\sigma})^2$, and in particular

$$\|E\| \leq 4kC_0 L(\tilde{\sigma})^2. \tag{3.50}$$

Proof Let $\tilde{\ell}_{ij} = |\tilde{v}_i - \tilde{v}_j|$. By the cosine rule we have

$$\left[\tilde{P}^{\mathsf{T}}\tilde{P}\right]_{ij} = \frac{1}{2}(\tilde{\ell}_{0i}^2 + \tilde{\ell}_{0j}^2 - \tilde{\ell}_{ij}^2),$$

and we obtain a bound on the magnitude of the coefficients of E:

$$\begin{aligned}\left|G_{ij} - \left[\tilde{P}^{\mathsf{T}}\tilde{P}\right]_{ij}\right| &\leq \frac{1}{2}\left(\left|\ell_{0i}^2 - \tilde{\ell}_{0i}^2\right| + \left|\ell_{0j}^2 - \tilde{\ell}_{0j}^2\right| + \left|\ell_{ij}^2 - \tilde{\ell}_{ij}^2\right|\right) \\ &\leq \frac{3}{2}(2 + C_0)C_0 L(\tilde{\sigma})^2 \\ &\leq 4C_0 L(\tilde{\sigma})^2.\end{aligned}$$

This leads us to a bound on $s_1(E) = |E|$. Indeed, the magnitude of the column vectors of E is bounded by $\sqrt{k}$ times a bound on the magnitude of their coefficients, and the magnitude of $s_1(E)$ is bounded by $\sqrt{k}$ times a bound on the magnitude of the column vectors. We obtain Equation (3.50). □

We have the following extension of the "Thickness under distortion" Lemma 3.5.2 ([BDG13a, §4.2]):

Lemma 3.8.3 (Abstract Euclidean simplex) *Suppose $\tilde{\sigma} = \{\tilde{v}_0, \dots, \tilde{v}_k\} \subset \mathbb{R}^n$, and $\{\ell_{ij}\}_{0 \le i,j \le k}$ is a set of positive numbers defined for all $0 \le i \ne j \le k$ such that $\ell_{ij} = \ell_{ji}$, and such that*

$$||\tilde{v}_i - \tilde{v}_j| - \ell_{ij}| \le C_0 L(\tilde{\sigma})$$

for all $0 \le i < j \le k$.

If

$$C_0 = \frac{\eta t(\tilde{\sigma})^2}{4} \qquad \text{with} \quad 0 \le \eta \le 1, \tag{3.51}$$

then there exists a Euclidean simplex $\sigma = \{v_0, \dots, v_k\}$ whose edge lengths are described by the numbers ℓ_{ij}. Let $\tilde{P}$ and P be matrices whose i^{th} column is given by $\tilde{v}_i - \tilde{v}_0$, and $v_i - v_0$ respectively. Then

$$s_k(P) \ge (1 - \eta) s_k(\tilde{P}),$$

and the thickness of σ satisfies

$$t(\sigma) \ge \frac{4}{5\sqrt{k}}(1 - \eta) t(\tilde{\sigma}).$$

Proof If $\tilde{\sigma}$ is degenerate, then by (3.51), $\{\ell_{ij}\}$ is the set of edge lengths of $\tilde{\sigma}$ and there is nothing to prove. Therefore, assume $t(\tilde{\sigma}) > 0$.

Let G be the matrix defined by Equation (3.48), and define the matrix E by $G = \tilde{P}^{\mathsf{T}}\tilde{P} + E$, and let x be a unit eigenvector of G associated with the smallest eigenvalue μ_k. Then

$$\begin{aligned} \mu_k = x^{\mathsf{T}} G x &= x^{\mathsf{T}} \tilde{P}^{\mathsf{T}} \tilde{P} x + x^{\mathsf{T}} E x \\ &\ge s_k(\tilde{P})^2 - s_1(E) \\ &= \left(1 - \frac{s_1(E)}{s_k(\tilde{P})^2}\right) s_k(\tilde{P})^2. \end{aligned}$$

From Lemma 3.5.1 we have $s_k(\tilde{P})^2 \ge k t(\tilde{\sigma})^2 L(\tilde{\sigma})^2$, and by Lemma 3.8.2 $s_1(E) \le 4k C_0 L(\tilde{\sigma})^2$, so by the definition (3.51) of C_0, we have that

$$\mu_k \ge (1 - \eta) s_k(\tilde{P})^2,$$

and thus G is positive semi-definite, and the first inequality is satisfied because $\mu_k = s_k(P)^2$ and $\sqrt{1-\eta} \geq 1-\eta$.

In order to obtain the thickness bound, we employ Lemma 3.8.1. Since thickness is independent of the vertex labelling, we may assume that some vertex other than v_0 realises the minimal altitude in σ (if necessary, we relabel the vertices of $\tilde{\sigma}$ and σ, maintaining the correspondence). Then using Lemma 3.8.1 and Lemma 3.5.1 we have

$$kt(\sigma)L(\sigma) \geq s_k(P) \geq (1-\eta)s_k(\tilde{P}) \geq (1-\eta)\sqrt{k}t(\tilde{\sigma})L(\tilde{\sigma}).$$

The stated thickness bound follows since $\frac{L(\tilde{\sigma})}{L(\sigma)} \geq \frac{1}{1+C_0} \geq \frac{4}{5}$. □

Now we examine whether the simplices of the complex $\mathcal{A}$ of Theorem 3.2 meet the requirements of Lemma 3.8.3. If $\sigma \in \mathcal{A}$, with $p \in \sigma$, then we can use the Rauch theorem 3.5.4 to compare σ with the Euclidean simplex $\sigma(p) \in T_pM$. Under the assumptions of Theorem 3.2, we have $\left\|d\exp_p\right\| \leq 1 + \frac{\Lambda h^2}{2}$, and $\left\|d\exp_p^{-1}\right\| \leq 1 + \frac{\Lambda h^2}{3}$. Thus

$$\ell_{ij} - |v_i(p) - v_j(p)| \leq \frac{\Lambda h^2}{2} |v_i(p) - v_j(p)|,$$

and

$$|v_i(p) - v_j(p)| - \ell_{ij} \leq \frac{\Lambda h^2}{3}\ell_{ij} \leq \frac{\Lambda h^2}{3}\left(1 + \frac{\Lambda h^2}{2}\right)|v_i(p) - v_j(p)| \leq \frac{\Lambda h^2}{2}|v_i(p) - v_j(p)|,$$

and we can use

$$C_0 = \frac{\Lambda h^2}{2} \tag{3.52}$$

in Lemma 3.8.3. Thus in order to guarantee that the ℓ_{ij} describe a non-degenerate Euclidean simplex, we require that

$$\Lambda h^2 = \frac{\eta t_0^2}{2},$$

for some non-negative $\eta < 1$.

Under the conditions of Theorem 3.2 we may have $h^2\Lambda = \frac{nt_0^2}{36}$, which gives us $\eta = \frac{n}{18}$. Thus when $n \geq 18$ we require stronger bounds on the scale than those imposed by Theorem 3.2 if we wish to ensure the existence of a piecewise flat metric on $\mathcal{A}$. Reducing the curvature controlled constraint on h in Theorem 3.2 by a factor of $1/\sqrt{n}$ gives us $\eta = \frac{1}{18}$, and Lemma 3.8.3 yields:

Proposition 3.8.4 *If the requirements of Theorem 3.2, are satisfied when the scale parameter* (3.5) *is replaced with*

$$h = \min\left\{\frac{\iota_M}{4}, \frac{t_0}{6\sqrt{\Lambda}}\right\},$$

then the geodesic distances between the endpoints of the edges in $\mathcal{A}$ defines a piecewise flat metric on $\mathcal{A}$ such that each simplex $\sigma \in \mathcal{A}$ satisfies

$$t(\sigma) > \frac{3}{4\sqrt{n}} t_0.$$

3.8.2 Metric distortion of the barycentric coordinate map

In the context of Theorem 3.2 the barycentric coordinate map on each simplex defines a piecewise smooth homeomorphism $H : |\mathcal{A}| \to M$. If the condition of Proposition 3.8.4 is also met, then $\mathcal{A}$ is naturally endowed with a piecewise flat metric. We wish to compare this metric with the Riemannian metric on M. It suffices to consider an n-simplex $\sigma \in \mathcal{A}$, and establish bounds on the singular values of the differential dH. If $p \in \sigma$, then we can write $H\big|_{\boldsymbol{\sigma}_{\mathbb{E}}} = b \circ \mathcal{L}_p$, where $\mathcal{L}_p : \boldsymbol{\sigma}_{\mathbb{E}} \to \boldsymbol{\sigma}_{\mathbb{E}}(p)$ is the linear map that sends $\sigma \in \mathcal{A}$ to $\sigma(p) \in T_pM$.

A bound on the metric distortion of a linear map that sends one Euclidean simplex to another is a consequence of the following (reformulation of [BDG13a, Lem A.4]):

Lemma 3.8.5 (Linear distortion bound) *Suppose that P and $\tilde{P}$ are non-degenerate $k \times k$ matrices such that*

$$\tilde{P}^{\mathsf{T}}\tilde{P} = P^{\mathsf{T}}P + E. \tag{3.53}$$

Then there exists a linear isometry $\Phi : \mathbb{R}^k \to \mathbb{R}^k$ such that

$$\left\|\tilde{P}P^{-1} - \Phi\right\| \leq \frac{s_1(E)}{s_k(P)^2}.$$

Proof Multiplying by $P^{-T} := (P^{\mathsf{T}})^{-1}$ on the left, and by P^{-1} on the right, we rewrite Equation (3.53) as

$$A^{\mathsf{T}}A = I + F, \tag{3.54}$$

where $A = \tilde{P}P^{-1}$, and $F = P^{-T}EP^{-1}$. Using the singular value decomposition $A = U_A\Sigma_A V_A^{\mathsf{T}}$, we let $\Phi = U_A V_A^{\mathsf{T}}$ so that

$$(A - \Phi) = U_A(\Sigma_A - I)V_A^{\mathsf{T}}. \tag{3.55}$$

From Equation (3.54) we deduce that $s_1(A)^2 \leq 1 + s_1(F)$, and also that $s_k(A)^2 \geq 1 - s_1(F)$. Using these two inequalities we find

$$\max_i |s_i(A) - 1| \leq \frac{s_1(F)}{1 + s_i(A)} \leq s_1(F),$$

and thus

$$\|\Sigma_A - I\| \leq s_1(F) \leq s_1(P^{-1})^2 s_1(E) = s_k(P)^{-2} s_1(E).$$

The result now follows from Equation (3.55). □

Lemma 3.8.5 implies:

Lemma 3.8.6 *Suppose $\sigma = \{v_0, \ldots, v_n\}$ and $\tilde{\sigma} = \{\tilde{v}_0, \ldots, \tilde{v}_n\}$ are two Euclidean simplices in $\mathbb{R}^n$ such that*

$$\left| |\tilde{v}_i - \tilde{v}_j| - |v_i - v_j| \right| \leq C_0 L(\sigma).$$

If $A : \mathbb{R}^n \to \mathbb{R}^n$ is the affine map such that $A(v_i) = \tilde{v}_i$ for all i, and $C_0 \leq \frac{2}{3}$, then for all $x, y \in \mathbb{R}^n$,

$$\left| |A(x) - A(y)| - |x - y| \right| \leq \eta |x - y|,$$

where

$$\eta = \frac{4C_0}{t(\sigma)^2}.$$

Proof Let P be the matrix whose i^{th} column is $v_i - v_0$, and let $\tilde{P}$ be the matrix whose i^{th} column is $\tilde{v}_i - \tilde{v}_0$. Then we have the matrix form $A(x) = \tilde{P}P^{-1}x + (\tilde{v}_0 - \tilde{P}P^{-1}v_0)$. It follows then from Lemma 3.8.5 that $\eta \leq s_n(P)^{-2} s_1(E)$, where $E = \tilde{P}^{\mathsf{T}}\tilde{P} - P^{\mathsf{T}}P$.

By Lemma 3.8.2, $s_1(E) \leq 4nC_0 L(\sigma)^2$, and by Lemma 3.5.1, $s_n(P)^2 \geq nt(\sigma)^2 L(\sigma)^2$, and the result follows. □

Observe that if A in Lemma 3.8.6 is a linear map, then the lemma states that $s_1(A) \leq 1 + \eta$ and $s_n(A) \geq 1 - \eta$. We use this to estimate the metric distortion of $H|_{\boldsymbol{\sigma}_{\mathbb{E}}} = b \circ \mathcal{L}_p$. Under the assumption of Proposition 3.8.4, specifically, given that $h \leq \frac{t_0}{6\sqrt{\Lambda}}$, we again exploit Equation (3.52), so

$$\left\|\mathcal{L}_p^{-1}\right\| \leq 1 + \frac{2\Lambda h^2}{t_0^2}$$

and, since $\|\mathcal{L}_p\|^{-1} = s_n(\mathcal{L}_p^{-1}) \geq 1 - \frac{2\Lambda h^2}{t_0^2}$, and the second term is less than $\frac{1}{2}$, we also have

$$\|\mathcal{L}_p\| \leq 1 + \frac{4\Lambda h^2}{t_0^2}.$$

Using Equation (3.47) we have

$$\|db\| \leq 1 + \frac{14\Lambda h^2}{t_0},$$

and

$$\left\|db^{-1}\right\| \leq 1 + \frac{28\Lambda h^2}{t_0}.$$

Recalling that $dH\big|_{\boldsymbol{\sigma}_{\mathbb{E}}} = (db)\mathcal{L}_p$, and $h^2 \leq \frac{t_0^2}{36\Lambda}$, we obtain

$$\|dH\| \leq 1 + \frac{20\Lambda h^2}{t_0^2},$$

and

$$\left\|dH^{-1}\right\| \leq 1 + \frac{32\Lambda h^2}{t_0^2}.$$

The bound on the differential of H and its inverse enables us to estimate the Riemannian metric on M using the piecewise flat metric on $\mathcal{A}$. The metric distortion bound on H is found with the same kind of calculation as exhibited in Equation (3.32), for example. We find:

Theorem 3.3 (Metric distortion) *If the requirements of Theorem 3.2, are satisfied with the scale parameter* (3.5) *replaced by*

$$h = \min\left\{\frac{\iota_M}{4}, \frac{t_0}{6\sqrt{\Lambda}}\right\},$$

then $\mathcal{A}$ is naturally equipped with a piecewise flat metric $d_{\mathcal{A}}$ defined by assigning to each edge the geodesic distance in M between its endpoints.

If $H : |\mathcal{A}| \to M$ is the triangulation defined by the barycentric coordinate map in this case, then the metric distortion induced by H is quantified as

$$|d_M(H(x), H(y)) - d_{\mathcal{A}}(x, y)| \leq \frac{50\Lambda h^2}{t_0^2} d_{\mathcal{A}}(x, y),$$

for all $x, y \in |\mathcal{A}|$.

3.9 Alternate criteria

We discuss alternative formulations of our results. In Section 3.9.1, we consider defining the quality of Riemannian simplices in terms of Euclidean simplices defined by the geodesic edge lengths of the Riemannian simplices. In Section 3.9.2 we compare thickness with a volume-based quality measure for simplices that we call *fatness*.

3.9.1 In terms of the intrinsic metric

We imposed a quality bound on a Riemannian simplex $\boldsymbol{\sigma}_M$ by imposing a quality bound on the Euclidean simplex $\sigma(p)$ that is the lift of the vertices of $\boldsymbol{\sigma}_M$ to T_pM. This was convenient for our purposes, but the quality of $\boldsymbol{\sigma}_M$ could also be characterised directly by its geodesic edge lengths.

As discussed in Section 3.8.1, we can use the smallest eigenvalue of the matrix (3.48) G to characterise the quality of $\boldsymbol{\sigma}_M$: When $\mu_n(G) \geq 0$, there is a Euclidean simplex $\boldsymbol{\sigma}_{\mathbb{E}}$ with the same edge lengths as $\boldsymbol{\sigma}_M$, however we have the inconvenience that the lower bound (3.49) on $t(\boldsymbol{\sigma}_{\mathbb{E}})$ with respect to $\mu_k(G)$ is not valid for all choices of vertex labels.

This inconvenience can be avoided if a volumetric quality measure is used, such as the fatness discussed in Section 3.9.2. Determinant-based criteria for Euclidean simplex realisability are discussed by Berger [Ber87a, §9.7], for example.

In any event, we will express the alternate non-degeneracy criteria for $\boldsymbol{\sigma}_M$ in terms of the thickness of the associated Euclidean simplex $\boldsymbol{\sigma}_{\mathbb{E}}$. Using Proposition 3.2.5, and the Rauch theorem 3.5.4, we have the following reformulation of the non-degeneracy criteria of Theorem 3.1:

Proposition 3.9.1 (Non-degeneracy criteria) *If $\rho < \rho_0$ defined in Equation* (3.3)*, and the geodesic edge lengths of $\boldsymbol{\sigma}_M \subset B_\rho \subset M$ define a Euclidean simplex $\boldsymbol{\sigma}_{\mathbb{E}}$ with*

$$t(\boldsymbol{\sigma}_{\mathbb{E}}) \geq 3\sqrt{\Lambda} L(\boldsymbol{\sigma}_{\mathbb{E}}) \tag{3.56}$$

then $\boldsymbol{\sigma}_M$ is non-degenerate. As in Theorem 3.1, the assertion holds if ρ replaces $L(\boldsymbol{\sigma}_{\mathbb{E}})$ in the lower bound (3.56)*.*

Proof By Lemma 3.5.4 we have for any $x \in B_\rho$

$$|v_i(x) - v_j(x)| \leq \left(1 + \frac{\Lambda(2\rho)^2}{3}\right) \ell_{ij},$$

and

$$\ell_{ij} \leq \left(1 + \frac{\Lambda(2\rho)^2}{2}\right) |v_i(x) - v_j(x)|\,.$$

Therefore

$$\begin{aligned} |\,|v_i(x) - v_j(x)| - \ell_{ij}\,| &\leq \Lambda 2\rho^2 \left(1 + \frac{\Lambda 4\rho^2}{3}\right) \ell_{ij} \\ &\leq 4\Lambda\rho^2 \ell_{ij}. \end{aligned}$$

Then using $C_0 = 4\Lambda\rho^2$ in Lemma 3.5.2, we see that $\sigma(x)$ is non-degenerate if $t(\boldsymbol{\sigma}_{\mathbb{E}}) > \sqrt{8}\sqrt{\Lambda}\rho$, and the result follows from Proposition 3.2.5, and the remarks at the end of Section 3.2.2. □

The scale parameter h in Theorem 3.2 is in fact a strict upper bound on the geodesic edge lengths ℓ_{ij} in $\mathcal{A}$. A similar argument to the proof of Proposition 3.9.1 allows us to restate Theorem 3.2 by employing a thickness bound on the Euclidean simplices with edge lengths ℓ_{ij}:

Proposition 3.9.2 (Triangulation criteria) *Suppose M is a compact n-dimensional Riemannian manifold with sectional curvatures K bounded by $|K| \leq \Lambda$, and $\mathcal{A}$ is an abstract simplicial complex with finite vertex set $\mathcal{P} \subset M$. Define a quality parameter $t_0 > 0$, and let*

$$h = \min\left\{\frac{\iota_M}{4}, \frac{t_0}{8\sqrt{\Lambda}}\right\}.$$

If

1. *For every simplex $\sigma = \{p_0, \ldots, p_n\} \in \mathcal{A}$, the edge lengths $\ell_{ij} = d_M(p_i, p_j)$ satisfy $\ell_{ij} < h$, and they define a Euclidean simplex $\boldsymbol{\sigma}_{\mathbb{E}}$ with $t(\boldsymbol{\sigma}_{\mathbb{E}}) \geq t_0$.*
2. *The balls $\{B_M(p; h)\}_{p\in\mathcal{P}}$ cover M, and for each $p \in \mathcal{P}$ the secant map of $\exp_p^{-1}$ realises $\underline{\mathrm{St}}(p)$ as a full star.*

then $\mathcal{A}$ triangulates M, and the triangulation is given by the barycentric coordinate map on each simplex.

Proof By the argument in the proof of Proposition 3.9.1, using h instead of 2ρ, we see that for any $x, y \in B_M(p; h)$ we have

$$\left|\left|\exp_p^{-1}(x) - \exp_p^{-1}(y)\right| - d_M(x, y)\right| \leq \Lambda h^2 d_M(x, y).$$

Then using $C_0 = \Lambda h^2 = \frac{\eta t_0^2}{4}$ in Lemma 3.5.2, we get

$$\eta = \frac{4\Lambda h^2}{t_0^2} \leq \frac{1}{16}.$$

It follows that if $\sigma \in \mathcal{A}$, with $p \in \sigma$, then

$$t(\sigma(p)) \geq \frac{4}{5\sqrt{n}}(1-\eta)t_0 \geq \frac{3}{4\sqrt{n}}t_0.$$

The bound on h then implies that $h \leq \frac{\sqrt{n}t(\sigma(p))}{6\sqrt{\Lambda}}$, and so the result of Theorem 3.2 applies. □

3.9.2 In terms of fatness

Many alternative quality measures for simplices have been employed in the literature. Thickness is employed by Munkres [Mun68], using a slightly different normalisation than ours. It is also very popular to use a volume-based quality measure such as that employed by Whitney [Whi57]. In this section we introduce Whitney's quality measure, which we call *fatness*, and we compare it with thickness.

If σ is a j-simplex, then its *volume*, may be defined for $j > 0$ as

$$\mathrm{vol}^j(\sigma) = \frac{1}{j!}\prod_{i=1}^{j} s_i(P),$$

where P is the $m \times j$ matrix whose i^{th} column is $p_i - p_0$ for $\sigma = \{p_0, \cdots, p_j\} \subset \mathbb{R}^m$. If $j = 0$ we define $\mathrm{vol}^0(\sigma) = 1$. Alternatively, the volume may be defined inductively from the formula

$$\mathrm{vol}^j(\sigma) = \frac{a_p(\sigma)\,\mathrm{vol}^{j-1}(\sigma_p)}{j}. \tag{3.57}$$

The *fatness* of a j-simplex σ is the dimensionless quantity

$$\Theta(\sigma) = \begin{cases} 1 & \text{if } j = 0 \\ \frac{\mathrm{vol}^j(\sigma)}{L(\sigma)^j} & \text{otherwise.} \end{cases}$$

Lemma 3.9.3 (Fatness and thickness) *For any j-simplex σ*

$$t(\sigma)^j \leq \Theta(\sigma) \leq \prod_{k=1}^{j} t(\sigma^k) \leq \frac{t(\sigma)}{(j-1)!},$$

where $\sigma = \sigma^j \supset \sigma^{j-1} \supset \cdots \supset \sigma^1$ is any chain of faces of σ such that for each $i < j$, σ^i has maximal volume amongst all the facets of σ^{i+1}.

Proof It follows directly from the volume formula (3.57) that if σ^{k-1} is a face with maximal volume in $\sigma^k = \{p_k\} \cup \sigma^{k-1}$, then p_k is a vertex with minimal altitude in σ^k. Order the vertices of $\sigma = \{p_0, \ldots, p_j\}$ so that $\sigma^k = \{p_0, \ldots, p_k\}$ for each $k \leq j$. Then, inductively expanding the volume formula (3.57), we get

$$\mathrm{vol}(\sigma^j) = \prod_{k=1}^{j} \frac{a_{p_k}(\sigma^k)}{k}.$$

The inequality $\Theta(\sigma) \leq \prod_{k=1}^{j} t(\sigma^k)$ then follows from the definitions of thickness and fatness, and the observation that $L(\sigma) \geq L(\sigma^k)$ for all $k \leq j$. Also from the definition of thickness we have the trivial bound $t(\sigma^k) \leq \frac{1}{k}$, from which the rightmost inequality follows.

The lower bound also follows from induction on Equation (3.57). Using the same chain of faces and vertex labelling we get

$$\begin{aligned}
\Theta(\sigma) &= \frac{a_{p_j}(\sigma)}{jL(\sigma)} \frac{\mathrm{vol}(\sigma^{j-1})}{L(\sigma)^{j-1}} \\
&= t(\sigma)\Theta(\sigma^{j-1}) \frac{L(\sigma^{j-1})^{j-1}}{L(\sigma)^{j-1}} \\
&\geq t(\sigma) t(\sigma^{j-1})^{j-1} \frac{L(\sigma^{j-1})^{j-1}}{L(\sigma)^{j-1}} \qquad \text{inducive hypothesis} \\
&= t(\sigma) \left(\frac{a_{p_{j-1}}(\sigma^{j-1})}{(j-1)L(\sigma)} \right)^{j-1} \\
&\geq t(\sigma)^j.
\end{aligned}$$

□

Although Lemma 3.9.3 gives the impression that fatness corresponds roughly to a power of thickness, we observe that thickness and fatness coincide for triangles, as well as edges, and vertices.

Lemma 3.9.3, provides a way to express our results in terms of fatness instead of thickness. For example, the quality bound for non-degeneracy in Theorem 3.1

$$t(\sigma(p)) > 10\sqrt{\Lambda}\rho,$$

is attained if

$$\Theta(\sigma(p)) > \frac{10\sqrt{\Lambda}\rho}{(n-1)!}.$$

3.10 Simplices modelled on spaces of constant curvature

In this section we revisit our discussion of non-degeneracy criteria for Riemannian simplices on manifolds M whose sectional curvatures K are bounded by Λ, that is $|K| \leq \Lambda$. We focus in particular on the approach based on the Topogonov comparison theorem, see Section 3.6. In Section 3.6 we compared simplices on the manifold to Euclidean simplices ($\sigma^{\mathbb{E}}(v_r)$) in the tangent space of the manifold. This comparison is unnatural if the manifold has large, nearly constant negative or positive curvature. One would expect that the Riemannian simplices ($\boldsymbol{\sigma}_M$) on a manifold that is close to a space of constant curvature can have low quality but still be non-degenerate. Because spaces of constant curvature are totally geodesic a simplex is non-degenerate if and only if the quality is zero. In this section we continue to denote spaces of constant curvature by $\mathbb{H}(K)$, regardless whether the curvature K is positive or negative.

3.10.1 Overview of results

We prove the following results:

In case the manifold has positive curvature:

Theorem 3.10.10 *Let M be a manifold with bounded positive sectional curvatures K, that is $0 < \Lambda_- \leq K \leq \Lambda_+$. Suppose that $v_0, \ldots, v_n$ are vertices on M. Let us assume*[10] *that all vertices lie within a geodesic ball of radius $\frac{1}{2}\tilde{D}$ with centre v_r, where $\tilde{D} \leq 1/(2\sqrt{\Lambda_+})$. Under these assumptions the Riemannian simplex with vertices $v_0, \ldots, v_n$ on M is non-degenerate if*

$$\frac{Q_{\mathbb{H}(\Lambda_{mid})}(\sigma_{\mathbb{H}(\Lambda_{mid})}(v_r))}{(2\tilde{D})^{2n}} \geq n\,|\Lambda_- - \Lambda_+|\,\tilde{D}^2$$

with $Q_{\mathbb{H}(\Lambda_{mid})}$ the simplex quality

$$\begin{aligned} &Q_{\mathbb{H}(\Lambda_{mid})}(\sigma_{\mathbb{H}(\Lambda_{mid})}(v_r)) \\ &\quad = \min_{y \in \mathbb{H}(\Lambda_{mid})} \max_j \left\{ \det \left(\frac{1}{\Lambda_{mid}} \sin\left(\sqrt{\Lambda_{mid}}\, d_{\mathbb{H}(\Lambda_{mid})}(y, v_i(v_r))\right) \cdot \right.\right. \\ &\qquad\qquad \left.\left. \sin\left(\sqrt{\Lambda_{mid}} d_{\mathbb{H}(\Lambda_{mid})}(y, v_l(v_r))\right) \cos\theta_{il} \right)_{i,l \neq j} \right\}, \end{aligned} \tag{3.58}$$

[10] This bound is stronger than necessary. In fact it suffices for the lengths of geodesics in the proof below to be bounded by $\tilde{D}$.

$\sigma_{\mathbb{H}(\Lambda_{mid})}(v_r)$ the simplex on $\mathbb{H}(\Lambda_{mid})$ with vertices $v_i(v_r)$ defined by $v_i(v_r) = \exp_{\mathbb{H}(\Lambda_{mid})} \circ \exp^{-1}_{v_r,M}(v_i)$ and

$$\Lambda_{mid} = \frac{1}{2}(\Lambda_- + \Lambda_+).$$

The negative curvature case is more involved.

Theorem 3.10.11 *Let M be a manifold with bounded negative sectional curvatures K, that is $\Lambda_- \leq K \leq \Lambda_+ < 0$. Suppose that $v_0, \ldots, v_n$ are vertices on M. Let us assume that all vertices lie within a geodesic ball of radius $\frac{1}{2}\tilde{D}$ with centre v_r. Under these assumptions the Riemannian simplex with vertices $v_0, \ldots, v_n$ on M is non-degenerate if*

$$\begin{aligned}|\Lambda^{\mathbb{H}}_{mid}|^n Q_{\mathbb{H}(\Lambda^{\mathbb{H}}_{mid})}(\sigma_{\mathbb{H}(\Lambda^{\mathbb{H}}_{mid})}(v_r)) > \; & n(\sinh\sqrt{|\Lambda_-|}\tilde{D})^{2(n-1)} \\ & \cdot \left(2 + 2\cosh\left(\sqrt{|\Lambda_-|}\tilde{D}\right) + |\Lambda_-|^2\cosh^2\left(\sqrt{|\Lambda_-|}\tilde{D}\right)\frac{11\tilde{D}^4}{4!}\right) \\ & \cdot \left||\Lambda_-|\cosh^2(\sqrt{|\Lambda_-|}\tilde{D}) - |\Lambda_+|\cosh^2(\sqrt{|\Lambda_+|}\tilde{D})\right| |\Lambda^{\mathbb{H}}_{mid}|\frac{11\tilde{D}^4}{2\cdot 4!}.\end{aligned}$$

with $\sigma_{\mathbb{H}(\Lambda^{\mathbb{H}}_{mid})}(v_r)$ the simplex on $\mathbb{H}(\Lambda^{\mathbb{H}}_{mid})$ with vertices $v_i(v_r) = \exp_{\mathbb{H}(\Lambda^{\mathbb{H}}_{mid})} \circ \exp^{-1}_{v_r,M}(v_i)$, $Q_{\mathbb{H}(\Lambda^{\mathbb{H}}_{mid})}(\sigma_{\mathbb{H}(\Lambda^{\mathbb{H}}_{mid})}(v_r))$ the simplex quality

$$\begin{aligned}Q_{\mathbb{H}(\Lambda^{\mathbb{H}}_{mid})} = \min_{x\in N}\max_j \Bigg\{ & \det\Bigg(\frac{1}{|\Lambda^{\mathbb{H}}_{mid}|}\sinh\left(\sqrt{|\Lambda^{\mathbb{H}}_{mid}|}d_{\mathbb{H}^n(\Lambda^{\mathbb{H}}_{mid})}(x, v_i(v_r))\right) \\ & \sinh\left(\sqrt{|\Lambda^{\mathbb{H}}_{mid}|}d_{\mathbb{H}^n(\Lambda^{\mathbb{H}}_{mid})}(x, v_l(v_r))\right)\cos\theta_{il}\Bigg)_{i,l\neq j}\Bigg\},\end{aligned}$$

where N equals to any geodesic ball with radius $2\tilde{D}$ centred at any of the vertices and $\Lambda^{\mathbb{H}}_{mid}$ satisfies

$$\begin{aligned}&\left||\Lambda^{\mathbb{H}}_{mid}|\cosh^2\sqrt{\Lambda^{\mathbb{H}}_{mid}}\tilde{D} - |\Lambda_-|\cosh^2\sqrt{|\Lambda_-|}\tilde{D}\right| \\ =\;&\left||\Lambda^{\mathbb{H}}_{mid}|\cosh^2\sqrt{\Lambda^{\mathbb{H}}_{mid}}\tilde{D} - |\Lambda_+|\cosh^2\sqrt{|\Lambda_+|}\tilde{D}\right| \\ =\;&\frac{1}{2}\left||\Lambda_-|\cosh^2\sqrt{|\Lambda_-|}\tilde{D} - |\Lambda_+|\cosh^2\sqrt{|\Lambda_+|}\tilde{D}\right|.\end{aligned}$$

Quality

In Theorems 3.10.10 and 3.10.11 we have introduced qualities for simplices of constant curvature. In the elliptic case this quality has a nice geometric interpretation (the hyperbolic case is slightly more involved).

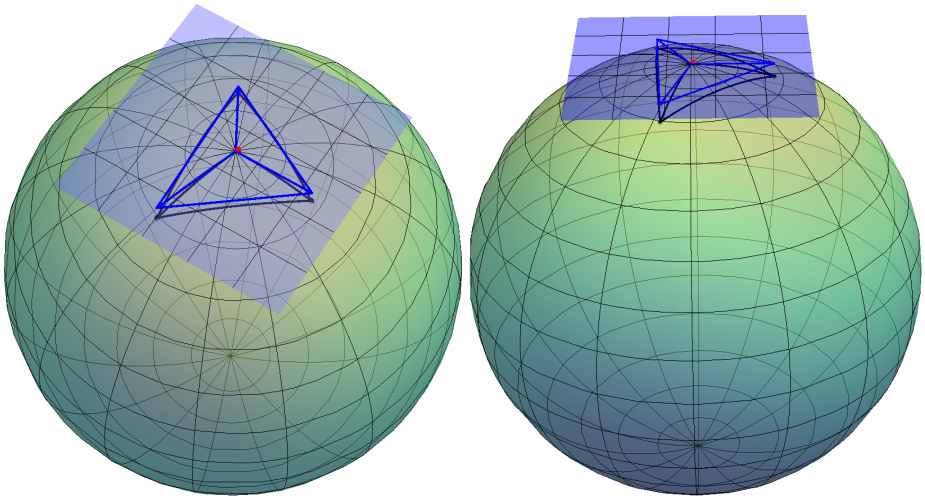

Figure 3.9: Geometric interpretation of the quality of a simplex on a space of positive constant curvature, top and side view.

The determinant

$$\det\left(\frac{1}{\Lambda_{\text{mid}}}\sin\left(\sqrt{\Lambda_{\text{mid}}}\,d_{\mathbb{H}(\Lambda_{\text{mid}})}(y,v_i)\right)\sin\left(\sqrt{\Lambda_{\text{mid}}}d_{\mathbb{H}(\Lambda_{\text{mid}})}(y,v_l)\right)\cos\theta_{il}\right)_{i,l\neq j},$$

in Theorem 3.10.10 gives the volume of a parallelepiped. This parallelepiped can be found as follows: We embed the sphere in Euclidean space in the standard manner, that is as a co-dimension one round sphere. We take the tangent space at y and the vertices v_i on the tangent space via the normal of the tangent space. The parallelepiped is given by the vectors from y to the projected vertices, see Figure 3.9.

The search for the point for which the maximum volume is minimized in (3.58), should remind one of following: In Euclidean space the barycentre of a simplex with vertices $v_0,\ldots,v_n$ is the point x for which the volumes of all dimensional simplices with vertices $x,v_0,\ldots,v_{j-1},v_{j+1},\ldots,v_n$ are equal. This means that maximum volume of the simplices is minimized.

Comparing Theorem 3.6.6 and Theorem 3.10.10

Using the geometric intuition we just developed, it is easy to compare Theorem 3.10.10 to the result of Section 3.6:

Theorem 3.6.6 *Let $v_0, \ldots, v_n$ be a set of vertices lying in a Riemannian manifold M, whose sectional curvatures are bounded in absolute value by Λ, within a convex geodesic ball of radius D centred at any one of the vertices (v_r) and such that $\sqrt{\Lambda}D < 1/2$. If $\sigma^{\mathbb{E}}(v_r)$, the convex hull of $(\exp_{v_r}^{-1}(v_i))_{i=0}^n = (v_i(v_r))_{i=0}^n$ in $T_{v_r}M$, satisfies*

$$\left(\frac{n!vol(\sigma^{\mathbb{E}}(v_r))}{(n+1)(2D)^n}\right)^2 > \tfrac{25}{24} n\Lambda D^2, \tag{3.43}$$

then the Riemannian simplex with vertices $v_0, \ldots, v_n$ is non-degenerate, that is diffeomorphic to the standard n-simplex.

For this comparison we note that

$$\det\left(\frac{1}{\Lambda_{\text{mid}}}\sin\left(\sqrt{\Lambda_{\text{mid}}}\, d_{\mathbb{H}(\Lambda_{\text{mid}})}(y, v_i)\right)\sin\left(\sqrt{\Lambda_{\text{mid}}} d_{\mathbb{H}(\Lambda_{\text{mid}})}(y, v_l)\right)\cos\theta_{il}\right)_{i,l\neq j},$$

tends to

$$\det(v_0(v_r) - x(v_r), \ldots, v_{j-1}(v_r) - x(v_r), v_{j+1}(v_r) - x(v_r), \ldots, v_n(v_r) - x(v_r))^2 \tag{3.59}$$

so that $Q_{\mathbb{H}(\Lambda_{\text{mid}})(\sigma_{\mathbb{H}(\Lambda_{\text{mid}})}(v_r))}$ tends to $(\frac{n!}{n+1}\text{vol}(\sigma^{\mathbb{E}}(v_r)))^2$. This means conditions in Theorem 3.6.6 and Theorem 3.10.10 coincide in the limit except that the prefactor is slightly better for Theorem 3.10.10 and Λ replaced by $|\Lambda_- - \Lambda_+|$. This replacement by $|\Lambda_- - \Lambda_+|$ is the significant step we make in this section.

Starting with the hyperbolic quality measure $Q_{\mathbb{H}(\Lambda^{\mathbb{H}}_{\text{mid}})}(\sigma_{\mathbb{H}(\Lambda^{\mathbb{H}}_{\text{mid}})}(v_r))$ also tends to $(\frac{n!}{n+1}\text{vol}(\sigma^{\mathbb{E}}(v_r)))^2$. However, due to the complicated nature of the quality bounds in Theorem 3.10.11 it is harder to compare to Theorem 3.6.6. In Section 3.10.5 we shall see that the quality bounds are proportional to $|\Lambda_- - \Lambda_+|$. Again it is this proportionality that sets these results apart.

3.10.2 Overview of the proof method

Recapitulation of Section 3.6

In Section 3.6 we assumed that a set of points $\{v_0, \ldots, v_n\}$ in a convex ball was given in M. The sectional curvatures K of M were supposed to be bounded that is $|K| \leq \Lambda$. The points $v_0, \ldots, v_n$ we think of as vertices of the Riemannian simplex. The point x is an arbitrary point in the convex ball that contains the vertices. We choose a vertex v_r from the vertex set. It is quality of the simplex $(\sigma^{\mathbb{E}}(v_r))$ found by taking the convex hull of the image of $v_0, \ldots, v_n$ under the

inverse exponential map $\exp_{v_r}^{-1}$ that (in the end) is used in the conditions for non-degeneracy of the Riemannian simplex.

To provide the conditions in Section 3.6 we started with $\exp_{v_r}^{-1}(x), \exp_{v_r}^{-1}(v_0)$, $\ldots, \exp_{v_r}^{-1}(v_n)$ and used the following steps:

1. Use the Toponogov comparison theorem to bound the difference between the lengths of the geodesics connecting vertices v_i and v_j and the lengths the geodesics connecting vertices x and v_i on the one hand and the corresponding (via the map $\exp_{\mathbb{H}(\pm\Lambda)} \circ \exp_{v_r}^{-1}$) lengths of geodesics on spaces of constant curvature $\mathbb{H}(\pm\Lambda)$ on the other.

2. Prove that the lengths of these geodesics are not far from what you would expect in the Euclidean case (via the map $\exp_M^{-1}$) if the vertices and x lie close together relative to the bounds on the sectional curvature on M.

3. Given these approximate lengths of the geodesics we again use the Toponogov comparison theorem and explicit calculations on spaces of constant curvature to give estimates on difference between the inner products between tangents to the geodesics from x to the vertices and the expectation in the Euclidean case.

4. $n \times n$ of these inner products between the tangents of geodesics from x to the vertices are put into a single Gram matrix. The determinant of this matrix is non-zero if and only if the tangents to the geodesics emanating from x are linearly independent. A result by Friedland describes the behaviour of the determinant under perturbations of the entries. This means that the determinant of the Gram matrix is close to the determinant of the Gram matrix one expects in the Euclidean case, to be precise the matrix with entries $(\exp_{v_r}^{-1}(v_i) - \exp_{v_r}^{-1}(x)) \cdot (\exp_{v_r}^{-1}(v_l) - \exp_{v_r}^{-1}(x))$. This allows us to give conditions that guarantee that there are n tangents to the geodesics emanating from x that are linearly independent, based on the quality of the simplex you would expect in the Euclidean case ($\sigma^{\mathbb{E}}(v_r)$).

5. If for every x in a sufficiently large convex neighbourhood some n tangents to the geodesics emanating from x and going to the vertices are linearly independent, the simplex is non-degenerate.

Overview of this section, that is Section 3.10

In this section we are interested in Riemannian simplices on manifolds whose sectional curvatures are very close to constant, meaning that the sectional curvature K satisfies $\Lambda_- \leq K \leq \Lambda_+$ with $|\Lambda_- - \Lambda_+|$ small relative to $|\Lambda_-|$. This means that we always suppose that $0 < \Lambda_-$ or $\Lambda_+ < 0$. We have to distinguish between

positive sectional curvature (elliptic) and negative sectional curvature (hyperbolic). Because the sectional curvatures are very close to constant, comparing the manifold to Euclidean space is unnatural. Instead we compare to spaces of constant curvature Λ_{mid} if the curvature is positive and $\Lambda^{\mathbb{H}}_{\text{mid}}$ if the curvature is negative, whose sectional curvature lies in the interval $[\Lambda_-, \Lambda_+]$.

In the elliptic case we shall compare to the space with constant curvature

$$\Lambda_{\text{mid}} = \frac{1}{2}(\Lambda_- + \Lambda_+).$$

The hyperbolic case will be more involved. In particular the non-degeneracy conditions will be in terms of the quality of the simplex $\sigma_{\mathbb{H}(\Lambda^{(\mathbb{H})}_{\text{mid}})}(v_r)$ with vertices

$$\exp_{\mathbb{H}(\Lambda^{(\mathbb{H})}_{\text{mid}})} \circ \exp^{-1}_{v_r,M}(v_i),$$

where $\exp_{v_r,M}$ denotes the exponential function of M at v_r. Here $\Lambda^{(\mathbb{H})}_{\text{mid}}$ stands for one of the alternatives, namely Λ_{mid} or $\Lambda^{\mathbb{H}}_{\text{mid}}$.Quality measures for constant curvature spaces are not common and no such measure suited to our need existed previously. We introduce a quality measure in Section 3.10.3 that is suited.

Our steps to provide quality bounds that guarantee non-degeneracy of the simplex shall be the following:

1. Use the Toponogov comparison theorem to bound the difference between the lengths of the geodesics connecting vertices v_i and v_j and the lengths the geodesics connecting vertices x and v_i on the one hand and the corresponding (via the map $\exp_{\mathbb{H}(\Lambda_+)} \circ \exp^{-1}_{v_r,M}$ and $\exp_{\mathbb{H}(\Lambda_-)} \circ \exp^{-1}_{v_r,M}$, respectively) lengths of geodesics on spaces of constant curvature $\mathbb{H}(\Lambda_-)$ and $\mathbb{H}(\Lambda_+)$.

   This step is identical to first step above, except that we use the more refined curvature bounds Λ_- and Λ_+ instead of $\pm\Lambda$.

2. Prove that the lengths of these geodesics are not far from what you would expect on the space $\mathbb{H}(\Lambda^{(\mathbb{H})}_{\text{mid}})$ (via the map $\exp_{\mathbb{H}(\Lambda^{(\mathbb{H})}_{\text{mid}})} \circ \exp^{-1}_{v_r,M}$) if the vertices and x lie close together relative to the bounds on the sectional curvature on M. It is at this point where the analyses in the elliptic and hyperbolic cases really start to differ.

   Clearly this step differs from the corresponding step above because $\mathbb{H}(\Lambda^{(\mathbb{H})}_{\text{mid}})$ replaces Euclidean space.

3. Given these approximate lengths of the geodesics we can again use the Toponogov comparison theorem and explicit calculations on spaces of con-

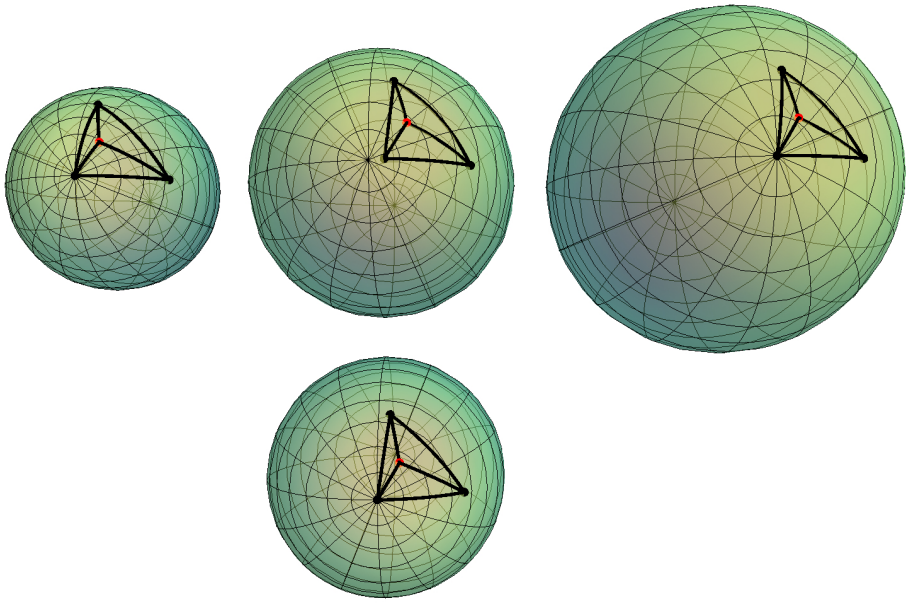

Figure 3.10: Pictorial overview (top view) of our approach in the case of positive curvature, the negative curvature case is similar but difficult to depict:
Above we see from left to right a small sphere, an ellipsoid and a large sphere. Below we see a sphere of mediocre size. The small sphere is the example of $\mathbb{H}(\Lambda_+)$, the large sphere of $\mathbb{H}(\Lambda_-)$ and the sphere of mediocre size of $\mathbb{H}(\Lambda_{\text{mid}})$. The ellipsoid is the manifold M.
The vertices on M are depicted in black, as are the vertices on the spaces of constant curvature left, right and below. The vertices on M are transplanted on spaces of constant curvature by the maps $\exp_{\mathbb{H}(\Lambda_+)} \circ \exp_{v_r,M}^{-1}$, $\exp_{\mathbb{H}(\Lambda_-)} \circ \exp_{v_r,M}^{-1}$ and $\exp_{\mathbb{H}(\Lambda_{\text{mid}})} \circ \exp_{v_r,M}^{-1}$, respectively. The same holds for the arbitrary point x (red).
The angles between the tangents to the geodesics emanating from the red point on M (the ellipsoid in the middle) are by the Topogonov comparison theorem close to the corresponding angles in the spaces of constant curvature (left and right). In turn these spaces of constant curvature are similar to the space with curvature Λ_{mid} (middle bottom).

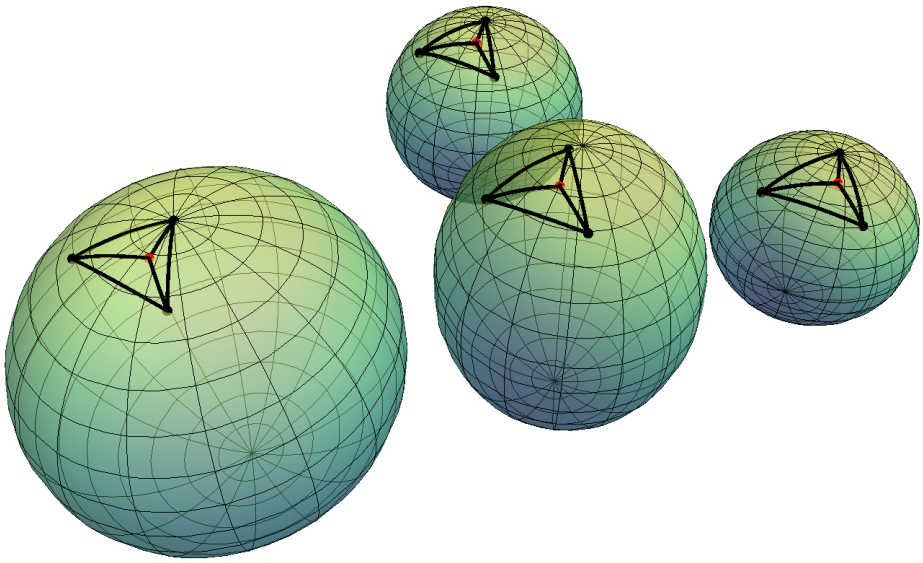

Figure 3.11: Side view of Figure 3.10.

stant curvature to give estimates on difference between the following[11] 'inner products':

$$\frac{1}{\Lambda_{\text{mid}}} \sin \sqrt{\Lambda_{\text{mid}}} d_M(x, v_i) \sin \sqrt{\Lambda_{\text{mid}}} d_M(x, v_j) \cos \theta_{ij,M} \qquad \text{(elliptic)}$$

$$\frac{1}{\Lambda^{\mathbb{H}}_{\text{mid}}} \sinh \sqrt{\Lambda^{\mathbb{H}}_{\text{mid}}} d_M(x, v_i) \sinh \sqrt{\Lambda^{\mathbb{H}}_{\text{mid}}} d_M(x, v_j) \cos \theta_{ij,M} \qquad \text{(hyperbolic),}$$

with $\theta_{ij,M}$ the angle between the geodesics from x to v_i and v_j, and the expectation of these 'inner products' in $\mathbb{H}(\Lambda^{(\mathbb{H})}_{\text{mid}})$. As before elliptic refers to positive sectional curvature, here $\Lambda_{\text{mid}} > 0$, and hyperbolic refers to negative sectional curvature, here $\Lambda^{\mathbb{H}}_{\text{mid}} < 0$.

This step differs from the one we used in the recapitulation of Section 3.6 because we no longer use the standard inner product.

[11] The inner products introduced here have a nice geometric interpretation, which is easiest to see for the elliptic sphere: Suppose that the sphere ($\mathbb{H}(\Lambda_{\text{mid}})$) is embedded in Euclidean space in the standard manner, that is as a round sphere of codimension one. In this setting these inner products are the inner products between the vectors in $T_x\mathbb{H}(\Lambda_{\text{mid}})$ that go from x to the projection vertices onto the tangent space $T_x\mathbb{H}(\Lambda_{\text{mid}})$, where the projection goes via the normal to $T_x\mathbb{H}(\Lambda_{\text{mid}})$. We shall get back to this in more detail below.

4. $n \times n$ of these 'inner products' are put into a pseudo Gram matrix. We shall introduce this pseudo Gram matrix below. The determinant of this matrix is non-zero if and only if the tangents to the geodesics emanating from x are linearly independent. A result by Friedland describes the behaviour of the determinant under perturbations of the entries. This means that the determinant of the Gram matrix is close to the determinant of the Gram matrix one expects for $\mathbb{H}(\Lambda^{(\mathbb{H})}_{\text{mid}})$. This allows us to give conditions that guarantee that there are n tangents to the geodesics emanating from x that are linearly independent, based on the quality of the simplex you would expect in the the constant curvature case.

   This step only differs from the fourth step we mentioned in the recapitulation of Section 3.6 in that 'inner products' are different.

5. If for every x in a sufficiently large convex neighbourhood some n tangents to the geodesics emanating from x and going to the vertices are linearly independent, the simplex is non-degenerate.

   This step is identical to the fifth step in the overview of the approach of Section 3.6.

The main building blocks for this approach where we model our intrinsic simplices on simplices on spaces of constant curvature are the pseudo Gram matrices to which we dedicate our first subsection. The calculations necessary to compare different spaces of constant curvature are the topic of the second subsection. The comparison of spaces of different constant curvature will mainly focus on the cosine rule in imitation of Lemmas 3.6.2 and 3.6.3. In the third subsection we combine the results to Theorems 3.10.10 and 3.10.11.

3.10.3 Simplex quality on constant curvature spaces

In this subsection we shall introduce an alternative for the Gram matrix that is specific to spaces of non-trivial constant curvature. In this section $\mathbb{H}(1/r^2)$, the n-sphere with radius r and therefore sectional curvature $1/r^2$, will be assumed to be isometrically embedded in Euclidean space with co-dimension one. This means that we view it as round sphere in the traditional sense. The hyperbolic sphere $\mathbb{H}(-1/r^2)$, the hyperbolic n-sphere with imaginary radius r and therefore sectional curvature $-1/r^2$, is often viewed as embedded using the Minkowski or Hyperboloid model. This is an embedding as the 'upper' connected component of a two sheeted hyperboloid, given by $-x_0^2 + x_1^2 + \cdots + x_n^2 = -r^2$, in Minkowski space with metric[12] $\mathrm{d}s^2 = -\mathrm{d}x_0^2 + \mathrm{d}x_1^2 + \cdots + \mathrm{d}x_n^2$.

[12] The other choice would yield a negatively definite metric.

As in Section 3.6 we shall mostly denote distances as $d_M(x, y)$. In this section M is often a space of constant curvature. The exception will be when we are in Euclidean space and we want to emphasize that it is a vector space in the hope to remind the reader of similar statements in Section 3.6. If so we shall write $|x - y|$. So $|x - y|$ is used interchangeably with $d_{\mathbb{R}^{n+1}}(x, y)$, but in the one case x and y are thought of as vectors and the other as points in Euclidean space.

We discuss the elliptic case first, because the geometric interpretation is easier. Our first lemma helps to establish that the alternative Gram matrices, which we shall define below, for spaces of constant curvature are indeed a measure of quality. By which we mean that the alternative Gram matrix is zero if and only if a reasonable degeneracy occurs.

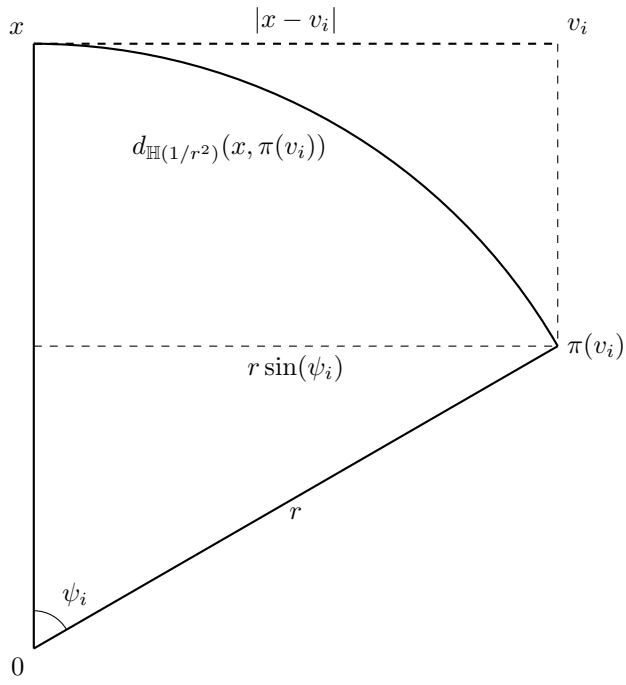

Figure 3.12: Intersection of the sphere with x, v_i and $\pi(v_i)$. Because of lack of space we have introduced the notation $\psi_i = d_{\mathbb{H}(1/r^2)}(x, \pi(v_i))/r$.

Remark 3.10.1 *We note that a space of constant sectional curvature $1/r^2$ is a sphere that can be embedded as a round sphere of co-dimension one in Euclidean space. The radius of this sphere is r.*

Lemma 3.10.2 *Suppose that $x, v_0, \ldots, v_{n-1}$ are the vertices of a simplex in $L \subset \mathbb{R}^{n+1}$, where L is an n-dimensional linear subspace, such that $d_{\mathbb{R}^{n+1}}(x, v_i) \leq d$. Furthermore let $(\mathbb{H}(1/r^2))(y, r)$ be a sphere in $\mathbb{R}^{n+1}$ with centre y, such that $x \in (\mathbb{H}(1/r^2))(y, r)$ and the tangent space $T_x(\mathbb{H}(1/r^2))(y, r)$ coincides with L and $d < r$. We emphasize that $x \in L$. Denote by π the projection from L onto $(\mathbb{H}(1/r^2))(y, r)$ via the normal of L. The domain of this map is $B^n_L(x, r)$ the ball in L centred at x with radius r. See Figure 3.12 for a sketch. Then*

$$\det\left(d_{(\mathbb{H}(1/r^2))}(x, \pi(v_i))d_{(\mathbb{H}(1/r^2))}(x, \pi(v_l))\cos\theta_{il}\right)_{0\leq i,l\leq n-1} = 0,$$

where $\theta_{ij} = \angle v_i x v_j$, if and only if

$$\det(|x - v_i||x - v_l|\cos\theta_{il})_{0\leq i,l\leq n-1} =$$
$$\det\left(r^2 \sin\left(\frac{d_{(\mathbb{H}(1/r^2))}(x, \pi(v_i))}{r}\right)\sin\left(\frac{d_{(\mathbb{H}(1/r^2))}(x, \pi(v_l))}{r}\right)\cos\theta_{il}\right)_{0\leq i,l\leq n-1} = 0.$$

Proof We can assume that $x \neq v_i$ for all i, because if $x = v_i$ for some i there is nothing to prove. Due to linearity of the determinant we have

$$\begin{aligned}
&\det(d_{(\mathbb{H}(1/r^2))}(x, \pi(v_i))d_{\mathbb{H}(1/r^2)}(x, \pi(v_l))\cos\theta_{il}) \\
&\quad = \left(\prod_i d_{\mathbb{H}(1/r^2)}(x, \pi(v_i))\right)\det\left(d_{\mathbb{H}(1/r^2)}(x, \pi(v_l))\cos\theta_{il}\right) \\
&\quad = \left(\prod_i d_{\mathbb{H}(1/r^2)}(x, \pi(v_i))\right)\left(\prod_l d_{\mathbb{H}(1/r^2)}(x, \pi(v_l))\right)\det(\cos\theta_{il}) \\
&\quad = \left(\prod_i d_{\mathbb{H}(1/r^2)}(x, \pi(v_i))^2\right)\det(\cos\theta_{il})
\end{aligned}$$

and similarly

$$\begin{aligned}
&\det(|x - v_i||x - v_l|\cos\theta_{il}) \\
&\quad = \det\left(r\sin\left(\frac{d_{\mathbb{H}(1/r^2)}(x, \pi(v_i))}{r}\right)r\sin\left(\frac{d_{\mathbb{H}(1/r^2)}(x, \pi(v_l))}{r}\right)\cos\theta_{il}\right) \\
&\quad = \left(\prod_i r\sin\left(\frac{d_{\mathbb{H}(1/r^2)}(x, \pi(v_i))}{r}\right)\right)^2\det(\cos\theta_{il}). \qquad (3.60)
\end{aligned}$$

Given that by assumption $|x - v_i| \neq 0$ and

$$\sin\left(\frac{d_{(\mathbb{H}(1/r^2))}(x, \pi(v_i))}{r}\right) \neq 0,$$

for all i the claim follows. □

We shall refer to a matrix of the form

$$\left(r^2 \sin\left(\frac{d_{\mathbb{H}(1/r^2)}(x,v_i)}{r}\right)\sin\left(\frac{d_{\mathbb{H}(1/r^2)}(x,v_l)}{r}\right)\cos\theta_{il}\right)$$

as a spherical pseudo Gram matrix.

We use the pseudo Gram matrix to introduce a quality measure $Q_{\mathbb{H}(1/r^2)}$ for simplices on the sphere with vertices $v_0,\ldots,v_n$

$$\begin{aligned}&Q_{\mathbb{H}(1/r^2)}(\sigma)\\ &= \min_{x\in\mathbb{H}(1/r^2)} \max_j \left\{\det\left(r^2\sin\left(\frac{d_{\mathbb{H}(1/r^2)}(x,v_i)}{r}\right)\right.\right.\\ &\qquad\left.\left.\sin\left(\frac{d_{\mathbb{H}(1/r^2)}(x,v_l)}{r}\right)\cos\theta_{il}\right)_{i,l\neq j}\right\}. \qquad (3.61)\end{aligned}$$

By the notation $i,l\neq j$ we mean to imply that $i,j\in\{0,\ldots,j-1,j+1,\ldots,n\}$. If we view the sphere $Q_{\mathbb{H}(1/r^2)}$ as being embedded in the Euclidean space $\mathbb{R}^{n+1}$ this has the interpretation

$$\begin{aligned}Q_{\mathbb{H}(1/r^2)}(\sigma) &= \min_{x\in\mathbb{H}(1/r^2)} \max_j\{\det\left(\tilde{\pi}_x v_i\cdot\tilde{\pi}_x v_l\right)_{i,l\neq j}\}\\ &= \min_{x\in\mathbb{H}(1/r^2)} \max_j\{\left(\det\left(\tilde{\pi}_x v_i\right)_{i\neq j}\right)^2\}, \qquad (3.62)\end{aligned}$$

where $\tilde{\pi}_x$ is the projection onto the hyperplane characterized by the normal x, that is tangent to $\mathbb{H}(1/r^2)$. This interpretation follows from (3.60).

In our definition we have chosen specifically to let x run over the entire sphere. In particular we include the case where all vertices are equally parsed on the equator. In this case the quality is zero. This is in accordance with our intuition because we would not know on which hemisphere to draw the simplex.

Now we shall give some lower bounds on the quality $Q_{\mathbb{H}(1/r^2)}$. These bounds should strengthen our intuition. Let us consider the simplex $\{0,v_0,\ldots,v_n\}$ in $\mathbb{R}^{n+1}$. Suppose that $B(y,\rho)$ is a ball that lies inside this simplex. Clearly the choice of hyperplane onto which one projects this ball does not influence the volume of the projected ball. Let us denote the volume of the projected ball is $\mathrm{vol}(\pi_x(B(y,\rho)))$. Equation (3.62) now implies that $Q_{\mathbb{H}(1/r^2)} > \mathrm{vol}(\pi_x(B(y,\rho)))^2$.

This completes our discussion of quality in the elliptic setting and we continue to the hyperbolic case.

The direct analogue of Lemma 3.10.2 holds for the Minkowski or hyperboloid model of hyperbolic spaces of constant curvature. For this setting we therefore we introduce the hyperbolic pseudo Gram matrix

$$\left(r^2\sinh\left(\frac{d_{\mathbb{H}^n(-1/r^2)}(x,v_i)}{r}\right)\sinh\left(\frac{d_{\mathbb{H}^n(-1/r^2)}(x,v_l)}{r}\right)\cos\theta_{il}\right)$$

as well as the quality measure for simplices on the hyperbolic sphere with vertices $v_0, \ldots, v_n$ for some neighbourhood N

$$Q_{\mathbb{H}(-1/r^2)} = \min_{x \in N} \max_j \left\{ \det \left(r^2 \sinh \left(\frac{d_{\mathbb{H}^n(-1/r^2)}(x, v_i)}{r} \right) \right. \right. \\ \left. \left. \sinh \left(\frac{d_{\mathbb{H}^n(-1/r^2)}(x, v_l)}{r} \right) \cos \theta_{il} \right)_{i,l \neq j} \right\}. \quad (3.63)$$

Remark 3.10.3 *Unfortunately the geometric interpretation is more difficult in this hyperbolic setting and we have not (yet) been able to provide a discussion similar to the one for spaces of positive curvature above.*

3.10.4 Approximating cosine rules

In this section we derive the analogues of Lemma 3.6.2, given in Lemmas 3.10.4 and 3.10.6, and Lemma 3.6.3, given in Lemmas 3.10.8 and 3.10.9.

In Lemmas 3.10.4 and 3.10.6 one assumes that a, b and c are the lengths of the edges of a geodesic triangle in a space of constant curvature $\pm 1/k^2$ and γ the enclosed angle, see the sketch below. This means that a, b, c and γ satisfy the cosine rule for a space of curvature $\pm 1/k^2$, that is (3.13) or (3.14). If $\pm 1/l^2$ is close to $\pm 1/k^2$, then a, b, c and γ 'nearly satisfy' the cosine rule for a space of curvature $\pm 1/l^2$. We will quantify 'nearly satisfy' in Lemmas 3.10.4 and 3.10.6. This result is essential to compare hinges.

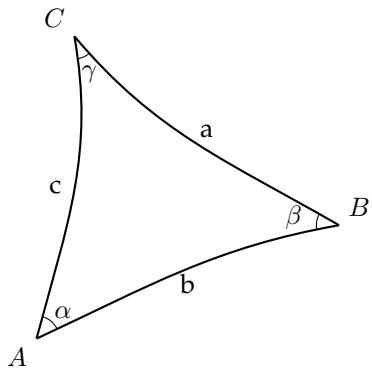

In Lemmas 3.10.8 and 3.10.9 we assume that a, b and c are given up to some error. Once more a, b and c are the lengths of the edges of a geodesic triangle in a space of constant curvature $\pm 1/k^2$. In Lemmas 3.10.8 and 3.10.9 we derive

some bounds on

$$\sin\frac{b}{l}\sin\frac{c}{l}\cos\alpha$$

and

$$\sinh\frac{b}{l}\sinh\frac{c}{l}\cos\alpha,$$

respectively.

We shall first discuss the elliptic and then the hyperbolic case.

Cosine rule for spaces of positive curvature

We want to compare the cosine rule in two spaces of positive curvature. To be precise we will prove the following

Lemma 3.10.4 *Let*

$$0 < l \le k \qquad a, b, c \le \frac{1}{2}l \qquad a, b, c \le d_{max}.$$

If a, b, c *and* γ *satisfy*

$$k^2\cos\frac{c}{k} - k^2\cos\frac{a}{k}\cos\frac{b}{k} = k^2\sin\frac{a}{k}\sin\frac{b}{k}\cos\gamma \tag{3.64}$$

a, b, c *and* γ *also satisfy*

$$l^2\cos\frac{c}{l} - l^2\cos\frac{a}{l}\cos\frac{b}{l} = l^2\sin\frac{a}{l}\sin\frac{b}{l}\cos\gamma + R_T(a, b, c)$$

with

$$R_T(a, b, c) \le \left|\frac{1}{l^2} - \frac{1}{k^2}\right| \frac{11 d_{max}^4}{4!}.$$

Here R_T *stands for the total remainder, because it is found by studying remainders in the Taylor series of the constituents in* (3.64).

The assumption $k \ge l$ is only used to streamline the calculations, in the sense that it can be replaced by $k > 0$ and $a, b, c \le \frac{1}{2}k$. We shall prove this statement by examining the individual terms in (3.64). Our estimates are based on Taylor's theorem with remainder in one and multiple variables.

We start with the first term on the left hand side of the cosine rule, we multiply by k and l respectively to ensure that the quadratic terms cancel

$$\begin{aligned} l^2 \cos\frac{c}{l} - k^2 \cos\frac{c}{k} &= l^2 - k^2 - R_{pc}(c) \\ |R_{pc}(c)| &\leq \frac{c^4}{4!} \sup_{c\in[0,l/2]} \left| l^2 \partial_c^4 \cos\frac{c}{l} - k^2 \partial_c^4 \cos\frac{c}{k} \right| \\ &= \frac{c^4}{4!} \sup_{c\in[0,l/2]} \left| \frac{1}{l^2} \cos\frac{c}{l} - \frac{1}{k^2} \cos\frac{c}{k} \right| \\ &\leq \left| \frac{1}{l^2} - \frac{1}{k^2} \right| \frac{c^4}{4!}, \end{aligned}$$

the notation R_{pc} is used to remind us of the fact that it is a remainder, in the sense of Taylor, and we consider perturbations of the cosine, hence pc. The supremum is assumed in $c = 0$ because

$$\frac{1}{l^n} \cos\frac{c}{l} - \frac{1}{k^n} \cos\frac{c}{k}$$

is monotone in c, which can be seen by taking the derivative and noting that

$$\frac{k^{n+1}}{l^{n+1}} > 1 \qquad\qquad \frac{\sin\frac{c}{k}}{\sin\frac{c}{l}} < 1.$$

For the other terms we need the following estimates

Lemma 3.10.5 *Provided $k \geq l > 0$ and $a/l, b/l < 1/2$, we have that*

$$\frac{1}{l^2} \cos\frac{a}{l} \cos\frac{b}{l} - \frac{1}{k^2} \cos\frac{a}{k} \cos\frac{b}{k} \leq \frac{1}{l^2} - \frac{1}{k^2}$$

and

$$\frac{1}{l^2} \sin\frac{a}{l} \sin\frac{b}{l} - \frac{1}{k^2} \sin\frac{a}{k} \sin\frac{b}{k} \leq \frac{1}{l^2} - \frac{1}{k^2}$$

Proof The first inequality is equivalent to

$$\frac{1}{k^2} - \frac{1}{k^2} \cos\frac{a}{k} \cos\frac{b}{k} \leq \frac{1}{l^2} - \frac{1}{l^2} \cos\frac{a}{l} \cos\frac{b}{l}$$

it therefore suffices to prove that

$$x^2 - x^2 \cos ax \cos bx$$

is monotone increasing in x on the given domain, which can be seen by differentiating and equating to zero and noting that there is no solution given the conditions on a and b:

$$\begin{aligned}&\partial_x(x^2 - x^2\cos ax\cos bx)\\&\quad = 2x - 2x\cos ax\cos bx + x^2 a\sin ax\cos bx + x^2 b\cos ax\sin bx = 0\\&\quad 2 + xa\sin ax\cos bx + xb\cos ax\sin bx = 2\cos ax\cos bx\end{aligned}$$

and considering the Taylor series at $x = 0$. The last equality has no solutions except $x = 0$ under the assumptions because $0 \leq ax, bx \leq 1/2$ implies that

$$xa\sin ax\cos bx + xb\cos ax\sin bx \geq 0 \qquad\qquad \cos ax\cos bx \leq 1$$

with the equality only achieved if $x = 0$ or trivial a, b. Similarly the second inequality can be proven

$$\frac{1}{l^2}\sin\frac{a}{l}\sin\frac{b}{l} - \frac{1}{k^2}\sin\frac{a}{k}\sin\frac{b}{k} \leq \frac{1}{l^2} - \frac{1}{k^2}$$

is equivalent to

$$\frac{1}{k^2} - \frac{1}{k^2}\sin\frac{a}{k}\sin\frac{b}{k} \leq \frac{1}{l^2} - \frac{1}{l^2}\sin\frac{a}{l}\sin\frac{b}{l}$$

which follows from the monotonicity of $x^2(1 - \sin ax\sin bx)$ in x, which is again established by taking the derivative and equating to zero

$$\begin{aligned}&\partial_x(x^2(1 - \sin ax\sin bx))\\&\quad = 2x(1 - \sin ax\sin bx) - x^2(b\sin ax\cos bx + a\cos ax\sin bx) = 0,\end{aligned}$$

which has no solutions except $x = 0$ because in the given domain

$$2\sin ax\sin bx + bx\sin ax\cos bx + ax\cos ax\sin bx \leq \frac{3}{2}$$

which completes the proof of the second inequality. Note that this is the only place where we really use the assumption $a, b, c \leq \frac{1}{2}l$. □

With this intermediate result we can return to the proof of Lemma 3.10.4, where we apply the result of Lemma 3.10.5 almost immediately.

Using Taylor's theorem for multiple variables we have

$$k^2\cos\frac{a}{k}\cos\frac{b}{k} - l^2\cos\frac{a}{l}\cos\frac{b}{l} = k^2 - l^2 + R_{pcc}(a, b)$$

with

$$|R_{pcc}(a,b)| \leq \left|\frac{1}{l^2} - \frac{1}{k^2}\right| \frac{5d_{\max}^4}{4!}.$$

This follows from the fact that

$$\partial_a^i \partial_b^j (k^2 \cos\frac{a}{k}\cos\frac{b}{k} - l^2 \cos\frac{a}{l}\cos\frac{b}{l} - (k^2 - l^2)) = 0$$

for $0 \leq i \leq 3-j$, $0 \leq j \leq 3$ and

$$\begin{aligned}
&|\partial_a^i \partial_b^j (k^2 \cos\frac{a}{k}\cos\frac{b}{k} - l^2 \cos\frac{a}{l}\cos\frac{b}{l} - (k^2 - l^2))| \\
&\quad = \begin{cases} |\frac{1}{k^2}\cos\frac{a}{k}\cos\frac{b}{k} - \frac{1}{l^2}\cos\frac{a}{l}\cos\frac{b}{l}| & \text{if } i+j=4 \text{ and } i,j \text{ even}, \\ |\frac{1}{l^2}\sin\frac{x}{l}\sin\frac{y}{l} - \frac{1}{k^2}\sin\frac{x}{k}\sin\frac{y}{k}|, & \text{if } i+j=4 \text{ and } i,j \text{ odd}, \end{cases} \\
&\quad \leq \left|\frac{1}{l^2} - \frac{1}{k^2}\right|,
\end{aligned}$$

where in the last line we used the result of Lemma 3.10.5.

Likewise we have that

$$\begin{aligned}
l^2 \sin\frac{a}{l}\sin\frac{b}{l} - k^2 \sin\frac{a}{k}\sin\frac{b}{k} &= R_{pss}(x) \\
|R_{pss}(x)| &\leq \left|\frac{1}{l^2} - \frac{1}{k^2}\right| \frac{5d_{\max}^4}{4!}
\end{aligned}$$

This follows from exactly the same reasoning

$$\partial_a^i \partial_b^j (l^2 \sin\frac{a}{l}\sin\frac{b}{l} - k^2 \sin\frac{a}{k}\sin\frac{b}{k}) = 0$$

for $0 \leq i \leq 3-j$, $0 \leq j \leq 3$ and

$$\begin{aligned}
&|\partial_a^i \partial_b^j (l^2 \sin\frac{a}{l}\sin\frac{b}{l} - k^2 \sin\frac{a}{k}\sin\frac{b}{k})| \\
&\quad = \begin{cases} |\frac{1}{l^2}\sin\frac{x}{l}\sin\frac{y}{l} - \frac{1}{k^2}\sin\frac{x}{k}\sin\frac{y}{k}| & \text{if } i+j=4 \text{ and } i,j \text{ even}, \\ |\frac{1}{k^2}\cos\frac{a}{k}\cos\frac{b}{k} - \frac{1}{l^2}\cos\frac{a}{l}\cos\frac{b}{l}|, & \text{if } i+j=4 \text{ and } i,j \text{ odd}, \end{cases} \\
&\quad \leq \left|\frac{1}{l^2} - \frac{1}{k^2}\right|,
\end{aligned}$$

where again in the last line we used the result of Lemma 3.10.5.

We can now combine these estimates and apply them to the cosine rule, which we multiply by k^2 and write down in different order for convenience. Assuming that $k > l > 0$, $a/l, b/l, c/l \leq \frac{1}{2}$ and $a, b, c \leq d_{\max}$, we see

$$\begin{aligned} k^2 \cos\frac{c}{k} - k^2 \cos\frac{a}{k}\cos\frac{b}{k} &= k^2 \sin\frac{a}{k}\sin\frac{b}{k}\cos\gamma \\ l^2 \cos\frac{c}{l} - l^2 \cos\frac{a}{l}\cos\frac{b}{l} - R_{pc}(c) + R_{pcc}(a,b) &= l^2 \sin\frac{a}{l}\sin\frac{b}{l}\cos\gamma \\ &\quad - R_{pss}(a,b)\cos\gamma \\ l^2 \cos\frac{c}{l} - l^2 \cos\frac{a}{l}\cos\frac{b}{l} &= l^2 \sin\frac{a}{l}\sin\frac{b}{l}\cos\gamma \\ &\quad + R_T(a,b,c) \end{aligned}$$

with

$$R_T(a,b,c) \leq \left|\frac{1}{l^2} - \frac{1}{k^2}\right| \frac{11 d_{\max}^4}{4!}.$$

This completes the proof of Lemma 3.10.4.

Cosine rule for spaces of negative curvature

We now want to compare the cosine rule in two spaces of negative curvature, like we have done for spaces of positive curvature in Lemma 3.10.4. To be precise we prove the following lemma

Lemma 3.10.6 *Assuming that $k \geq l > 0$, and $a, b, c \leq d_{max}$, we have that if a, b, c and γ satisfy*

$$k^2 \cosh\frac{c}{k} - k^2 \cosh\frac{a}{k}\cosh\frac{b}{k} = -k^2 \sinh\frac{a}{k}\sinh\frac{b}{k}\cos\gamma$$

they also satisfy

$$l^2 \cosh\frac{c}{l} - l^2 \cosh\frac{a}{l}\cosh\frac{b}{l} = -l^2 \sinh\frac{a}{l}\sinh\frac{b}{l}\cos\gamma + R_T(a,b,c)$$

with

$$R_T(a,b,c) \leq \left|\frac{1}{l^2}\cosh^2\frac{d_{max}}{l} - \frac{1}{k^2}\cosh^2\frac{d_{max}}{k}\right| \frac{11 d_{max}^4}{4!}.$$

Again the assumption $k \geq l$ is only used to streamline the calculations, in the sense that it can be replaced by $k > 0$. We shall follow the same procedure as in the elliptic case.

By Taylor's we see

$$l^2 \cosh \frac{c}{l} - k^2 \cosh \frac{c}{k} = l^2 - k^2 - R_{pch}(c),$$

with

$$\begin{aligned} |R_{pch}(c)| &\leq \frac{c^4}{4!} \sup_{c \in [0, d_{\max}]} \left| l^2 \partial_c^4 \cosh \frac{c}{l} - k^2 \partial_c^4 \cosh \frac{c}{k} \right| \\ &= \frac{c^4}{4!} \sup_{c \in [0, d_{\max}]} \left| \frac{1}{l^2} \cosh \frac{c}{l} - \frac{1}{k^2} \cosh \frac{c}{k} \right| \\ &\leq \left| \frac{1}{l^2} \cosh \frac{d_{\max}}{l} - \frac{1}{k^2} \cosh \frac{d_{\max}}{k} \right| \frac{c^4}{4!} \end{aligned}$$

The supremum is assumed in $c = d_{\max}$ because

$$\frac{1}{l^2} \cosh \frac{c}{l} - \frac{1}{k^2} \cosh \frac{c}{k}$$

is monotone in c, which can be seen by taking the derivative

$$\frac{1}{l^3} \cosh \frac{c}{l} - \frac{1}{k^3} \cosh \frac{c}{k}.$$

and observing that $\frac{1}{l} \geq \frac{1}{k}$ and $\cosh \frac{c}{l} \geq \cosh \frac{c}{k}$, because the hyperbolic cosine seen as a function from $\mathbb{R}_+$ to $\mathbb{R}_+$ is monotone.

For the remaining terms we again need a sub-lemma:

Lemma 3.10.7 *Provided $k \geq l \geq 0$ and $a, b, c \leq d_m$, we have that*

$$\frac{1}{l^2} \cosh \frac{a}{l} \cosh \frac{b}{l} - \frac{1}{k^2} \cosh \frac{a}{k} \cosh \frac{b}{k} \leq \frac{1}{l^2} \cosh^2 \frac{d_{max}}{l} - \frac{1}{k^2} \cosh^2 \frac{d_{max}}{k}$$

and

$$\begin{aligned} \frac{1}{l^2} \sinh \frac{a}{l} \sinh \frac{b}{l} - \frac{1}{k^2} \sinh \frac{a}{k} \sinh \frac{b}{k} &\leq \frac{1}{l^2} \sinh^2 \frac{d_{max}}{l} - \frac{1}{k^2} \sinh^2 \frac{d_{max}}{k} \\ &\leq \frac{1}{l^2} \cosh^2 \frac{d_{max}}{l} - \frac{1}{k^2} \cosh^2 \frac{d_{max}}{k} \end{aligned}$$

Proof The first two inequalities follow from the fact that both functions are monotone if one leaves one of the variables fixed. Monotonicity is proven by noting that the derivative is of the form

$$\frac{1}{l^3} \cosh \frac{y}{l} \sinh \frac{z}{l} - \frac{1}{k^3} \cosh \frac{y}{k} \sinh \frac{z}{k} = 0$$

which has no non-trivial solutions because $\cosh$ and $\sinh$ are monotone. The final inequality follows from

$$\frac{1}{k^2} = \frac{1}{k^2}\left(\cosh^2\frac{d_{\max}}{k} - \sinh^2\frac{d_{\max}}{k}\right) \leq \frac{1}{l^2}\left(\cosh^2\frac{d_{\max}}{l} - \sinh^2\frac{d_{\max}}{l}\right) = \frac{1}{l^2}$$

□

Using Taylors theorem for multiple variables we have

$$k^2\cosh\frac{a}{k}\cosh\frac{b}{k} - l^2\cosh\frac{a}{l}\cosh\frac{b}{l} = k^2 - l^2 + R_{pchch}(a,b)$$

with

$$|R_{pchch}(a,b)| \leq \left|\frac{1}{l^2}\cosh^2\frac{d_{\max}}{l} - \frac{1}{k^2}\cosh^2\frac{d_{\max}}{k}\right|\frac{5d_{\max}^4}{4!}.$$

This follows from the fact that

$$\partial_a^i\partial_b^j\left(k^2\cosh\frac{a}{k}\cosh\frac{b}{k} - l^2\cosh\frac{a}{l}\cosh\frac{b}{l} - (k^2-l^2)\right)\Big|_{a=b=0} = 0$$

for $0 \leq i \leq 3-j, 0 \leq j \leq 3$ and

$$\begin{aligned}
&|\partial_a^i\partial_b^j(k^2\cosh\frac{a}{k}\cosh\frac{b}{k} - l^2\cosh\frac{a}{l}\cosh\frac{b}{l})| \\
&= \begin{cases} |\frac{1}{k^2}\cosh\frac{a}{k}\cosh\frac{b}{k} - \frac{1}{l^2}\cosh\frac{a}{l}\cosh\frac{b}{l}| & \text{if } i+j=4 \text{ and } i,j \text{ even}, \\ |\frac{1}{l^2}\sinh\frac{x}{l}\sinh\frac{y}{l} - \frac{1}{k^2}\sinh\frac{x}{k}\sinh\frac{y}{k}|, & \text{if } i+j=4 \text{ and } i,j \text{ odd}, \end{cases} \\
&\leq \left|\frac{1}{l^2}\cosh^2\frac{d_{\max}}{l} - \frac{1}{k^2}\cosh^2\frac{d_{\max}}{k}\right|,
\end{aligned}$$

where in the last line we used the result of Lemma 3.10.7.

Likewise we have that

$$\begin{aligned}
l^2\sinh\frac{a}{l}\sinh\frac{b}{l} - k^2\sinh\frac{a}{k}\sinh\frac{b}{k} &= R_{pshsh}(x) \\
|R_{pshsh}(x)| &\leq \left|\left(\frac{1}{l^2}\cosh^2\frac{d_{\max}}{l} - \frac{1}{k^2}\cosh^2\frac{d_{\max}}{k}\right)\frac{5d_{\max}^4}{4!}\right|
\end{aligned}$$

This follows from exactly the same reasoning

$$\partial_a^i\partial_b^j(l^2\sinh\frac{a}{l}\sinh\frac{b}{l} - k^2\sinh\frac{a}{k}\sinh\frac{b}{k}) = 0$$

for $0 \leq i \leq 3-j$, $0 \leq j \leq 3$ and

$$\begin{aligned}
&|\partial_a^i \partial_b^j (l^2 \sinh\frac{a}{l}\sinh\frac{b}{l} - k^2 \sinh\frac{a}{k}\sinh\frac{b}{k})| \\
&= \begin{cases} |\frac{1}{l^2}\sinh\frac{x}{l}\sinh\frac{y}{l} - \frac{1}{k^2}\sinh\frac{x}{k}\sinh\frac{y}{k}| & \text{if } i+j=4 \text{ and } i,j \text{ even}, \\ |\frac{1}{k^2}\cosh\frac{a}{k}\cosh\frac{b}{k} - \frac{1}{l^2}\cosh\frac{a}{l}\cosh\frac{b}{l}|, & \text{if } i+j=4 \text{ and } i,j \text{ odd}, \end{cases} \\
&\leq \left| \frac{1}{l^2}\cosh^2\frac{d_{\max}}{l} - \frac{1}{k^2}\cosh^2\frac{d_{\max}}{k} \right|,
\end{aligned}$$

where again in the last line we used the result of Lemma 3.10.7.

We can now combine these estimates and apply them to the hyperbolic cosine rule, which we multiply by k^2 and write down in different order for convenience. Assuming that $k > l > 0$ and $a, b, c \leq d_{\max}$, we see

$$\begin{aligned}
k^2\cosh\frac{c}{k} - k^2\cosh\frac{a}{k}\cosh\frac{b}{k} &= -k^2\sinh\frac{a}{k}\sinh\frac{b}{k}\cos\gamma \\
l^2\cosh\frac{c}{l} - l^2\cosh\frac{a}{l}\cosh\frac{b}{l} - R_{pch}(c) + R_{pchch}(a,b) &= -l^2\sinh\frac{a}{l}\sinh\frac{b}{l}\cos\gamma \\
&\quad + R_{pshsh}(a,b)\cos\gamma \\
l^2\cosh\frac{c}{l} - l^2\cosh\frac{a}{l}\cosh\frac{b}{l} &= -l^2\sin\frac{a}{l}\sin\frac{b}{l}\cos\gamma \\
&\quad + R_{TH}(a,b,c)
\end{aligned}$$

with

$$R_{TH}(a,b,c) \leq \left| \frac{1}{l^2}\cosh^2\frac{d_{\max}}{l} - \frac{1}{k^2}\cosh^2\frac{d_{\max}}{k} \right| \frac{11 d_{\max}^4}{4!}$$

This completes the proof of Lemma 3.10.6 and therefore our discussion of the cosine rule.

The cosine with 'errors' in lengths for spaces of positive constant curvature

We can now give the analogues for Lemma 3.6.3, in case we compare to spaces of constant curvature instead of Euclidean space.

In the following lemma we start with a geodesic triangle on $\mathbb{H}(1/k^2)$ of which the lengths of the edges are approximately known. By approximately known we mean that the lengths of the edges a, b and c are close to the lengths a_l, b_l and c_l, the lengths of the edges of a geodesic triangle on $\mathbb{H}(1/l^2)$. The edges with length a_l, b_l and c_l will themselves be given as hinges, for example a_l satisfies

$$l^2\cos\frac{a_l}{l} = l^2\cos\frac{a_1}{l}\cos\frac{a_2}{l} + l^2\sin\frac{a_1}{l}\sin\frac{a_2}{l}\cos\gamma_a.$$

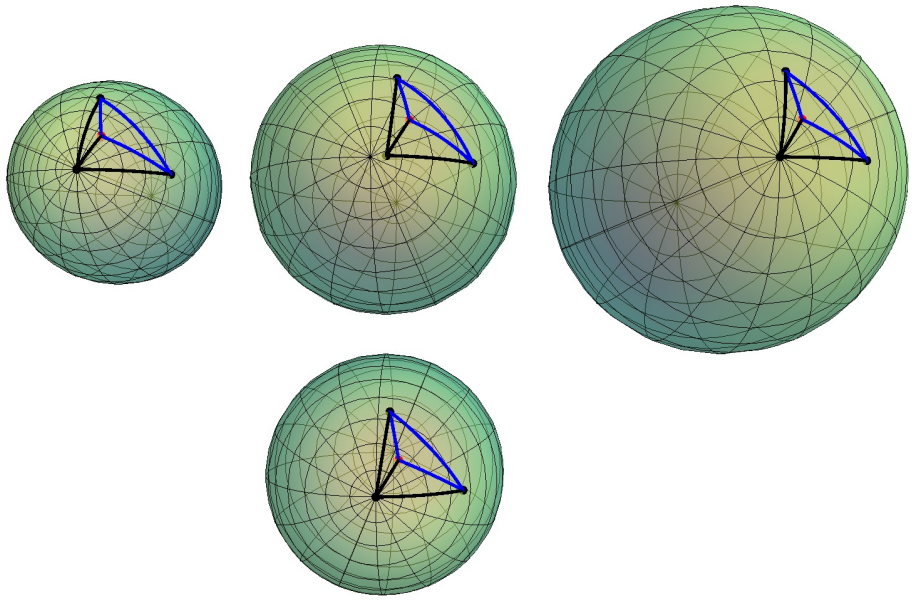

Figure 3.13: The role of Lemma 3.10.8 is the following:
Above we see from left to right a small sphere, an ellipsoid and a large sphere. Below we see a sphere of mediocre size. The small sphere is the example of $\mathbb{H}(\Lambda_+)$, the large sphere of $\mathbb{H}(\Lambda_-)$ and the sphere of mediocre size of $\mathbb{H}(\Lambda_{\text{mid}})$. The ellipsoid is the manifold M.
The vertices on M are depicted in black, as are the vertices on the spaces of constant curvature left, right and below. The vertices on M are transplanted on spaces of constant curvature by the maps $\exp_{\mathbb{H}(\Lambda_+)} \circ \exp_{v_r,M}^{-1}$, $\exp_{\mathbb{H}(\Lambda_-)} \circ \exp_{v_r,M}^{-1}$ and $\exp_{\mathbb{H}(\Lambda_{\text{mid}})} \circ \exp_{v_r,M}^{-1}$, respectively. The same holds for the arbitrary point x (red).
In v_r is the point from which black geodesics emanate. Our criteria for non-degeneracy will be in terms of the simplex with vertices $\exp_{\mathbb{H}(\Lambda_{\text{mid}})} \circ \exp_{v_r,M}^{-1}(v_i)$. This means that we think of the black edges as 'known'. The blue edges are only 'approximately known'. Lemma 3.10.8 gives us bounds on the 'difference' between the 'inner products' (of the form $\sin\frac{a}{l}\sin\frac{b}{l}\cos\gamma$) of edges on $\mathbb{H}(\Lambda_+)$ or $\mathbb{H}(\Lambda_-)$ and $\mathbb{H}(\Lambda_{\text{mid}})$.
The worst case scenario are the 'inner products' for geodesic triangles of which all edges are blue, that is all edge lengths are 'approximately known'. Lemma 3.10.8 focusses on this.

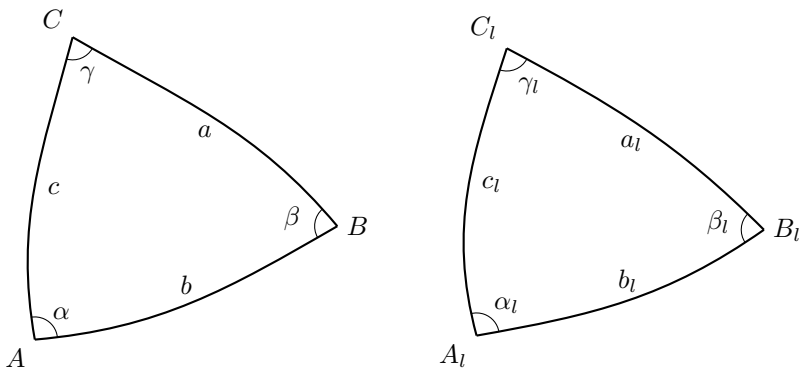

Figure 3.14: Two geodesic triangles on spaces of different constant curvature with the angles and edge lengths as used in Lemma 3.10.8 indicated.

The role of this lemma in Section 3.10.5 is to give us approximate values of the 'inner products' (of the form $\sin\frac{a}{l}\sin\frac{b}{l}\cos\gamma$), see Figure 3.13 for an overview. These 'inner products' are the entries in the pseudo Gram matrix.

Lemma 3.10.8 *Let $\mathbb{H}(+1/k^2)$ and $\mathbb{H}(+1/l^2)$ be spaces of positive constant sectional curvature, where for convenience we assume that $k > l > 0$. Moreover let the edge-lengths (a, b, c) of a geodesic triangle on $\mathbb{H}(+1/k^2)$ satisfy*

$$\begin{aligned} l^2\cos\frac{a}{l} &= l^2\cos\frac{a_l}{l} + R_{T_a},\\ l^2\cos\frac{b}{l} &= l^2\cos\frac{b_l}{l} + R_{T_b}\\ l^2\cos\frac{c}{l} &= l^2\cos\frac{b_l}{l} + R_{T_c} \end{aligned}$$

with

$$\begin{aligned} l^2\cos\frac{a_l}{l} &= l^2\cos\frac{a_1}{l}\cos\frac{a_2}{l} + l^2\sin\frac{a_1}{l}\sin\frac{a_2}{l}\cos\gamma_a\\ l^2\cos\frac{b_l}{l} &= l^2\cos\frac{b_1}{l}\cos\frac{b_2}{l} + l^2\sin\frac{b_1}{l}\sin\frac{b_2}{l}\cos\gamma_b\\ l^2\cos\frac{c_l}{l} &= l^2\cos\frac{c_1}{l}\cos\frac{c_2}{l} + l^2\sin\frac{c_1}{l}\sin\frac{c_2}{l}\cos\gamma_c \end{aligned}$$

and

$$|R_{T_a}|, |R_{T_b}|, |R_{T_c}| \leq \left|\frac{1}{l^2} - \frac{1}{k^2}\right| \frac{11 d_{max}^4}{4!},$$

and

$$a, a_1, a_2, b, b_1, b_2, c, c_1, c_2 \leq \frac{1}{2}l \qquad a, a_1, a_2, b, b_1, b_2, c, c_1, c_2 < d_{max},$$

then

$$|l^2 \sin\frac{b}{l}\sin\frac{c}{l}\cos\alpha - l^2\sin\frac{b_l}{l}\sin\frac{c_l}{l}\cos\alpha_l| \leq 2\left|\frac{1}{l^2} - \frac{1}{k^2}\right| d_{max}^4,$$

with

$$l^2 \sin\frac{b_l}{l}\sin\frac{c_l}{l}\cos\alpha_l = l^2\cos\frac{a_l}{l} - l^2\cos\frac{b_l}{l}\cos\frac{c_l}{l}.$$

Here the notation for the lengths and angles of a geodesic triangle is as in Figure 3.14.

Clearly we can formulate Lemma 3.10.8 for each of the angles α, β and γ, as in Figure 3.14. We have chosen α over γ and β. The reason for this is that γ is used in Lemma 3.10.4 (elliptic) and Lemma 3.10.6 (hyperbolic) as a given quantity, while in Lemma 3.10.8 the angle is (approximately) determined based on (approximate) lengths of edges.

Proof Because a, b, c are the edge lengths of a geodesic triangle on $\mathbb{H}(+1/k^2)$ we have, by Lemma 3.10.4, that

$$l^2\cos\frac{a}{l} - l^2\cos\frac{b}{l}\cos\frac{c}{l} = l^2\sin\frac{b}{l}\sin\frac{c}{l}\cos\alpha + R_T(a,b,c)$$

with

$$R_T(a,b,c) \leq \left|\frac{1}{l^2} - \frac{1}{k^2}\right| \frac{11 d_{\max}^4}{4!}.$$

Filling in our assumptions we see that

$$\begin{aligned}
l^2\cos\frac{a_l}{l} + R_{T_a} - (l^2\cos\frac{b_l}{l} + R_{T_b})(\cos\frac{c_l}{l} + \frac{R_{T_c}}{l^2}) - R_T \\
= l^2\sin\frac{b}{l}\sin\frac{c}{l}\cos\alpha \\
l^2\cos\frac{a_l}{l} - l^2\cos\frac{b_l}{l}\cos\frac{c_l}{l} + R_{T_b}\cos\frac{c_l}{l} + R_{T_c}\cos\frac{b_l}{l} + R_{T_b}\frac{R_{T_c}}{l^2} + R_{T_a} - R_T \\
= l^2\sin\frac{b}{l}\sin\frac{c}{l}\cos\alpha \\
l^2\sin\frac{b_l}{l}\sin\frac{c_l}{l}\cos\alpha_l + R_{T_b}\cos\frac{c_l}{l} + R_{T_c}\cos\frac{b_l}{l} + R_{T_b}\frac{R_{T_c}}{l^2} + R_{T_a} - R_T \\
= l^2\sin\frac{b}{l}\sin\frac{c}{l}\cos\alpha.
\end{aligned}$$

Because

$$\begin{aligned}\left|\frac{R_{T_c}}{l^2}\right| &\leq \frac{11}{4!}\left|\frac{1}{l^4}-\frac{1}{k^2l^2}\right| d_{\max}^4 \\ &\leq \frac{11}{4!}\left|\frac{1}{l^4}-\frac{1}{k^2l^2}\right| \left(\frac{l}{2}\right)^4 \\ &= \frac{11}{2^4 4!}\end{aligned}$$

we have that

$$\begin{aligned}&|R_{T_b}\cos\frac{c_l}{l}+R_{T_c}\cos\frac{b_l}{l}+R_{T_b}\frac{R_{T_c}}{l^2}+R_{T_a}-R_T| \\ &\qquad\leq |R_{T_b}|+|R_{T_c}|+\frac{11}{2^4 4!}|R_{T_b}|+|R_{T_a}|+|R_T| \\ &\qquad\leq (4+\frac{11}{2^4 4!})\frac{11}{4!}\left|\frac{1}{l^2}-\frac{1}{k^2}\right| d_{\max}^4 \\ &\qquad\leq 2\left|\frac{1}{l^2}-\frac{1}{k^2}\right| d_{\max}^4\end{aligned}$$

□

The cosine with 'errors' in lengths for spaces of negative constant curvature

Similarly, for hyperbolic spaces we have

Lemma 3.10.9 *Let $\mathbb{H}(-1/k^2)$ and $\mathbb{H}(-1/l^2)$ be spaces of negative constant sectional curvature, where for convenience we assume that $k > l > 0$. Moreover let the edge-lengths (a, b, c) of a geodesic triangle on $\mathbb{H}(-1/k^2)$ satisfy*

$$\begin{aligned}l^2\cosh\frac{a}{l} &= l^2\cosh\frac{a_l}{l}+R_{T_a}, \\ l^2\cosh\frac{b}{l} &= l^2\cosh\frac{b_l}{l}+R_{T_b} \\ l^2\cosh\frac{c}{l} &= l^2\cosh\frac{c_l}{l}+R_{T_c}\end{aligned}$$

with

$$\begin{aligned}l^2\cosh\frac{a_l}{l} &= l^2\cosh\frac{a_1}{l}\cosh\frac{a_2}{l}-l^2\sinh\frac{a_1}{l}\sinh\frac{a_2}{l}\cos\gamma_a \\ l^2\cosh\frac{b_l}{l} &= l^2\cosh\frac{b_1}{l}\cosh\frac{b_2}{l}-l^2\sinh\frac{b_1}{l}\sinh\frac{b_2}{l}\cos\gamma_b \\ l^2\cosh\frac{c_l}{l} &= l^2\cosh\frac{c_1}{l}\cosh\frac{c_2}{l}-l^2\sinh\frac{c_1}{l}\sinh\frac{c_2}{l}\cos\gamma_c\end{aligned}$$

and

$$|R_{T_a}|, |R_{T_b}|, |R_{T_c}| \leq \left| \frac{1}{l^2} \cosh^2 \frac{d_{max}}{l} - \frac{1}{k^2} \cosh^2 \frac{d_{max}}{k} \right| \frac{11 d_{max}^4}{4!},$$

and

$$a, a_1, a_2, b, b_1, b_2, c, c_1, c_2 < d_{max},$$

then

$$\begin{aligned} |l^2 \sinh \frac{b}{l} \sinh \frac{c}{l} \cos\alpha - & l^2 \sinh \frac{b_l}{l} \sinh \frac{c_l}{l} \cos\alpha_l| \\ & \leq \left(2 + 2\cosh \frac{d_{max}}{l} + \frac{1}{l^4} \cosh^2 \left(\frac{d_{max}}{l} \right) \frac{11 d_{max}^4}{4!} \right) \\ & \quad \cdot \left| \frac{1}{l^2} \cosh^2 \frac{d_{max}}{l} - \frac{1}{k^2} \cosh^2 \frac{d_{max}}{k} \right| \frac{11 d_{max}^4}{4!}, \end{aligned}$$

with

$$l^2 \sinh \frac{b_l}{l} \sinh \frac{c_l}{l} \cos\alpha_l = l^2 \cosh \frac{b_l}{l} \cosh \frac{c_l}{l} - l^2 \cosh \frac{a_l}{l}$$

Note that we no longer impose bound on the lengths with respect to l or k as we did in the elliptic case.

Proof Because a, b, c are the edge lengths of a geodesic triangle on $\mathbb{H}(-1/k^2)$ Lemma 3.10.6 yields

$$l^2 \cosh \frac{c}{l} - l^2 \cosh \frac{a}{l} \cosh \frac{b}{l} = -l^2 \sinh \frac{a}{l} \sinh \frac{b}{l} \cos\gamma + R_T(a, b, c)$$

with

$$R_T(a, b, c) \leq \left| \frac{1}{l^2} \cosh^2 \frac{d_{\max}}{l} - \frac{1}{k^2} \cosh^2 \frac{d_{\max}}{k} \right| \frac{11 d_{\max}^4}{4!}.$$

Filling in our assumptions we see that

$$\begin{aligned} l^2 \cosh \frac{a_l}{l} + R_{T_a} - (l^2 \cosh \frac{b_l}{l} + R_{T_b})(\cosh \frac{c_l}{l} + \frac{R_{T_c}}{l^2}) - R_T & \\ = -l^2 \sinh \frac{b}{l} \sinh \frac{c}{l} \cos\alpha & \\ l^2 \cosh \frac{a_l}{l} - l^2 \cosh \frac{b_l}{l} \cosh \frac{c_l}{l} + R_{T_b} \cosh \frac{c_l}{l} + R_{T_c} \cosh \frac{b_l}{l} + R_{T_b} \frac{R_{T_c}}{l^2} + R_{T_a} - R_T & \\ = -l^2 \sinh \frac{b}{l} \sinh \frac{c}{l} \cos\alpha & \\ l^2 \sinh \frac{b_l}{l} \sinh \frac{c_l}{l} \cos\alpha_l - R_{T_b} \cosh \frac{c_l}{l} - R_{T_c} \cosh \frac{b_l}{l} - R_{T_b} \frac{R_{T_c}}{l^2} - R_{T_a} + R_T & \\ = l^2 \sinh \frac{b}{l} \sinh \frac{c}{l} \cos\alpha. & \end{aligned}$$

We now have that

$$\begin{aligned}
&|-R_{T_b}\cosh\frac{c_l}{l}-R_{T_c}\cosh\frac{b_l}{l}-R_{T_b}\frac{R_{T_c}}{l^2}-R_{T_a}+R_T|\\
&\qquad\leq|R_{T_b}|\cosh\frac{d_{\max}}{l}+|R_{T_c}|\cosh\frac{d_{\max}}{l}+|R_{T_b}|\left|\frac{R_{T_c}}{l^2}\right|+|R_{T_a}|+|R_T|\\
&\qquad\leq\left(2+2\cosh\frac{d_{\max}}{l}+\frac{1}{l^4}\cosh^2\left(\frac{d_{\max}}{l}\right)\frac{11d_{\max}^4}{4!}\right)\\
&\qquad\quad\cdot\left|\frac{1}{l^2}\cosh^2\frac{d_{\max}}{l}-\frac{1}{k^2}\cosh^2\frac{d_{\max}}{k}\right|\frac{11d_{\max}^4}{4!}.
\end{aligned}$$

□

3.10.5 Determining non-degeneracy

In this section we combine the results of Sections 3.10.3 and 3.10.4 with bounds on determinants from Section 3.6.1 to give criteria that guarantee non-degeneracy, much in the same way as we did in Subsection 3.6.3. As before we shall first treat the elliptic and then the hyperbolic case.

Recapitulation of the overview of the Section 3.10

In this section, that is Section 3.10, we compare to general spaces of constant curvature instead of to Euclidean spaces. This means that our geometrical picture is slightly different from the one sketched in figure 3.6, a pictorial overview of this section is given in Figure 3.10 and Figure 3.11, see also Figure 3.13.

We start in the same manner as we did in the Euclidean case:
We are given a manifold M whose sectional curvatures K are bounded by $0 < \Lambda_- \leq K \leq \Lambda_+$ or $\Lambda_- \leq K \leq \Lambda_+ < 0$, and a set of vertices $v_0, \ldots, v_n$ on the manifold. We know that if σ_M is an intrinsic simplex with these vertices, then σ_M is non-degenerate if for all $x \in \sigma_M$ we can find an independent set of n tangent vectors to geodesics to the vertices $v_0, \ldots, v_n$ emanating from x.

In Section 3.6 we used the Toponogov comparison theorem twice, first to estimate all the edge lengths of geodesic triangles whose vertices are elements of the set $\{x, v_0, \ldots, v_n\}$ in terms of the lengths of the corresponding (Rauch[13]) edges in spaces of constant curvature. If the simplex on the space of constant curvature was sufficiently small, the lengths of these edges would be close to those in Euclidean space. To be precise we compared with the simplex lifted to the tangent space $T_{v_r}M$ with the inverse of the exponential map. We could then repeat the trick to prove that for sufficiently small simplices the same holds

[13]See definition 3.3.1.

for the angles between tangents from geodesics emanating from x. The angle estimates were used to prove that: If the lifted simplex was of sufficient quality we are able to find for each x a set of n independent tangent vectors, establishing non-degeneracy.

In this section, that is Section 3.10, we no longer go from the spaces of constant curvature, that give lower and upper bounds on the edge lengths and angles with the Toponogov comparison theorem, to Euclidean space, but compare to a space of constant curvature. Here we compare to the simplex $\sigma_{\mathbb{H}(\Lambda_{\text{mid}})}(v_r)$ on a space with constant curvature Λ_{mid} such that the length of the edges emanating from v_r and the angles between the tangents of geodesics at v_r are the same as on M is the model we use. To put it in other words the vertices of $\sigma_{\mathbb{H}(\Lambda_{\text{mid}})}(v_r)$ are $\exp_{\Lambda_{\text{mid}}} \circ \exp^{-1}_{v_r,M}(v_i)$.

Degeneracy criteria for simplices on spaces of constant positive curvature

Let us now make these statements more precise. We define

$$\Lambda_{\text{mid}} = \frac{1}{2}(\Lambda_- + \Lambda_+).$$

Note that this is the arithmetic mean of the upper and lower bounds on the sectional curvature and has nothing to do with the mean curvature. Let us further assume that all distances involved are bounded from above by $1/(2\sqrt{\Lambda_-})$ and some maximum distance $\tilde{D}$. By the Toponogov comparison theorem we have that $d_M(y,z)$ the distances between $y, z \in \{x, v_0, \dots v_n\}$ in M are bounded by those in $\mathbb{H}(\Lambda_-)$ and $\mathbb{H}(\Lambda_+)$. Or in other words we have that

$$d_{\mathbb{H}(\Lambda_+)}(y_{\Lambda_+}, z_{\Lambda_+}) \leq d_M(y,z) \leq d_{\mathbb{H}(\Lambda_-)}(y_{\Lambda_-}, z_{\Lambda_-})$$

where $y_K = \exp_{\mathbb{H}(K)} \circ \exp_{v_r,M}(y)$. Because we use the exponential map at v_r regard v_r as a fixed point and we shall not use the notation $(v_r)_K$, but write v_r regardless. The distances $d_{\mathbb{H}(\Lambda_-)}(y_{\Lambda_-}, z_{\Lambda_-})$ and $d_{\mathbb{H}(\Lambda_+)}(y_{\Lambda_+}, z_{\Lambda_+})$ satisfy

$$\begin{aligned}
&\frac{1}{\Lambda_-}\cos\left(\sqrt{\Lambda_-}d_{\mathbb{H}(\Lambda_-)}(y,z)\right)\\
&=\frac{1}{\Lambda_-}\cos\left(\sqrt{\Lambda_-}d_M(y,v_r)\right)\cos\left(\sqrt{\Lambda_-}d_M(z,v_r)\right)\\
&\quad+\frac{1}{\Lambda_-}\sin\left(\sqrt{\Lambda_-}d_M(y,v_r)\right)\sin\left(\sqrt{\Lambda_-}d_M(z,v_r)\right)\cos\theta_{\angle_M y v_r z}
\end{aligned}$$

and

$$\begin{aligned}
&\frac{1}{\Lambda_+}\cos\left(\sqrt{\Lambda_+}d_{\mathbb{H}(\Lambda_+)}(y,z)\right)\\
&\quad=\frac{1}{\Lambda_+}\cos\left(\sqrt{\Lambda_+}d_M(y,v_r)\right)\cos\left(\sqrt{\Lambda_+}d_M(z,v_r)\right)\\
&\qquad+\frac{1}{\Lambda_+}\sin\left(\sqrt{\Lambda_+}d_M(y,v_r)\right)\sin\left(\sqrt{\Lambda_+}d_M(z,v_r)\right)\cos\theta_{\angle_M yv_rz},
\end{aligned}$$

where $\theta_{\angle_M yv_rz}$ denotes the angle between the tangents to the geodesics on M from v_r to y and v_r to z. Using Lemma 3.10.4 we see that

$$\begin{aligned}
&\frac{1}{\Lambda_{\text{mid}}}\cos\left(\sqrt{\Lambda_{\text{mid}}}d_{\mathbb{H}(\Lambda_-)}(y,z)]\right)\\
&\quad=\frac{1}{\Lambda_{\text{mid}}}\cos\left(\sqrt{\Lambda_{\text{mid}}}d_M(y,v_r)\right)\cos\left(\sqrt{\Lambda_{\text{mid}}}d_M(z,v_r)\right)\\
&\qquad+\frac{1}{\Lambda_{\text{mid}}}\sin\left(\sqrt{\Lambda_{\text{mid}}}d_M(y,v_r)\right)\sin\left(\sqrt{\Lambda_{\text{mid}}}d_M(z,v_r)\right)\cos\theta_{\angle_M yv_rz}+R_{T_1}
\end{aligned}$$

and

$$\begin{aligned}
&\frac{1}{\Lambda_{\text{mid}}}\cos\left(\sqrt{\Lambda_{\text{mid}}}d_{\mathbb{H}(\Lambda_+)}(y,z)\right)\\
&\quad=\frac{1}{\Lambda_{\text{mid}}}\cos\left(\sqrt{\Lambda_{\text{mid}}}d_M(y,v_r)\right)\cos\left(\sqrt{\Lambda_{\text{mid}}}d_M(z,v_r)\right)\\
&\qquad+\frac{1}{\Lambda_{\text{mid}}}\sin\left(\sqrt{\Lambda_{\text{mid}}}d_M(y,v_r)\right)\sin\left(\sqrt{\Lambda_{\text{mid}}}d_M(z,v_r)\right)\cos\theta_{\angle_M yv_rz}+R_{T_2},
\end{aligned}$$

with

$$|R_{T_1}|,|R_{T_2}|\leq\frac{1}{2}\left|\Lambda_--\Lambda_+\right|\frac{11\tilde{D}^4}{4!},$$

so that

$$\begin{aligned}
&\frac{1}{\Lambda_{\text{mid}}}\cos\left(\sqrt{\Lambda_{\text{mid}}}d_M(y,z)\right)\\
&\quad=\frac{1}{\Lambda_{\text{mid}}}\cos\left(\sqrt{\Lambda_{\text{mid}}}d_M(y,v_r)\right)\cos\left(\sqrt{\Lambda_{\text{mid}}}d_M(z,v_r)\right)\\
&\qquad+\frac{1}{\Lambda_{\text{mid}}}\sin\left(\sqrt{\Lambda_{\text{mid}}}d_M(y,v_r)\right)\sin\left(\sqrt{\Lambda_{\text{mid}}}d_M(z,v_r)\right)\cos\theta_{\angle_M yv_rz}+R_T,
\end{aligned}\tag{3.65}$$

with the same bound on $|R_T|$.

We are now going to study the $\sin a \sin b \cos\gamma$ terms we discussed in Section 3.10.3. These generalize the $ab\cos\gamma$ terms we use in the Gram-matrix in the Eulcidean case, see Section 3.6.3. The point we focus on is x.

Thanks to (3.65) we have the (approximate) lengths of all geodesics. So we can now apply the Toponogov comparison theorem for a second time. The Toponogov comparison theorem gives us that

$$\begin{aligned} d_{\mathbb{H}^n(\Lambda_-)}(x_{\Lambda_-}, y_{\Lambda_-}) \geq d_M(x,y) \geq d_{\mathbb{H}^n(\Lambda_+)}(x_{\Lambda_+}, y_{\Lambda_+}) \\ \cos\theta_{\mathbb{H}^n(\Lambda_-)} \geq \cos\theta_M \geq \cos\theta_{\mathbb{H}^n(\Lambda_+)}, \end{aligned}$$

where we identify angles in the obvious manner using $\exp_{\mathbb{H}(\Lambda_\pm)} \circ \exp_M^{-1}$, in the same way as we do the points. From these inequalities we infer that

$$\begin{aligned} &\frac{1}{\Lambda_{\text{mid}}} \sin\left(\sqrt{\Lambda_{\text{mid}}} d_{\mathbb{H}^n(\Lambda_-)}(x_{\Lambda_-}, y_{\Lambda_-})\right) \sin\left(\sqrt{\Lambda_{\text{mid}}} d_{\mathbb{H}^n(\Lambda_-)}(x_{\Lambda_-}, z_{\Lambda_-})\right) \cdot \\ &\qquad\qquad \cos\theta_{\angle_{\Lambda_-^x} yxz} \\ &\geq \frac{1}{\Lambda_{\text{mid}}} \sin\left(\sqrt{\Lambda_{\text{mid}}} d_M(x,y)\right) \sin\left(\sqrt{\Lambda_{\text{mid}}} d_M(x,z)\right) \cos\theta_{\angle_M yxz} \\ &\geq \frac{1}{\Lambda_{\text{mid}}} \sin\left(\sqrt{\Lambda_{\text{mid}}} d_{\mathbb{H}^n(\Lambda_+)}(x_{\Lambda_+}, y_{\Lambda_+})\right) \sin\left(\sqrt{\Lambda_{\text{mid}}} d_{\mathbb{H}^n(\Lambda_+)}(x_{\Lambda_+}, z_{\Lambda_+})\right) \cdot \\ &\qquad\qquad \cos\theta_{\angle_{\Lambda_+^x} yxz}, \end{aligned}$$

where $\angle_{\Lambda_\pm^x} yxz$ denotes the angle between the tangents of the geodesics from x to $\exp_{\mathbb{H}(\Lambda_\pm)} \circ \exp_{x,M}^{-1}(y)$ and from x to $\exp_{\mathbb{H}(\Lambda_\pm)} \circ \exp_{x,M}^{-1}(z)$. We can now use the result of Lemma 3.10.8 to see that

$$\begin{aligned} &\left| \frac{1}{\Lambda_{\text{mid}}} \sin\left(\sqrt{\Lambda_{\text{mid}}} d_{\mathbb{H}^n(\Lambda_\pm)}(x_{\Lambda_\pm}, y_{\Lambda_\pm})\right) \sin\left(\sqrt{\Lambda_{\text{mid}}} d_{\mathbb{H}^n(\Lambda_\pm)}(x_{\Lambda_\pm}, z_{\Lambda_\pm})\right) \cdot \right. \\ &\qquad\qquad \cos\theta_{\angle_{\Lambda_\pm^x} yxz} \\ &- \frac{1}{\Lambda_{\text{mid}}} \sin\left(\sqrt{\Lambda_{\text{mid}}} d_{\mathbb{H}^n(\Lambda_{\text{mid}})}(x_{\Lambda_{\text{mid}}}, y_{\Lambda_{\text{mid}}})\right) \sin\left(\sqrt{\Lambda_{\text{mid}}} d_{\mathbb{H}^n(\Lambda_{\text{mid}})}(x_{\Lambda_{\text{mid}}}, z_{\Lambda_{\text{mid}}})\right) \cdot \\ &\qquad\qquad \left. \cos\theta_{\angle_{\Lambda_{\text{mid}}} yxz} \right| \\ &\leq |\Lambda_- - \Lambda_+| \, \tilde{D}^4, \end{aligned}$$

where $\Lambda_\pm$ should be interpreted either Λ_- or Λ_+ and

$$\angle_{\Lambda_{\text{mid}}} yxz$$

is the angle between the tangents to the geodesics from $\exp_{\mathbb{H}(\Lambda_{\text{mid}})} \circ \exp_{v_r,M}^{-1}(x)$ to $\exp_{\mathbb{H}(\Lambda_{\text{mid}})} \circ \exp_{v_r,M}^{-1}(y)$ and from $\exp_{\mathbb{H}(\Lambda_{\text{mid}})} \circ \exp_{v_r,M}^{-1}(x)$ to $\exp_{\mathbb{H}(\Lambda_{\text{mid}})} \circ \exp_{v_r,M}^{-1}(z)$.

Here we went from angles determined by the exponential map at x to those determined by the exponential map at v_r, this is possible because Lemma 3.10.8 only takes lengths of geodesics as input.

This means

$$\begin{aligned}
&\left| \frac{1}{\Lambda_{\text{mid}}} \sin\left(\sqrt{\Lambda_{\text{mid}}} d_M(x,y)\right) \sin\left(\sqrt{\Lambda_{\text{mid}}} d_M(x,z)\right) \cos\theta_{\angle_M yxz} \right. \\
&- \frac{1}{\Lambda_{\text{mid}}} \sin\left(\sqrt{\Lambda_{\text{mid}}} d_{\mathbb{H}^n(\Lambda_{\text{mid}})}(x_{\Lambda_{\text{mid}}}, y_{\Lambda_{\text{mid}}})\right) \sin\left(\sqrt{\Lambda_{\text{mid}}} d_{\mathbb{H}^n(\Lambda_{\text{mid}})}(x_{\Lambda_{\text{mid}}}, z_{\Lambda_{\text{mid}}})\right) \cdot \\
&\qquad \left. \cos\theta_{\angle_{\Lambda_{\text{mid}}} yxz} \right| \\
&\leq |\Lambda_- - \Lambda_+| \, \tilde{D}^4. \qquad (3.66)
\end{aligned}$$

We can now exploit (3.66) to prove that the (rescaled) pseudo Gram matrix

$$\left(\frac{\sin\left(\sqrt{\Lambda_{\text{mid}}} d_M(x,v_i)\right) \sin\left(\sqrt{\Lambda_{\text{mid}}} d_M(x,v_l)\right) \cos\theta_{il}}{(2\tilde{D})^2 \Lambda_{\text{mid}}} \right)_{i,l\neq j}, \qquad (3.67)$$

with $\theta_{\angle_M v_i x v_l} = \theta_{il}$ is non-degenerate. Here we use Lemma 3.10.2 which says that the determinant of (3.67) is zero if and only if the vectors $\exp_{x,M}^{-1}(v_i)$ with $i \neq j$ are linearly independent. We use the result by Friedland, see Section 3.6.1, to give condition that guarantee that the determinant of (3.67) is non-zero. Because of the role of $\max\{\|A\|_\infty, \|A+E\|_\infty\}$, where in this case A is (3.67) and $A+E$ is the approximate Gram matrix, it is important to note that

$$\left| \frac{\sin\left(\sqrt{\Lambda_{\text{mid}}} d_M(x,v_i)\right) \sin\left(\sqrt{\Lambda_{\text{mid}}} d_M(x,v_l)\right) \cos\theta_{il}}{(2\tilde{D})^2 \Lambda_{\text{mid}}} \right| \leq 1. \qquad (3.68)$$

This follows from the observation that if $y_{\max} < \pi/2$ then

$$\sup_{y\in[0,y_{\max}]} \frac{\sin(y)}{y_{\max}} \leq 1.$$

We are now able to conclude that

$$\begin{aligned}
&\left| \det\left(\frac{\sin\left(\sqrt{\Lambda_{\text{mid}}} d_M(x,v_i)\right) \sin\left(\sqrt{\Lambda_{\text{mid}}} d_M(x,v_l)\right) \cos\theta_{il}}{(2\tilde{D})^2 \Lambda_{\text{mid}}} \right)_{i,l\neq j} \right| \\
&\geq \left| \det\left(\sin\left(\sqrt{\Lambda_{\text{mid}}} d_{\mathbb{H}^n(\Lambda_{\text{mid}})}(x_{\Lambda_{\text{mid}}}, (v_i)_{\Lambda_{\text{mid}}})\right) \cdot \right. \right. \\
&\qquad \left. \left. \frac{\sin\left(\sqrt{\Lambda_{\text{mid}}} d_{\mathbb{H}^n(\Lambda_{\text{mid}})}(x_{\Lambda_{\text{mid}}}, (v_l)_{\Lambda_{\text{mid}}})\right) \cos\theta_{\angle_{\Lambda_{\text{mid}}} v_i x v_l}}{(2\tilde{D})^2 \Lambda_{\text{mid}}} \right)_{i,l\neq j} \right| \\
&\qquad - n\,|\Lambda_- - \Lambda_+| \, \tilde{D}^2 \qquad (3.69)
\end{aligned}$$

Combining Lemma 3.10.2 and Lemma 3.6.4 and using that if for all x there is a j such that the pseudo Gram matrix above is non-degenerate then the simplex is non-degenerate we have

Theorem 3.10.10 *Let M be a manifold with bounded positive sectional curvatures K, that is $0 < \Lambda_- \leq K \leq \Lambda_+$. Suppose that $v_0, \ldots, v_n$ are vertices on M. Let us assume*[14] *that all vertices lie within a geodesic ball of radius $\frac{1}{2}\tilde{D}$ with centre v_r, where $\tilde{D} \leq 1/(2\sqrt{\Lambda_+})$. Under these assumptions the Riemannian simplex with vertices $v_0, \ldots, v_n$ on M is non-degenerate if*

$$\frac{Q_{\mathbb{H}(\Lambda_{mid})}(\sigma_{\mathbb{H}(\Lambda_{mid})}(v_r))}{(2\tilde{D})^{2n}} \geq n\,|\Lambda_- - \Lambda_+|\,\tilde{D}^2$$

with $Q_{\mathbb{H}(\Lambda_{mid})}$ the simplex quality

$$\begin{aligned} &Q_{\mathbb{H}(\Lambda_{mid})}(\sigma_{\mathbb{H}(\Lambda_{mid})}(v_r)) \\ &\quad = \min_{y \in \mathbb{H}(\Lambda_{mid})} \max_j \left\{ \det \left(\frac{1}{\Lambda_{mid}} \sin\left(\sqrt{\Lambda_{mid}}\, d_{\mathbb{H}(\Lambda_{mid})}(y, v_i(v_r))\right) \cdot \right.\right. \\ &\qquad\qquad \left.\left. \sin\left(\sqrt{\Lambda_{mid}} d_{\mathbb{H}(\Lambda_{mid})}(y, v_l(v_r))\right) \cos\theta_{il} \right)_{i,l \neq j} \right\}, \end{aligned}$$

$\sigma_{\mathbb{H}(\Lambda_{mid})}(v_r)$ the simplex on $\mathbb{H}(\Lambda_{mid})$ with vertices $v_i(v_r)$ defined by $v_i(v_r) = \exp_{\mathbb{H}(\Lambda_{mid})} \circ \exp^{-1}_{v_r, M}(v_i)$ and

$$\Lambda_{mid} = \frac{1}{2}(\Lambda_- + \Lambda_+).$$

Degeneracy criteria for simplices on spaces of constant negative curvature

We can perform similar calculations for the hyperbolic case but the result is significantly more complicated due to the fact that the hyperbolic cosine is not bounded by one. Moreover we will not impose a bound on $\tilde{D}$ in the negative curvature setting.

Let us start by defining $\Lambda^{\mathbb{H}}_{\text{mid}}$ as the negative solution to the following equa-

[14] This bound is stronger than necessary. In fact it suffices for the lengths of geodesics in the proof below to be bounded by $\tilde{D}$.

tion:

$$\begin{aligned}
&\left| |\Lambda^{\mathbb{H}}_{\text{mid}}| \cosh^2\left(\sqrt{\Lambda^{\mathbb{H}}_{\text{mid}}}\tilde{D}\right) - |\Lambda_-| \cosh^2\left(\sqrt{|\Lambda_-|}\tilde{D}\right)\right| \\
&= \left| |\Lambda^{\mathbb{H}}_{\text{mid}}| \cosh^2\left(\sqrt{\Lambda^{\mathbb{H}}_{\text{mid}}}\tilde{D}\right) - |\Lambda_+| \cosh^2\left(\sqrt{|\Lambda_+|}\tilde{D}\right)\right| \\
&= \frac{1}{2}\left| |\Lambda_-| \cosh^2\left(\sqrt{|\Lambda_-|}\tilde{D}\right) - |\Lambda_+| \cosh^2\left(\sqrt{|\Lambda_+|}\tilde{D}\right)\right|.
\end{aligned}$$

We shall once more employ the bounds Friedland, see Section 3.6.1. In order to be able to do so we need, similarly to (3.68), that

$$\sinh\left(\sqrt{|\Lambda^{\mathbb{H}}_{\text{mid}}|}a\right)\sinh\left(\sqrt{|\Lambda^{\mathbb{H}}_{\text{mid}}|}b\right)\cos\gamma \leq \sinh^2\left(\sqrt{|\Lambda_-|}\tilde{D}\right).$$

So that, using Lemma 3.10.9 and similarly to (3.69), we have

$$\begin{aligned}
&\left|\det\left(\sinh\left(\sqrt{\Lambda^{\mathbb{H}}_{\text{mid}}}d_M(x,v_i)\right)\sinh\left(\sqrt{\Lambda^{\mathbb{H}}_{\text{mid}}}d_M(x,v_l)\right)\cos\theta_{ij}\right)_{i,l\neq j}\right| \\
\geq &\left|\det\left(\sinh\left(\sqrt{\Lambda^{\mathbb{H}}_{\text{mid}}}d_{\mathbb{H}^n(\Lambda^{\mathbb{H}}_{\text{mid}})}(x_{\Lambda^{\mathbb{H}}_{\text{mid}}},(v_i)_{\Lambda^{\mathbb{H}}_{\text{mid}}})\right)\cdot\right.\right. \\
&\left.\left.\sinh\left(\sqrt{\Lambda^{\mathbb{H}}_{\text{mid}}}d_{\mathbb{H}^n(\Lambda^{\mathbb{H}}_{\text{mid}})}(x_{\Lambda^{\mathbb{H}}_{\text{mid}}},(v_l)_{\Lambda^{\mathbb{H}}_{\text{mid}}})\right)\cos\theta_{\angle_{\Lambda^{\mathbb{H}}_{\text{mid}}}v_i x v_l}\right)_{i,l\neq j}\right| \\
&- n(\sinh^2\sqrt{|\Lambda_-|}\tilde{D})^{n-1} \\
&\cdot\left(2+2\cosh\left(\sqrt{|\Lambda_-|}\tilde{D}\right)+|\Lambda_-|^2\cosh^2\left(\sqrt{|\Lambda_-|}\tilde{D}\right)\frac{11\tilde{D}^4}{4!}\right) \\
&\cdot\left||\Lambda_-|\cosh^2\sqrt{|\Lambda_-|}\tilde{D}-|\Lambda_+|\cosh^2\sqrt{|\Lambda_+|}\tilde{D}\right||\Lambda^{\mathbb{H}}_{\text{mid}}|\frac{11\tilde{D}^4}{2\cdot 4!}.
\end{aligned}$$

From which we infer that

Theorem 3.10.11 *Let M be a manifold with bounded negative sectional curvatures K, that is $\Lambda_- \leq K \leq \Lambda_+ < 0$. Suppose that $v_0,\ldots,v_n$ are vertices on M. Let us assume that all vertices lie within a geodesic ball of radius $\frac{1}{2}\tilde{D}$ with centre v_r. Under these assumptions the Riemannian simplex with vertices $v_0,\ldots,v_n$ on M*

is non-degenerate if

$$|\Lambda^{\mathbb{H}}_{mid}|^n Q_{\mathbb{H}(\Lambda^{\mathbb{H}}_{mid})}(\sigma_{\mathbb{H}(\Lambda^{\mathbb{H}}_{mid})}(v_r)) > \; n(\sinh\sqrt{|\Lambda_-|}\tilde{D})^{2(n-1)} \cdot \left(2 + 2\cosh\left(\sqrt{|\Lambda_-|}\tilde{D}\right) + |\Lambda_-|^2\cosh^2\left(\sqrt{|\Lambda_-|}\tilde{D}\right)\frac{11\tilde{D}^4}{4!}\right) \cdot \left||\Lambda_-|\cosh^2(\sqrt{|\Lambda_-|}\tilde{D}) - |\Lambda_+|\cosh^2(\sqrt{|\Lambda_+|}\tilde{D})\right| |\Lambda^{\mathbb{H}}_{mid}|\frac{11\tilde{D}^4}{2\cdot 4!}.$$

with $\sigma_{\mathbb{H}(\Lambda^{\mathbb{H}}_{mid})}(v_r)$ *the simplex on* $\mathbb{H}(\Lambda^{\mathbb{H}}_{mid})$ *with vertices* $v_i(v_r) = \exp_{\mathbb{H}(\Lambda^{\mathbb{H}}_{mid})} \circ \exp^{-1}_{v_r,M}(v_i)$, $Q_{\mathbb{H}(\Lambda^{\mathbb{H}}_{mid})}(\sigma_{\mathbb{H}(\Lambda^{\mathbb{H}}_{mid})}(v_r))$ *the simplex quality*

$$Q_{\mathbb{H}(\Lambda^{\mathbb{H}}_{mid})} = \min_{x\in N}\max_j \left\{\det\left(\frac{1}{|\Lambda^{\mathbb{H}}_{mid}|}\sinh\left(\sqrt{|\Lambda^{\mathbb{H}}_{mid}|}d_{\mathbb{H}^n(\Lambda^{\mathbb{H}}_{mid})}(x, v_i(v_r))\right) \sinh\left(\sqrt{|\Lambda^{\mathbb{H}}_{mid}|}d_{\mathbb{H}^n(\Lambda^{\mathbb{H}}_{mid})}(x, v_l(v_r))\right)\cos\theta_{il}\right)_{i,l\neq j}\right\},$$

where N *equals to any geodesic ball with radius* $2\tilde{D}$ *centred at any of the vertices and* $\Lambda^{\mathbb{H}}_{mid}$ *satisfies*

$$\begin{aligned}&\left||\Lambda^{\mathbb{H}}_{mid}|\cosh^2\sqrt{\Lambda^{\mathbb{H}}_{mid}}\tilde{D} - |\Lambda_-|\cosh^2\sqrt{|\Lambda_-|}\tilde{D}\right| \\ =\;&\left||\Lambda^{\mathbb{H}}_{mid}|\cosh^2\sqrt{\Lambda^{\mathbb{H}}_{mid}}\tilde{D} - |\Lambda_+|\cosh^2\sqrt{|\Lambda_+|}\tilde{D}\right| \\ =\;&\frac{1}{2}\left||\Lambda_-|\cosh^2\sqrt{|\Lambda_-|}\tilde{D} - |\Lambda_+|\cosh^2\sqrt{|\Lambda_+|}\tilde{D}\right|.\end{aligned}$$

The bounds are far more complicated than the elliptic case and thus more difficult to interpret, however if $|\Lambda_- - \Lambda_+|$ tends to zero so does

$$\left||\Lambda_-|\cosh^2\left(\sqrt{|\Lambda_-|}\tilde{D}\right) - |\Lambda_+|\cosh^2\left(\sqrt{|\Lambda_+|}\tilde{D}\right)\right|.$$

This can be made more precise using the mean value theorem which states that for a function f there exists a $c \in [a, b]$ such that

$$f'(c) = \frac{f(b) - f(a)}{b - a}.$$

Applying this to $x \cosh^2 \sqrt{x}\tilde{D}$ we see that

$$\begin{aligned}
&\left||\Lambda_-| \cosh^2\left(\sqrt{|\Lambda_-|}\tilde{D}\right) - |\Lambda_+| \cosh^2\left(\sqrt{|\Lambda_+|}\tilde{D}\right)\right| \\
&= |\Lambda_+ - \Lambda_-| \left|\cosh^2\left(\sqrt{|\tilde{\Lambda}|}\tilde{D}\right) + \tilde{D}\sqrt{|\tilde{\Lambda}|} \sinh\left(\sqrt{|\tilde{\Lambda}|}\tilde{D}\right) \cosh\left(\sqrt{|\tilde{\Lambda}|}\tilde{D}\right)\right| \\
&\leq |\Lambda_+ - \Lambda_-| \left|\cosh^2\left(\sqrt{|\Lambda_-|}\tilde{D}\right) + \tilde{D}\sqrt{|\Lambda_-|} \sinh\left(\sqrt{|\Lambda_-|}\tilde{D}\right) \cosh\left(\sqrt{|\Lambda_-|}\tilde{D}\right)\right|,
\end{aligned}$$

with $\tilde{\Lambda} \in [\Lambda_-, \Lambda_+]$, where we used that

$$\cosh^2\left(\sqrt{x}\tilde{D}\right) + \tilde{D}\sqrt{x} \sinh\left(\sqrt{x}\tilde{D}\right) \cosh\left(\sqrt{x}\tilde{D}\right)$$

is monotone increasing for $x \geq 0$.

This implies that if one has a set of points on a manifold which is close to a space of constant curvature, in the sense of the sectional curvature, then very small quality is required to guarantee non-degeneracy, where we regard the lower bound on the sectional curvature and the distance between the vertices as fixed.

Part II

Topological methods for the analysis of the cosmic web

Chapter 4

Introduction

The second part of this thesis is dedicated to questions that arose from cosmology. Section 4.1 gives a very brief introduction of cosmology. Section 4.2 defines Gaussian random fields. Section 4.3 gives an introduction to some aspects of topology, especially homology theory, intended for readers from outside mathematics. Finally Section 4.4 gives an overview of the second part of this thesis.

4.1 Cosmology

In Section 4.1.1 we discuss the evolution of the universe at large scales. According to the Cosmological principle the universe is approximately uniform at these scales. By uniform we mean that it is homogeneous and isotropic. While models of a uniform universe provide a good description of the global universe. In addition, they also provide a context for the generation of small inhomogeneities in the early universe, the seeds of all structure and objects in the universe. These small inhomogeneities are (almost) Gaussian. By Gaussian we mean that they are described by a Gaussian random field. The geometry and topology of Gaussian random fields will be the main topic of this part of the thesis.

In Section 4.1.2 we discuss how the inhomogeneities evolve into the intricate structure of the present day universe at a smaller scale.

For further reading on general relativity and cosmology we refer to Misner, Thorne and Wheeler [MTW73], Wald [Wal84], Carroll [Car03] and Weinberg [Wei08]. For further reading on the origins and evolution of structure we refer to Weinberg [Wei08], Peebles [Pee80], lectures by Van de Weijgaert [vdW], Van de Weijgaert and Bond[WB08] and Brandenberger [Bra04].

4.1.1 A history of uniform spacetime

General Relativity

In special relativity space and time are combined into a single entity, called spacetime. Special relativity does not describe gravity.

The key idea of Einstein for the combination of special relativity and gravitation was the Einstein equivalence principle. The Einstein equivalence principle can be explained by the Einstein lift experiment. This is a thought experiment which says that if a physicist is contained in a sufficiently small box (the lift) he cannot distinguish the consequences of the acceleration of the box from the consequences of the box being in a gravitational field.

The Einstein equivalence principle implies that a theory of gravity should locally reduce to special relativity. This gave Einstein the idea that in 'general' spacetime should be a four dimensional pseudo-Riemannian manifold with signature[1] $-+++$. Locally a pseudo-Riemannian manifold is well approximated by its tangent space, on which we can impose the rules of special relativity. The difference in acceleration due to gravity from one point to another can be encoded by the curvature (tensor) of the manifold. The fact that spacetime is curved is an effect of the presence of matter.

In special relativity mass and energy are equivalent ($E = mc^2$) and energy and momentum are combined (into a four-vector). This means that the 'source' of gravity should no longer be mass as in classical mechanics, but some combination of energy and momentum. This 'source' is the so-called energy momentum tensor $T_{\mu\nu}$. The theory of curved spacetime is called general relativity. The physics of general relativity reduces to Newtonian gravitation in the weak field small velocity limit.

The Einstein equations

The consideration above led to the Einstein field equations [Ein15]. The Einstein field equations determine the geometry of spacetime. If we include the cosmo-

[1] The signature $+--$ is also possible. We follow Misner, Thorne and Wheeler [MTW73] and Wald [Wal84] in our choice.

logical constant Λ, these read[2]

$$R_{\mu\nu} - \frac{1}{2}g_{\mu\nu}R + g_{\mu\nu}\Lambda = \frac{8\pi G}{c^4}T_{\mu\nu}, \tag{4.1}$$

where $R_{\mu\nu}$ denotes the Ricci curvature tensor, R the scalar curvature, $g_{\mu\nu}$ the metric, G Newton's gravitational constant, c the speed of light and $T_{\mu\nu}$ the energy momentum tensor. We shall normalize the speed of light by taking $c = 1$. The cosmological constant was originally introduced by Einstein to accommodate a static universe. Our universe is not static, as was established in the 1920s. This led to a temporary decrease in interest in the cosmological constant. More recently (the 1990s) the effects of a cosmological constant have been observed. Before we can discuss this in more detail we first need to introduce the models for uniform space.

Friedmann and Lemaître

In 1922 Friedmann published a model [Fri22, Fri99a] of a positively curved uniform universe that was dynamic, that is it expanded (and in some cases collapsed), followed in 1924 by a model [Fri24, Fri99b] for negatively curved space. Lemaître [Lem27, Lem13] independently described the same model as Friedmann for positively curved space.

What we mean by positively and negatively curved universes is best explained by giving the Robertson-Walker metric[3]:

$$ds^2 = g_{\mu\nu}\mathrm{d}x^\mu \mathrm{d}x^\nu = -\mathrm{d}t^2 + a(t)^2\left(\frac{\mathrm{d}r^2}{1-kr^2} + r^2(\mathrm{d}\theta^2 + \sin^2\theta \mathrm{d}\phi^2)\right), \tag{4.2}$$

where we used the Einstein summation convention. The names of Robertson [Rob35, Rob36a, Rob36b] and Walker [Wal37] are attached to this metric because they were the first to prove that (4.2) is the most general expression for a metric for homogeneous and isotropic (uniform) universe (in concurrence with the cosmological principle). The coordinates we denote by x^μ with $\mu = 0, \ldots, 3$ in

[2]We have chosen to write the Λ term on the left hand side of equation (4.1). The left hand side of the Einstein equation is traditionally reserved for geometric terms, while the right hand side contains the terms having a matter origin. Writing the $g_{\mu\nu}\Lambda$ term on the right hand side therefore has huge physical and philosophical implications. If it is written on this side of the Einstein equation it is called Dark Energy. Various models for Dark Energy having more or less the same effect as the $g_{\mu\nu}\Lambda$ have been proposed, often under the name Quintessence, no empirical evidence for a deviation from $g_{\mu\nu}\Lambda$ has been found to date. For those familiar with Dark energy models, Planck (together with some earlier observations) [PAA+14b] found $w_{\text{eff}} = -1.04^{+0.72}_{-0.69}$, while $w_{\text{eff}} = -1$ corresponds to a cosmological constant.

[3]Also known as the Friedmann-Robertson-Walker, Friedmann-Lemaître-Robertson-Walker and Friedmann-Lemaître metric.

general and by t, r, θ, ϕ in this particular case. The function $a(t)$ is called the scale factor and reflects the expansion of the universe. The curvature factor is denoted by k. The universe is called positively curved if $k > 0$, flat if $k = 0$ and negatively curved if $k < 0$. Because the 'space' is a space of constant curvature this is also called uniform spacetime. The 'space' part of (4.2) has sectional curvature k. Observations indicate that $k = 0$. We shall discuss this in more detail below.

Evolution of the universe

The assumption that the metric is of the form (4.2) greatly simplifies the Einstein equations. In this setting the evolution of $a(t)$ is relatively easily determined for various models of the energy content.[4] The growth (shrinking) of the scale factor a is referred to as expansion (collapse) of the universe. For the energy content as determined by observations the universe has a beginning, that is a t such that $a(t) = 0$. The distances on the space of constant curvature shrink to zero as a tends to zero from above. The beginning of the universe is known as the Big Bang.

The observation of the expansion

In the 1920s the expansion of the universe was observationally established by Lemaître [Lem27, Lem13] and Hubble [Hub29]. The observations indicated a roughly linear relation[5] between the distance from earth to galaxies and their 'apparent' velocity. The 'apparent' velocity was measured by a redshift. Redshift is a shift in frequency of the light, in this case due to expansion of the universe. The distance was derived from the observed brightness of so called standard candles (stars of which the absolute or intrinsic brightness is precisely known). The fact that the linear relation between the 'apparent' velocity is rough is due to the so-called peculiar velocity. To be precise the 'apparent' velocity is the combines the contributions of the recessional velocity and the (relatively small) peculiar velocity. The recessional velocity is due to the expansion of the universe. The peculiar velocity is a consequence of local mass concentrations and deficits.

The observation of the cosmological constant and flatness of the universe

The appearance of the cosmological constant was rejected by Einstein after the expansion of the universe had been observed. The cosmological constant how-

[4] The energy in the universe is determined by the dark energy (or cosmological constant), dark matter, radiation and baryonic matter.

[5] In a sufficiently small galactic neighbourhood. For galaxies that are very far away one needs to take (the details of) the evolution of the universe into account.

ever has in the meantime been observed by studying distant supernovae [RFC+98, PAG+99]. This has been confirmed by other observations. See [FTH08] for an overview. Among these observations we should mention the WMAP [BHH+03] and Planck [PAA+14a] satellites, that observed the cosmic microwave background radiation. The cosmic microwave background will play an important role also in the rest of this story and we shall come back to it below. The observations also indicate that k in equation (4.2) is zero. We also say that the universe is flat.

Decoupling and recombination

The ongoing expansion of the universe implies that the universe was denser and hotter in the past. This means that there was a time when the universe was so dense that photons (light) could not propagate freely in the hot substance known as plasma. Because the universe was expanding it also cooled down. Some 380,000 years[6] after Big Bang the matter cooled down to some 3000 degrees Kelvin[7] and went through a phase transition so that the electrons and protons together formed hydrogen. This is known as recombination. This meant that photons were no longer scattered by the electrons and thus the universe became transparent. This is known as decoupling. Decoupling means that there was virtually no interaction between the photons and other matter from that point onward.[8] The name last scattering is also attached to the same phenomenon.

The Cosmic Microwave Background

As mentioned above the photons present in the universe effectively stopped interacting with matter. This means that from decoupling onward these photons propagate freely through the universe in every direction. These freely propagating photons are called the Cosmic Microwave Background.

The Cosmic Microwave Background has first been observed by Arno Penzias and Robert Wilson [PW65] in the 1960s. Because of the expansion of the universe these photons have redshifted and the currently observed temperature of the Cosmic Microwave Background is $2.7255 \pm 0.0006K$, see [Fix09]. Later observations by the COBE [SBK+92], WMAP [BHH+03] and Planck [PAA+14a] satellites have shown Cosmic Microwave Background to be very isotropic and the tiny deviations from the mean to be nearly Gaussian in nature, see Figure 4.1. By Gaussian in nature we mean that they are well described by a Gaussian random field, which we shall introduce in Section 4.2.

[6] Here of course we extrapolate.

[7] This is not an instantaneous process. The ionization percentage drops from over 97% for $T = 4200\ K$ to less than 0.5% for $T = 3000\ K$, see Section 2.3 of [Wei08].

[8] There is one exception called the Sunyaev-Zel'dovich effect.

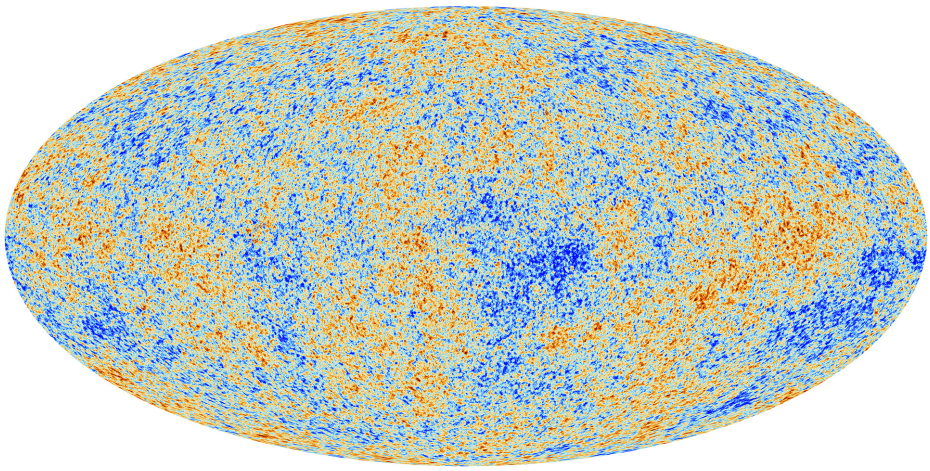

Figure 4.1: The Cosmic Microwave Background, as measured by Planck [PAA+14a], after the removal of the foreground and artefacts. The deviations from the average lie between $-500\,\mu K$ (dark blue) and $500\,\mu K$ (dark red).

The horizon problem

The isotropic nature of the Cosmic Microwave Background poses a problem. In general relativity information cannot be exchanged at speeds greater than the speed of light. For a given observer the boundary of the set of all past events of which the information may have reached the observer is called the particle horizon for that observer. The size of the horizon limits the scale at which isotropy can exist. Precisely because when no information can be exchanged between two regions of space you would expect their properties to be independent.

The Friedman-Lemaître-Robertson-Walker model based on the observed energy content of the universe is also called the cosmological standard model. For the cosmological standard model the horizon for any point before or at the time that the universe became transparent encloses a region in space that corresponds to small parts of the observed Cosmic Microwave Background. For the cosmological standard model the angular diameter (on the sky) for which causal contact existed is of order 1°, see Section 4.1 of [Wei08].[9] The fact that causal contact should be of order 1° while the Cosmic Microwave Background has a temperature of $2.7255 \pm 0.0006K$ in every direction is known as the horizon problem.

[9] This corresponds to a larger volume in space than one might expect because the visible universe is about three times as large as one would naively expect because of the expansion of the universe.

Inflation

One solution to the horizon problem is the incorporation [Gut81, Lin82] into the model of a period of very rapid expansion in the very early universe, called Inflation, so that regions that could exchange information in the very early stages of the universe are blown up to scales far beyond those that correspond to the observed Cosmic Microwave Background. Inflation also explains why the universe is almost flat and we do not observe exotic particles, in particular magnetic monopoles, that would be created at the very high temperatures that existed just after the Big Bang. To be precise we do not observe these exotic particles because after inflation there are only a few exotic particles left in a large volume.

Inflation implies that not only exotic particles, but all particles present before or at the beginning of inflation are diluted. In quantum field theoretical terms this can be reformulated as the fields that existed at the beginning of inflation being greatly redshifted.

The generation of fluctuations

While explaining these global fine-tuning problems of the standard Friedmann-Lemaître-Robertson-Walker Universe models, inflation also suggests the nature of the origin of fluctuations in the early Universe, the seeds for the formation of all structure in the Universe.

The generation of fluctuations in the early universe is a form of particle creation in curved spacetime. We may understand particle creation in curved spacetime starting with a quantum mechanical system in the ground state. To the ground state one associates a particular wave function. Now suppose that space expands and the wave function gets stretched, then the system is no longer in the ground state but is the superposition of the ground state and some excited states (as in Fourier decompositions). In quantum field theory this is interpreted as particle creation,[10] or in this case more specifically as the creation of cosmological perturbations.

We refer to Brandenberger [Bra04] for a pedagogical introduction and [MFB92] for an extensive overview of the quantum mechanical origins of the (tiny) fluctuations in the Cosmic Microwave Background. In Section 4.2 we will see two arguments that imply that the fluctuations are (nearly) Gaussian.

[10] This is because of wave-particle duality. The notion of a particle in a quantum field theory on curved spacetime is a very subtle one. For a full discussion of quantum field theory on curved spacetime we refer to [Wal94].

4.1.2 The Cosmic Web

Over the past decades, ever more ambitious galaxy redshift surveys have unveiled the existence of an intriguing spatial organization of matter on scales of a few up to hundreds of Megaparsecs.[11] At these scales the Universe still resides in a state of moderate dynamical evolution. From the first hints of superclustering in the seventies to the progressively larger and more detailed three-dimensional maps of interconnected large scale structure that emerged in the eighties, nineties and especially post-2000, we now have a clear paradigm. Galaxies, intergalactic gas and dark matter exist in a wispy weblike spatial arrangement consisting of dense compact clusters, elongated filaments, and sheetlike walls, amidst large near-empty void regions, with similar patterns existing at higher redshift, albeit over smaller scales. The hierarchical nature of this mass distribution, marked by substructure over a wide range of scales and densities, has been clearly demonstrated. This complex morphological structure is known as the *Cosmic Web* [Zel70, BKP96, WB08].

It was the celebrated map of the first CfA redshift slice [dGH86] that showed the connection between the basic elements of the Cosmic Web that was going to emerge in more extensive mapping surveys. In recent years this view has been expanded dramatically to the present grand vistas offered by the 100,000s of galaxies in the 2dF – two-degree field – Galaxy Redshift Survey, the 2dFGRS see for example [CPJ$^+$03], the SDSS [TBS$^+$04] galaxy redshift survey, and recently in the 2MRS survey of the Local Universe [HJS$^+$05] and the VIPERS deep probe of the cosmic galaxy distribution at higher redshifts, see for example [GSG$^+$14]. These and many other redshift surveys have unequivocally established the reality of the Cosmic Web and its structural components. A telling illustration of the weblike galaxy distribution in the local Universe is the map of galaxy positions in a thin slice through the Sloan Digital Sky Survey, shown in Figure 4.2.

Cosmic Structure Formation

The generally accepted theoretical framework for the formation of structure is that of gravitational instability [Pee80]. The gravitational instability scenario assumes the early universe to have been almost perfectly smooth, with the exception of tiny density deviations with respect to the global cosmic background density and the accompanying tiny velocity perturbations from the general Hubble expansion.

The minor density deviations vary from location to location. At one place the density will be slightly higher than the average global density, while a few Megaparsecs further the density may have a slightly smaller value than on av-

[11] In astronomy distance are measured in parsecs. One parsec equals about three light years.

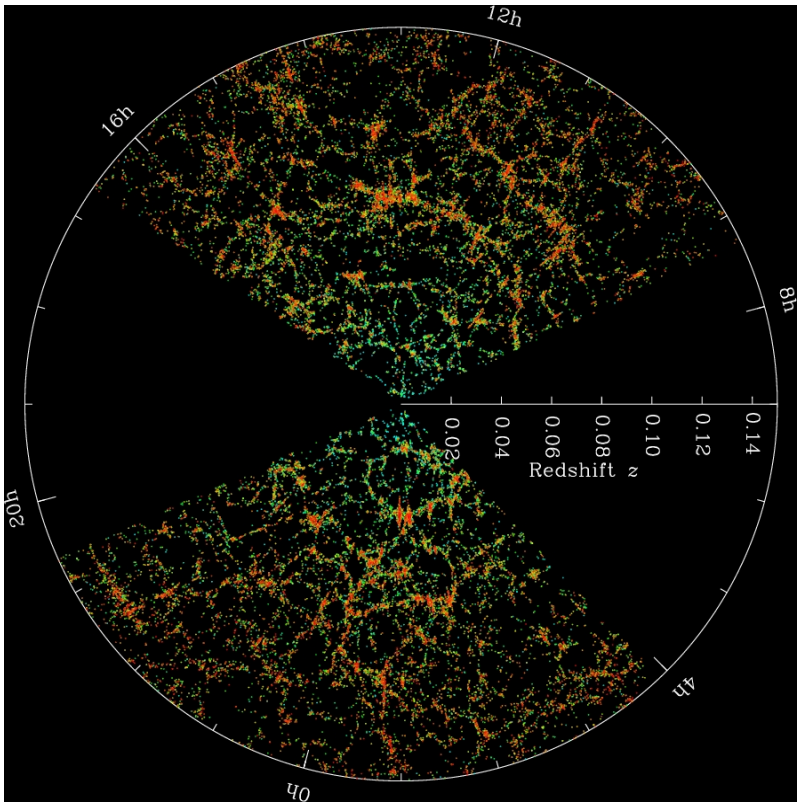

Figure 4.2: Slice of the galaxy distribution found by the Sloan Digital Sky Survey (third data release). The distances are given in terms of the redshift. Both clusters and the filaments connecting the clusters stand out. Credited to M. Blanton and the Sloan Digital Sky Survey.

erage. The observed fluctuations in the temperature of the cosmic microwave background radiation are a reflection of these density perturbations, so that we know that the primordial density perturbations have been in the order of 10^{-5} [SBK+92, BHH+03, PAA+14a].

Gravitational Instability

The originally minute local deviations from the average density of the Universe, and the corresponding deviations from the global cosmic expansion velocity (the Hubble expansion), will start to grow under the influence of the corres-

ponding gravity perturbations. The gravitational force acting on each patch of matter in the universe is the total sum of the gravitational attraction by all matter throughout the universe. Evidently, in a homogeneous Universe the gravitational force is the same everywhere. In a universe with minute density perturbations this will be no longer true, the density perturbations will induce local differences in gravity.

The resulting formation and moulding of structure is fully described by three equations, the *continuity equation*, expressing mass conservation, the *Euler equation* for accelerations driven by the gravitational force for dark matter and gas, and pressure forces for the gas, and the *Poisson-Newton equation* relating the gravitational potential to the mass density distribution in the Universe. In slightly overdense regions around density peaks, the excess gravitational attraction slows down the expansion relative to the mean, while underdense regions expand more rapidly. When a positive density fluctuation becomes sufficiently overdense it can come to a halt, turn around and start to contract. As long as pressure forces do not counteract the infall, the overdensity will grow without bound, assembling more and more matter by accretion from the surroundings, ultimately fully collapsing in a gravitationally bound and virialized object.

By contrast, voids emerge out of the density troughs in the primordial Gaussian field of density fluctuations. As a result of their underdensity voids represent a region of weaker gravity, resulting in an effective repulsive peculiar gravitational influence. Initially underdense regions therefore expand faster than the Hubble flow, and thus expand with respect to the background Universe. As matter streams out of the void, the density within the void decreases. Of course, the density deficit of voids is strictly limited: they cannot become more empty than empty. It is the prime reason why void structure will be fundamentally different from that of the structure of clusters.

Non-linear structure growth

Once the gravitational clustering process has progressed beyond the initial linear growth phase we see the emergence of complex patterns and structures in the density field. Highly illustrative of the intricacies of the structure formation process is that of one of state-of-the-art N-body computer simulations, the Millennium-II simulation, see [SWJ$^+$05, BSW$^+$09].

Figure 4.3 shows three sets of each four time frames out of this massive 10^{10} particle simulation of the matter distribution in the standard ΛCDM cosmology. The frames show thin sections through the box of $100h^{-1}\mathrm{Mpc}$ size. The time frames correspond to redshifts $z = 6.20$, $z = 2.07$, $z = 0.99$ and $z = 0$. The earliest time frame is close to the epoch when the first dwarf galaxies formed. The first column of frames contains the Dark Matter particle distribution in a

$15h^{-1}\mathrm{Mpc}$ thick slice of the full $100h^{-1}\mathrm{Mpc}$ box, the second column zooms in on the central $40h^{-1}\mathrm{Mpc}$. The third column shows the evolution of the central $15h^{-1}\mathrm{Mpc}$ region around the emerging compact massive cluster.

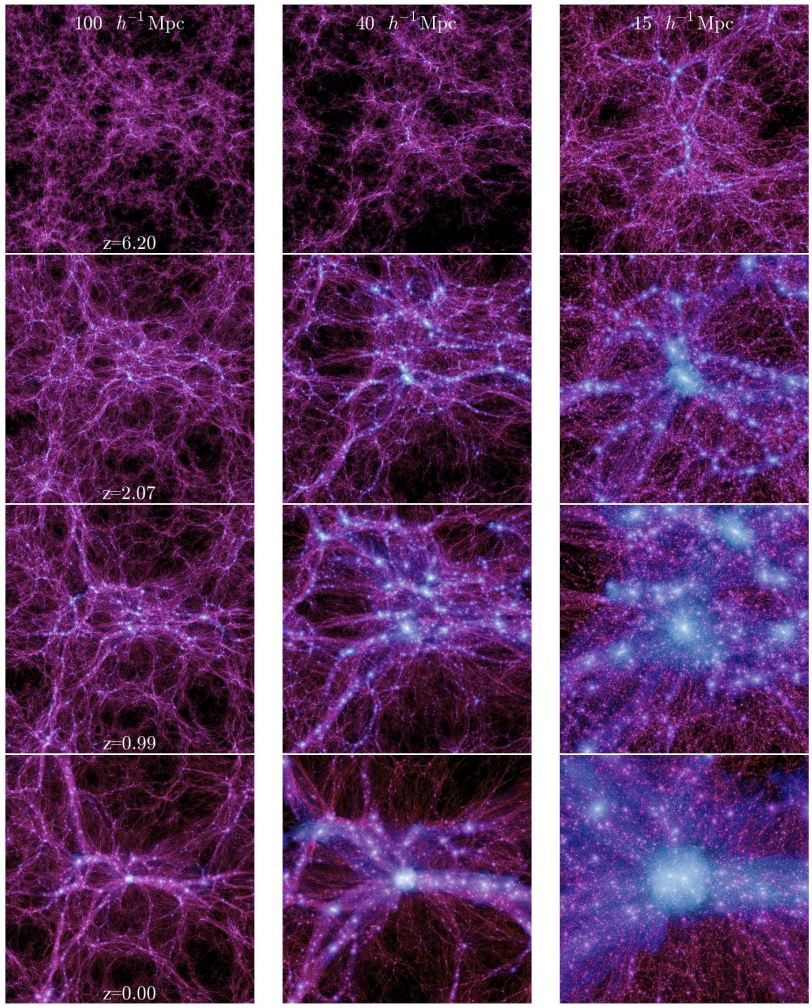

Figure 4.3: The structures found by the Millennium II simulation for different times and scales [BSW+09]. The time is indicated by the redshift parameter z, where $z = 0$ corrsponds to present day universe and $z = 6.2$ to some 12 billion years ago. The distances are measure in $h^{-1}Mpc$ which equals nearly 5 million light years.

The first set provides a beautiful picture of the unfolding Cosmic Web, starting from a field of mildly undulating density fluctations towards that of a pronounced and intricate filigree of filamentary features, dented by dense compact clumps at the nodes of the network. The second set of frames depicts in meticulous detail the formation of the filamentary network connecting into the cluster which are the transport channels for matter to flow into the cluster. Clearly visible as well is the hierarchical nature in which not only the cluster builds up but also the filamentary network. At first consisting of a multitude of small scale edges, they quickly merge into a few massive elongated channels. Equally interesting to see is the fact that the dark matter distribution is far from homogeneous: a myriad of tiny dense clumps indicate the presence of the dark halos in which galaxies – or groups of galaxies – will or have formed.

Large N-body simulations like the Millennium simulation and the many others currently available all reveal a few "universal" characteristics of the (mildly) nonlinear cosmic matter distribution. The most prominent characteristics of the Megaparsec universe are:

- Hierarchical clustering
- Anisotropic & Weblike spatial geometry
- Voids

Each of these aspects deserve some further discussion.

Hierarchical Structure Formation

Perhaps the most significant and characteristic property is the *hierarchical nature* of the cosmic matter distribution. Over a wide range of spatial and mass scales objects and/or structures are embedded within structures of a larger dimension and a lower density. The resulting scenario of structure formation is one in which the first objects to form are small compact objects which subsequently merge with their surroundings as the larger scale density excess in which they are embedded condenses out of the cosmic background. Small scale perturbations evolve substantially faster than the ones on larger scales and will emerge first as genuine recognizable objects.

Extended features still in the process of collapsing, or collapsed objects which have not yet fully virialized, often contain a large amount of smaller scale substructure at higher density which materialized at an earlier epoch. This substructure is a clear manifestation of the hierarchical development of structure in the Universe. Observationally we can recognize traces of the hierarchical formation process in the galaxy distribution on Megaparsec scales. The large unrelaxed filamentary and wall-like superclusters contain various rich clusters

of galaxies as well as a plethora of smaller galaxy groups, each of which has a higher density than the average supercluster density. Zooming in on even smaller scales, within groups large galaxies themselves are usually accompanied by a number of smaller satellites and dwarf galaxies. The imprint of hierarchical clustering may also be found in fully collapsed structures, such as clusters and even the halos of galaxies.

Anisotropic Collapse

The second key characteristic of the cosmic matter distribution is that of a *weblike geometry* marked by highly elongated filamentary, flattened planar structures and dense compact clusters surrounding large near-empty void regions (see Figure 4.4). In this section we focus on the backbone - or skeleton - of the Cosmic Web defined by these anisotropic filamentary and sheetlike patterns.

The recognition of the *Cosmic Web* as a key aspect in the emergence of structure in the Universe came with early analytical studies and approximations concerning the emergence of structure out of a nearly featureless primordial Universe. In this respect the Zel'dovich formalism [Zel70] played a seminal role. It led to view of structure formation in which planar pancakes form first, draining into filaments which in turn drain into clusters, with the entirety forming a cellular network of sheets. As borne out by a large sequence of N-body computer experiments of cosmic structure formation, weblike patterns in the overall cosmic matter distribution do represent a universal but possibly transient phase in the gravitationally driven emergence and evolution of cosmic structure. The N-body calculations have shown that weblike patterns defined by prominent anisotropic filamentary and planar features – and with characteristic large underdense void regions – are a natural manifestation of the gravitational cosmic structure formation process.

The existence of the Cosmic Web is a result of this tendency of matter concentrations to contract and evolve into anisotropic, elongated or flattened, structures. It is a manifestation of the generic *anisotropic* nature of gravitational collapse, a reflection of the intrinsic anisotropy of the gravitational force in a random density field.

Voids

The third major characteristic of the Megaparsec mass distribution is the existence of large underdense void regions. In terms of volume, they are the predominant features in the cosmic mass distribution [CvJF14].

Voids have been known as a feature of galaxy surveys since the first surveys were compiled [CR75, GT78, EJS80]. *Voids* are enormous regions with sizes

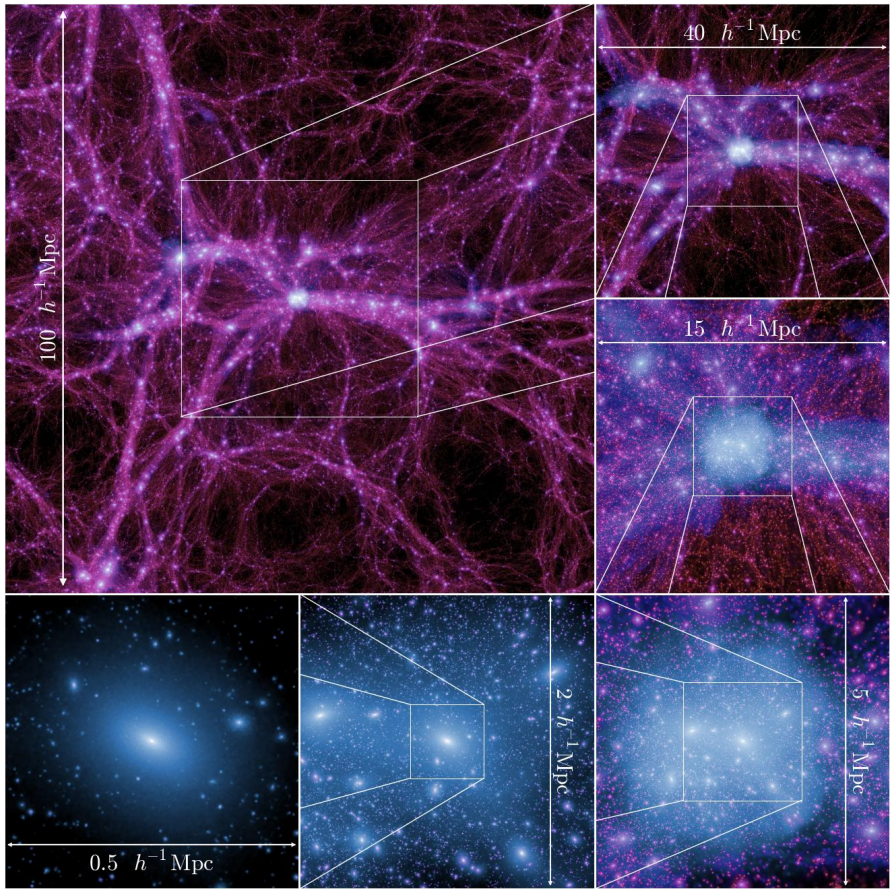

Figure 4.4: A zoom-in of the (present day) structure found by the Millennium II simulation [BSW+09]. The zoom-in focusses on a cluster and goes from $100h^{-1}Mpc$ (somewhat over 400 million lightyears) to $0.5h^{-1}Mpc$. The multi scale nature of the cosmic web is apparent.

in the range of $20 - 50h^{-1}$ Mpc that are practically devoid of any galaxy, usually roundish in shape and occupying the major share of space in the Universe. Forming an essential ingredient of the *Cosmic Web* [BKP96], they are surrounded by elongated filaments, sheetlike walls and dense compact clusters. Following the discovery by Ref. [KOSS81] and [KOSS87] of the most dramatic specimen, the Boötes void, a hint of their central position within a weblike arrangement came with the first CfA redshift slice [dGH86]. This view has been dramatically

endorsed and expanded by the redshift maps of the 2dFGRS, SDSS, 2MRS and VIPERS surveys [CPJ+03, TBS+04, HJS+05, GSG+14]. They have established voids as an integral component of the Cosmic Web. The SDSS map shown in Figure 4.2 provides a telling impression of this finding.

In a void-based description of the evolution of the cosmic matter distribution, voids mark the transition scale at which density perturbations have decoupled from the Hubble flow and contracted into recognizable structural features. On the basis of theoretical models of void formation one might infer that voids may act as the key organizing element for arranging matter concentrations into an all-pervasive cosmic network [Ick84, vv93, Sv04, Ara12]. As voids expand, matter is squeezed in between them, and sheets and filaments form the void boundaries.

As we have already discussed above, voids emerge out of the density troughs in the primordial Gaussian field of density fluctuations. As a result of their underdensity voids represent a region of weaker gravity, resulting in an effective repulsive peculiar gravitational influence. Initially underdense regions therefore expand faster than the Hubble flow, and thus expand with respect to the background Universe. The flow in and around the void is dominated by the outflow of matter from the void, culminating into the void's own expansion near the outer edge. Various studies have found strong indications for the imprint of voids in the peculiar velocity flows of galaxies in the Local Universe, see for example [Dek94, Rv07, TSK+08, TCHP14].

In recent years, there has been a strongly growing interest in voids as a key constituent of the large scale Universe. A major incentive for this has been the recognition that the number density, sizes and shapes of voids are sensitive probes of global cosmological parameters, dark matter [MW90, DR94, RM96] and dark energy [PL07a, PL07b, LW10, BvDP12, SLWW12, HSW14].

4.2 A Gaussian random field primer

This section will give a rough introduction to Gaussian random fields. Most of the time we shall ignore questions regarding convergence and existence. It is almost entirely based on [Adl81, AT07, Chr92, Abr97, BBKS86, vdWB96, PUP02, Jon97, Jon15].

4.2.1 Literature overview

'The geometry of random fields' by Adler [Adl81] is perhaps the classic reference of those on which we base this introduction. The book by Adler and Taylor [AT07] is of all these sources the most general in its treatment. This makes it somewhat abstract. The book by Christakos [Chr92] is written with applications of general random fields in mind, although in geophysics. The emphasis on applications makes it more accessible to practitioners but it is still fairly mathematically rigorous. The review of Abrahamsen [Abr97] is somewhat in line with [Chr92]. Papoulis and Unnikrishna Pillai [PUP02] gives a classic and general introduction to (as the title of the book says) probability, random variables and stochastic processes. Useful lecture notes by Jones [Jon97] do much the same but with Cosmological applications in mind and a special focus on Gaussian random fields. The book [Jon15] by the same author should also be mentioned. Bardeen, Bond, Kaiser and Szalay [BBKS86] apply the results on Gaussian random fields to Cosmology. Van de Weijgaert and Bertschinger [vdWB96] also comes from a cosmological background and focusses on constrained fields.

4.2.2 Random Fields

Before we can give the definition of a random field we first introduce a probability space. A probability space $(\Omega, \mathcal{F}, \mathbb{P})$ consists of a sample space Ω, a σ-algebra $\mathcal{F}$ and a probability measure $\mathbb{P}$ (the σ-algebra and measure give us sets that behave reasonable and a way to assign values to these sets compatible, in the finite dimensional case, with the standard integration on $\mathbb{R}^n$), such that the Kolmogorov axioms hold:

- $\mathbb{P}(\Omega) = 1$ (the total probability of all events is 1).
- $0 \leq \mathbb{P}(A) \leq 1$ for all sets $A \in \mathcal{F}$ (the probability of a event is never negative and at most one).
- if $A_i \cap A_j = \emptyset$ for all $i \neq j$ then

$$\mathbb{P}\left(\bigcup_i^{\infty} A_i\right) = \sum_{i=1}^{\infty} \mathbb{P}(A_i)$$

(the total probability of any (countable) number of mutually exclusive events to occur is the sum of the probability of the individual events).

A finite dimensional random variable, $X(u)$, with $u \in \Omega$ as defined above, is a nice (measurable) mapping X from $(\Omega, \mathcal{F})$ into $\mathbb{R}^d$. The (cumulative) distribution function is defined by

$$\mathbb{P}((-\infty, x_1] \times \cdots \times (-\infty, x_d]) = F(x),$$

The derivative

$$\varphi(x) = \frac{\partial^d F(x)}{\partial x_1 \cdots \partial x_d},$$

if it exists, is called the probability density function. We can now write

$$\mathbb{P}(A) = \int_A \varphi(x) \mathrm{d}x.$$

The conditional probability density is defined as

$$\varphi(x_{k+1}, \ldots, x_d \mid x_1, \ldots, x_k) = \frac{\varphi(x_1, \ldots, x_d)}{\tilde{\varphi}(x_1, \ldots, x_k)},$$

with

$$\tilde{\varphi} = \frac{\partial^k}{\partial x_1 \cdots \partial x_k} \mathbb{P}((-\infty, x_1] \times \cdots \times (-\infty, x_k] \times \mathbb{R}^{d-k}).$$

The conditional probability density is related to the conditional probability (conditioned on lower dimensional half spaces) by

$$\begin{aligned} &\varphi(x_{k+1}, \ldots, x_d \mid x_1, \ldots, x_k) \\ &\quad = \frac{\partial^{d-k}}{\partial x_{k+1} \cdots \partial x_d} \mathbb{P}((-\infty, x_{k+1}] \times \cdots \times (-\infty, x_d] \mid x_1, \ldots, x_k), \end{aligned}$$

here the condition on the point should be interpreted as a limit because the condition on sets of measure zero needs some justification.
The expectation value of a random variable (or its mean value) can now be defined as

$$m = \langle X \rangle = \mathbb{E}(X) = \int_{\mathbb{R}} x \varphi(x) \mathrm{d}x.$$

The mean is also known as the first moment. This can be generalized to the expectation value of a function g of the random variable

$$\langle g(x) \rangle = \mathbb{E}(g(X)) = \int_{\mathbb{R}} g(x) \varphi(x) \mathrm{d}x.$$

There are a number of such expectation values of particular interest:

- The covariance or central second moment

$$c_{ij} = \mathbb{E}((X_i - m_i)(X_j - m_j)) = \int_{\mathbb{R}} (x_i - m_i)(x_j - m_j)\varphi(x)\mathrm{d}x.$$

- The variance

$$\sigma_i^2 = c_{ii} = \mathbb{E}((X_i - m_i)^2) = \int_{\mathbb{R}} (x_i - m_i)^2\varphi(x)\mathrm{d}x.$$

- The second order correlation function or two point correlation function

$$\langle X_i X_j \rangle = \mathbb{E}(X_i X_j) = \int_{\mathbb{R}} x_i x_j \varphi(x)\mathrm{d}x.$$

  This is also known as the non-central second moment or non-central covariance. Note that some authors choose to normalize the correlation function by

$$\frac{1}{\sqrt{\sigma_i^2}\sqrt{\sigma_j^2}}.$$

- The higher order correlation functions or n-point correlation functions

$$\langle X_i X_j \dots X_k \rangle = \mathbb{E}(X_i X_j \dots X_k) = \int_{\mathbb{R}} x_i x_j \dots x_k \varphi(x)\mathrm{d}x.$$

- The characteristic function, the Fourier transform of the probability density function,

$$\Phi(\omega) = \mathbb{E}(e^{i\omega \cdot X}) = \int_{\mathbb{R}} e^{i\omega \cdot x}\varphi(x)\mathrm{d}x,$$

  with $\cdot$ the usual inner product.

We can now give the definition of a random field, following [AT07]:

Definition 4.2.1 *Let $(\Omega, \mathcal{F}, P)$ be a probability space and $\mathbb{R}^n$ Euclidean space. Then a 'nice' (measurable) mapping $f : \Omega \to Fun(\mathbb{R}^n, \mathbb{R})$, where $Fun(\mathbb{R}^n, \mathbb{R})$ denotes the space of all real-valued functions on $\mathbb{R}^n$, is called an n-dimensional random field.*

Alternatively, following to [Chr92], we can also put the emphasis on individual points (by restriction): Let $s_1, \dots s_2, \dots$ be an (countable) infinite sequence of random points in $\mathbb{R}^n$. Then the random field $f(s)$ is a family of random variables $\{x_1, x_2, \dots\}$ at points $s_1, \dots s_2, \dots$, where each random variable is defined on $(\Omega, \mathcal{F})$ and takes values in $\mathbb{R}$.
Usually some additional conditions on the existence of various expectation values are added, which we shall ignore because they are mostly automatically satisfied for Gaussian random fields.

4.2.3 Gaussian random fields

A real valued random variable X is said to be Gaussian or normally distributed, with mean m, if it has the probability density function

$$\varphi(x) = \frac{1}{\sqrt{2\pi}\sigma} e^{-(x-m)^2/(2\sigma^2)},$$

for some $\sigma > 0$. An $\mathbb{R}^d$-valued random variable $X = (X_1, \dots, X_d)$ is called a multivariate Gaussian if for every $(\alpha_1, \dots, \alpha_d) \in \mathbb{R}^d$, the real-valued variable $\sum \alpha_i X_i$ is Gaussian. In this case we have a $m \in \mathbb{R}^d$, and a $d \times d$-matrix C whose entries are the covariances c_{ij} (that is $(C)_{ij} = c_i j$), such that the probability density function reads

$$\varphi(x) = \frac{1}{\sqrt{(2\pi)^d \det(C)}} e^{-\frac{1}{2}(x-m)^t C^{-1}(x-m)}. \tag{4.3}$$

This means that all correlation functions of the field are determined by the two point correlation function. Below we shall see that the same holds for the derivatives of the field. This in turn implies that a Gaussian random field is completely determined by the two point correlation function.

We are now able to give the central definition:

Definition 4.2.2 *A random field $\phi : \Omega \to Fun(\mathbb{R}^n, \mathbb{R})$ is called a Gaussian random field if the restriction of $Fun(\mathbb{R}^n, \mathbb{R})$ to any finite number of points $s_1, \dots, s_d \in \mathbb{R}^n$, denoted by $f_{s_1}, \dots f_{s_d}$ together form a multivariate Gaussian $(f_{s_1}, \dots f_{s_d})$.*

The functions

$$\begin{aligned} m(s) &= \mathbb{E}(f_s) \\ C(s,t) &= \mathbb{E}((f_s - m_s)(f_t - m_t)) \end{aligned}$$

are called the mean and covariance functions of the Gaussian random field.

From this point onward we assume that the mean is zero, unless stated otherwise. Moreover, to emphasize that we think of f as a function we shall write $f(s)$, instead of f_s

We emphasize that both the multivariate Gaussian and Gaussian random field are determined completely by their mean (which we now assume to be trivial) and covariance. These two suffice to define the probability density. Moreover, we have that

$$\mathbb{E}(f(s_1)f(s_2)\dots f(s_k)) = \sum_{\text{pairings}} \prod_{\text{pairs}} \mathbb{E}(f(s_i)f(s_j)), \tag{4.4}$$

which can be written, using the $\langle\,\rangle$ notation to emphasize the relation with quantum field theory, as

$$\langle f(s_1)f(s_2)\dots f(s_k)\rangle = \sum_{\text{pairings}} \prod_{\text{pairs}} \langle f(s_i)f(s_j)\rangle.$$

Alternatively, one can define a Gaussian random field as a field of which the correlation functions satisfy (4.4). This point of view is emphasized in [Wei08], because (4.4) can be viewed as a classical analogue of Wick's theorem (where the f_{s_i} are replaced by quantum mechanical operators and ordering therefore is taken into account). The density fluctuations in the early universe are believed to arise from the fluctuations of one or more nearly free quantum fields and therefore satisfy Wick's theorem, explaining why in the classical limit one would expect the fields to satisfy (4.4). This definition is equivalent to Definition 4.2.2 because of a result by Kolmogorov. Kolmogorov extension theorem says that a probability measure is uniquely determined by the correlation functions. This means in particular that if all correlations are compatible with the classical analogue of Wick's theorem the field is Gaussian. We refer to Section 1.2 of [Sim79] for a discussion.

Having touched on the importance of Gaussian random fields in Physics we should also mention the other argument put forward in favour of a Gaussian random field being a good model for physical phenomena such as the Cosmic Microwave Background, namely the central limit theorem. The central limit theorem in the most elementary (one dimensional) form, see Section 7.4 of [PUP02], says the following: Suppose we have a sequence of independent random variables X_i with mean m_i and covariance σ_i^2 and probability density ϕ_i. The mean and variance of the sum

$$X = X_1 + \ldots + X_n$$

are given by

$$m = m_1 + \ldots + m_n \qquad\qquad \sigma^2 = \sigma_1^2 + \ldots + \sigma_n^2$$

and the density by

$$\phi = \phi_1 * \ldots * \phi_n$$

where $*$ denotes convolution. If X is properly scaled we have, under fairly general conditions, that the density ϕ approaches a Gaussian as n tends to infinity, that is in the limit

$$\phi(x) \sim \frac{1}{\sqrt{2\pi\sigma^2}} e^{-(x-m)^2/2\sigma^2},$$

where $\sim$ denotes proportionality. For a full discussion we refer the reader to Section 4.4 of [Chr92] and the references mentioned there.

Using a path integral-like approach one sometimes writes

$$e^{-S[f]}$$

for the generalized probability function, with

$$S[f] = \frac{1}{2} \iint f(s) K(s,t) f(t) \mathrm{d}s \, \mathrm{d}t,$$

where

$$\int K(s,t) C(t,u) \mathrm{d}t = \delta_D(t-u)$$

and where δ_D denotes the Dirac δ-distribution. The S above is often referred to as the action, in direct analogy of the quantum field theory case. Note however that in this path-integral-like approach the measures involved in the generalized probability function now are over spaces of functions.

4.2.4 Properties of Gaussian fields

We shall be interested in geometric properties of Gaussian random fields, for which we must introduce a notion of differentiability. This notion is based on the usual definition of the derivative

$$\frac{\partial f}{\partial s_i}(s) = \lim_{h \to 0} \frac{f(s + h e_i) - f(s)}{h},$$

where e_i is the i^{th} basis vector. The stochastic derivative (in the mean square sense) is defined as the the random field $\partial f / \partial s_i$ for which

$$\lim_{h \to 0} \mathbb{E} \left(\left(\frac{f(s + h e_i) - f(s)}{h} - \frac{\partial f}{\partial s_i}(s) \right)^2 \right).$$

This definition can clearly be extended to include higher derivatives. Using the correlation function we are also able to obtain expressions for the covariance of f and its derivatives. We have the following result, see section 4.3 of [Chr92] for a full discussion:[12] The partial derivative $\partial^\nu f(s)/(\partial s_{i_1} \dots \partial s_{i_\nu})$ exists in the sense we defined above if and only if

$$\mathbb{E}\left(\frac{\partial^\nu f(s)}{\partial s_{i_1} \dots \partial s_{i_\nu}} \frac{\partial^\nu f(t)}{\partial t_{i_1} \dots \partial t_{i_\nu}}\right) = \frac{\partial^{2\nu} C(s,t)}{\partial s_{i_1} \dots \partial s_{i_\nu} \partial t_{i_1} \dots \partial t_{i_\nu}}$$

exists and is finite at all diagonal points $t = s$. Furthermore if both $\partial^\nu f(s)/(\partial s_{i_1} \dots \partial s_{i_\nu})$ and $\partial^\mu f(t)/(\partial t_{i_1} \dots \partial t_{i_\mu})$ exist, then

$$\mathbb{E}\left(\frac{\partial^\nu f(s)}{\partial s_{i_1} \dots \partial s_{i_\nu}} \frac{\partial^\mu f(t)}{\partial t_{i_1} \dots \partial t_{i_\mu}}\right) = \frac{\partial^{\nu+\mu} C(s,t)}{\partial s_{i_1} \dots \partial s_{i_\nu} \partial t_{i_1} \dots \partial t_{i_\mu}}. \tag{4.5}$$

Such results are generally proven using a reasoning we shall roughly sketch for $\mathbb{E}(\partial_s f(s) \partial_t f(t))$, the covariance of the derivatives of a one dimensional field:

$$\begin{aligned}
&\mathbb{E}(\partial_s f(s) \partial_t f(t)) \\
&= \lim_{\epsilon_1, \epsilon_2 \to 0} \mathbb{E}\left(\frac{f(s+\epsilon_1) - f(s)}{\epsilon_1} \frac{f(t+\epsilon_2) - f(t)}{\epsilon_2}\right) \\
&= \lim_{\epsilon_1, \epsilon_2 \to 0} \frac{\mathbb{E}\left(f(s+\epsilon_1) f(t+\epsilon_2) - f(t) f(s+\epsilon_1) - f(s) f(t+\epsilon_2) + f(s) f(t)\right)}{\epsilon_1 \epsilon_2} \\
&= \lim_{\epsilon_1, \epsilon_2 \to 0} \frac{C(s+\epsilon_1, t+\epsilon_2) - C(s+\epsilon_1, t) - C(s, t+\epsilon_2) + C(s,t)}{\epsilon_1 \epsilon_2} \\
&= \frac{\partial^2 C(s,t)}{\partial s \partial t}.
\end{aligned}$$

From this sketch we can see that n-point correlation functions of derivatives of fields can be expressed in derivatives of 2-point functions, because we can use formula (4.4) to go from n-point to 2-point functions before taking the limits $\epsilon_i \to 0$ (in what in our example is the second line). It follows directly that the n-point correlation functions of derivatives of fields are completely determined by the 2-point functions in the same manner as the n-point correlation functions of the fields themselves and thus are Gaussian. It is therefore not unusual, see [BBKS86], if one considers a Gaussian random field and some of its derivatives in a small number of points to put the correlations between the fields and those derivatives at the specified points in a single correlation matrix C, so that the probability density function is the same as in (4.3).

[12] Chapter 9 of [PUP02] gives a weaker, but easier result, section 1.4.2 of [AT07] treats the same and is more sophisticated.

Let us now introduce some further definitions and notation. We call a Gaussian random field isotropic if the correlation function only depends on the distance between the two points considered, that is

$$C(s,t) = C(r),$$

with $r = |s-t|$. In this case we have that for the Fourier components $\hat{f}(k)$ of $f(x)$

$$f(x) = \int \frac{\mathrm{d}k}{(2\pi)^n} \hat{f}(k) e^{-ik\cdot x},$$

satisfy

$$\mathbb{E}(\hat{f}(k)^* \hat{f}(k')) = (2\pi)^3 P(k) \delta_D(k-k'),$$

where $P(k)$ is referred to as the power spectrum.

4.3 Topology for Cosmologists

This section gives an overview of some aspects of algebraic topology and Morse theory as well some differential topology. Some of the standard works on algebraic topology are [Mun84, DFN90, Hat01]. Edelsbrunner and Harer [EH10] also give an introduction to algebraic topology with a focus on computational aspects and persistence. It is this book that we shall follow in Sections 4.3.2 and 4.3.4. Milnor [Mil73] is the classical introduction to Morse Theory. Section 4.3.3 will follow Milnor [Mil73] closely.

4.3.1 Topology and the Euler characteristic

Topology is the branch of mathematics concerned with the properties of spaces that are preserved under continuous deformations such as stretching and bending, but not tearing.[13]

The Euler characteristic

One of the most useful tools of topology are so-called invariants that can be used to distinguish for example surfaces up to these deformations. One of the oldest

[13]To be more precise one does not distinguish spaces for which there is a continuous, piecewise smooth or smooth bijection whose inverse is also continuous, piecewise smooth or smooth in topology. A bijection is a one to one mapping, that is every point is mapped to a unique point and every point in the image is reached. These bijections are referred to as homeomorphisms, piecewise smooth homeomorphisms and diffeomorphisms. The branch of topology that concentrates on diffeomorphisms is called differential topology. Below we shall often assume smoothness for simplicity.

The word topology also refers to a collection of all open sets in a space. A topology on a space is all that is necessary to define continuous mappings. A space endowed with a topology is called a topological space.

Another branch of topology is knot theory. This branch considers the particular embedding in a low dimensional space, traditionally of a single deformed circle but nowadays of more general spaces. Knot theory for example distinguishes the following two embeddings of two circles (with unit radius) in three dimensional Euclidean space: In the first embedding the circles lie in parallel planes in three space and in the second each circle is centred on a point of the other circle, but coincide nowhere. These two configurations cannot be deformed into one another in three dimensional space, without intersections. Although the two pairs of circles are clearly diffeomorphic and can be deformed into one another in a sufficiently high dimensional space.

The concept of continuous deformations can be formalized by homotopy and isotopy. Given two (continuous, piecewise smooth or smooth) functions $f, g : X \to Y$ a homotopy between f and g is a (continuous, piecewise smooth or smooth) function $H : X \times [0,1] \to Y$ such that $H|_0 = f$ and $H|_1 = f$. Here we usually think of $[0,1]$ as a time interval. For example let us choose X and Y to be the cylinder $S^1 \times [0,1]$, f the identity and $g : (x_1, x_2) \mapsto (x_1, 0)$, then f and g are homotopic. An isotopy is a homotopy such that for all $t \in [0,1]$, H_t is an embedding (a homeomorphism on the image).

There is a version of homotopy theory that focusses on space and not functions. In such a case spaces are called homotopy equivalent or of the same homotopy type.

topological invariants used in this field is the so called Euler characteristic. The Euler Characteristic of a surface can be defined as the alternating sum of the number of simplices, that is vertices (v), edges (e) and triangles (t)

$$\chi = v - e + t \tag{4.6}$$

of a triangulation. This definition generalizes to any dimension. By triangulation we mean a 'neat' subdivision of the surface into triangles, edges and vertices, or in general into simplices. A set of simplices, together with an adjacency relation is called a simplicial complex. Simplicial complices allow us to consider the triangulation of a space or surface. We will view triangulations in two slightly different ways, namely as being 'painted' on the space or surface and as a simplicial complex per se. From the definition (4.6) it is clear that the Euler characteristic is additive. By additive we mean that if a surface is composed of multiple disjoint pieces the Euler characteristic of the entire surface is the sum of the Euler characteristics of the constituent parts.

The Euler characteristic for topological spheres

We can verify that the Euler characteristic is an invariant for two triangulations of the topological 2-sphere: the boundaries of the tetrahedron and the octahedron. The boundary of tetrahedron consist of 4 vertices, 6 edges and 4 triangles, which yields $\chi = 4-6+4 = 2$. The boundary of the octahedron has 6 vertices, 12 edges and 8 triangles, which again gives $\chi = 6-12+8 = 2$. From this example it is immediately clear that the number of vertices, edges and triangles themselves are not topological invariants.

The genus

The Euler characteristic of a single surface without boundary in Euclidean space can be expressed in terms of the genus g

$$\chi = 2 - 2g.$$

The genus is defined as the maximum number of non-intersecting closed curves (circles) such that if we cut along these curves the surface is not split into two or more pieces. For example, the genus of the sphere is zero because if we remove one point, say the south pole, and flatten the surface we get the plane and every closed curve on the plane has an inside and outside so that if we cut along such a curve we get two pieces. The boundary of a doughnut (torus) has genus one because if it lies flat on a surface we can cut along a circle that is furthest from the centre and end op with a surface that can be flattened into a cylinder, which in

turn will be cut into two by cutting along any closed curve on it. Roughly speaking the genus is the number of holes through which one can put ones finger to grab hold of it.

Betti numbers

As mentioned above the number of triangles edges and vertices are not themselves topological invariants. However there exists an equivalent definition of the Euler characteristic in terms of topological invariants, namely the Betti numbers β_i,

$$\chi = \beta_0 - \beta_1 + \beta_2,$$

where roughly speaking β_0 is the number of components, β_1 is the number of (independent) loops and β_2 is the number of surfaces without a boundary. Our next subsection will venture to make the definition of these Betti number a bit more precise.

4.3.2 Homology

While the Euler characteristic can topologically distinguish between connected, closed surfaces (by which we mean that if the Euler characteristics of two smooth surfaces are equal then they can be smoothly[14] deformed into each other conversely if they can be smoothly deformed into one another, then the Euler characteristic is the same), it has no discriminative power if applied to 3-manifolds without boundaries, which is the most direct generalization of surfaces. One can prove that the Euler characteristic is zero for each $3-$manifold.[15]

The Euler Poincaré formula

Above we have noted that the Euler characteristic is equal to the alternating[16] sum $\beta_0 - \beta_1 + \beta_2$, where β_0 is the number of components, β_1 is the number of (independent) loops and β_2 is the number of surfaces without a boundary. These constituents of the sum do allow a generalization. In fact we can write the Euler characteristic in any dimension as the alternating sum of Betti numbers, that is

$$\chi = \beta_0 - \beta_1 + \dots.$$

This formula is known as the Euler-Poincaré formula. Betti numbers are topological invariants, meaning that they are the same for two manifolds if they can be smoothly deformed into one another. The converse is not true (even in three dimensions). That is, there are smooth manifolds that have identical Betti numbers but are not the same, to be precise they are not homeomorphic.[17]

Assigning numbers to vertices, edges, ...

We will now introduce these Betti numbers of a space without being very rigorous, by which we mean that we shall often say that a space or map is nice or well-behaved without specifying the conditions. To do so it is easiest to assume that the space of which we want to find the Betti number is nicely triangulated, that is, subdivided into simplices[18] so that an entire neighbourhood of a triangle is well-behaved. To define the Betti numbers mentioned before we now consider particular subsets of the set of all simplices in the triangulation of our space (or manifold). We take a (fixed) triangulation of the manifold (in this case our finite

[14] Smooth means that one can take any number of derivatives of all variables and these derivatives are continuous with respect to all variables.

[15] This in fact holds in any odd dimension and is a consequence of the so-called Poincaré duality.

[16] By alternating sum we mean the sum with alternating signs.

[17] The most famous example of this is the three-dimensional Poincaré's homology sphere.

[18] The higher dimensional equivalent of triangles, such as the tetrahedron in three dimensions.

size universe) and a closed [19] subcomplex, that is a closed subset of the triangulation. To each simplex (vertex, edge, ...) we formally assign a number 0 or 1 depending on whether we include the simplex in the complex or set, see figure 4.5.

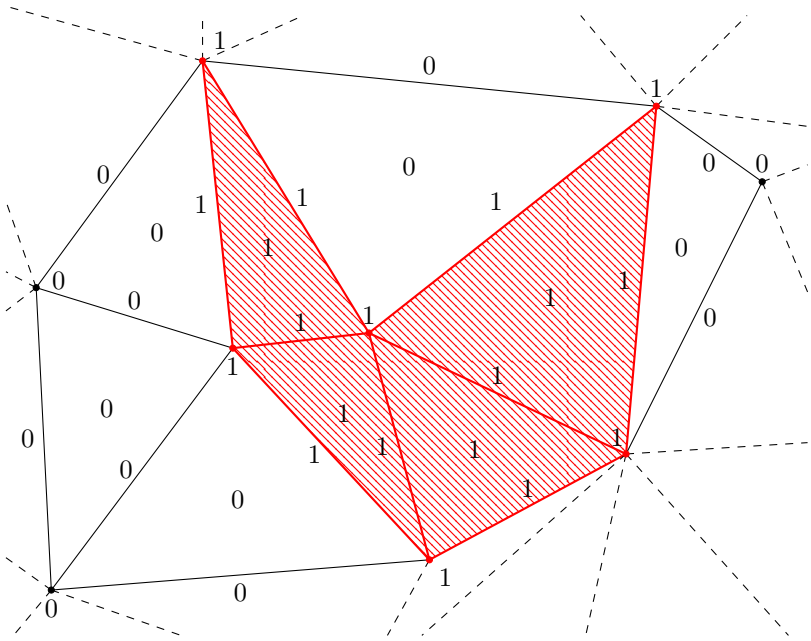

Figure 4.5: Example of a 2-chain.

Adding and subtracting numbers assigned to simplices

We can formally add and subtract these triangulations with numbers assigned to the simplices by adding and subtracting the values for the individual simplices, modulo 2. Modulo 2 calculus only[20] uses 0 and 1 and $0 \pm 0 = 0$, $0 \pm 1 = 1 \pm 0 = 1$ and $1 \pm 1 = 0$. To put it in other words, we are only interested in the first digit if we write the number in binary. The set $\{0, 1\}$ with the modulo 2 calculus is denoted by $\mathbb{Z}_2$, $\mathbb{Z}/2\mathbb{Z}$ or $\mathbb{F}_2$. We will perform all our calculations using $\mathbb{Z}_2$.

[19] By closed we mean that the boundary is included in the set, for example a triangle is part of the set then so are its edges and vertices.

[20] Formally, we identify $\{\ldots -4, -2, 0, 2, 4, 6, 8, \ldots\}$ with $\bar{0}$, which is also written as 0 for simplicity, and $\{\ldots -3, -1, 1, 3, 5, 7, \ldots\}$ with $\bar{1}$, which is also written as 1.

Chains

A set, such as our simplices with numbers attached, with addition and subtraction operations is called a group. A set of closed d-dimensional simplices ($d-$simplices) or the corresponding member in the group is called a $d-$chain.

The boundary of chains

For a d-dimensional chain we may consider its boundary, which has a very specific meaning. For example, the boundary of a triangle consists of its three edges (without regard to the dimension of the space in which the triangle lies). Another important example is an (ordered) set of n edges where the endpoint of an edge is the starting point of the next edge (of course the end of the last edge is the beginning of the first, possibly with further self-intersection in the vertices[21]), has no boundary. A d-chain that has no boundary is called a d-cycle.

Calculating the boundary

To be entirely precise we give a method to calculate the boundary of a d-chain: For each d-dimensional simplex in the chain we take the $(d-1)$-dimensional boundary (for a tetrahedron these are the faces). The formal sum of these boundary elements (using the $\mathbb{Z}_2$ calculus) for all d-simplices in the d-chain is the boundary of the d-chain. The boundary of a chain has itself no boundary, it is a cycle. This is obvious in the example of the triangle, where the boundary is a topological circle (which means that it can be deformed in the standard circle in a nice manner). In the Euclidean plane every loop of edges is the boundary of a number of patches that can be deformed to disks, see figure 4.6. [22]

The example of the torus

For the torus this is not the case, as we shall explain. For our explanation we shall think of the torus as a surface of revolution around the z-axis, see figure 4.7. The way we see the torus does not matter but this description makes the discussion of our examples much easier, because we can refer to specific circles on the torus. With this description of the torus in mind, we see that either one of the two circles that form the intersection of the torus and xz-plane can not be written as the boundary of a disk-like region. In this example we do not want

[21] There is a topological theory which considers only nice loops and surfaces,this is called the theory of homotopy groups. However computations in this theory are very hard, especially in higher dimensions. This is one of the reasons why the famous Poicaré conjecture was so hard to prove. Because of our need of concrete results this theory is not of much use to us.

[22] If the loop does not have self intersections and lies in two dimensions, this is true in a very nice manner, this result is known as the Schönflies theorem.

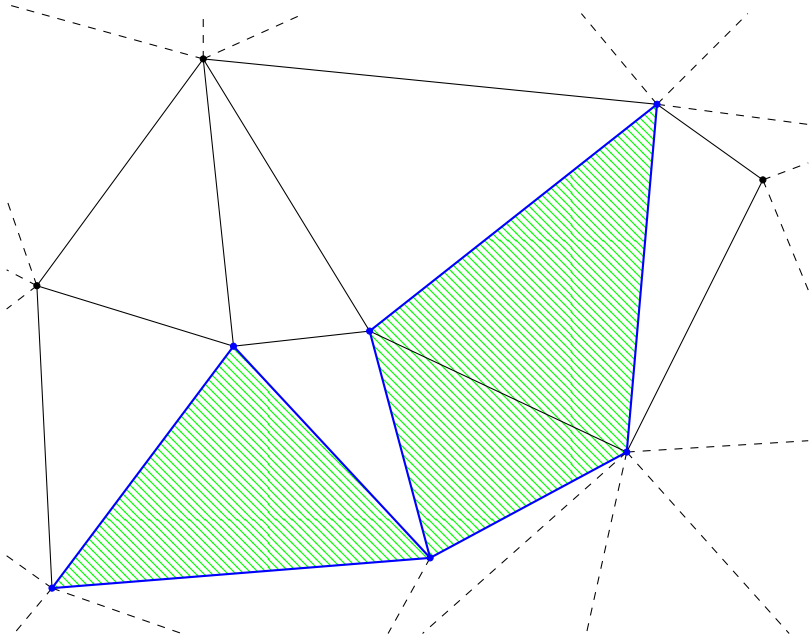

Figure 4.6: In Euclidean space every 1-cycle (blue) is the boundary of a 2-chain (green).

to distinguish between any of the circles we find by intersecting the torus with any plane which contains the $z-$axis. The reason for this is that in topology we do not distinguish between two objects that can be smoothly deformed into one another and two such circles can be deformed into one another by rotation around the z-axis.

Identification

In general it can be very difficult to see if two objects can be deformed into one another. We therefore need a criterion which is easier to verify. Thus we do not distinguish the two circles on the torus if they form the boundary of a two-dimensional piece of the torus. In the case of the circles mentioned before there clearly is a cylindrical piece of the torus which has both as boundary, see figure 4.7. We will use the word identify to indicate that we do not distinguish between two objects (in this case circles).

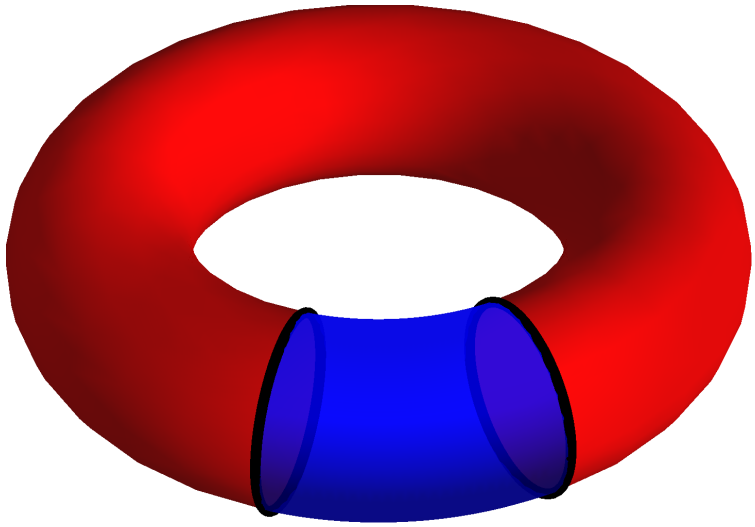

Figure 4.7: Two 1-cycles on the torus can be identified, for together they are the boundary of a 2-chain. Individually neither of these 1-cycles are the boundary of a 2-chain.

Equivalence classes and cosets

Identification will be used very often so we discuss it in some detail. We start with a set of objects (circles in our example) and give some ground on which to distinguish them. This ground needs to be compatible in the sense that if we cannot distinguish a and b from each other nor b and c then we cannot distinguish a and c. Now we can collect all elements that cannot be distinguished in a set. This set is called an equivalence class. In homological context it is usually called a coset, we shall come back to this later.

Betti numbers

The Betti numbers formalize and generalize the identification of circles on the torus if they are the boundary of a cylindrical piece.

Cycles

The generalization of the circles in our example will be d-cycles, d-chains that do not have a boundary. Cycles generalizes the circle in our example greatly. For

example if our space is $\mathbb{R}^3$, a torus (correctly triangulated in a nicely triangulated space) is such a cycle.

The homology group: identifying cycles

d-cycles can be formally added and subtracted because they are chains. We now identify two d-cycles if they form the boundary of a $(d+1)$-chain. A family of cycles that can be identified with one another in this manner is called a coset. These cosets can be added and subtracted similarly to individual chains. We add or subtract cosets A and B, by choosing elements $a \in A$ and $b \in B$ (called representatives of the cosets) and add or subtract these to find a new element $a \pm b$. The element we thus find is an element of some coset. Let us call this coset C. We say that C is the outcome of the sum and write $A \pm B = C$. One can show that the choice of $a \in A$ and $b \in B$ does not influence the outcome. These cosets form a group that is known as the d^{th} homology group and is denoted by H_d.

The homology group as linear space

We now revert to the description of a set of simplices as a formal sum of all simplices in the triangulation with ones as coefficient if an element of the set and zeros otherwise. We can identify this set with an element in a linear space, where every simplex corresponds to a coordinate with a coefficient modulo 2. To such a linear space we can associate a dimension. This dimension is the number of linearly independent vectors. The dimension of the homology group H_d is referred to as the d^{th} Betti number (β_d). The number of elements in the linear space is 2^{β_d}, because for each base vector of the linear space, we may chose a coefficient to be 0 or 1. The number of 'base vectors' in a group is called the rank. We stress that we regard H_d as a linear space.

The 'universe'

The 'universe' in most cosmological simulations, is a three-dimensional box (cube) of finite size, where we identify opposite faces of the box. This space is also called a flat 3-torus ($\mathbb{T}^3$). We wish to introduce some specific terminology and discuss heuristics for the 3-torus. In this setting only β_0, β_1, β_2 and β_3 may be non-zero. Moreover, β_3 equals 0 unless the subset is $\mathbb{T}^3$ itself in which case $\beta_3 = 1$. The first three Betti numbers have intuitive interpretations: β_0 is the number of components, β_1 is the number of loops, and β_2 is the number of shells in the subset. Often, it is convenient to consider the complement of the subset, for which $\beta_0 - 1$ is the number of gaps between the components, β_1 the number of tunnels going through the loops, and β_2 the number of voids enclosed by the shells.

4.3.3 Morse Theory

In the previous section we have developed homology theory and arrived at topological invariants, among others Betti numbers, that help us to distinguish two different objects (often manifolds) topologically. In this section we are going to decompose manifolds into building blocks, using fairly general functions on the manifolds, so called Morse functions. We refer to Milnor [Mil73] for further reading. The discussion in this section will not be focused on a specific dimension. For example we shall often speak of manifolds, the reader is of course free to think of embedded surfaces. The functions we consider will be smooth, meaning that a sufficient number of derivatives exist and are continuous. We shall not specify the exact number of derivatives that need to exist for the statements to hold.

The two pillars of Morse theory

Morse theory is based on two observations concerning smooth functions (f) on a smooth manifold M:

- Suppose that the gradient $\mathrm{grad}(f)$ is non-zero along the level set $M_{f=c} = \{x \in M \mid f(x) = c\}$. Then for sufficiently small[23] ϵ the sublevel set $M_{f\leq c+\epsilon} = \{x \in M \mid f(x) \leq c + \epsilon\}$ can be smoothly deformed[24] into the sublevel set $M_{f\leq c} = \{x \in M \mid f(x) \leq c\}$.

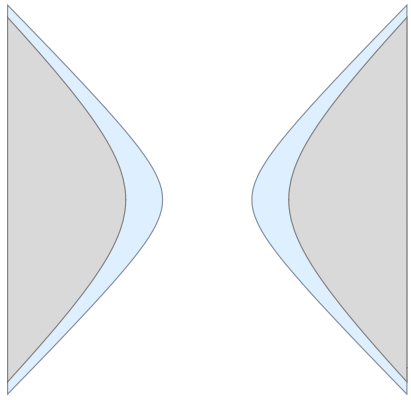

Figure 4.8: The sublevel sets can be deformed into one another (by diffeomorphisms) if $\mathrm{grad}(f)$ is non-zero. In this example f is a hyperbolic paraboloid.

[23] We think of ϵ as positive, but the statement also holds for negative ϵ.
[24] Using the flow of $\mathrm{grad}(f)$.

- Suppose that the gradient $\mathrm{grad}(f)$ is zero at a single isolated point x on M for which $f(x) = c$ and the second order derivatives are well behaved in x. Then for sufficiently small[25] ϵ the sublevel set $M_{f\leq c+\epsilon} = \{x \in M \mid f(x) \leq c + \epsilon\}$ can be smoothly moulded from the sublevel set $M_{f\leq c-\epsilon} = \{x \in M \mid f(x) \leq c - \epsilon\}$ to which an extra object is attached. Moreover this extra object, sometimes called a handle, can be shrunk[26] to a k-cell (a topological k dimensional ball). The dimension of the k-cell can be determined studying the second order Taylor approximation of f in the point x.

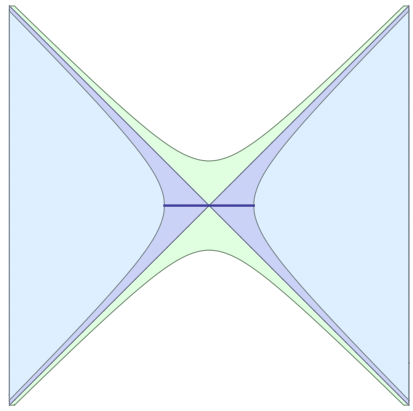

Figure 4.9: Here we see the example of the attachment of a 1-cell if f goes through a value where $\mathrm{grad}(f)$ is zero. We have depicted the critical sublevel set, as well sublevel sets for values above and below the critical value. A cell is attached to the sublevel set for a value of the function below the critical level.

We shall now make the statements above more precise, before we consider an example. The example will be the classical one namely the torus of revolution.

Cells and CW-complexes

A k-cell can be defined as

$$C_k = \{x \in \mathbb{R}^k : |x| \leq 1\}.$$

An well behaved object consisting of such cells (of various dimension) is called a CW-complex. These CW-complexes serve as some kind of 'skeleton' for the manifold.

[25] Here $\epsilon > 0$.

[26] Often is said that they have the same homotopy type.

Attaching cells to CW-complexes

In the context of Morse theory CW-complex are build by consecutively attaching cells. The attaching of a k-cell [27] means we glue C_k on the boundary of C_k to the pre-existing topological space Y (the 'previous' CW-complex). Formally we identify the points on ∂C_k with points in the pre-existing topological space Y using a continuous map from the boundary ∂C_k to Y, we refer the reader to Section I.1 of [Mil73] for more details.

Morse functions

Let f be a smooth real valued function on a manifold M. A point $p \in M$ is called a critical point of f, if in local coordinates

$$\frac{\partial f}{\partial x^i}(p) = 0,$$

for all i. The value at which this occurs is called a critical value. A critical point is called non-degenerate if and only if the matrix

$$\left(\frac{\partial^2 f}{\partial x_i \partial x_j}(p) \right) \tag{4.7}$$

is non-singular, that is if its determinant is non-zero. The matrix given in equation (4.7) is called the Hessian in local coordinates or simply the Hessian. A function is called a Morse function, or just Morse, if all critical points are non-degenerate. We shall always assume that f is smooth so the Hessian is a symmetric matrix. The number of negative eigenvalues of this matrix is called the index of f.

The lemma of Morse

Roughly speaking the index of f determines the f completely in a small neighbourhood. More precisely, we have the following lemma of Morse:

Lemma 4.3.1 *Let p be a non-degenerate critical point for f. Then there is a local coordinate system $(x_1, \dots x_n)$ centred at p such that*

$$f = f(p) - x_1^2 - \dots - x_\lambda^2 + x_{\lambda+1}^2 + \dots + x_n^2,$$

where λ is the index of f at p.

[27] There also exists so called handle decompositions of manifolds, where the manifold itself and not the CW-complex is decomposed. These handles can be thought of as thickened versions of the cells. We refer to [RS72] for a full discussion.

Once more, the two pillars of Morse theory

We are now able to give precise versions of the two observations we started with:

Theorem 4.3.2 *Let f be a smooth real valued function on a manifold M. Let $a < b$ and suppose that the set $f^{-1}([a,b])$, consisting of all points $p \in M$ with $a \leq f(p) \leq b$, is compact and contains no critical points of f. Then $M_{f\leq a}$ is diffeomorphic to $M_{f\leq b}$.*

Theorem 4.3.3 *Let f be a smooth real function on M and p a non-degenerate critical point with index λ. Setting $f(p) = c$, suppose that $f^{-1}([c-\epsilon, c+\epsilon])$ is compact and contains no critical point of f other than p for some $\epsilon > 0$. Then, for all sufficiently small ϵ the set $M_{f\leq c+\epsilon}$ has the homotopy type of $M_{f\leq c-\epsilon}$ with a λ-cell attached.*

If two manifolds have the same homotopy type we mean that using homotopy theory they can not be distinguished. As we have seen in Section 4.3.2 this roughly means that they can be deformed into one another, but with certain degeneracies. For example a cylinder and a circle are homotopic. Theorem 4.3.3 in particular implies that the Betti numbers of $M_{f\leq c+\epsilon}$ and $M_{f\leq c-\epsilon}$ with a λ-cell attached (in the correct manner) are the same. We refer the reader to Section I.3 of [Mil73] for the proofs.

Approximating functions by Morse functions

Morse functions (functions all of whose critical points are non-degenerate) are dense[28] in the set of all smooth functions, meaning that any given smooth function can be approximated arbitrarily well by Morse functions.

[28]This statement should be interpreted using the appropriate topology on the space of functions, see Chapter 6 of [Hir76].

A Morse function on the torus

We shall now illustrate the theory we have just developed in a specific example. In our example M is the torus of revolution embedded in $\mathbb{R}^3$ such that the symmetry axis of the torus is horizontal and f is induced by the height (vertical or z-direction), see figures 4.10-4.16. We shall review the development of the topology of the sublevel set from the empty set to the full torus, as the value of f increases.

From the empty set to a single point

For sufficiently low value of c we have that $M_{f\leq c}$ is empty. The transition to a non-empty set occurs when the horizontal plane is tangent to the torus for the first time, see figure 4.10. We shall refer to a specific height as the level. Let us call this level c_0. Because the horizontal plane indicating the value of f is tangent to the surface the gradient $\mathrm{grad}(f)$ restricted to the surface is zero. This means that there is a so called critical point and c_0 is a critical value. The second order Taylor series of f restricted to the surface gives a paraboloid, which means that f has local (or in this case global) minimum here. This means that the critical point is of index 0. The sublevel set M_{c_0}consists of a single point and thus can be shrunk (trivially) to a single point. The CW-complex therefore also consists of a single point, which is also called a 0-cell in this context. One says that by crossing the singular value a 0-cell is added to the complex.

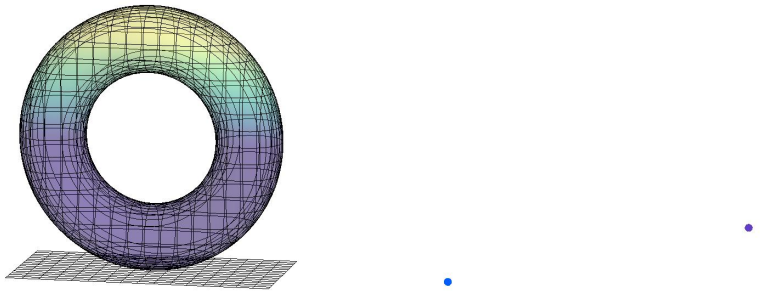

Figure 4.10: The plane indicating the level of f is tangent to the torus (left), the sublevel set (middle) consists of a single point as does the CW-complex (right).

The topological disk

Between the critical value we have seen above and next, that is with respect to the increasing value of f, the topology does not change. This means that all sublevel sets in this range can be smoothly deformed into one another. The sublevel sets can be shrunk to a single point, so that the CW-complex still consists of a single point. We have illustrated this in Figure 4.11.

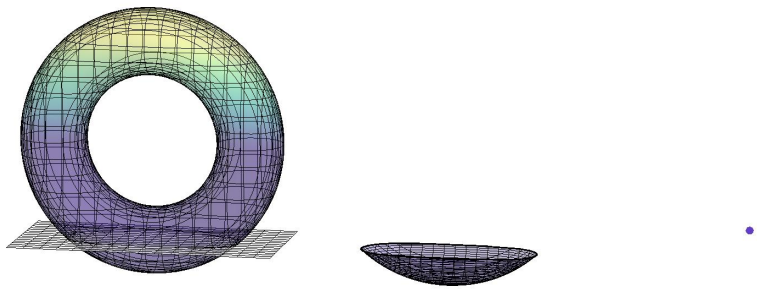

Figure 4.11: The plane indicating the level of f and the torus intersect in a regular manner (left), the sublevel set (middle), can still can shrunk to a single point (right) without tearing.

From a disk to a disk with two points on the boundary identified

Once the horizontal plane is again tangent to the surface the topology changes, see figure 4.12. The second order Taylor approximation of f gives a saddle. So the critical point has index 1. The sublevel set can no longer be shrunk to a point but to a circle. A 1-cell, that is a curve, beginning and ending at the point previously present is attached to the CW-complex.

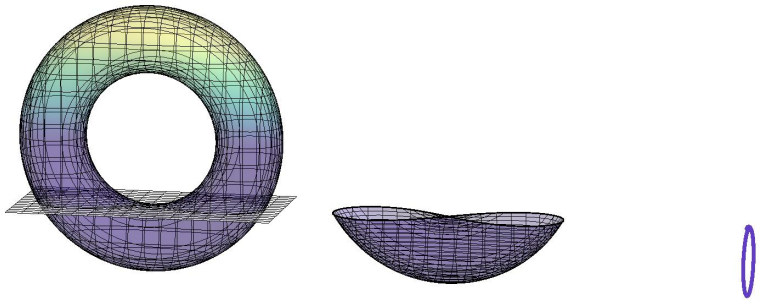

Figure 4.12: The plane indicating the level of f is again tangent to the torus (left). The boundary of the sublevel set (middle) is therefore non-smooth. A 1-cell is attached to the CW-complex (right).

The cylinder

Between successive critical points, see figure 4.13, the sublevel set is a topological cylinder with smooth boundary.

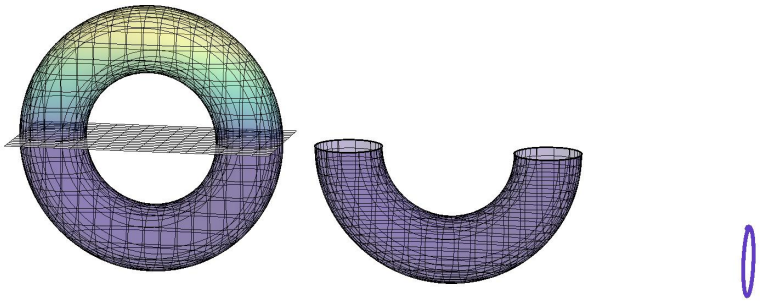

Figure 4.13: The plane indicating the level of f and the torus intersect in a regular manner (left). The sublevel set (middle) can still can shrunk to a circle (right).

The cylinder with two points on the boundary identified

Again we see, in figure 4.14, that the topology of the sublevel set changes when the horizontal plane is once again tangent to the surface. Just as for the previous critical value the critical point is a saddle point, that is it has index 1. The sublevel set can be shrunk to two intersecting closed curves (topological circles). This is equivalent to saying that a 1-cell is attached to the CW-complex.

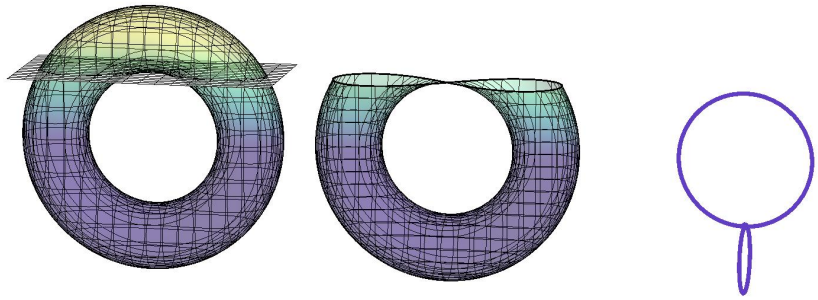

Figure 4.14: The plane indicating the level of f is once more tangent to the torus (left). This implies that the boundary of the sublevel set (middle) is non-smooth. Another 1-cell is added to the CW-complex (right).

The torus with a point left out

Between critical values the topology of the sublevel set (without boundary) is that of a torus with a point left out, see figure 4.15.

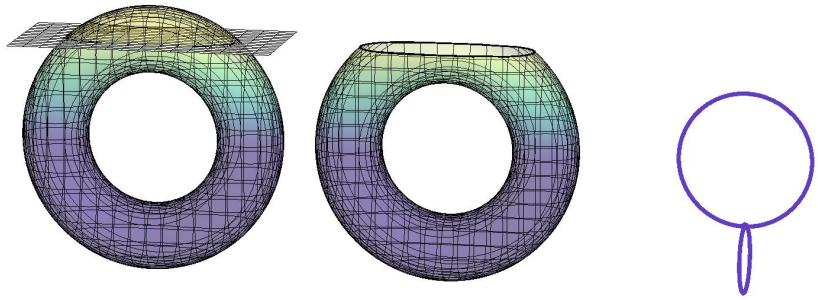

Figure 4.15: The plane indicating the level of f and the torus intersect in a regular manner (left), the sublevelset (middle), can still can shrunk to two intersecting circles (right).

Completing the torus

The final change (figure 4.16) in topology takes place as the horizontal plane coincides with the tangent plane to the highest point of the torus. The Taylor series up to second order of f, the restricted to the surface gives a paraboloid with negative coefficients, which means that f has local (or in this case global)

maximum here. This is equivalent to saying that f has a critical point of index 2. A 2-cell, roughly speaking an object that can be made by continuously stretching a disk, is attached to the CW-complex, to create a topological torus.

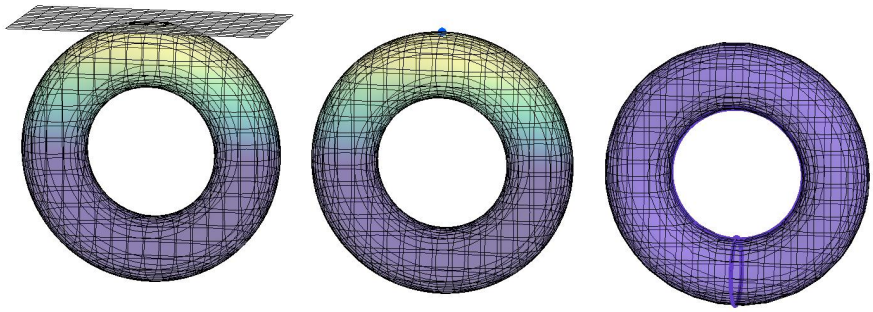

Figure 4.16: The plane indicating the level of f is once more tangent to the torus (left) and the torus is complete (middle). A 2-cell is added to the CW-complex (right).

This concludes our discussion of the example of the torus of revolution.

4.3.4 Persistence

Having discussed Morse theory and homology we are now ready to combine both into persistent homology or Persistence for short. For further reading on this we refer to [EH10]. Again this section is anything but mathematically rigid.

From Morse theory to Homology

In the section on Morse theory we have argued that the topology of a sublevel set does not change unless the Morse function f attains a critical value. If it encounters a critical value with index d we are able to create the sublevel set found below the critical value from the one above the critical value, by glueing in a piece that can be moulded from an d-dimensional disk. This object moulded from a d-dimensional disk we have called a handle and the d-dimensional disk a d-cell. An object consisting of cells we named a CW-complex. The glueing procedure at the crossing of critical point is echoed in a very nice manner by the Betti numbers.

Example merger connected components: two dimensions

For example let us assume the sublevel sets consists of two disjoint parts before the critical value of index one that are connected by a curve at the crossing of the value, see figure 4.17. Then the number of connected components (β_0) drops by one, as illustrated in two dimensions by figure 4.17.

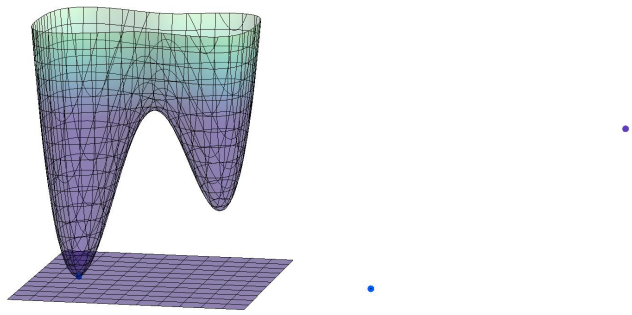

(a) A connected component (β_0) is born as we cross the first singular value. Once more we depict the surface and the level on the left, the sublevelset in the middle and the CW-complex on the right.

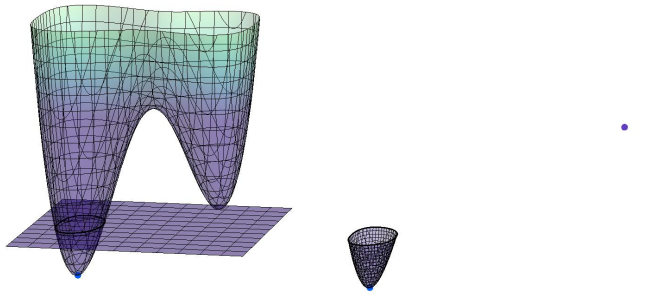

(b) Between critical points the topology is stable.

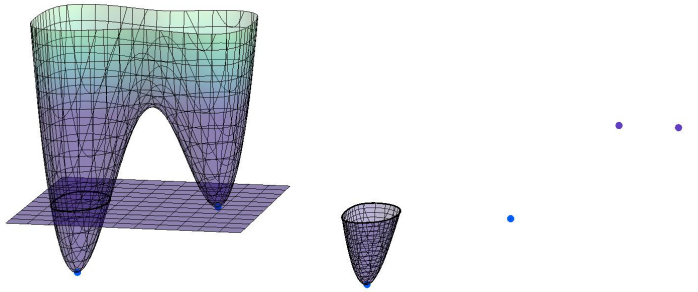

(c) At the crossing of the second critical point another 0-cycle is born. β_0 increases by one.

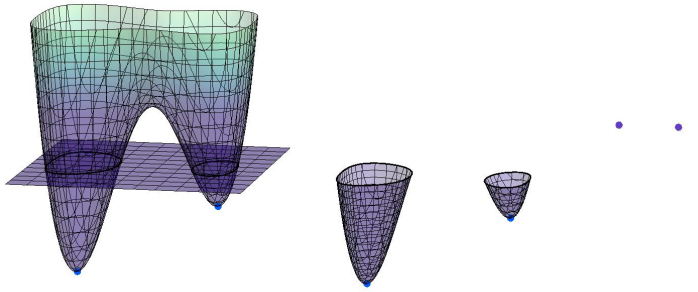

(d) The two connected components persist for a short while.

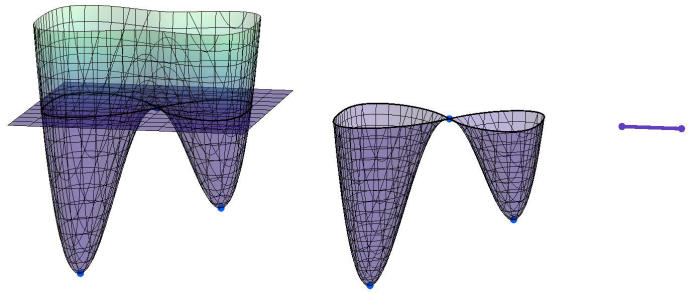

(e) At the encounter of a critical point of index 1 the two connected components merge into a single connected component. The 0-cycle that was created last is killed due to the so called elder rule.

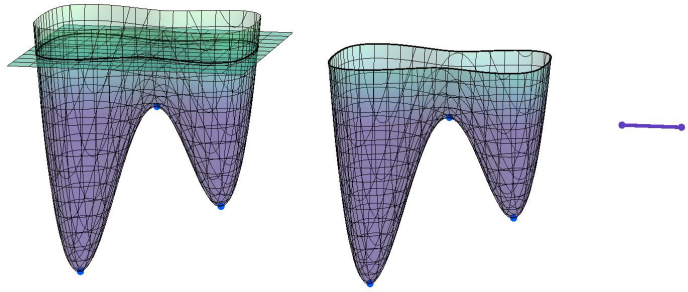

(f) After the final critical point the topology of the sublevel set is again that of a topological disk.

Figure 4.17: An example of the creation of a connected component that persists and one that is merged into the other connected component.

Example merger connected components: arbitrary dimensions

In any dimension this still holds because if two points (0-cycles) belong to the same connected component we can draw a curve (which we regard in this context as a 1-chain) connecting these two points. This means that the two points belong to the same coset, as defined above. Which in turn implies that in this case after crossing the critical value the dimension of H_0, β_0 is one smaller than before, the other homology groups (H_d) are unaffected. This decrease of the dimension by one will be associated to a death, alternatively we shall say that one connected component has died. A full definition of death will follow.

Example creation of loop that does not persist

As we have seen there is another scenario possible for the evolution of the topology at the crossing of a critical value of index 1. Again we start with two connected components. However in this case one of the connected components remains unaffected by the crossing of the critical value while the other undergoes a change by the attachment of a curve γ_0 (1-cell).

The evolution of the homology groups

Let us assume that γ_0 is attached to q_1 and q_2, two points both on one of the connected components. Because the curve is attached to a single connected component we can find a curve connecting q_1 and q_2 inside this connected component (γ_1). These curves γ_0 and γ_1 together form a loop (1-cycle). This 1-cycle was not present before the critical point was crossed, nor can it be the boundary of any two-dimensional chain because γ_0 is completely isolated. This means that in this case by crossing the critical value the dimension of H_1 (β_1) increases by one, while the other homology groups remain unaffected. The fact that the other homology groups are unaffected can be understood in the following manner: As the added handle can be shrunk to a one-dimensional disk it does not contribute to higher dimensional objects such as 2-cycles.

Birth

The increase of the dimension of the homology group will be associated to the birth of the cycle consisting of γ_0 and γ_1. We use this terminology: the cycle consisting of γ_0 and γ_1 is born. The birth and death of a non-persistent 1-cycle is illustrated in figure 4.18.

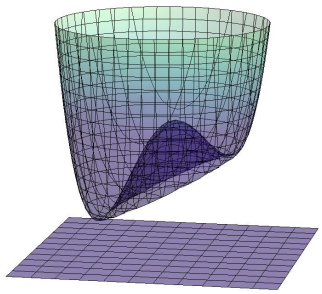

(a) For sufficiently low values of f the sublevel set and the CW-complex is empty. Trivially all Betti numbers of the sublevel set are zero.

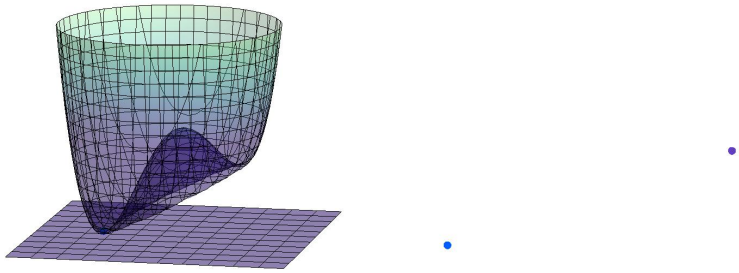

(b) Once we reach the first critical point a connected component is born, here both the sublevel set (middle) and CW-complex (right) consist of a single point. β_0 increases by one.

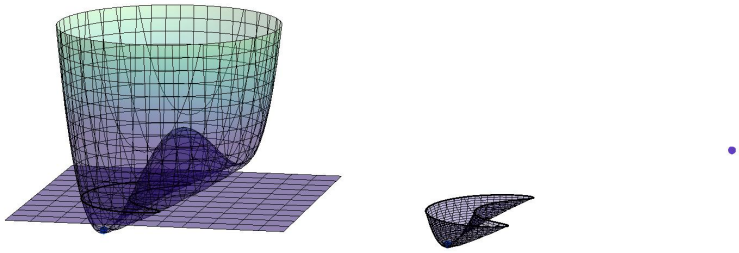

(c) In between critical points the sublevel set (middle) is a topological disk and its CW-complex (right) is a point.

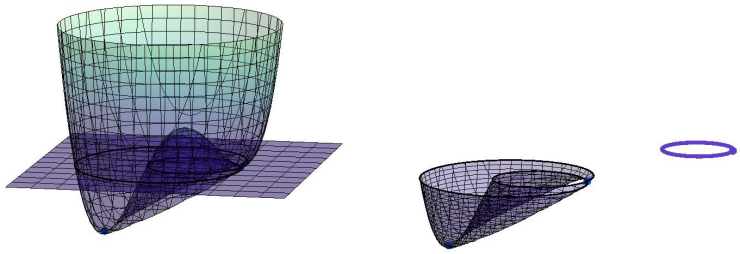

(d) As we go through a critical point of index 1 a loop is created, to be precise the 1-cycles in one coset are no longer the boundary of a co-chain. This is reflected by the CW-complex. We say that a 1-cycle is born.

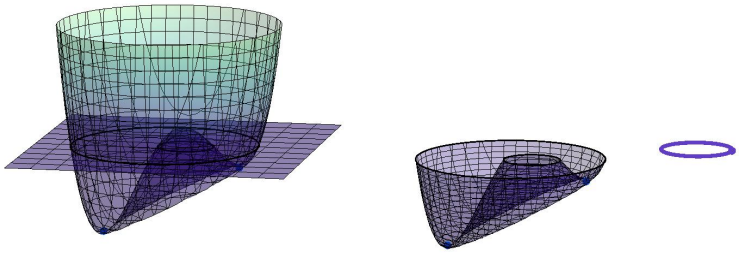

(e) The topology is stable between critical points.

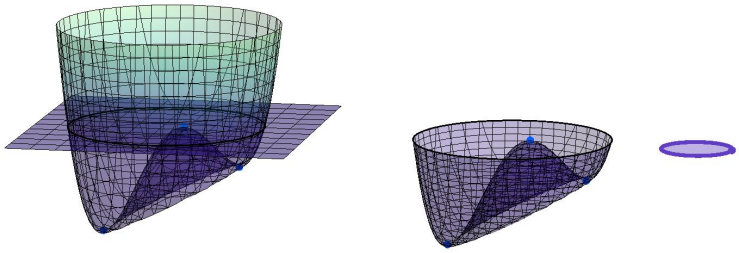

(f) This critical point is a local minimum, the 1-cycle was born in (d) dies. This can be seen because the 1-cycles that are in the same coset as what is in this figure the boundary of the sublevel set, now clearly are the boundary of topological disk. This topology is well reflected by the CW-complex.

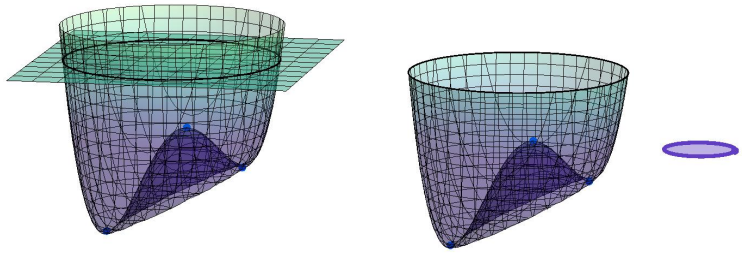

(g) After the final critical point the topology is that of a topological disk. One connected component persists.

Figure 4.18: An example of the creation of a persistent connected component and a loop that dies after a small increase of the level.

The general evolution of the Betti numbers

One can argue that in general β_m (the dimension of H_m) increases by one or β_{m-1} (the dimension of H_{m-1}) decreases by one if we go through a critical point of index m and attach the corresponding m-cell to the super level set. Note that the boundary of the m-cell is a cycle both before and after the attachment of the cell itself. We can now distinguish two cases. The boundary of the m-cell after attachment was either the boundary of an m-chain in the space before the critical point or it was not.

- If it was, then the m-cell and this m-chain together form a m-chain that has no boundary. This new m-chain can not be the boundary of some other chain because the m-cell is isolated. This implies that we have a new (family of) m-cycle. This means that the dimension β_m of H_M increases by one.

- If it was not, then the boundary of the m-cell was a cycle that defined a non-trivial element in H_{m-1} before the crossing of the critical value. This is because by definition cycles are identified if they are the boundary of chain. After crossing of the critical value the boundary of the m-cell is the boundary of a chain, namely the m-cell we just attached. So the boundary of the m-cell is now after attachment identified with the trivial element 0 in H_{m-1}, while before it spanned (was the basis vector of) a one dimensional subspace. This means that the dimension β_{m-1} of H_{m-1} drops by one.

Evolution in terms of linear spaces

Because the spaces H_d are linear spaces we can think of the linear map (think of matrices) between[29] $H_0 \times H_1 \times \ldots \times H_t = \tilde{H}_{\text{before}}$ and $H_0 \times H_1 \times \ldots \times H_t = \tilde{H}_{\text{after}}$. This mapping will be denoted by $\tilde{H}_{\text{before}} \to \tilde{H}_{\text{after}}$. Before and after refers to before and after the passage of a critical value. We use t to denote the top dimension in the equations above.

For n-dimensional manifolds we have that $t = n$. To understand this we have to go back to the definition of chains we have seen in Section 4.3.2. If the manifold is n-dimensional there are no simplices of dimension greater than n in its triangulation. This implies that the homology groups above this dimension are also trivial.

[29]Here $\times$ denotes the Cartesian product, we are familiar with this concept in Euclidean space where we write $\mathbb{R} \times \mathbb{R} = \mathbb{R}^2$ and $\mathbb{R} \times \mathbb{R}^2 = \mathbb{R}^3$. Here $\mathbb{R}$, $\mathbb{R}^2$ and $\mathbb{R}^3$ denote one-, two- and three-dimensional space, respectively.

Evolution for complicated Morse functions

We now consider the setting where we have a very complicated Morse function f with a great number of critical values. In this case we want to keep track of the changes to the homology of the super levelset after crossing of each critical value. This means that we require a complete picture of the so-called sequence of linear maps[30]

$$\tilde{H}_{r_0} \to \tilde{H}_{r_1} \to \ldots \to \tilde{H}_{r_n}, \tag{4.8}$$

with $r_0 > \nu_0 > r_1 > \ldots > \nu_n > r_n$, where the ν_i denote the critical values of the density function and the r_i denote the regular values of the function. To relate this notation to the one used before we note that every $\tilde{H}_{r_i} \to \tilde{H}_{r_{i+1}}$ in the sequence should be interpreted as $\tilde{H}_{\text{before}} \to \tilde{H}_{\text{after}}$ for the critical point ν_{i+1}. We note that for sufficiently large values there are no points for which the density function attains this (or greater) value, therefore the super level set is empty, which means $\tilde{H}_{r_0} = 0$. The sequence (4.8) contains a great deal of information on the topology. We shall encode this information so that it is easy to represent in pictures. [31]

Filtrations

Note that we have

$$M_{f>r_0} \subseteq M_{f>r_1} \subseteq \ldots \subseteq M_{f>r_n},$$

where we used the notation of Section 4.3.3. Such a sequence of sets that of which the elements lie in one another as indicated here is called a filtration.

Defining birth and death

For each base vector v in the linear space $\tilde{H}_{r_i}$ we can check if it is the image of some (base) vector w in $\tilde{H}_{r_{i-1}}$ under the linear map $\tilde{H}_{r_{i-1}} \to \tilde{H}_{r_i}$. If this is not the case we say that v is born at $\tilde{H}_{r_i}$. Let us assume that v is indeed born at $\tilde{H}_{r_i}$. We can now follow v as it is mapped by composition of linear maps (think of products of matrices) to $\tilde{H}_{r_{i+1}}, \tilde{H}_{r_{i+2}}, \ldots$. Typically there are spaces $\tilde{H}_{r_{j-1}}$ and $\tilde{H}_{r_j}$ so that the image of v is non-zero in $\tilde{H}_{r_{j-1}}$ but is mapped to zero under the map $\tilde{H}_{r_{j-1}} \to \tilde{H}_{r_j}$. That is, v is not in the kernel or null space of the mapping

$$\tilde{H}_{r_i} \to \ldots \to \tilde{H}_{r_{j-1}},$$

[30] This is NOT an example of an exact sequence.

[31] The representation we choose does not throw away information; we shall be able to reconstruct the entire sequence of linear maps from our representation.

but it is in the kernel or null space of

$$\tilde{H}_{r_i} \to \ldots \to \tilde{H}_{r_j}.$$

In this case we say that v dies at h_j. We define the associated birth-death pair to be (ν_i, ν_j), the pair of critical points associated to $\tilde{H}_{r_i}$ and $\tilde{H}_{r_j}$ respectively. Here one must bear in mind that here a choice is involved.

The elder rule

The choice we mentioned above is best illustrated by our example of two connected components that merge into one, see figure 4.17. We have to chose which of the two connected components dies. By agreement the oldest survives, that is the connected component that arose at the smallest value for f. This is called the elder rule. We call the difference of both values between the two elements of the pair the persistence or 'the time for which v survives'.

Persistence diagrams and barcodes

As we mentioned above the information on birth-death pairs can be represented in diagrams. Suppose that for each d-cycle we have its birth death pair (ν_i, ν_j). A persistence diagram represents all these points in a two dimensional graph. A bar code represents the birth death pair (ν_i, ν_j) by drawing a line from ν_i to ν_j. All these lines are then depicted underneath each other.

The Morse inequalities

We conclude our discussion with the Morse inequalities: Above we have seen that a critical point of index 1 of a Morse can have two effects on the Betti numbers of the sublevel sets, either β_0 decreases by one or β_1 increases by one. Equivalent statements hold for critical points of index i, with the exception of index 0, because there is no β_{-1}. This observation gives us

- The Euler characteristic is also equal to the alternating sum of the number of critical points with index i
- The weak Morse inequalities, which bound the i^{th} Betti number from above by the number of critical points with index i.

The latter can be strengthened to the Morse inequalities

$$C_\lambda^\# - C_{\lambda-1}^\# + \ldots \pm C_0^\# \geq \beta_\lambda - \beta_{\lambda-1} + \ldots \pm \beta_0,$$

where $C_i^\#$ denotes the number of critical points of index i. For a proof of the Morse inequalities we refer the reader to Section I.5 of [Mil73].

4.3.5 Lipschitz-Killing curvatures

In our discussion of the Lipschitz-Killing curvatures, we shall focus on the so-called tube results. These relate geometric quantities of a manifold to the volume of a tubular neighbourhood. We shall also discuss the Hadwiger's formula, a formula that gives the Lipschitz-Killing curvatures in terms of topological quantities. As before we shall not go into specific conditions on differentiability but assume that every function or map is sufficiently smooth.

Literature review

For an extensive treatment of the volume of tubes we refer the reader to Berger and Gostiaux [BG88], Adler and Taylor [AT07] and Morvan [Mor08]. Berger and Gostiaux [BG88] treat tubes in a purely differential geometric setting. Adler and Taylor [AT07] focusses specifically on Gaussian random fields. We shall follow Adler and Taylor [AT07] as much as possible. Morvan [Mor08] gives an overview, which is less detailed than the other two books.

Gauss curvature and the shape operator

The shape operator $S(v)$ is defined as $-\nabla_v \nu$ with ν the normal vector field, roughly speaking the normal of the surface translated to the origin. The space operator can be seen as a linear operator (matrix) from the tangent space to itself. The shape operator is related to the Gaussian curvature by $K = \det S$. The shape operator (seen as matrix) is in the right coordinate system equal to

$$\begin{pmatrix} k_1 & 0 \\ 0 & k_2 \end{pmatrix}.$$

The principal curvatures k_1, k_2, the inverses of the maximum and minimum radii of the osculating circles. This means that $K = k_1 k_2$. The mean curvature is given by $k_1 + k_2$. The Gaussian curvature in two dimensions is also given by $R_{abcd} = K(g_{ac}g_{bd} - g_{ad}g_{bc})$, with R_{abcd} the Riemann tensor and g_{ab} the metric.

The three dimensional tube formula

The tubular neighbourhood of a manifold are all points in the ambient space that lie within a given radius from the manifold. The tubular neighbourhood of a curve in two dimensional Euclidean space is depicted in Figure 4.19. In Appendix 4.A.1 we will prove that the volume of the tubular neighbourhood of a two dimensional manifold M is given by

$$\text{Vol}(\text{tube}(M, \epsilon)) = 2A(M)\epsilon + \frac{2}{3}\epsilon^3 \int_M K \mathrm{d}A. \tag{4.9}$$

We have denoted the tubular neighbourhood of M with radius ϵ by tube(M, ϵ) This formula is remarkable because of two things:

- Both terms in (4.9) are intrinsic, meaning that they refer to the manifold M (or the Riemannian structure with which it is endowed) and not to its embedding in Euclidean space.

- The second term on the right hand side of (4.9) is in fact topological in nature, because of the Gauss-Bonnet theorem:

$$\int K \mathrm{d}A = 2\pi\chi(M). \tag{4.10}$$

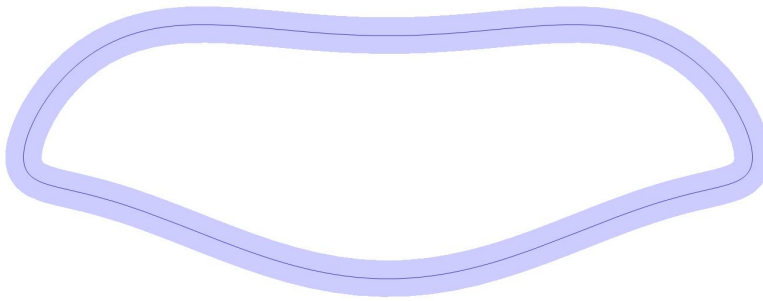

Figure 4.19: Tubular neighbourhood of a smooth closed curve in two dimensions.

The Gauss-Bonnet formula

The Gauss-Bonnet theorem is of great importance both here and in the following chapters. Although the full proof of the (two dimensional) Gauss-Bonnet theorem is somewhat subtle, we have given a rough sketch in Appendix 4.A.2. The Gauss-Bonnet theorem can be generalized to arbitrary (even) dimension, for which we refer the reader to [Spi75c] or [Che44]. The Gauss-Bonnet theorem is however in some sense quite unique. This will be the topic of chapter 5.

The tube formula in arbitrary dimension

The tube formula (4.9) also generalizes to higher dimensions, see [BG88] page 235:

Theorem 4.3.4 *Let M be a d-dimensional submanifold of an n dimensional Euclidean space. The volume of the ϵ-neighbourhood of M, also called the ϵ-tube of M, is a polynomial in ϵ:*

$$\mathit{Vol}(\mathit{tube}(M,\epsilon)) = \sum_{i=0}^{\lfloor d/2 \rfloor} a_{2i}\epsilon^{n-d+2i}, \tag{4.11}$$

where

$$a_{2i} = \frac{1}{n-d+2i}\int_M K_{2i}\mathrm{d}\mu,$$

with $\mathrm{d}\mu$ the volume form on M and K_{2i} the Weyl curvatures.

The Weyl curvatures are intrinsic in nature, in particular they can be expressed in terms of the Riemann tensor, see [Wey39].

From the tube formula to the Lipschitz-Killing curvatures

There is a reformulation of (4.11) for which roughly speakin the js in a_j do not run over $2i$, but the odd cases, which are zero, are included. If one includes these and normalizes, using the volume of the j-dimensional unit ball ω_j, the elements of the extended sequence of a_j are referred to as Lipschitz-Killing curvatures. To be precise

$$\mathrm{Vol}(\mathrm{tube}(M,\epsilon)) = \sum_{j=0}^{n} \omega_{n-j}\mathcal{L}_j(M)\epsilon^{n-j}$$

defines the Lipschitz-Killing curvatures $\mathcal{L}_j(M)$. Sometimes the intrinsic nature of the Lipschitz-Killing curvatures is used to define them directly using the Riemann tensor. These expressions can be found in Section 7.6 of [AT07], or by comparing to [Wey39]. It must be noted that this point of view is not propagated in [AT07].

From the Lipschitz-Killing curvatures to the Minkowski functionals

Reversing the order and altering the normalization of the Lipschitz-Killing curvatures gives the Minkowski functionals

$$\mathcal{M}_j(M) = (j!\omega_j)\mathcal{L}_{n-j}(M).$$

Using the Minkowski functionals the tube formula reads

$$\text{Vol}(\text{tube}(M,\epsilon)) = \sum_{j=0}^{n} \mathcal{M}_j(M)\frac{\epsilon^j}{j!}.$$

The Minkowski functionals for two dimensional surfaces in three dimensional Euclidean can now be read of from (4.9). In case of convex bodies, one also encounters the terms Quermass intergrals and Steiner functionals, for various versions of what are basically Lipschitz-Killing curvatures/Minkowski functionals. To add to the confusion all of these are referred to as intrinsic volumes.

Crofton's formula

Interestingly enough the Lipschitz-Killing curvatures can also be expressed in terms of topological quantities. The simplest example of such a formula is Crofton's formula, see Section 1.7.C of [DC76]. Let γ be a regular curve of length l in the plane. A straight line $L_s(\theta, r_{\text{ol}})$ in the plane shall be given by

$$L_s(\theta, r_{\text{ol}}) = \{(x,y) \in \mathbb{R}^2 \mid x\cos\theta + y\sin\theta = r_{\text{ol}}\}$$

Any straight line in the plane define the multiplicity $n_i(\theta, r_{\text{ol}})$ to be the number of intersection points of the curve γ and $L_s(\theta, r_{\text{ol}})$. With these definitions we can give Crofton's formula:

$$\frac{1}{2}\iint n_i(\theta, r_{ol})\mathrm{d}r_{ol}\mathrm{d}\theta = l.$$

Santaló's formula

More generally the Lipschitz-Killing curvatures can be expressed in terms of an integral over the Euler characteristic of the intersection between planes of a certain dimension and the manifold. To be precise

$$\mathcal{L}_j = \begin{pmatrix} n \\ j \end{pmatrix} \frac{\omega_n}{\omega_{n-j}\omega_j} \int_{\text{Eucl}(n)} \chi(M \cap h_{\text{Eucl}} E_{n-j})\mathrm{d}h_{\text{Eucl}},$$

with $\text{Eucl}(n)$ the Euclidean group, the symmetry group of n-dimensional Euclidean space, $h_{\text{Eucl}} \in \text{Eucl}(n)$ and $\mathrm{d}h_{\text{Eucl}}$ the standard measure[32] on $\text{Eucl}(n)$. This formula is called Hadwiger's formula, although Hadwiger is only associated to the convex case, or Santaló's formula who treated the general case, see also [San76]. For a proof of Hadwiger's formula we refer the reader to Section 17.5 of [Mor08] which gives a proof based on a more general result by Chern [Che52].

[32] the Haar measure normalized to be the Lesbesgue measure on the translations and the invariant probability measure on the rotations.

Further generalizations

We remark that a far reaching generalization has been discovered by Schapira [Sch91, Sch95] within the field of sheaf theory. This generalization has been propagated by Ghrist, see for example [BG09]. The generalization by Schapira states that under certain conditions a manifold in Euclidean space is completely reconstructible once all the Euler characteristics of the intersections of linear subspaces of appropriate dimension and the manifold are known. Schapira gives the following example: One can reconstruct a body in $\mathbb{R}^3$ from the knowledge of the number of connected components and holes of all its intersections by two dimensional affine slices.

4.4 Overview

Understanding the properties of the Cosmic Microwave Background and the large scale structure to which it gave rise, is one of the main objectives of modern cosmology, as discussed in Section 4.1. We have argued that the density perturbations in the early universe are well approximated by Gaussian random fields.

The Euler characteristic in cosmology

As early as the 1980s [BBKS86, HGIW86] it was realized that the density of Euler characteristic of super- or sublevel sets was important for the study of Gaussian random fields. The significance of the Euler characteristic follows, among others, from the following:

- For sufficiently high levels the Euler Characteristic equals the number of peaks, see [Adl81, BBKS86].
- The Euler Characteristic is independent from the two point function or Power spectrum and three point function, giving another way to measure deviations from the Gaussian random field.

The interest of the Euler characteristic is enhanced by the fact that its density can be expressed as an integral using the Gauss-Bonnet theorem or by using the fact that the Euler characteristic is the alternating sum of critical points of a Morse function. These integrals can in fact be evaluated [Adl81, HGIW86, AT07].

Other topological invariants in topology

Recently, see for example van de Weijgaert et al. [vdWPJ+11] or van de Weijgaert et al. [vdWVE+11], the importance of other topological invariants such as Betti number for the study of the large scale structure of the universe was realised. The topology of both so called alpha shapes and sub- or superlevel sets now sees active research.

Morse Functions and alpha shapes

Our explanation of persistence, Section 4.3.4, focussed on sub- or superlevel sets. The existence of a continuous function, in a cosmological context this is the density, is necessary for level sets to be defined. For a study of the Betti numbers (not persistence) of Gaussian random fields, we refer the reader to [PPC+13] and (for semi-analytic results in two dimensions) to [FvEvdW+15]. Alpha shapes are used in the study of discrete point sets. Roughly speaking alpha shapes of

a point set in Euclidean space associated with radius r is the union of the balls of radius r centred on the points in the point set. These are beginning to be used, among others, in the study of the galaxy distribution in the present day universe. This thesis focusses on the topology of superlevel sets or level sets.

Interest from cosmologists in persistence

The interest from cosmologists in persistence, see Section 4.3.4, is a natural consequence of the studies mentioned before [vdWPJ+11, vdWVE+11, PPC+13]. Persistence is currently being applied to, among others, cosmological models [PEvdW+15], Gaussian random fields, and simulations of the universe for different dark energy models, see [Nev13].

Interest from mathematics

The efforts to understand the topology of the universe coincide with interest by Alder et al. [ABN+10] in the persistence of Gaussian random fields, as well as renewed interest in Euler integration from applied mathematics, see for example [BG09]. Critical points of two and three dimensions Gaussian random fields in the meantime have gained renewed interest from the Cosmological community [GPP12].

Contribution

The studies of the topology of Gaussian random fields and models for the universe are all numerical in nature. The exceptions are the Euler characteristic and the critical points of the Gaussian random field. The contributions of this part of the thesis are the following:

- In chapter 5 we prove that other topological invariants, such as Betti numbers, can not be found using straightforward integration technique, such as those used to determine the Euler characteristic. This means that the numerical methods used in the study of the topology of the universe are necessary.
- In chapter 6 we show that the positive part of the Gauss curvature of the isodensity sets of a Gaussian random field does not provide reasonable bounds on the number of connected components of of the superlevel sets.

As a corollary of these results we have that the topological quantities such as the persistence of a Gaussian random field are not encoded in the Lipschitz-Killing curvatures, discussed in Section 4.3.5.

4.A Appendix

In these appendices we give a some proofs that were omitted from Section 4.3.5. Here we shall discuss the the tube formula in the setting of a surface embedded in three dimensions. The main reason why we include this is because the relatively straightforward proof collected here is scattered over the literature. A sketch of the proof of the Gauss-Bonnet theorem is included because the ideas of the proof are relatively easy to understand and because the Gauss-Bonnet theorem plays an essential role in Chapters 5 and 6.

4.A.1 The tube formula in three dimensions

In this appendix we will prove the tube formula for surfaces in three dimensional Euclidean space

$$\text{Vol}(\text{tube}(M,\epsilon)) = 2A(M)\epsilon + \frac{2}{3}\epsilon^3 \int_M K \mathrm{d}A. \tag{4.9}$$

Our approach is based on exercises 3.12 in [Spi75a] and 5.3.7 in [O'N06] as well as bibliography point A.II.b of [Spi75c].

We will use the shape operator $S(v) = -\nabla_v \nu$ with ν the normal vector field.

Let $M \subset \mathbb{R}^3$ be a compact surface with normal ν. Then

$$M_\epsilon = \{p + \epsilon\nu(p) : p \in M\}$$

is called the parallel surface of M. We have the following map

$$F : M \to M_\epsilon : p \mapsto p + \epsilon\nu(p). \tag{4.12}$$

For any tangent vector v we write $\bar{v} = F_*(v)$. Let $\alpha : (-\delta, \delta) \to M$ be a curve such that $\alpha(0) = p$ and $\alpha'(p) = v$. Let $\bar{\alpha} = F \circ \alpha$, now we have that

$$\bar{v} = \bar{\alpha}'(0) = \frac{d}{ds}\bigg|_{s=0} (\alpha(s) + \epsilon\nu(\alpha(s)) = v + \epsilon\nu'(p+sv)|_{s=0} = v - \epsilon S(v).$$

Or directly

$$\bar{v} = F_*(v) = \nabla_v(p + \epsilon\nu(p)) = v + \epsilon\nabla_v\nu = v - \epsilon S(v),$$

where we identify tangent vectors with elements in $\mathbb{R}^3$. Note that this implies that $0 \neq \bar{v}$ if $v \neq \epsilon S(v)$, so that M_ϵ is an immersed surface for all $|\epsilon| < |k_1|^{-1}, |k_2|^{-1}$, with k_1, k_2 the principal curvatures. The principal curvatures are

the eigenvalues of the shape operator S, seen as linear operator from the tangent space to itself. Using the identities

$$\begin{aligned} S(v) \times S(w) &= K(p)v \times w \\ S(v) \times w + v \times S(w) &= 2H(p)v \times w, \end{aligned}$$

see for example lemma 5.3.4 of [O'N06], we now have

$$\begin{aligned} \bar{v} \times \bar{w} &= v \times w - \epsilon(v \times S(w) + S(v) \times w) + \epsilon^2 S(v) \times S(w) \\ &= v \times w - 2\epsilon H v \times w + \epsilon^2 K v \times w. \end{aligned}$$

This implies that the volume element $\mathrm{d}\bar{A}_\epsilon$ of M_ϵ is related to the volume element $\mathrm{d}A$ of M by

$$F^*(\mathrm{d}\bar{A}_\epsilon) = (1 - 2\epsilon H + \epsilon^2 K)\mathrm{d}A.$$

Integration then yields

$$A(M_\epsilon) = A(M) - 2\epsilon \int_M H \mathrm{d}A + \epsilon^2 \int_M K \mathrm{d}A,$$

By integrating over ϵ we can find the volume[33] enclosed between M and M_ϵ, that is

$$V(M, M_\epsilon) = A(M)\epsilon - \epsilon^2 \int_M H \mathrm{d}A + \frac{1}{3}\epsilon^3 \int_M K \mathrm{d}A. \tag{4.13}$$

Here we ignore any possible issues regarding self-intersections, due to the fact that beyond a distance called the reach from a surface there is no longer a unique closest point on the manifold, see [Fed59] and [Fed96] for a discussion. From (4.13) we conclude that the volume enclosed by $M_{-\epsilon}$ and M_ϵ, that is the tube, is

$$\text{Vol}(\text{tube}(M, \epsilon)) = V(M_{-\epsilon}, M_\epsilon) = 2A(M)\epsilon + \frac{2}{3}\epsilon^3 \int_M K \mathrm{d}A. \tag{4.9}$$

This concludes our discussion.

[33] This is straightforward because the normal on corresponding points on parallel surfaces is equal.

4.A.2 Sketch of the proof of the Gauss-Bonnet theorem

In this appendix we give a rough sketch of the idea of the proof of the Gauss-Bonnet theorem.

By straightforward calculation, see theorem 3.9 of [Spi99], one can prove that for a triangle whose edges are geodesics with vertices v_1, v_2, v_3 on a surface we have that

$$\int_{\triangle v_1 v_2 v_3} K \mathrm{d}A = \varphi_1 + \varphi_2 + \varphi_3 - \pi, \tag{4.14}$$

with $\varphi_i = \angle v_i$. Now suppose that we have triangulated (subdivided into triangles) the surface such that all edges are geodesics, then

$$\sum_{\text{triangles}} \Big(\sum_{i=1}^{3} \varphi_i - \pi \Big) = \sum_{\text{triangles}} \int_{\text{triangle}} K \mathrm{d}A.$$

We can now reorder the summation and use that the angles adjacent to a single vertex sum to 2π, to see that

$$\int_M K \mathrm{d}A = \sum_{\text{vertices}} 2\pi - \sum_{\text{triangles}} \pi = 2\pi v - \pi t,$$

with v the number of vertices and t the number of triangles. Every triangle has three edges, but every edge is shared by two triangles so that $2e = 3t$, with e the number of edges. Rewriting this as $-t = 2t - 2e$, we find that

$$\int K \mathrm{d}A = 2\pi(v - e + t) = 2\pi\chi(M).$$

Chapter 5

A geometrical take on invariants of low-dimensional manifolds found by integration

5.1 Introduction

The Gauss-Bonnet theorem relates the integral of some intrinsic quantity whose origins lie in the field of differential geometry, namely the Gaussian curvature, to some topological invariant, the Euler characteristic. For higher dimensional manifolds the Gauss-Bonnet theorem can be generalized, using the theory of characteristic classes. For a very elegant exposition we refer to Milnor and Stasheff [MS74] or alternatively Spivak [Spi75c]. Abrahamov [Abr51] proved that the invariants thus produced are unique, up to some equivalence. See Gilkey [Gil84] for a modern (and more extensive) treatment. Below we provide a proof of a similar statement for two and three dimensional manifolds, based solely on geometrical arguments, in contrast to the more algebraic approach taken in the literature.
The formulation of the main result will be along the lines of the following question proposed by I.M. Singer: 'Suppose that f is a scalar valued invariant of the metric such that $t(M) = \int f \mathrm{dVol}$ is independent of the metric. Then is there some universal constant c so that $t(M) = c\chi(M)$?' This question has reportedly ([Gil84]) been answered in the affirmative by E. Miller.

The proof as discussed by Gilkey is somewhat algebraic in nature and fo-

cusses on the invariance of $f = F(g, \partial g, \ldots)$ under coordinate transformations. Fortunately the functions which are well behaved can be easily found and be listed, using a theorem by Weyl on the invariants of the orthogonal group. The invariant functions thus found are linear combinations of contractions of Riemann tensors and their derivatives. The functions can be further distinguished based on their behaviour under rescaling of the metric. If the product of the function and the volume form is invariant under this rescaling it is a candidate for a topological invariant.[1] For example in two dimensions the Gaussian curvature is the only such function (up to some remainder whose integral is zero). It can be shown that all such functions yields topological invariants.

Our geometrical proof relies heavily on the classification of two dimensional closed surfaces and on Heegaard splitting. A discussion of the classification can be found in [Hir76] or [Mas77], for the latter we refer to [Fom87] or [Sti93].

We complete our discussion by some remarks on generalizations.

[1] A line of reasoning one also encounters in the work by Abrahamov.

5.2 Surfaces

Theorem 5.2.1 *Let f be a function on two dimensional real Riemannian compact manifolds, which is completely determined by the metric, in the sense that f locally can be written as $f(x) = F(g(x), \partial g(x), \ldots)$ where g denotes the metric, independent of the topology of the base manifold. Suppose the integration*

$$I_f(M) \equiv \int_M f \, \mathrm{d}Vol,$$

where $\mathrm{d}Vol$ indicates the volume form, of f over an orientable[2] manifold M yields a topological invariant $t_f(M)$ for all surfaces. We write $t_f(M)$ to emphasize the dependence on f. Then there exists a real number c_f, depending only on f, such that $t_f(M) = c_f \, \chi(M)$, where χ denotes the Euler characteristic.

Proof First we note that the space of Riemannian metrics on a manifold is connected. This is obvious because if g and $\tilde{g}$ are metrics then so is $\lambda g + (1-\lambda)\tilde{g}$ for all $\lambda \in [0, 1]$. This means that we can assume without loss of generality that M is isometrically embedded in $\mathbb{R}^3$, because we can choose $\tilde{g}$ to be the standard metric of M. Now let f be a function as described in the theorem, such that

$$\int_M f \, \mathrm{dVol} = t$$

is a topological invariant. Suppose that for the two sphere $\mathbb{S}^2$ we have

$$\int_{\mathbb{S}^2} f \, \mathrm{dVol} = 2c,$$

where c is some constant. From this we can conclude that for the sphere $t = c\chi(M)$.

We can now deform the two-sphere as follows. A small region is pushed outwards and bent -in a sufficiently smooth manner- such that this region contains three equally spaced parallel cylinders pieces all of the same radius. We can now cut in the cylindrical part along the plane orthogonal to the cylinder and reassemble the parts so that we recover a topological sphere but also get a torus. The integral is not altered because integrals are additive. The procedure is illustrated in figure 5.1. Because the integral is clearly additive for unions this implies that

$$\int_{C_1} f \mathrm{dVol} = 0,$$

[2]Clearly the integral over a non-orientable manifold does not make sense.

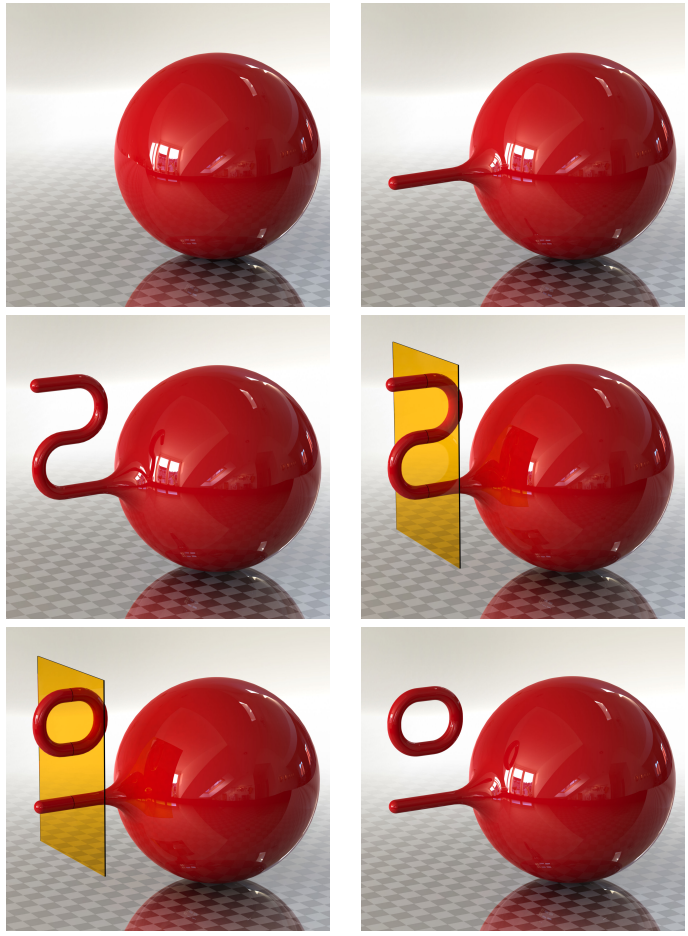

Figure 5.1: From left to right, top to bottom we have depicted: the sphere, the deformation (in two steps), the deformed surface with cutting lines indicated by the yellow glass plane and the reassembled surfaces (with and without cutting lines).

where C_1 is a surface of genus 1. Generally we shall denote a surface of genus g by C_g.

The rest of the proof is inductive in nature. We begin with a topological genus-g torus and two spheres. We deform these surfaces so that the spheres contain a piece of a cylinder, both of the same radius, and the n-torus such that

it contains two pieces of the cylinder, again of the same radius, so that if these pieces are deleted one of the remaining surfaces is itself a topological cylinder. We again cut the cylindrical pieces in half and reassemble the part so that we have a genus-$g-1$ torus and a sphere. As sketched in figure 5.2.

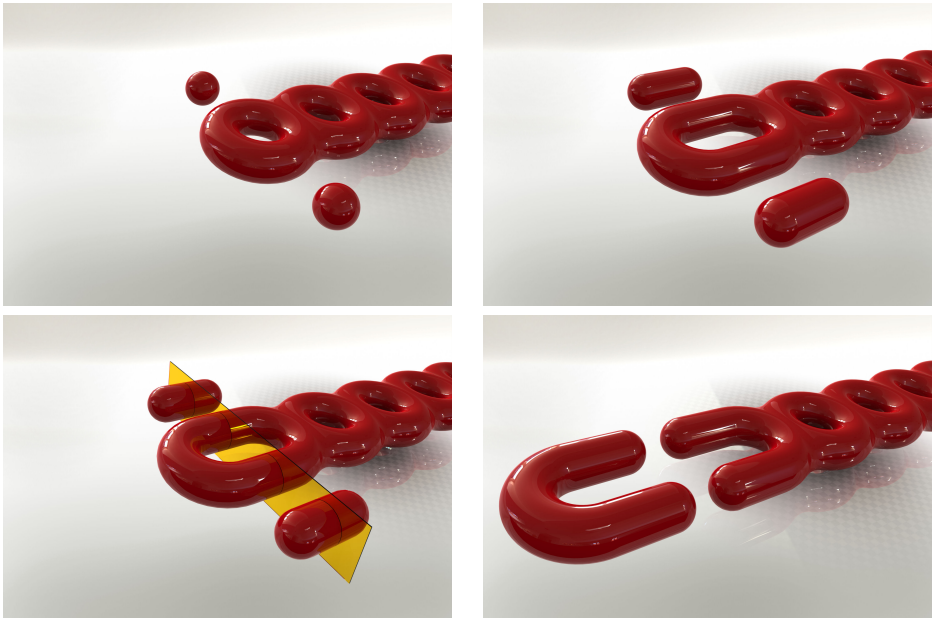

Figure 5.2: From left to right, top to bottom we have depicted: An n-holed torus and two spheres, the same surfaces deformed, the deformed surfaces with the lines along which we cut indicated by yellow glass plane and the reassembled surfaces.

We can now conclude that

$$\int_{C_g} f \mathrm{dVol} + 2 \int_{\mathbb{S}^2} f \mathrm{dVol} = \int_{C_{g-1}} f \mathrm{dVol} + \int_{\mathbb{S}^2} f \mathrm{dVol}$$

and thus by induction that

$$\int_{C_g} f \mathrm{dVol} = c(2-2g) = c\,\chi(C_g).$$

By the classification of all 2-manifolds we have proven the theorem for all two dimensional real manifolds embedded in $\mathbb{R}^3$. □

Remark 5.2.2 *In theorem 5.2.1 we assumed that f gives us a topological invariant for all surfaces, in fact the conclusion can be drawn for a given manifold M, if $\int f \mathrm{d}Vol$ is an invariant for S^2, $S^1 \times S^1$ and M.*

The proof of this statement differs from that above in that instead of the induction step illustrated in figure 5.2, we consider a genus g surface and $2g$ balls and perform the cut and paste operation for each hole simultaneously.

5.3 Three dimensions

We will now focus on the three dimensional case. The intuition for the following proof is much strengthened by the remark that a Morse function h on some manifold M can always be interpreted as height function. This can be easily seen as follows: Let M be isometrically embedded in $\mathbb{R}^n$, possibly using the Nash embedding theorem. Then we can add the value of the Morse function as another coordinate to a point $p \in M \subset \mathbb{R}^n$, so that the manifold M is embedded in $\mathbb{R}^{n+1}$ and the last coordinate is the height.

Theorem 5.3.1 *Let f be a function on three dimensional real Riemannian compact manifolds, which is completely determined by the metric, in the sense that f locally can be written as $f(x) = F(g(x), \partial g(x), \dots)$ where g denotes the metric, independent of the topology of the base manifold. If the integration*

$$I_f(M) \equiv \int_M f \, \mathrm{d}Vol$$

of f over a manifold M yields a topological invariant $t_f(M)$, for all 3-manifolds. Then we have $t(M) = 0$.

Proof The first step in our proof will consist of showing that if $M = C_g \times \mathbb{S}^1$ we have that

$$\int_M f \, \mathrm{dVol} = 0.$$

To show this we shall consider a manifold N, that admits a Heegaard splitting of genus g. This means that the manifold N can be represented as the attachment of two three-dimensional manifolds, which are both homeomorphic to a three-dimensional ball with g handles, with respect to a diffeomorphism of their boundaries. We further have that there exists a Morse function h on N with one minimum and one maximum and all critical points of index 1, 2 correspond to the critical values c_1 and c_2 respectively with $c_1 < c_2$, see [Fom87]. This has been schematically represented in the leftmost picture in figure 5.3. [3]

We now define for every surface C_g of genus g, some metric induced by an embedding in $\mathbb{R}^3$, exhibiting $\mathbb{Z}_2$ symmetry. We shall refer to this Riemannian

[3]Note that conversely a Heegaard splitting also gives a Morse function in a natural manner. Namely we start with Morse functions on both g-handled balls, by simply taking a Morse function on the standard g-handled ball and pulling back via the diffeomorphisms to the g-handled balls in question. Now theorem 1.4 and lemma 3.7 of [Mil65a], give a differentiable structure on the union with a smooth structure compatible with the given differentiable structure on the different parts, moreover such that the Morse functions on both parts piece together to a smooth function.

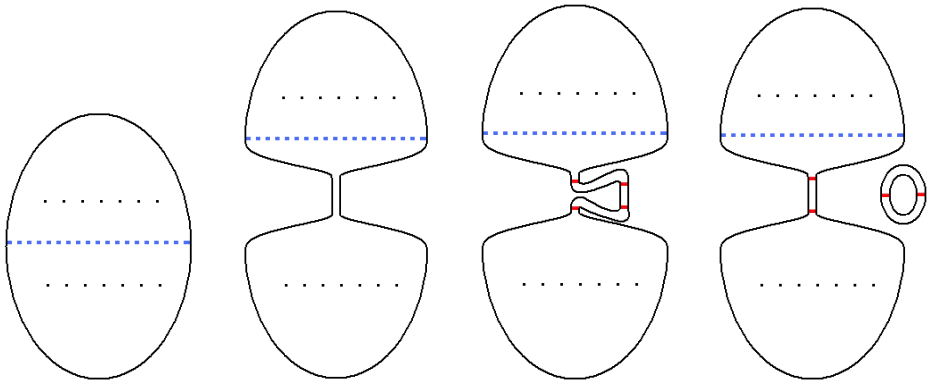

Figure 5.3: From left to right we have sketched: A manifold admitting a Heegaard splitting; the critical points of the Morse function are indicated as dots and the attachment by a blue dashed line, the same manifold with a small part of it brought to a standard $C_g \times [-\delta, \delta]$ metric, the deformed surface with cutting lines (red) indicated and the reassembled surfaces.

manifold as the standard surface of genus g. In the following we view N as embedded in $\mathbb{R}^k$. Let f be as in theorem 5.2.1 such that

$$\int_N f \, \mathrm{dVol},$$

is a topological invariant t. For some sufficiently small $[a_1, b_1] \subset \mathbb{R}$, with $c_1 < a_1 < \alpha_1 < \beta_1 < b_1 < c_2$, we smoothly and isotopically deform $h^{-1}([a_1, b_1]) \cap M \sim C_g \times [a_1, b_1]$, so that $h^{-1}([\alpha_1, \beta_1]) \cap M$ becomes isometric to the standard $C_g \times [\alpha_1, \beta_1] \subset \mathbb{R}^4 \subset \mathbb{R}^k$ given by the standard C_g and the ordinary Cartesian product. We shall now deform this part of the manifold so that it consists of a straight piece and two pieces which are straight at the beginning and the end but are bent in the middle so that if we cut along the the boundaries of the pieces and reassemble we recover the original manifold and $C_g \times \mathbb{S}^1$. The procedure is sketched in figure 5.3. From this we conclude that

$$\int_N f \, \mathrm{dVol} = \int_N f \, \mathrm{dVol} + \int_{C_g \times \mathbb{S}^1} f \, \mathrm{dVol},$$

where we again used local isotopy and the additivity of integration. Therefore,

$$\int_{C_g \times \mathbb{S}^1} f \, \mathrm{dVol} = 0.$$

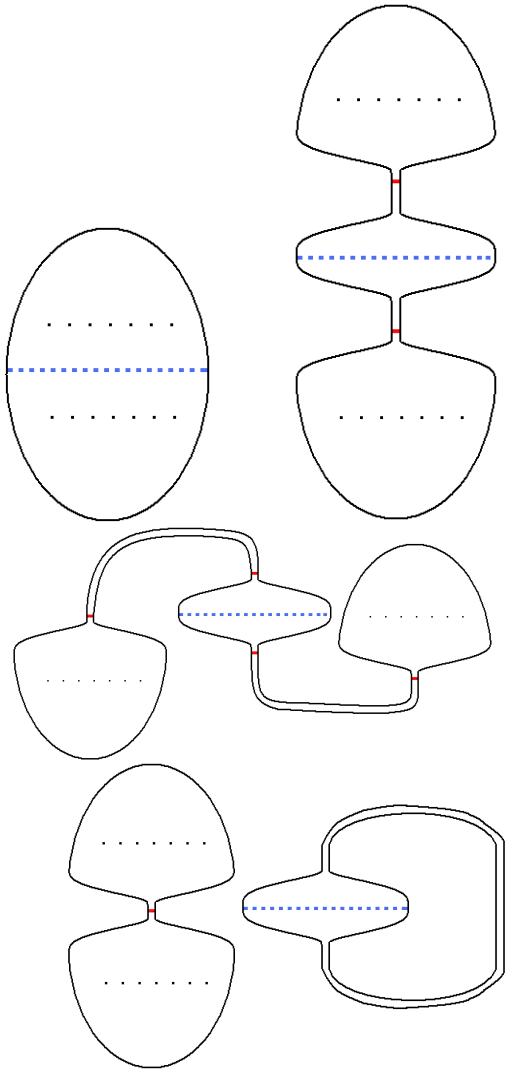

Figure 5.4: A Heegaard splitting, then the same manifold with two small parts brought to a standard metric both on another side of the 'attachment line', cutting lines (red) are also indicated, and finally the reassembled surface (two connected components).

The next part of the proof relies on the fact that the sphere ($\mathbb{S}^3$) allows a Heegaard splitting of every genus g, see [Fom87]. Let M be a manifold which allows a Heegaard splitting of genus g. We now deform two pieces of the manifold into parts isometric to $C_g \times [\alpha_1, \beta_1]$ and $C_g \times [\alpha_2, \beta_2]$, with $\alpha_1 < \beta_1 < \alpha_2 < \beta_2$, so that for all $p_1 \in (\alpha_1, \beta_1)$ and $p_2 \in (\alpha_2, \beta_2)$ both $h^{-1}((-\infty, p_1)) \cap M$ and $h^{-1}(p_2, \infty) \cap M$ are topological spheres with g handles whose boundary is isometric to the standard genus g surface, as discussed above. We can now smoothly deform $h^{-1}((p_1, q_1)) \cap M$ and $h^{-1}((q_2, p_2)) \cap M$, with $p_1 < q_1 < \beta_1$ and $\alpha_2 < q_2 < p_2$ (see figure 5.4), such that if we cut along the p_i and q_i lines and reassemble (possibly using $\mathbb{Z}_2$ symmetry) we recover two topological manifolds, with given topology. One of the manifolds we thus construct is a manifold admitting a Heegaard splitting of genus g. The attachment diffeomorphism, of the latter, on the boundary of the sphere with g handles is the identity. This manifold shall be denoted by $M_g^{S(3D)}$. The other manifold T_{C_g} is a mapping torus, found by taking $C_g \times I$, where I denotes the interval, and glueing the ends together by a glueing homeomorphism. The entire procedure is sketched in figure 5.4.

For a mapping torus we again have that

$$\int_{T_{C_g}} f \mathrm{dVol} = 0,$$

with f locally defined in terms of the metric. This can be seen as follows: consider T_{C_g} and deform part of it such that it is isometric to $[a, b] \times C_g$. Now introduce a second copy of T_{C_g} and cut in the parts isometric to $[a, b] \times C_g$. The two disjoint parts are now both diffeomorphic to $[c, d] \times C_g$. We can now deform the parts isometric to $[a, b] \times C_g$ and glue them together such that we get the trivial mapping torus $C_g \times S^1$. See figure 5.5 for a sketch. From this construction we can conclude that

$$2 \int_{T_{C_g}} f \mathrm{dVol} = \int_{C_g \times S^1} f \mathrm{dVol} = 0.$$

This means that by deforming, cutting and pasting a manifold M, which allows a Heegaard splitting of genus g, we find the following equalities

$$\int_M f \, \mathrm{dVol} = \int_{M_g^{S(3D)}} f \, \mathrm{dVol} + \int_{C_g \times \mathbb{S}^1} f \, \mathrm{dVol} = \int_{M_g^{S(3D)}} f \, \mathrm{dVol} + 0,$$

where f is as defined in the theorem. If we now use that the sphere ($\mathbb{S}^3$) allows a Heegaard splitting of every genus g we find that

$$\int_M f \, \mathrm{dVol} = \int_{M_g^{S(3D)}} f \, \mathrm{dVol} = \int_{\mathbb{S}^3} f \, \mathrm{dVol}. \tag{5.1}$$

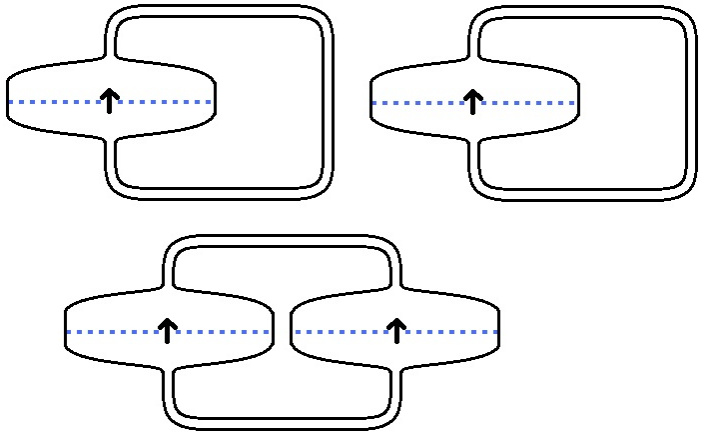

Figure 5.5: Two non-trivial mapping tori that are reassembled into a trivial mapping torus. We use arrows to indicate the direction in which we traverse, this makes the difference between a glueing homeomorphism and its inverse.

Following this observation, we are able to use the result of the first part of the proof,

$$\int_{C_g \times \mathbb{S}^1} f \, \mathrm{dVol} = 0.$$

This immediately translates into

$$\int_{\mathbb{S}^2 \times \mathbb{S}^1} f \, \mathrm{dVol} = 0.$$

We notice that both $\mathbb{S}^3$ and $\mathbb{S}^2 \times \mathbb{S}^1$ allow a Heegaard splitting of genus 1, so that

$$\int_{\mathbb{S}^3} f \, \mathrm{dVol} = \int_{M_1^{S^{(3D)}}} f \, \mathrm{dVol} = \int_{\mathbb{S}^2 \times \mathbb{S}^1} f \, \mathrm{dVol} = 0. \tag{5.2}$$

Combining equations (5.1) and (5.2) yields

$$\int_M f \, \mathrm{dVol} = 0,$$

for any manifold M and $f = f(g, \partial g, \ldots)$ a function determined by the metric and all its derivatives. □

Remark 5.3.2 *In theorem 5.3.1 we assumed that f gives us a topological invariant for all 3-manifolds, in fact the conclusion can be drawn for a given manifold M allowing a Heegaard splitting of genus g, if $\int f \mathrm{d}Vol$ is an invariant for S^3, $S^1 \times C_g$, mapping tori T_{C_g}, $M_1^{S(3D)}$ and M, where C_g is a surface of genus g and $M_1^{S(3D)}$ as defined above.*

This is clear from inspection of the proof of theorem 5.3.1.

5.4 Higher dimensions

One can wonder about generalizations of the methods stated above to manifolds of general dimension. Some of these generalizations are immediately obvious, for example the procedure sketched in figure 5.3 can be used in any dimension so see that for f and t as in the theorem

$$\int_{M^{d-1}\times\mathbb{S}^1} f \,\mathrm{dVol} = t$$

implies that $t = 0$, where M^{d-1} is any manifold of dimension $d-1$ occurring as level set.

Using a sophisticated result given in [KKNO73], we can use cut and paste techniques to provide results equivalent to those of theorems 5.2.1 and 5.3.1 in higher dimensions. To explain this, we briefly recall some notions from [KKNO73]. Let M be a closed manifold and $N \subset M$ a closed submanifold of codimension 1 with trivial normal bundle. If one cuts M open along N one obtains a manifold M' with boundary $\partial M' = N + N$. Pasting the boundary together in a different manner gives a new closed manifold $\tilde{M}$. $\tilde{M}$ is said to have been obtained by cutting and pasting M (Schneiden und Kleben in German or SK for short).

We shall assume that a topological invariant $t \in \mathbb{R}$ for n-dimensional manifolds is compatible with disjoint unions, that is if $M = M_1 + M_2$ then $t(M) = t(M_1) + t(M_2)$. Such t is called an SK-invariant if whenever M_1 and M_2 are compact n-manifolds with diffeomorphic boundaries and $\phi, \psi : \partial M_1 \to \partial M_2$ orientation preserving diffeomorphisms, then

$$t(M_1 \cup_\phi -M_2) = t(M_1 \cup_\psi -M_2).$$

Here $-M_2$ means M_2 with reversed orientation and $M_1 \cup_\phi -M_2$ means M_1 pasted to M_2 along the boundary by ϕ and smoothed.[4]

Corollary 1.4 of [KKNO73] now states that any SK-invariant for smooth manifolds is a linear combination of the Euler characteristic and the signature in the oriented case.

By the generalisation of the constructions in Sections 5.2 and 5.3 the invariants found by integration are SK-invariants and thus linear combinations of the Euler characteristic and the signature.

[4] There is an analogous definition in the non-oriented case.

Chapter 6

Bounds on Betti numbers in three dimensions

In the previous chapter we have seen that it is impossible to find expressions for any topological invariant except the Euler characteristic, using only local geometric information. In this chapter we broaden our interest and include practical bounds on topological invariants of the level or super level sets of Gaussian random fields in our considerations. In the particular case of a co-dimension one submanifold in Euclidean space, one bound (apart from the Morse inequalities) comes to mind: For an even[1] dimensional closed compact hypersurfaces without boundary embedded in a Euclidean space of one dimension greater, one always finds parts of this surface with positive curvature.

This can be used to give bounds on the number of connected components (β_0), and somewhat indirectly on the other Betti numbers. To be precise in Section 6.1.2 of the Preliminaries we shall see that for two dimensional surfaces

$$\int_{\Sigma} K\,\Theta(K)\mathrm{d}A \geq 4\pi\beta_0(\Sigma), \tag{6.1}$$

where K denotes the Gaussian curvature and Θ the Heaviside function. The Heaviside function is the distribution which is one for a positive and zero for a negative argument, that is

$$\Theta(x) = \begin{cases} 1 & \text{if } x \geq 0 \\ 0 & \text{if } x < 0. \end{cases}$$

[1]The even dimensionality is essential, see Chapters 4 and 5 or [MS74].

In the same section we shall also touch upon the indirect bounds on the other Betti numbers. In Section 6.2 we discuss in great detail the density expectation value of the left hand side of equation (6.1) for the case of a two dimensional isosurface of a Gaussian random field on $\mathbb{R}^3$. We provide an integral expression for this expectation value and numerically evaluate this integral. As in the previous chapter the result we achieve is negative in nature, that is the expectation value of the positive part of the Gaussian curvature does not yield practicable bounds on the number of connected components.

The Euler characteristic in the Gaussian random field literature

In our efforts to give the expectation value for the positive part of the Gaussian curvature, we shall also give an expression for the Euler Characteristic of an isosurface of a Gaussian random field in integral form. Our derivation is based on the Gauss-Bonnet theorem. In this sense it is unlike Adler [Adl81] (quoted in [BBKS86]), which uses that the Euler characteristic is the alternating sum of the number of critical points with a given index. The latter formula for the Euler characteristic arises from Morse theory and has been discussed in section 4.3.4. For a mainly numerical study of the density of critical points for two and three dimensional Gaussian random fields we refer to Gay, Pichon and Pogosyan [GPP12].

The approach used in [HGIW86] to calculate the expectation value of the Euler characteristic is also based on the Gauss-Bonnet theorem. In [HGIW86] space is subdivided using a body centred cubic tessellation, with a length scale that for now we shall consider fixed.

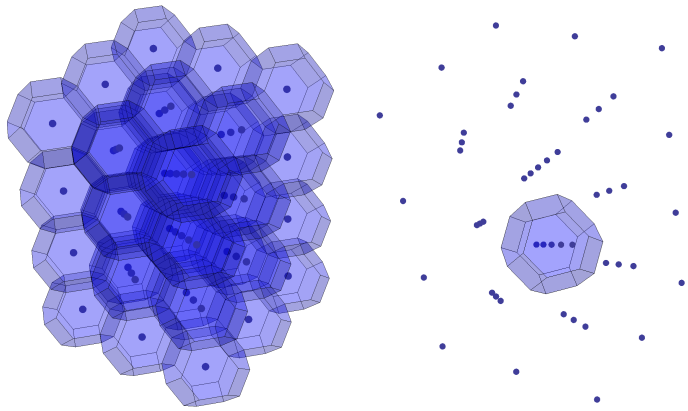

Figure 6.1: The body centred cubic (BCC) lattice (segment) with a single and all truncated octahedra indicated.

Truncated octahedra are the constituents of the tessellation. These truncated octahedrons are included in piecewise linear superlevel sets depending on whether the values of the Gaussian random fields at the centres are above some threshold.[2] Those truncated octahedra that are included are called positive, those that are not are called negative.

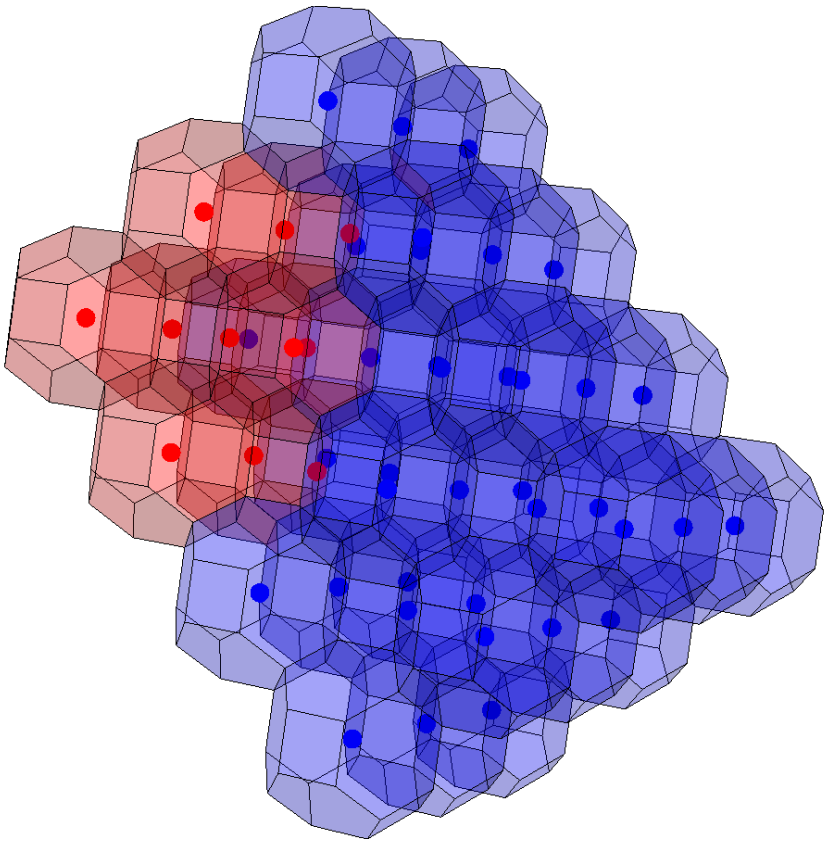

Figure 6.2: Those trucated octahedra for which the value of the Gaussian random fields at its centre lies above the threshold are indicated in red, the others in blue.

Each vertex on a truncated octahedron is shared between 4 octahedra in the tessellation. One can calculate the expectation for each of these octahedra to be positive or negative. This gives 6 different configurations classified as follows:

[2] Hamilton et al. [HGIW86] denotes the Gaussian random field by δ and the threshold by δ_c.

- All four are positive or negative.

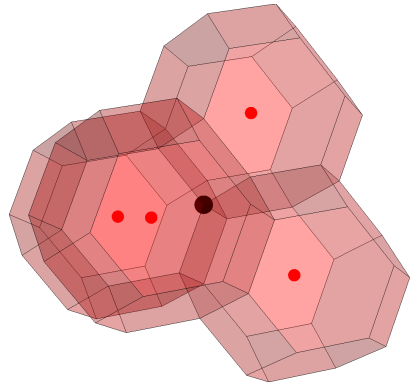

Figure 6.3: Here we indicate an arbitrary vertex on an arbitrary truncated polyhedron in the tessellation in black. All truncated octahedra that are adjacent to this vertex are above the threshold. We have not depicted the complementary configuration where all are below the threshold as it is identical. The angle deficit is zero.

- One is positive and the others negative or vice versa.

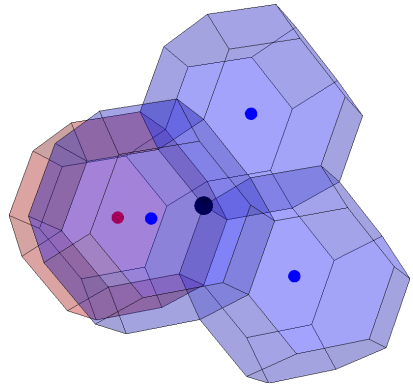

Figure 6.4: One truncated octahedra that is adjacent to this vertex is above the threshold. The angle deficit is $30°$. We have not depicted complementary configuration.

- Two are positive and two negative in two different configurations.

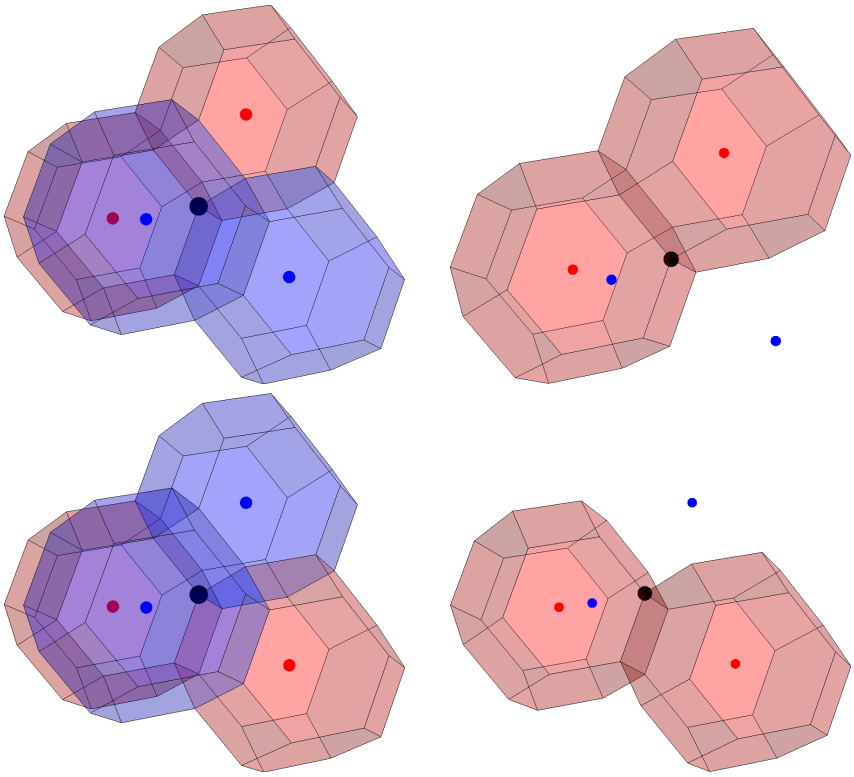

Figure 6.5: If two truncated octahedra are above the threshold there are two possibilities: the ones above the threshold share a hexagon (above) or a square (below). The angle deficits are $-60°$ and $-120°$, respectively. For both cases we have depicted the configuration including and excluding the octahedra below the threshold (blue if included).

For the latter two configurations one sees that there is an angle deficit on the 'isodensity surface' at the vertex. For the second point in our classification this deficit is positive. For the third point in our classification it is negative.

We can calculate the expectation value for each of the configurations and therefore the expectation value for the various positive and negative angle deficits. The angle deficit plays the role of the Gaussian curvature on a piecewise linear surface. Because of this it is possible to determine the Euler Characteristic of the 'isodensity surface', using a piecewise linear version of the Gauss-Bonnet theorem.

Let us assume that M is a surface in Euclidean space consisting of straight

triangles. The discrete or piecewise linear version of the Gauss-Bonnet theorem for M reads:

$$2\pi\chi(M) = \sum_{\text{vertices}} K_{\text{vertex}}, \tag{6.2}$$

where the sum is over all vertices and K_{vertex} denote the Gaussian curvature at a vertex. Gaussian curvature at a vertex equals the angle deficit at the vertex

$$K_{\text{vertex}} = 2\pi - \sum_{\text{adjacent}} \phi_{\text{adjacent}},$$

where the sum indicates the sum over all angle adjacent to the vertex.

The discrete Gauss-Bonnet theorem (6.2) is not difficult to prove. In the proof one uses:

- The sum of the angles of a triangle is π.
- The Euler characteristic χ satisfies $\chi = v - e + t$, with v the number of vertices, e the number of edges and t the number of triangles.
- Each triangle has three edges and each edge is shared between two triangles so that $3t = 2e$.

We now have

$$\begin{aligned}
\sum_{\text{vertices}} K_{\text{vertex}} &= \sum_{\text{vertices}} 2\pi - \sum_{\text{adjacent}} \phi_{\text{adjacent}} \\
&= 2\pi v - \sum_{\text{triangles}} \sum_{\text{angle}} \phi_{\text{angle}} \\
&= 2\pi v - \pi t \\
&= 2\pi v - 3\pi t + 2\pi t \\
&= 2\pi v - 2\pi e + 2\pi t \\
&= 2\pi\chi.
\end{aligned}$$

To approximate the isodensity surface of the tessellation needs to become finer, this means that we decrease the length scale which we assumed fixed. All contributions of positive and negative angle deficits diverge as the scale decreases, because of the choice of a tessellation. These divergences cancel if added to give the Euler Characteristic. The cancellation is a consequence of the Gauss-Bonnet theorem. Hamilton et al. [HGIW86] argues heuristically that this is natural. The approach presented in this chapter does not need to introduce divergent functions, but treats the smooth case.

The philosophy of Chapters 12 and 13 of [AT07] has also influenced this chapter. In Chapters 12 and 13 a sufficiently smooth manifold is endowed with the metric:

$$g_t(X_t, Y_t) = \mathbb{E}((X_t f) \cdot (Y_t f))$$

with f a Gaussian random field. The metric induced by the Gaussian random field can be used to give expressions for the mean Euler characteristic in terms of Lipschitz-Killing curvatures of this metric. This is the topic of Section 12.4 of [AT07]. In Chapter 13 [AT07] of an ingenious version of Hadwiger's formula is developed in the context of a manifold with a metric induced by a Gaussian random field. For a discussion of Hadwiger's formula we refer to Section 4.3.5.

Summary and contribution

To summarise; many expressions for the mean value of the Euler characteristic are available in various contexts, using either Morse theoretical arguments [Adl81, BBKS86], the Gauss-Bonnet theorem [HGIW86] or a combination of both and the Lipschitz-Killing curvature [AT07]. The use of the positive part of the Gaussian curvature as a bound on the number of connected components on the super level sets of a Gaussian Random field is new.

The main result is given in Figure 6.7. In this figure we give both our result for the Euler characteristic of the level set as well as the expectation value for the positive part of the Gaussian curvature. From which we are able to conclude the expectation value of the positive part of the Gaussian curvature does not yield practicable bounds on the number of connected components.

6.1 Preliminaries

In this section we discuss a number of results from the differential geometry of implicit surfaces, differential topology and some probability density function the last of which plays a central role in the astrophysical literature on Gaussian random fields.

6.1.1 Curvature of implicit surfaces

We shall give some classical formulae for the Gaussian and Mean curvatures of an implicit surface. We shall assume both the surfaces and the function to be smooth. These results can be found in the survey in the beginning of Chapter 3 of Spivak [Spi75a], Section 4 of Goldman [Gol05] and section 29 of [Kno13].

We consider an implicit surface defined by the equation $f(r_1, r_2, r_3) = c$, with c a constant. To begin, following [Gol05], we define the gradient $\operatorname{grad}(f)$, Hessian $H(f)$ and the adjoint of the Hessian $H^{\mathrm{ad}}(f)$ explicitly:

$$\operatorname{grad}(f) = \begin{pmatrix} f_1 \\ f_2 \\ f_3 \end{pmatrix}$$

$$H(f) = \begin{pmatrix} f_{11} & f_{12} & f_{13} \\ f_{12} & f_{22} & f_{23} \\ f_{13} & f_{23} & f_{33} \end{pmatrix}$$

$$H^{\mathrm{ad}}(f) = \begin{pmatrix} f_{22}f_{33} - f_{23}^2 & f_{23}f_{13} - f_{12}f_{33} & f_{12}f_{23} - f_{22}f_{13} \\ f_{13}f_{23} - f_{12}f_{33} & f_{11}f_{33} - f_{13}^2 & f_{12}f_{13} - f_{11}f_{23} \\ f_{12}f_{23} - f_{13}f_{22} & f_{21}f_{13} - f_{11}f_{23} & f_{11}f_{22} - f_{12}^2 \end{pmatrix},$$

with $f_i = \partial_{r_i} f$ and $f_{ij} = \partial_{r_i}\partial_{r_j} f$. We used the smoothness of f to interchange the order of differentiation. With these definitions the Gauss curvature reads

$$K = \frac{\operatorname{grad}(f)^t H^{\mathrm{ad}}(f) \operatorname{grad}(f)}{|\operatorname{grad}(f)|^4}$$

and the Mean curvature

$$K_M = \frac{\operatorname{grad}(f)^t H(f) \operatorname{grad}(f) - |\operatorname{grad}(f)|^2 \operatorname{Tr}(H(f))}{2|\operatorname{grad}(f)|^3}.$$

The principal curvatures k_1, k_2, the inverses of the maximum and minimum radii of the osculating circles, can be found using the mean and Gauss curvature

$$k_1, k_2 = K \pm \sqrt{K_M^2 - K}.$$

6.1.2 Convex hulls and Gauss-Bonnet

In this section we review some results from convex geometry.

In the following we consider a smooth positively oriented surface Σ with a single connected component embedded in $\mathbb{R}^3$. The convex hull of the surface $\text{CH}(\Sigma)$ is by definition convex and therefore its boundary is a topological sphere. We have given examples of convex hulls in two and three dimensions in figure 6.6. The boundary $\partial\text{CH}(\Sigma)$ is also smooth. This can be seen as follows if $x \in \partial\text{CH}(\Sigma)$ then there are two possibilities. Either $x \in \Sigma$ or there are at least two points $y_1, y_2 \in \Sigma$ so that x lies on the line connecting y_1 and y_2. If there are three points such that x lies in the interior of the convex hull of these points the point x is a planar point in $\partial\text{CH}(\Sigma)$ and the proof would be complete. Should there be only two points then we consider a neighbourhood of x and see that $\partial\text{CH}(\Sigma)$ is not smooth in a neighbourhood of x the surface Σ is not smooth in a neighbourhood of y_1 or y_2. This contradicts our assumption that Σ is smooth.

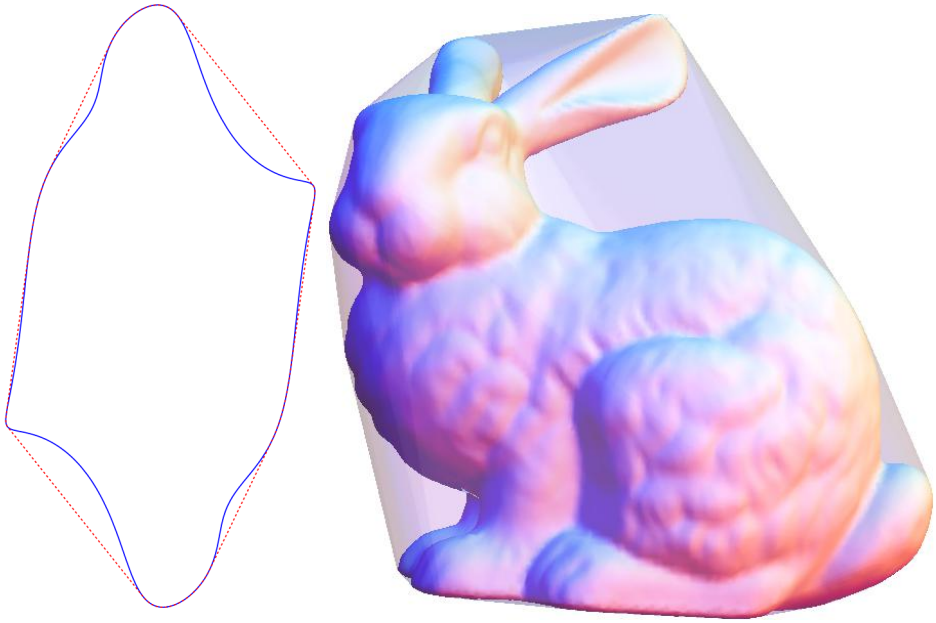

Figure 6.6: Examples of convex hulls. We have given a two and three dimensional example. We only depict the boundary of the convex hulls. The three dimensional example was made using the 'Stanford bunny' from the Wolfram example database.

Due to the Gauss-Bonnet theorem we have

$$\int_{\partial \mathrm{CH}(\Sigma)} K \mathrm{d}A = 4\pi.$$

For a discussion of the Gauss-Bonnet theorem we refer to Section 4.3.5. On the other hand, if for any $x \in \partial\mathrm{CH}(\Sigma)$ the Gaussian curvature at x as an element of $\mathrm{CH}(\Sigma)$ is positive definite, then $x \in \Sigma$. The proof is straightforward. Suppose that x does not lie on Σ, then there must be at least two points $y_1, y_2 \in \Sigma$ so that x lies on the line connecting y_1 and y_2. This line is an asymptotic curve[3] on the surface $\partial\mathrm{CH}(\Sigma)$ and therefore has non-positive curvature. Because $\mathrm{CH}(\Sigma)$ is by definition convex it follows that the curvature should be zero.

We can now combine this observation with the Gauss-Bonnet theorem to conclude that for each surface Σ of a single connected component

$$\int_{\Sigma} K\, \Theta(K) \mathrm{d}A_{\Sigma} \geq \int_{\partial \mathrm{CH}(\Sigma)} K \mathrm{d}A_{\partial \mathrm{CH}(\Sigma)} = 4\pi,$$

where Θ denotes the Heaviside function and $\mathrm{d}A_{\Sigma}$ and $\mathrm{d}A_{\partial \mathrm{CH}(\Sigma)}$ denote the respective area forms. This immediately implies that if we allow Σ to have multiple connected components, that then

$$\int_{\Sigma} K\, \Theta(K) \mathrm{d}A_{\Sigma} \geq \int_{\partial \mathrm{CH}(\Sigma)} K \mathrm{d}A_{\partial \mathrm{CH}(\Sigma)} = 4\pi\beta_0(\Sigma).$$

In this expression β_0 denotes the zeroth Betti number, which is the number of connected components. For a discussion of Betti numbers we refer to Section 4.3. This result can even be strengthened to

$$\int_{\Sigma} K\, \Theta(k_1)\Theta(k_2) \mathrm{d}A \geq 4\pi\beta_0(\Sigma), \tag{6.3}$$

with k_1, k_2 the principal curvatures. This result holds because for a convex surface all sectional curvatures are non-negative.

We can take this one step further: Suppose that Σ is itself the boundary of a full dimensional set S, inducing the orientation on Σ. In this case we are also able to infer topological bounds from those parts of the Gaussian curvature, for which the principal curvatures are negative. Let us consider the complement $\mathrm{comp}(S)$ of S. If S^c is a connected component of $\mathrm{comp}(S)$ then we can apply the same reasoning as above except that the normal of Σ is pointing inward into $\mathrm{comp}(S)$. This implies that

$$\int_{\partial S^c} K \Theta(-k_1)\Theta(-k_2) \mathrm{d}A \geq 4\pi.$$

[3] A discussion of asymptotic curves can be found in example [O'N06], [DC76] or [Spi99].

6.1.3 Expectation values of derivatives for Gaussian random fields

In the following section we give a probability density function that has been made completely explicit by [BBKS86]. It requires the introduction of a significant amount of notation in line with that article.

As mentioned in Section 4.2.3, one can combine probability distributions for the values of a Gaussian random field and its derivatives at a given fixed location into a single probability density distribution function. This probability distribution function is determined by a single correlation matrix. This has been done explicitly in Appendix A of [BBKS86] for an isotropic field for the field value and the values of the derivatives of the field up to second order at a given location. For more extensive probability functions including higher order terms relating physically to gravity we refer the reader to [vdWB96]. In these approaches the correlation matrix is even diagonalized and $\mathrm{SO}(3)$ symmetry is used to get rid of the off diagonal terms of the Hessian (the matrix of second order derivatives), so that the eigenvalues of the Hessian are the relevant variables.

We follow the so called Rice notation:

$$\eta_i = \partial_{r_i} f \qquad\qquad \zeta_{ij} = \partial_{r_i}\partial_{r_j} f.$$

We suppress the coordinate from the notation, that is we write for example η_i instead of $\eta_i(r)$, because the field is isotropic, as in Appendix A of [BBKS86]. The value of the field is indicated by ν. We are now able to define σ_0, σ_1 and σ_2 in terms of the correlation functions

$$\begin{aligned}
\langle f f\rangle &= \sigma_0^2 & \langle \eta_i \eta_j\rangle &= \frac{\sigma_1^2}{3}\delta_{ij}\\
\langle f \zeta_{ij}\rangle &= \frac{\sigma_1^2}{3}\delta_{ij} & \langle \zeta_{ij}\zeta_{kl}\rangle &= \frac{\sigma_2^2}{15}(\delta_{ij}\delta_{kl}+\delta_{ik}\delta_{jl}+\delta_{il}\delta_{jk}))\\
\langle f \eta_i\rangle &= 0 & \langle \eta_i \zeta_{jk}\rangle &= 0.
\end{aligned}$$

Here we used the $\langle\,\rangle$ notation instead of $\mathbb{E}$, as discussed in Section 4.2.3. In the same section we have seen (4.5) that these expectation values can be expressed in terms of covariance function, and thus the powerspectrum. With σ_0, σ_1 and σ_2 we may define

$$\gamma = \frac{\sigma_1^2}{\sigma_2\sigma_0}.$$

In addition, we assume that the eigenvalues of minus the Hessian $(-\zeta_{ij})$ are ζ_1, ζ_2 and ζ_3. The variables that allow diagonalization of the covariance matrix are

$$\sigma_2 x = -(\zeta_1+\zeta_2+\zeta_3) \quad \sigma_2 y = -\frac{1}{2}(\zeta_1-\zeta_3) \quad \sigma_2 z = -\frac{1}{2}(\zeta_1-2\zeta_2+\zeta_3) \qquad (6.4)$$

The joint distribution functions of the variables we have now introduced is

$$\phi(\nu,\eta,x,y,z)\mathrm{d}\nu\mathrm{d}^3\eta\mathrm{d}x\mathrm{d}y\mathrm{d}z = \frac{(15)^{5/2}}{32\pi^3}\frac{\sigma_0^3}{\sigma_1^3(1-\gamma^2)^{1/2}}|2y(y^2-z^2)|e^{-Q}\mathrm{d}\nu\mathrm{d}x\mathrm{d}y\mathrm{d}z\frac{\mathrm{d}^3\eta}{\sigma_0^3}, \quad (6.5)$$

with

$$Q = \frac{\nu^2}{2} + \frac{(x-\gamma\nu)^2}{2(1-\gamma^2)} + \frac{5}{2}(3y^2+z^2) + 3\frac{\eta_1^2+\eta_2^2+\eta_3^2}{2\sigma_1^2},$$

η a shorthand for the variables η_1 η_2 and η_3 and $\mathrm{d}^3\eta = \mathrm{d}\eta_1\mathrm{d}\eta_2\mathrm{d}\eta_3$. Here we follow the notation of Appendix A of [BBKS86], where the diagonalization is discussed in detail.

6.2 The expectation of the positive part of the Gaussian curvature

For the derivation of the mean value of the Euler characteristic and the mean value of the positive part of the Gaussian curvature we combine the results discussed above, in Section 6.1. As discussed in Section 6.1.2, the positive part of the Gaussian curvature provides bounds on the number of connected components in a three dimensional setting. These results are based on a theorem from distribution theory, Theorem 6.1.5 of [Hör90]:

Theorem 6.2.1 *If f is a real valued C^∞ function on a subset of $\mathbb{R}^n$ and if*

$$|\operatorname{grad}(f)| = \left(\sum_j |\partial_j f|^2\right)^{1/2} \neq 0,$$

when $f = 0$, then

$$f^*\delta_D = \mathrm{d}\mathit{Vol}_\Sigma / |\operatorname{grad}(f)|,$$

where $\mathrm{d}\mathit{Vol}_\Sigma$ is the Euclidean surface measure on the hypersurface

$$\Sigma = \{x \mid f(x) = 0\},$$

δ_D denotes the Dirac delta distribution and f^* denotes the pullback, which roughly speaking can interpreted by $f^*\delta_D(x) = \delta_D(f(x))$.

With this result and the Gauss-Bonnet theorem (4.10) we can write

$$\begin{aligned}\langle \chi_{\{f=0|_C\}} \rangle &= \left\langle \frac{1}{2\pi} \int_{f^{-1}(0)|_C} K \mathrm{d}A \right\rangle + \mathrm{t}(\partial C) \\ &= \left\langle \frac{1}{2\pi} \int_C |\operatorname{grad}(f)| K(f) f^*\delta_D \mathrm{dVol} \right\rangle + \mathrm{t}(\partial C) \\ &= \frac{1}{2\pi} \int_C \langle |\operatorname{grad}(f)| K(f) f^*\delta_D \rangle \mathrm{dVol} + \mathrm{t}(\partial C).\end{aligned}$$

Here we have denoted the surface defined by $f = 0$ restricted to a compact set C as explicitly as possible. The $\mathrm{t}(\partial C)$ refers to terms involving the boundary of C.

We are interested in the expectation value of the Euler characteristic χ per unit volume, so we may ignore the boundary terms, because their contribution is proportional to the area. This deserves a little explanation, if one wants to understand it at a non-heuristic level. For the explanation we need three results:

- The Gauss-Bonnet theorem for surfaces with boundary[4]

$$\int_{\Sigma} K \mathrm{d}A + \int_{\partial\Sigma} k_g \mathrm{d}s = 2\pi\chi(M), \tag{6.6}$$

  where k_g denotes the geodesic curvature of a curve.[5]

- The Euler characteristic obeys the inclusion-exclusion principle:

$$\chi(M \cup N) = \chi(M) + \chi(N) - \chi(M \cap N),$$

  with M and N two surfaces. This statement is true more generally, but we do not need this here.

- The circle and real line are the only one-dimensional topological manifolds of which the first is compact and the second not.

Using the same arguments as in the fully two dimensional case one can find an expectation value for k_g. To find an expectation value for the second term in (6.6) we need to integrate over the boundary ∂C, so that the contribution is proportional to the area, that is $\propto r^2$, instead of proportional to the volume, that is $\propto r^3$, with r the typical scale. If the total absolute Gaussian curvature of $\partial C \subset \mathbb{R}^3$ is constant with respect to the typical scale r, we can even see that up to leading order in r

$$\frac{1}{2\pi} \int_C \langle |\operatorname{grad}(f)| K(f) f^* \delta_D \rangle \mathrm{dVol}$$

gives

$$\langle \chi(\partial\{x \in C | f(x) \geq 0\}) \rangle.$$

We have that

$$\partial\{x \in C | f(x) \geq 0\} = f^{-1}(0)|_C \cup \{x \in \partial C | f(x) \geq 0\}.$$

Using the inclusion-exclusion principle we see that

$$\chi(\partial\{x \in C | f(x) \geq 0\}) = \chi(f^{-1}(0)|_C) + \chi(\{x \in \partial C | f(x) \geq 0\}) - \chi(f^{-1}(0)|_C \cap \{x \in \partial C | f(x) \geq 0\}).$$

[4]The Gauss-Bonnet theorem for surfaces with boundary can be found in for example [O'N06] as Theorem 7.5.

[5]The proof is a little more complicated than the one discussed in Section 4.3.5, because we need to prove the local Gauss-Bonnet formula (4.14) with non-geodesic boundaries.

Because $f^{-1}(0)|_C \cap \{x \in \partial C | f(x) \geq 0\}$ is assumed to be a smooth 1-dimensional manifold, see also Remark 6.2.3 below, and the only 1-dimensional compact manifolds are circles whose Euler characteristic is zero we in fact have:

$$\chi(\partial\{x \in C | f(x) \geq 0\}) = \chi(f^{-1}(0)|_C) + \chi(\{x \in \partial C | f(x) \geq 0\}).$$

Applying the Gauss-Bonnet theorem with boundary on both terms yields

$$\begin{aligned}\chi(\partial\{x \in C | f(x) \geq 0\}) =& \frac{1}{2\pi}\int_{f^{-1}(0)|_C} K \mathrm{d}A_{f^{-1}(0)|_C} \\ &+ \frac{1}{2\pi}\int_{\partial(f^{-1}(0)|_C)} k_g \mathrm{d}s_{f^{-1}(0)|_C} \\ &+ \frac{1}{2\pi}\int_{\{x\in\partial C | f(x)\geq 0\}} K \mathrm{d}A_{\{x\in\partial C|f(x)\geq 0\}} \\ &+ \frac{1}{2\pi}\int_{\{x\in\partial C | f(x)= 0\}} k_g \mathrm{d}s_{\{x\in\partial C|f(x)\geq 0\}}, \end{aligned} \tag{6.7}$$

where we have made the different domains and forms as explicit as possible. Note that although the domains of integration for the second and fourth term in equation (6.7) are equal, they differ because the geodesic curvature is taken with respect to $f^{-1}(0)$ and ∂C respectively. However, both of these terms can be argued to be proportional to the area of ∂C, as we did for one of them above. The third term is bounded from above by the total absolute Gaussian curvature of $\partial C \subset \mathbb{R}^3$. If C is a ball it is even bounded by 2. This means that the first term in (6.7) gives the leading contribution.

A discussion tackling the boundary from a Morse theoretical perspective can be found in Section 6.2 of [AT07].

Having discussed the boundary terms, which we shall ignore, we can now focus on

$$K^{\mathbb{E}} = \langle |\operatorname{grad}(f)| K(f) f^* \delta_D \rangle, \tag{6.8}$$

we shall not go into the normalization.[6] As a result of the bounds on the number of connected components, see Section 6.1.2, we are also interested in

$$K^{\mathbb{E}}_+ = \langle |\operatorname{grad}(f)| \Theta(K(f)) K(f) f^* \delta_D \rangle, \tag{6.9}$$

where Θ denotes the Heaviside function. Using the probability density function we reviewed in Section 6.1.3 and the formulae for the Gaussian curvature from Section 6.1.1 we can make $K^{\mathbb{E}}$ and $K^{\mathbb{E}}_+$ explicit. Note that because the Hessian

[6] We avoid this issue because in [HGIW86] there is a different normalization from that of [Adl81, BBKS86, AT07].

is diagonalized in Section 6.1.3, or to be more precise the probability density function is given in terms of the eigenvalues ζ_i of minus the Hessian $(-\zeta_{ij})$, the expressions for the Gaussian curvature simplify significantly:

$$K(\eta_1,\eta_2,\eta_3,\zeta_1,\zeta_2,\zeta_3)=\frac{\zeta_1\zeta_2\eta_3^2+\zeta_1\zeta_3\eta_2^2+\zeta_2\zeta_3\eta_1^2}{\left(\eta_1^2+\eta_2^2+\eta_3^2\right)^2}.$$

If written in terms of the variables x, y and z, see (6.4), the Gaussian curvature reads

$$\begin{aligned}K(\eta_1,\eta_2,\eta_3,x,y,z)=&\left(9(\eta_1^2+\eta_2^2+\eta_3^2)^2\right)^{-1}\cdot\\&(\sigma_2^2(x^2(\eta_1^2+\eta_2^2+\eta_3^2)\\&-x(3y(\eta_1^2-\eta_3^2)+z(\eta_1^2-2\eta_2^2+\eta_3^2))\\&-9\eta_2^2y^2+6yz(\eta_1^2-\eta_3^2)+z^2(-2\eta_1^2+\eta_2^2-2\eta_3^2))).\end{aligned}$$

The mean of the Gaussian curvature $K^{\mathbb{E}}$, see (6.8), now can be expressed as

$$K^{\mathbb{E}}=\int_{\mathbb{R}^6}\sqrt{\eta_1^2+\eta_2^2+\eta_3^2}K(\eta_1,\eta_2,\eta_3,x,y,z)\phi(\nu,\eta,x,y,z)\mathrm{d}\eta_1\mathrm{d}\eta_2\mathrm{d}\eta_3\mathrm{d}x\mathrm{d}y\mathrm{d}z, \tag{6.10}$$

with $\phi(\nu,\eta,x,y,z)$ as defined in (6.5). This naturally also implies that the mean of the positive part of the Gaussian curvature $K_+^{\mathbb{E}}$, see(6.9) can be expressed as

$$\begin{aligned}K_+^{\mathbb{E}}=\int_{\mathbb{R}^6}&\sqrt{\eta_1^2+\eta_2^2+\eta_3^2}K(\eta_1,\eta_2,\eta_3,x,y,z)\Theta(K(\eta_1,\eta_2,\eta_3,x,y,z))\cdot\\&\phi(\nu,\eta,x,y,z)\mathrm{d}\eta_1\mathrm{d}\eta_2\mathrm{d}\eta_3\mathrm{d}x\mathrm{d}y\mathrm{d}z,\end{aligned} \tag{6.11}$$

We have evaluated both integrals numerically using Mathematica with $\sigma_1 = \sigma_2 = 1$ and $\sigma_0 = 2$, the result of which is depicted in Figure 6.7. Mathematica reported error estimates of the order 10^{-6}, for both. In Figure 6.7 we have also added the normalized[7] version of the analytic expression for the mean Euler characteristic, that is

$$\chi\sim(\nu^2-1)e^{-\nu^2/2},$$

see [Adl81, BBKS86]. By comparing the analytic expression and the numerical results we find good agreement.

From figure 6.7 we are able to conclude that the bounds on the number of components arising from (6.9) do not contribute to our understanding. This can

[7] To avoid dependence on any convention[6] we have normalized using the $\nu = 0$ value.

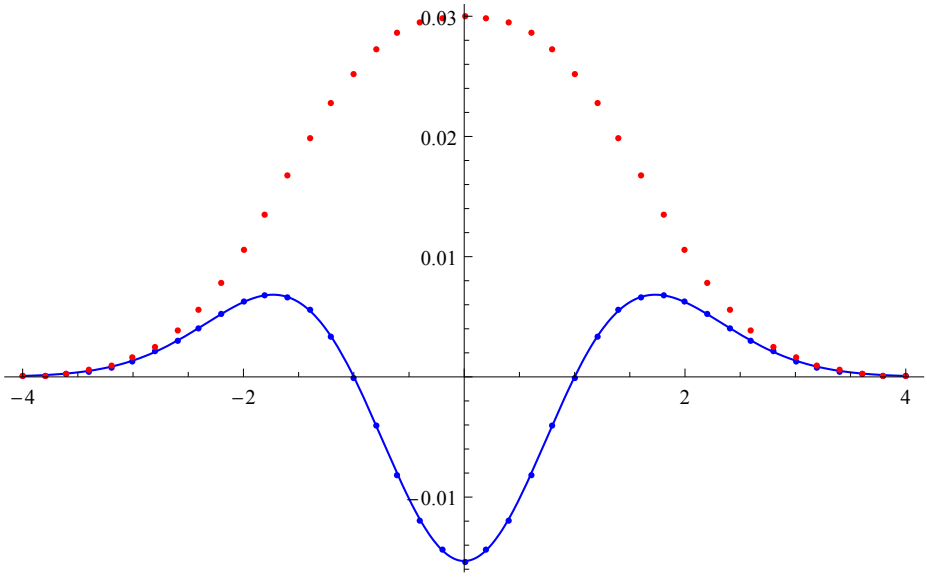

Figure 6.7: The numerical values for expectation value of Euler characteristic (6.10) (blue dots) and the positive part of the Gaussian curvature (6.9) (red dots) as functions of the threshold ν. The normalized version of the analytic prediction for the Euler characteristic χ, is added as a blue solid line.

be seen in two different ways. The first is numerical in nature; the bounds do not compare well to the numerical result for the number of connected component, see [PPC+13], inside the interval $[-3, 3]$. One at first glance may think that outside the interval $[-3, 3]$ information is gained, but the Morse inequalities already sufficed to conclude that the Euler Characteristic is dominated by the number of connected components. Which leads us to our second more theoretical point, the bounds from $K_+^{\mathbb{E}}$ are in fact comparable to the bounds from the Morse inequalities. For an extensive discussion and numerical results on the critical points of a Gaussian random field in three dimensions we refer the reader to Gay, Pichon and Pogosyan [GPP12].

Tighter bounds, see (6.3), could be found using

$$\langle |\operatorname{grad}(f)|\Theta(k_1(f))\Theta(k_2(f))K(f)f^*\delta_D\rangle, \tag{6.12}$$

with k_1 and k_2 the principal curvatures. However preliminary numerical results indicate that little will be gained by this.

We conclude our discussion with a number of remarks:

Remark 6.2.2 *It would be interesting to see whether it would be possible to gain tighter results after smoothing. By smoothing we mean a convolution with some function, for example a Gaussian function, so that the values of the Gaussian random field are 'averaged' in a small neighbourhood. It is possible that a significant part of the contributions to the positive part of the Gaussian curvature are very local in nature and thus would be easily removed by such a smoothing.*

Remark 6.2.3 *We have not provided regularity results and simply assume that the isosurfaces of a Gaussian random field are sufficiently smooth (with probability one). By Sard's lemma*[8] *and the implicit function theorem it would suffice for f to be a smooth Morse function to have the isosurfaces are smooth for almost all levels. For informative discussions of Sard's Lemma and the implicit function theorem we refer to [Mil65b] and [DK04] respectively. Conditions for a realisation of a Gaussian random field to be smooth*[9] *and Morse with probability one are discussed in Sections 1.4.2 and 11.3 of [AT07] respectively. It would be interesting to know if the conditions given in the two sections are in fact necessary for the level sets to be smooth.*

Remark 6.2.4 *Note that under such regularity assumptions one could also derive expectation values of a whole range of geometric quantities on isodensity surfaces. These geometric quantities need to behave reasonably on the boundary of compact sets.*

[8] This result is also formulated in terms of a measure, that is for all values of f except a set of measure zero f does not contain a critical point. This measure theoretical result should not be confused with the probability that a realisation is smooth.

[9] We also touched upon differentiability in Section 4.2. However necessary and sufficient conditions are given in [AT07] for a realisation to be C^k on a compactum with probability one.

Summary and acknowledgements

Summary

This summary and the thesis is subdivided into two parts namely:

- Extrinsic and intrinsic triangulations
- Topology and the structure in the universe

The two parts reflect the nature of the project that gave rise to this thesis.

Extrinsic and intrinsic triangulations

To be able to sketch the context in which this research took place we introduce manifolds, triangulations and embeddings.

Surfaces

The reader will be familiar with surfaces that lie in three dimensional Euclidean space. The (boundary of) any every day object can be thought of as a surface. An interesting example of this is the surface of the Earth. It is interesting because we are familiar with two ways of picturing it. The first one is as lying in Euclidean space, here we think of a picture from space. The second way is by means of an atlas,[1] see Figure 1. A chart in an atlas is the result of a mapping from the surface of the earth to a flat piece of paper.

Let us now think of a more general surface. If a surface is not flat, which the surface of the Earth for example is not, some of the geometry gets lost as one maps a piece of the earth's surface to a flat piece of paper. The geometry of the original surface can be 'stored' in an abstract method using what is called a Riemannian metric.

If you have a chart with a Riemannian metric, then we can put our finger at an arbitrary point on the chart. We can then move our finger a bit in an

[1] For the younger reader; an atlas is like a printed version of Google Earth.

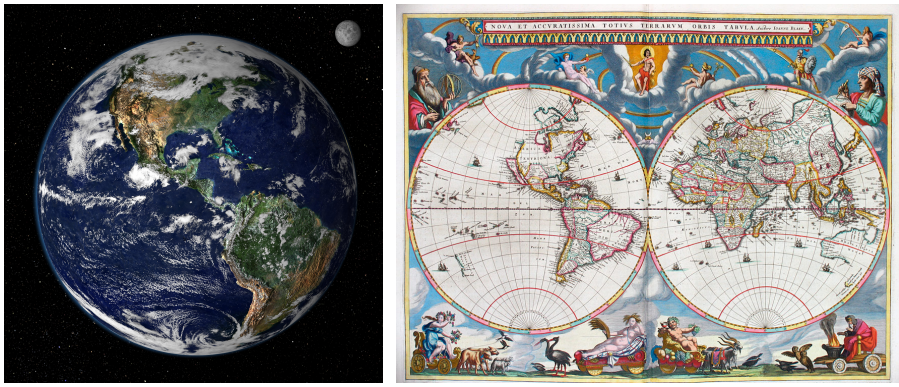

Figure 1: Left: The Earth as seen from space. Image reconstructed from data from NASA's Terra and GOES satellites by Reto Stöckli, Nazmi El Saleous, and Marit Jentoft-Nilsen.
Right: an image from the Blaeu atlas.

arbitrary direction on the chart. The Riemannian metric tells us what distance on the surface corresponds to the movement of our finger, see Figure 2. The Riemannian metric also 'stores' angles. One can use charts and the Riemannian metric to define surfaces, without the a priori need for a surfaces in Euclidean space.

It is important to note that any chart distorts the geometry. The Mercator projection for example preserves angles, but distorts area and length, while Peters projection preserves area, but distorts angles and lengths. The Riemannian metric's 'memory' is however perfect in that the geometry of the surface is completely encapsulated by it.

The Riemannian metric does not give us a unique way to reconstruct the way a surface is embedded in the Euclidean space. Let us make this clear by an example. Suppose we take a sheet of paper, lay it in front of us and draw a 5 centimetre long line on a sheet of paper and another 5 centimetre long line that intersects the former in the middle at an angle of $45°$. We can pick the sheet of paper up and bend it as if rolling it into a cylinder. This does not change the length of the lines nor the angle they make.

Both the flat sheet of paper in front of us and the bended version are 'embeddings' of the sheet of paper. To put it more abstractly the sheet of paper in front of us serves as a chart of both the bended piece we are holding and the piece itself, with the Riemannian metric given by the usual distances on a sheet of paper.

Because the Riemannian metric does not 'care' about the embedding it is

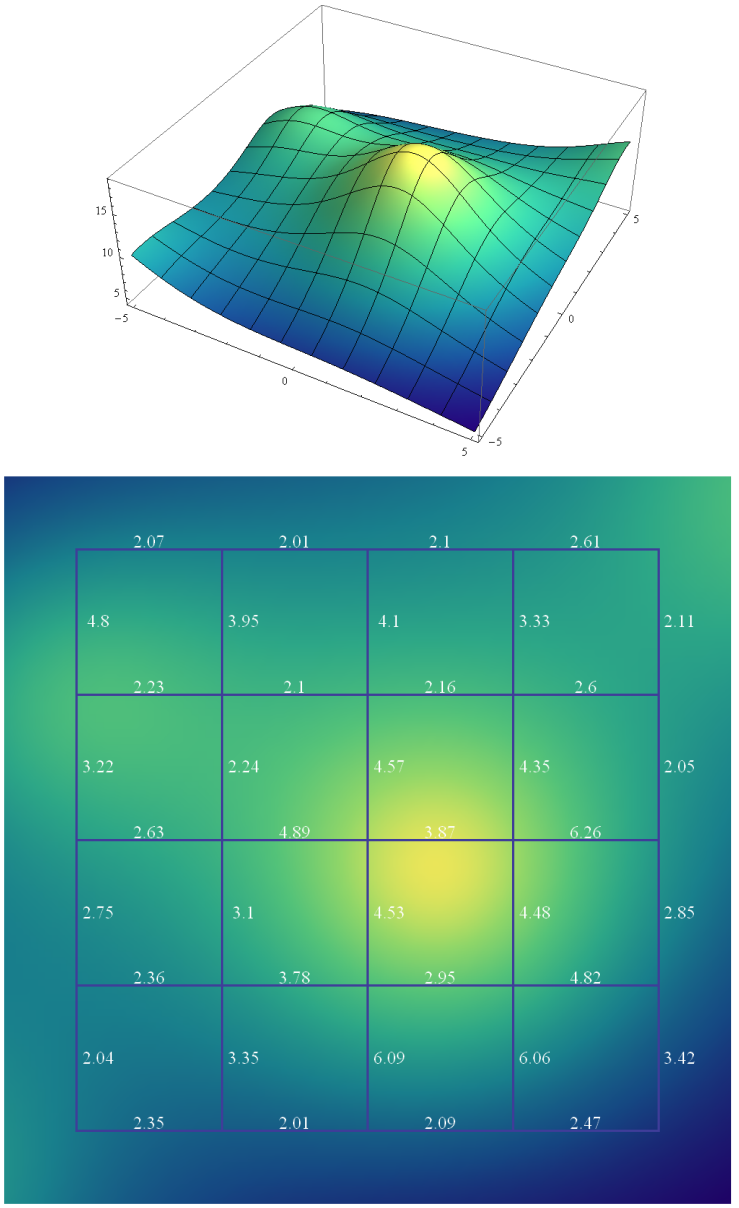

Figure 2: Above: a surface in Euclidean space. Below: A chart of the surface (found by vertical projection) with distances along the grid lines indicated.
A Riemannian metric can be thought of as an infinitely fine grid on such a map, with distances indicated, as well as information on the angles.

called intrinsic.

We have now described the two ways in which we view surfaces namely:

- Lying in Euclidean space. This is called an embedded surface. The space that surrounds the surface is called the ambient space.
- As given by a number of charts in an atlas, with a Riemannian metric.

Manifolds

Surfaces can be generalized to higher dimensional objects called manifolds, using the concept of charts in an atlas. The charts are in this setting segments of higher dimensional (Euclidean) space. The atlas of a three dimensional manifold, for example, would consist of a number of three dimensional 'boxes' that we would also call charts.

We can also generalize surfaces to manifolds by considering higher dimensional objects in large dimensional Euclidean space. For example, the two unit dimensional sphere in Euclidean space is given by the equation

$$x^2 + y^2 + z^2 = 1.$$

We can define a three dimensional unit sphere in four dimensions by the equation

$$x^2 + y^2 + z^2 + w^2 = 1. \tag{1}$$

Thanks to a result by Nash[2] the two ways to generalize a surface to a manifold are equivalent.

Triangles

Triangles are some of the elementary building blocks used in geometry. These building blocks can be generalized to higher dimensional simplices. A three dimensional simplex, for example, is a tetrahedron, see Figure 3.

The corners of a simplex are called vertices, lines connecting the vertices edges and the higher dimensional constituents faces.

We are interested in breaking up surfaces and manifolds into these elementary building blocks. This is called triangulating. We have considered two different ways in which we can triangulate:

[2]The recently diseased mathematician, known to the general audience because of the biographic film 'A beautiful mind'.

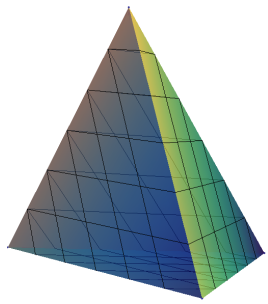

Figure 3: An elementary building block in three dimensions: a tetrahedron.

- We can view the surface as embedded in Euclidean space. In this setting the simplices are straight in the ambient space. We call it an *extrinsic triangulation*.
- We can view the surface as an abstract Riemannian manifold, that is without embedding. In this setting simplices are 'painted' on the surface and determined by the Riemannian metric. This is what we call an *intrinsic triangulation*.

Extrinsic triangulations

Most people that have been to the cinema in recent years, or own a television or a computer are familiar with extrinsic triangulations, because many computer images are build up from tiny (straight) triangles.

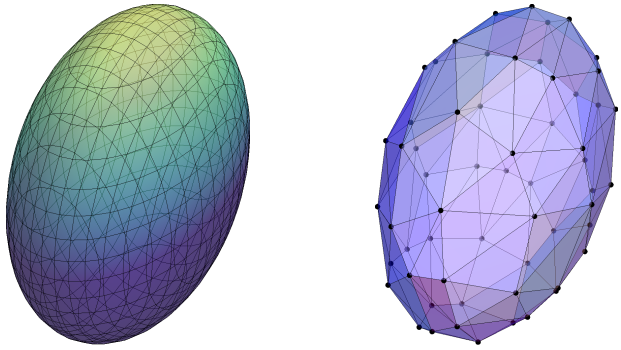

Figure 4: Left: an ellipsoid. Right: an extrinsic triangulation of the ellipsoid.

In our setting we shall assume that the surface to be captured on a screen is known and we want to approximate this surface by an extrinsic triangulation. One naturally would like to have realistic images. This means that the triangulation needs to be close to the given surface. The closeness of two surfaces will be given in term of the so-called Hausdorff distance d_H. The Hausdorff distance is a 'worst case scenario' distance between surfaces; it equals the maximum distance between the surface and the triangulation.

On the other hand we want to be efficient, by which we mean that we want to use as few vertices as possible. An optimal triangulation with m vertices is an extrinsic triangulation with m vertices such that d_H is as small as possible. It is clear that if we allow for more vertices we can achieve greater accuracy. We would like to think of the number of vertices as large. In the 1950s Fejes Tóth therefore suggested to look at

$$\frac{1}{A} = \lim_{m\to\infty} d_H m, \tag{2}$$

here m denotes the number of vertices, d_H is the Haussdorff distance (the measure for the accuracy of our approximation) and A is called the *Approximierbarkeit* or *approximation parameter*.

Expressions for the limit (2) and higher dimensional generalization of it are by now well understood if the surface (or manifold) is what we call convex. A surface is (locally) convex, if it is (locally) egg shaped, see Figure 5. A surface is (locally) non-convex if it is (locally) saddle shaped, see Figure 5.

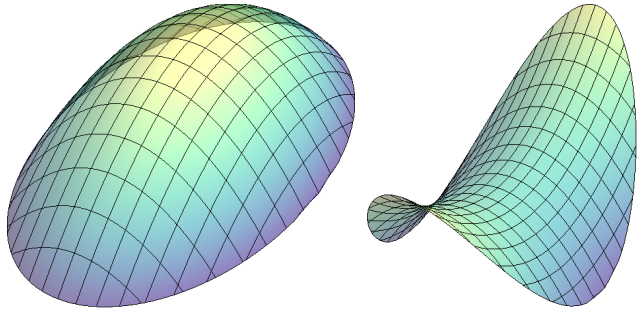

Figure 5: Left: An egg shaped convex surface. Right: A non-convex saddle.

The vertices of the triangulation can:

- lie on the surface (the triangulation of a convex surface is in this case called an inscribed polytope)
- be distributed such that the triangles touch the surface somewhere in the middle of the triangle (This is only possible if the surface is convex, the

triangulation of the convex surface is in this case called an circumscribed polytope)

- in general position, that is no constraint is given on the position of the vertices.

Our main results on extrinsic triangulations are as follows:

- We compare $\lim_{m\to\infty} d_H m$ for optimal triangulations of convex surfaces with the vertices on the surface to $\lim_{m\to\infty} d_H m$ for optimal triangulations of convex surfaces whose vertices are in general position. We find that they differ by a factor 2.
- We show that generally $\lim_{m\to\infty} d_H m$ depends on the embedding of the surface. To be precise we construct a sequence of embeddings E_k such that $\lim_{m\to\infty} d_H m$ for these embeddings increases roughly linearly with k. By a sequence of embeddings we mean that for each k we give a way for this Riemannian surface to be embedded in Euclidean space. Let us give a two dimensional example of such a sequence of embeddings. Suppose that we draw a number of loops, where each of the loops has the same length but are more and more curly. We have given an example in Figure 6. Our drawings are embeddings of the circle.

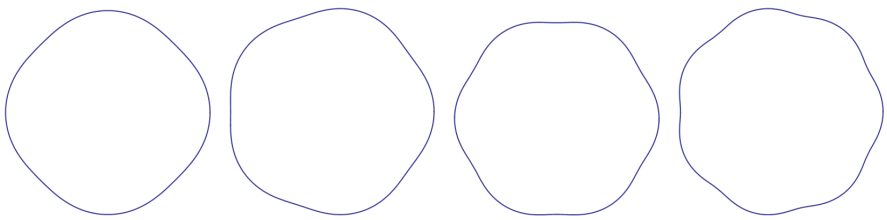

Figure 6: Elements in a sequence of embeddings of the circle in the plane.

- We study $\lim_{m\to\infty} d_H m$ for non-convex surfaces. This study involves the falsification of a claim by Fejes Tóth that $\lim_{m\to\infty} d_H m$ is zero for the one-sheeted hyperboloid. We find an expression for a lower bound on $\lim_{m\to\infty} d_H m$ for a large class of surfaces in three dimensional space, that can be attained. Finally we give an outline for a method to determine $\lim_{m\to\infty} d_H m$ for all surfaces in three dimensional space.

Intrinsic triangulations

For extrinsic triangulations we mainly focused on two dimensional surfaces. Our discussion of intrinsic triangles will consider arbitrary dimension. The fig-

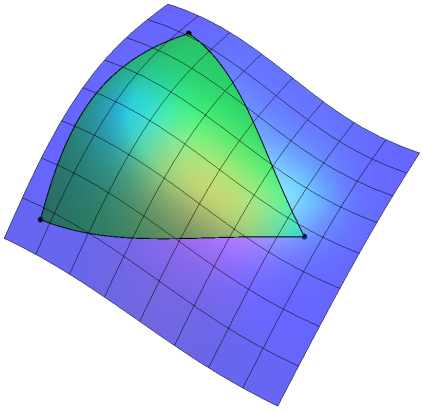

Figure 7: An intrinsic triangle on a surface.

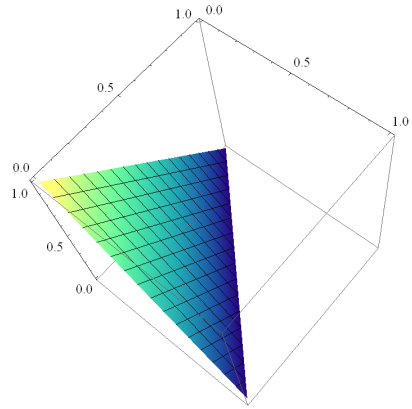

Figure 8: The two dimensional standard simplex.

ures we draw are however necessarily two dimensional, see for example Figure 7.

In Chapter 3 we introduce intrinsic simplices (triangles) and intrinsic triangulations. An intrinsic simplex is completely determined by the Riemannian structure on the manifold. The construction is based on so called Karcher means or Riemannian centres of mass. An intrinsic simplex is called non-degenerate if there is a 'nice' mapping from the standard simplex in Euclidean space to the intrinsic simplex. The two dimensional standard simplex is depicted in Figure 8. By 'nice' we mean that the map is one-to-one and the map is continuous in both directions. A mapping between a set A and a set B is called one-to-one if every point in A is mapped to a unique point in B and for every point in B there is a point in A that maps to it. A map is continuous if it has no sudden jumps.

The construction of intrinsic simplices has been studied before. We are the first to have treated the question of non-degeneracy in more than two dimensions, where the question is non-trivial.

We have also studied how one can subdivide a manifold into such intrinsic triangles, that is triangulate the manifold. Triangulations of manifolds were a topic of intense study from 1930 to 1960. The results gained in this period were based on the use of charts or embeddings. Because there is a freedom of choice in embeddings and charts, these classical results are not intrinsic.

The triangulations we consider are intrinsic, moreover we give explicit conditions on the shape and size of the triangles for these triangulations to exist.

Topology and the structure in the universe

The history of the universe

The history of our universe started with the big bang. In the beginning the universe was very hot and dense. After the big bang the universe immediately started to expand. As the universe expanded it also cooled down. This is comparable to bottle of deodorant that cools down if you empty it. However unlike a bottle of deodorant the universe does not have a nozzle, instead the volume increases as the universe evolves by the laws of General Relativity. Eventually the universe cooled down enough for it to become transparent.

The Cosmic Microwave Background

Before the universe became transparent is was very hot and glowed. Saying that the universe becomes transparent means (at quantum scale) that the light particles (photons) start to travel freely through the universe. Today we can still see the afterglow of the universe before it became transparent. This afterglow is called the Cosmic Microwave Background and has been measured, most recently by the Planck satellite, see Figure 9.

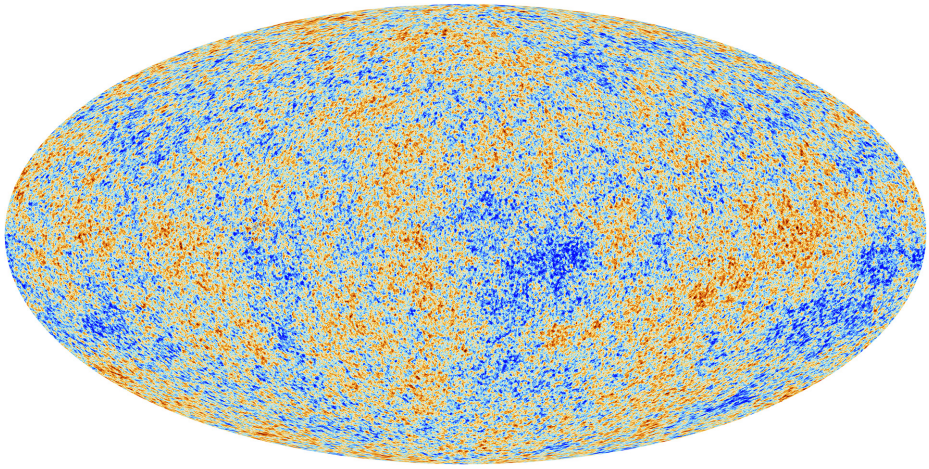

Figure 9: The Cosmic Microwave Background, as measured by Planck, after the removal of the foreground and artefacts. The deviations from the average lie between $-500\,\mu K$ (dark blue) and $500\,\mu K$ (dark red).

The temperature in the entire universe was almost the same when the universe became transparent. The deviation from the average temperature in the

Cosmic Microwave Background are well approximated by a so-called Gaussian random field. Cosmologists and theoretical physicists are interested in finding small aberrations from the predictions by Gaussian random fields in the Cosmic Microwave Background. These aberrations would be a unique source of information on the very early universe and could give insight in fundamental theories of nature.

Topology

Topology gives us tools that can help to detect these aberrations. Topology is the branch of mathematics concerned with the properties of spaces that are preserved under continuous deformations such as stretching and bending, but not tearing.

The tools require some explanation. We shall concentrate on the surface of equal temperature in the universe, at the time when the universe became transparent. This can be compared with lines of equal pressure studied by meteorologists and featured in almost every weather report, see for example Figure 10.

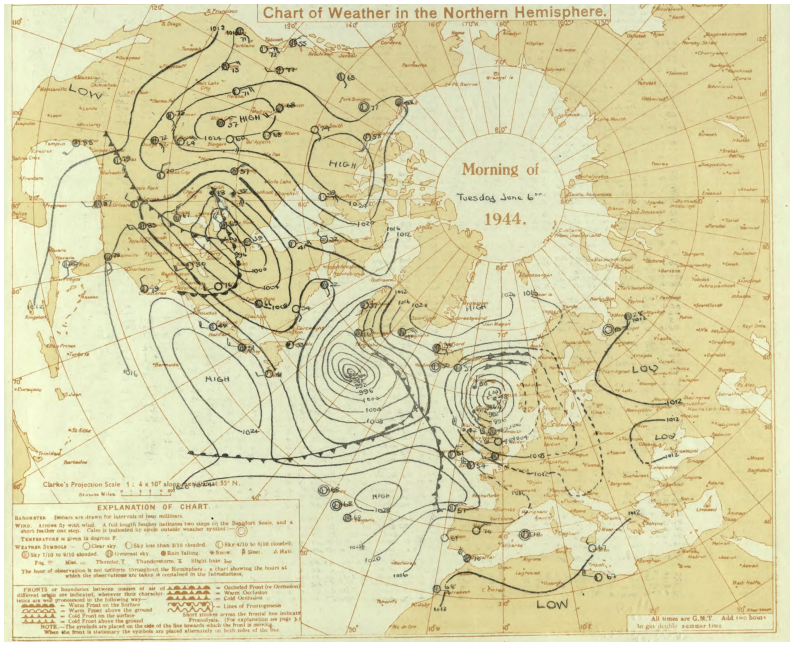

Figure 10: The weather map for D-Day, with isobars indicated. Courtesy of the Meteorological office, Air ministry, United Kingdom.

The surface of equal temperature can have multiple connected components. Just like there may be several high pressure areas each enclosed by lines of equal pressure. The number of connected components is a topological invariant, because it is preserved under continuous deformations.

Another topological invariant is the Euler characteristic χ. The Euler characteristic of a surface with a single connected component is given by

$$\chi = 2 - 2g,$$

with g the number of holes. See Figure 11 for an illustration. The Euler characteristic of a surface with multiple connected components is the sum of the Euler characteristic for the individual parts.

The Euler characteristic can be found by using the Gauss-Bonnet theorem. The Gauss-Bonnet theorem says that the integral of a local geometric property called the Gauss curvature equals the Euler characteristic. This is remarkable because it relates local geometry to the global topological properties of the surface.

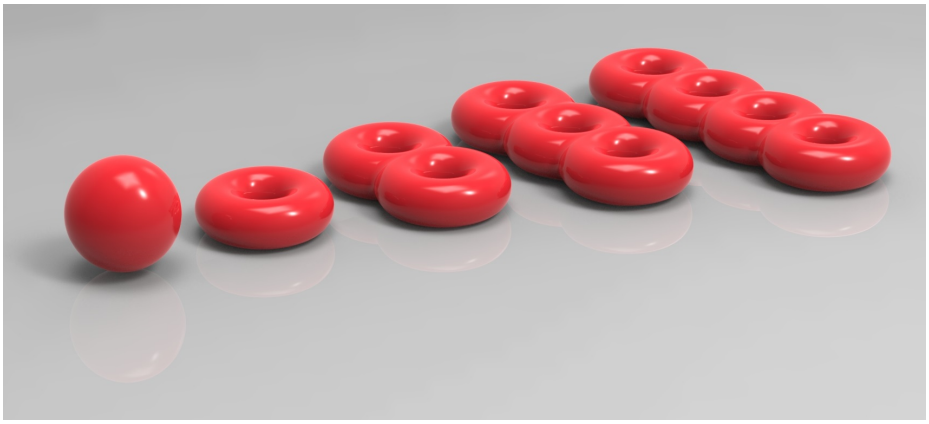

Figure 11: Surfaces with zero, one, two, three and four holes and therefore Euler characteristic 2, 0, -2, -4 and -6.

Numerical studies

The topological invariants of the surfaces of equal temperature in the universe help to characterize the deviations from the average and thus detect the aberrations from the Gaussian random field. These studies are at the moment being carried out by (among others) cosmologists, using numerical methods.

Numerical studies are absolutely necessary

In this thesis we prove that the result of the Gauss-Bonnet theorem is unique. By this we mean that the Euler characteristic is the only topological invariant that can be found by integrating a local geometric quantity. This implies that we really need numerical methods to study the topological invariants of surfaces of equal temperature in the universe. Even stronger, we can in general not even hope to find an estimate (based on the local geometry) for the number of connected components of the surfaces of equal temperature in the universe.

Samenvatting

Zowel dit proefschrift als deze samenvatting vallen uiteen in twee delen, namelijk:

- Extrinsieke en intrinsieke triangulaties
- Topologie en de structuur in het heelal.

Deze onderverdeling is het gevolg van de aard van het project waarbinnen het onderzoek heeft plaatsgevonden.

Extrinsieke en intrinsieke triangulaties

Om ons onderzoek te kunnen beschrijven introduceren wij variëteiten, triangulaties en inbeddingen.

Oppervlakken

De lezer is ongetwijfeld bekend met oppervlakken die in de drie dimensionale Euclidische ruimte liggen. De (randen van) alledaagse oppervlakken kunnen als dusdanig beschouwd worden. Een voorbeeld van zo'n oppervlak is het aardoppervlak. Dit oppervlak neemt een bijzondere plaats in omdat wij gewend zijn het op twee verschillende manieren te beschouwen: Ten eerste kunnen wij de aarde zien als oppervlak in de Euclidische ruimte, denk aan een foto van de aarde genomen vanuit de ruimte. Ten tweede bestuderen wij de aarde door middel van een atlas[1], zie Figuur 1. Een kaart is een afbeelding van het aardoppervlak op een vlak stuk papier.

Laat ons nu een willekeurig oppervlak beschouwen. Als een oppervlak niet plat is, zoals het aardoppervlak dat ook niet is, dan gaat meetkundige informatie verloren in de afbeelding van het oppervlak naar het platte stuk papier, de

[1] Voor de jongere lezer; een atlas is grof gezegd een geprinte versie van Google Earth.

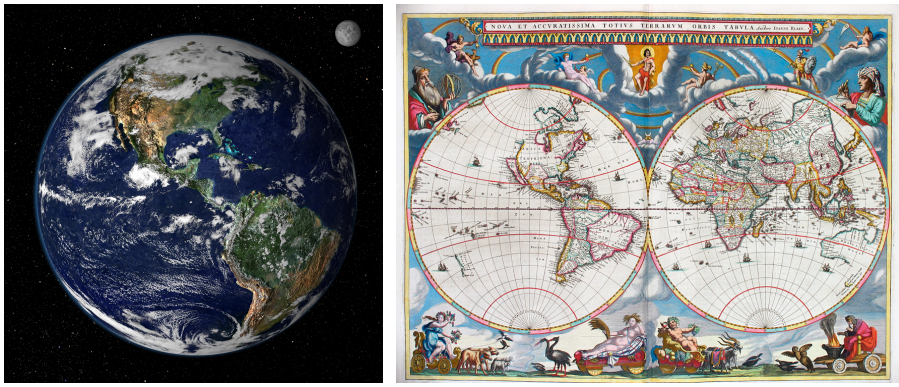

Figuur 1: Links: De aarde zoals gezien vanuit de ruimte. Beeld samengesteld uit data van NASA's Terra en GOES satellieten door Reto Stöckli, Nazmi El Saleous, en Marit Jentoft-Nilsen.
Rechts: een kaart uit de Blaeu atlas.

kaart. De meetkunde van het oorspronkelijke oppervlak kan echter opgeslagen worden met behulp van de Riemannse metriek.

Als je een vinger op een kaart plaatst waarop een Riemannse metriek gedefinieerd is en vervolgens je vinger in willekeurige richting beweegt, dan vertelt de Riemannse metriek met welke afstand op het oppervlak de beweging van je vinger overeenkomt, zie Figuur 2. De Riemannse metriek 'onthoudt' ook hoeken.

Je kunt oppervlakken definiëren met behulp van kaarten en de Riemannse metriek zonder uit te gaan van een oppervlak in Euclidische ruimte.

Zoals bekend verstoort iedere platte kaart van een stuk aaroppervlak de meetkunde van de aardbol. De Mercator projectie, bijvoorbeeld, behoudt hoeken, maar oppervlakten en lengten worden niet correct weergegeven. Dit in tegenstelling tot de Peters projectie, die oppervlak behoudend is, maar hoeken en afstanden verstoort. Het 'geheugen' van de Riemannse metriek is echter perfect, waarmee wij bedoelen dat alle meetkunde hiermee wordt vastgelegd, zij het op een abstracte manier.

De Riemannse metriek geeft ons echter geen unieke methode waarmee wij een oppervlak in de Euclidische ruimte kunnen construeren die door deze metriek beschreven wordt. Wij willen dit illustreren met behulp van een voorbeeld. Stel wij nemen een vel papier en tekenen hierop twee lijnen van 5 centimeter ieder, die elkaar in het midden snijden onder een hoek van $45°$. Wij kunnen nu het vel oppakken en buigen alsof wij het tot een cilinder willen rollen. Dit beïnvloedt de afstanden en de hoeken op het papier niet.

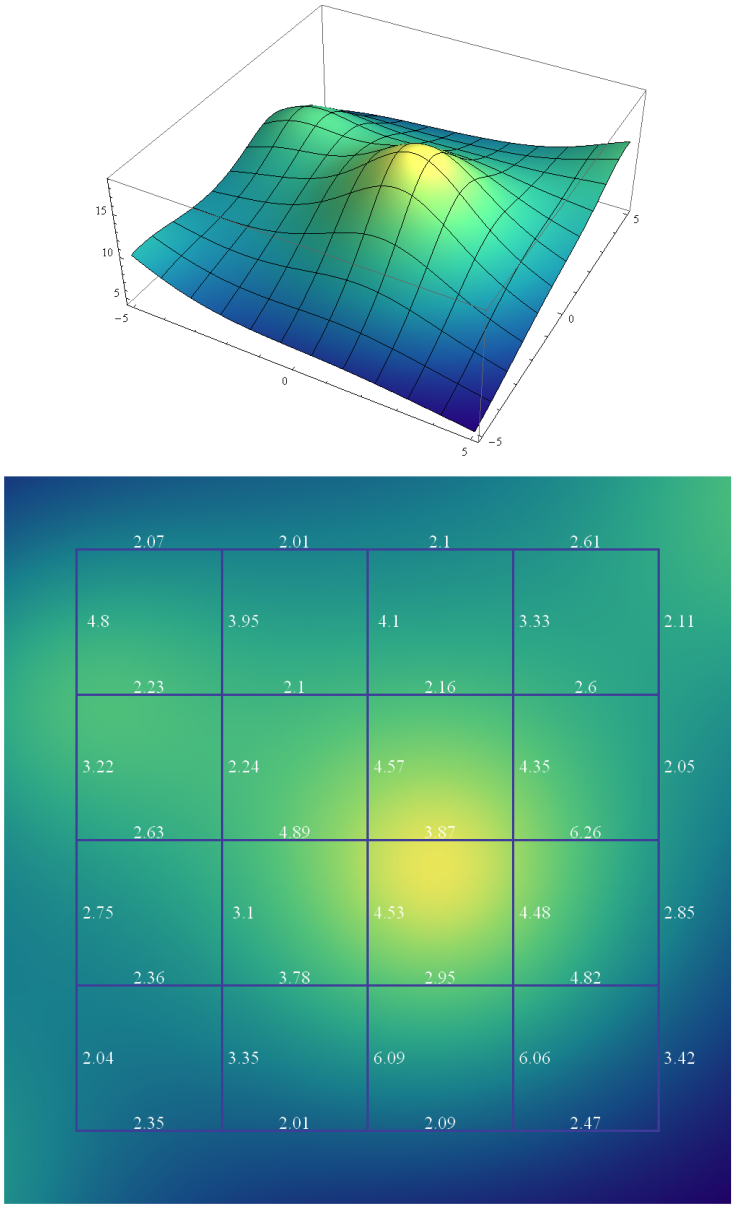

Figuur 2: Boven: Een oppervlak in de Euclidische ruimte. Beneden: Een kaart van het oppervlak (zoals gevonden door verticale projectie) met daarin afstanden langs de rasterlijnen aangegeven.
Een Riemannse metriek kan beschouwd worden als een oneindig fijne versie van zo'n raster, waarbij de afstanden zijn aangegeven, in combinatie met informatie over de hoeken.

Zowel het platte vel papier als de gebogen versie zijn inbeddingen van het vel papier in de ruimte. Anders gezegd het vlakke vel papier dient als kaart voor zowel zichzelf als de gebogen versie, met de gebruikelijke afstanden.

Omdat de Riemannse metriek onafhankelijk is van de inbedding wordt hij intrinsiek genoemd.

Samenvattend beschouwen wij oppervlakken dus op twee verschillende wijzen:

- Liggend in de Euclidische ruimte. Dit wordt een ingebed oppervlak genoemd. De ruimte, die het oppervlak bevat, heet de omgevingsruimte.
- Gegeven door middel van kaarten en een Riemannse metriek.

Variëteiten

Oppervlakken kunnen met behulp van kaarten gegeneraliseerd worden tot hoger dimensionale objecten die variëteiten worden genoemd. De kaarten in dit voorbeeld zijn stukken uit hoger dimensionale ruimte. De atlas van een drie dimensionale variëteit bestaat bijvoorbeeld uit drie-dimensionale 'dozen' die wij ook kaarten noemen.

Tevens kunnen zij oppervlakken generaliseren door hoger dimensionale objecten in Euclidische ruimte van nog hogere dimensie te beschouwen. Bijvoorbeeld, de twee dimensionale sfeer in drie dimensionale Euclidische ruimte wordt beschreven door de vergelijking

$$x^2 + y^2 + z^2 = 1.$$

Op dezelfde wijze kunnen wij een drie dimensionale sfeer in vier dimensionale Euclidische ruimte beschrijven:

$$x^2 + y^2 + z^2 + w^2 = 1. \tag{1}$$

Dankzij een resultaat van Nash[2] weten wij dat beide veralgemeniseringen van oppervlakken naar variëteiten equivalent zijn.

Driehoeken

Driehoeken zijn enkele van de elementaire bouwstenen die in de meetkunde worden gebruikt. Deze bouwstenen kunnen gegeneraliseerd worden naar simplices. Een drie dimensionale simplex, bijvoorbeeld, is een tetraëder zie Figuur 3.

[2]De recentelijk overleden wiskundige, bekend bij het grote publiek dankzij de film 'A beautiful mind'.

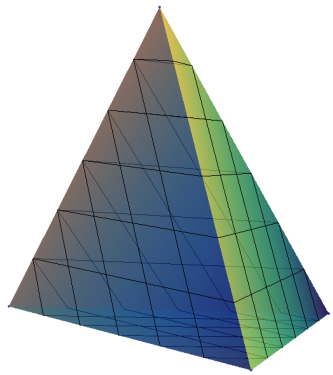

Figuur 3: Een drie-dimensionale elementaire bouwsteen: een tetraëder.

De hoekpunten van een simplex worden vertices genoemd, de lijnen die de vertices verbinden zijden en de hoger dimensionale onderdelen facetten.

Wij zijn geïnteresseerd in het opdelen van oppervlakken en variëteiten in deze elementaire bouwstenen. Dit opdelen wordt trianguleren genoemd. Wij hebben triangulaties op twee verschillende manieren opgevat:

- In het eerste geval gaan wij uit van een oppervlak ingebed in de Euclidische ruimte. In deze context zijn de simplices recht in de Euclidische omgevingsruimte. Wij noemen dit een *extrinsieke triangulatie*.

- In het tweede geval beschouwen wij een oppervlak als een abstracte Riemannse variëteit, dat wil zeggen zonder omliggende ruimte. In deze context zijn de simplices op het oppervlak 'geschilderd' op een wijze bepaald door de Riemannse metriek. Dit is wat wij een *intrinsieke triangulatie* noemen.

Extrinsieke triangulaties

Diegenen die de afgelopen jaren in een bioscoop zijn geweest, of een werkende televisie of een computer hebben gezien, zijn bekend met extrinsieke triangulaties. Dit komt omdat veel van de beelden die met behulp van een computer zijn gegenereerd zijn opgebouwd uit kleine (rechte platte) driehoeken.

Wij zullen in deze context aannemen dat het oppervlak gegeven is en dat wij dit oppervlak door een extrinsieke triangulatie benaderen. Wij willen graag nauwkeurige computeranimaties hebben. Dit betekent dat de triangulatie dichtbij het oppervlak moet liggen. Dichtbij wordt hier geïnterpreteerd in termen van

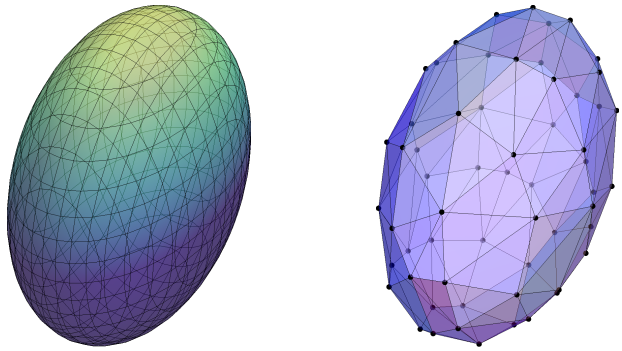

Figuur 4: Links: een ellipsoïde. Rechts: Een extrinsieke triangulatie van deze ellipsoïde

de Hausdorff afstand d_H. De Hausdorff afstand gaat uit van de slechtst mogelijke optie, het is de grootst mogelijke afstand tussen punten op het oppervlak en de triangulatie.

Tevens willen wij efficiënt zijn, waarmee wij bedoelen dat wij zo min mogelijk vertices gebruiken. Een optimale triangulatie met m vertices is een extrinsieke triangulatie met m vertices zodanig dat d_H zo klein mogelijk is. Het is duidelijk dat als wij meer vertices toelaten, dat dan de benadering preciezer kan. Wij zullen er ook vanuit gaan dat het aantal vertices groot is. In de jaren vijftig van de vorige eeuw heeft Fejes Tóth daarom voorgesteld om

$$\frac{1}{A} = \lim_{m \to \infty} d_H m, \tag{2}$$

te beschouwen, hier is m het aantal vertices. A wordt de *Approximierbarkeit* of de *approximatie parameter* genoemd.

Uitdrukkingen voor de limiet (2) en zijn hoger dimensionale generalisaties zijn bekend als het oppervlak (of de variëteit) convex is. Een oppervlak is (lokaal) convex, als het (lokaal) eivormig is, zie Figuur 5.

Verder willen wij een onderscheid aanbrengen gebaseerd op de posities van de vertices die wij toestaan. De vertices van een triangulatie kunnen:

- op het oppervlak liggen (indien het oppervlak convex is wordt er hier vaak gesproken van een ingeschreven polytoop)
- zo verdeeld zijn dat de simplices aan het oppervlak raken (Dit is alleen mogelijk als het oppervlak convex is, in dit geval wordt er gesproken van een omgeschreven polytoop)

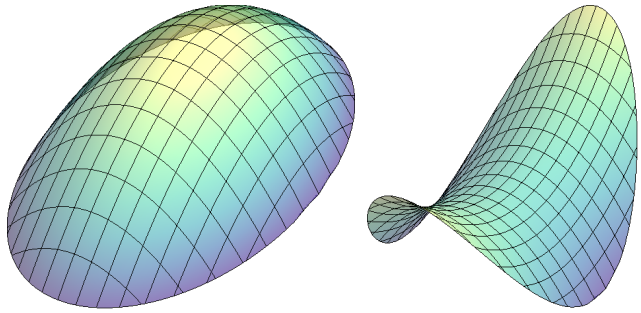

Figuur 5: Links: een eivormig (convex) oppervlak. Rechts: een (niet-convex) zadel.

- in algemene positie innemen, dat wil zeggen dat er geen eisen worden opgelegd.

De voornaamste resultaten die wij hebben geboekt aangaande extrinsieke resultaten zijn:

- Wij vergelijken $\lim_{m\to\infty} d_H m$ voor optimale triangulaties van convexe oppervlakken waarbij wij eisen dat de vertices op het oppervlak liggen met $\lim_{m\to\infty} d_H m$ voor optimale triangulaties van convexe oppervlakken waarbij wij geen eis opleggen aan de positie van de vertices. Het verschil blijkt een factor 2 te zijn.
- Wij tonen aan dat in het algemeen $\lim_{m\to\infty} d_H m$ afhankelijk is van de inbedding van het oppervlak. Om precies te zijn, construeren wij een serie van inbeddingen E_k zodat $\lim_{m\to\infty} d_H m$ grofweg lineair is met k. Met een serie van inbeddingen bedoelen wij dat voor elke k een inbedding geven van het Riemannse oppervlak in een hoger dimensionale Euclidische ruimte.

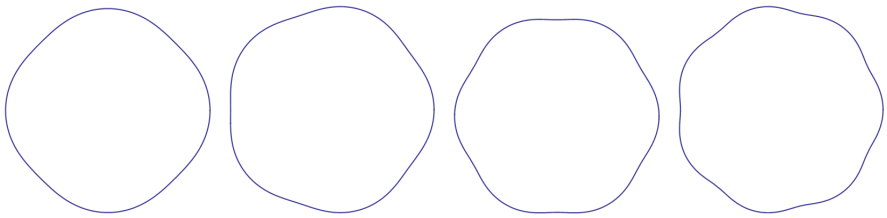

Figuur 6: De elementen in een serie inbeddingen van de cirkel in het twee dimensionale vlak.

Laat ons een twee dimensionaal voorbeeld geven van zo'n serie van inbeddingen. Stel dat wij een aantal lussen tekenen, die zichzelf niet doorsnijden, allen de zelfde lengte hebben, maar steeds golvender worden, zie Figuur 6. Deze tekeningen zijn inbeddingen van de cirkel.

- Wij bestuderen $\lim_{m\to\infty} d_H m$ voor niet convexe oppervlakken. In het bijzonder falsificeren wij een claim van Fejes Tóth die zegt dat $\lim_{m\to\infty} d_H m$ nul is voor de hyperboloïde met een samenhangs component. Tevens vinden wij een uitdrukking voor een ondergrens voor $\lim_{m\to\infty} d_H m$ voor een grote klasse oppervlakken in de drie dimensionale Euclidische ruimte. Tenslotte geven wij een methode om $\lim_{m\to\infty} d_H m$ voor alle oppervlakken in de drie dimensionale Euclidische ruimte te bepalen.

Intrinsieke triangulaties

Wat betreft extrinsieke triangulaties hebben wij ons voornamelijk gericht op twee dimensionale oppervlakken, terwijl wij ons in the geval van intrinsieke triangulaties willekeurige dimensie toestaan. Noodzakelijkerwijs moeten wij ons beperken tot het tekenen van twee dimensionale figuren, zie bijvoorbeeld Figuur 7.

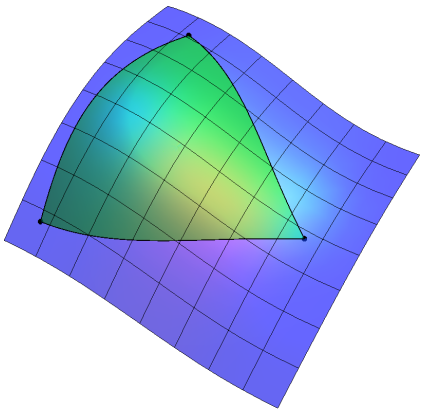

Figuur 7: Een intrinsieke driehoek op een oppervlak.

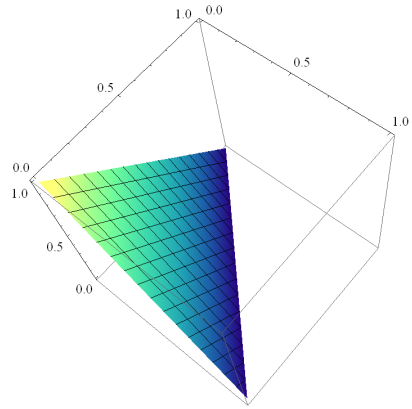

Figuur 8: De twee dimensionale standaard-simplex.

In Hoofdstuk 3 bespreken wij intrinsieke simplices (de veralgemeniseerde driehoeken) en intrinsieke triangulaties. Een intrinsieke simplex is een simplex die volledig door de Riemannse structuur op de variëteit is bepaald. De constructie is gebaseerd op Karcher gemiddelden of Riemannse massa middelpunten. Een intrinsieke simplex wordt niet-gedegenereerd genoemd als er een

'fraaie' afbeelding bestaat van de standaard-simplex in Euclidische ruimte naar de intrinsieke simplex. De twee dimensionale standaard-simplex is afgebeeld in Figuur 8. Met een 'fraaie' bedoelen wij een een-op-een afbeelding die continu is in beide richtingen. Een afbeelding van de verzameling A naar de verzameling B is een-op-een als er ieder punt in A op een uniek punt in B wordt afgebeeld en er voor ieder punt in B een orgineel in A te vinden is. Een afbeelding is continu als er geen sprongen zijn.

De constructie van intrinsieke simplices is bekend. Wij zijn echter de eersten die niet-gedegenereerdheid behandelen in meer dan twee dimensies, waar dit een niet triviaal vraagstuk is.

Wij bestuderen ook het opdelen van variëteiten in zulke intrinsieke simplices, dat wil zeggen het trianguleren van een variëteit. Triangulaties van variëteiten zijn in het verleden uitgebreid bestudeerd, met name van 1930 tot 1960. In de studies die toen zijn uitgevoerd gebruikte men echter altijd inbeddingen of expliciete kaarten, dit betekent dat er sprake was van keuzevrijheid, wat weer betekent dat de triangulaties niet intrinsiek waren. De triangulaties die wij onderzoeken zijn dat wel, bovendien geven wij expliciete voorwaarden waar de individuele driehoeken qua vorm en grootte aan moeten voldoen.

Topologie en de structuur van het universum

De geschiedenis van het universum

Het universum is begonnen met de Oerknal. Het vroege universum was heet en dicht. Direct na de Oerknal begon het universum uit te dijen. Door de uitdijing koelde de materie in het universum af. Dit werkt volgens hetzelfde principe als de afkoeling van een fles deodorant door deze leeg te spuiten. Het universum heeft in tegenstelling tot de fles deodorant geen spuitstuk. Het volume van het universum neemt toe omdat het evalueert volgens de wetten van de algemene relativiteitstheorie. Door de uitdijing van het universum werd de materie in het universum uiteindelijk voldoende verdund en afgekoeld om doorzichtig te worden.

De kosmische achtergrond straling

Voordat de materie in het universum transparant werd was de materie erg heet en gloeide. De transparantie van het universum betekent op zeer kleine schaal dat de licht deeltjes (fotonen) vrij door het universum begonnen de bewegen. Hieruit volgt dat wij op dit moment de nagloed van het nog niet transparante universum kunnen zien. Deze nagloed wordt de kosmische achtergrond straling genoemd en is geobserveerd, meest recentelijk door de Planck satelliet, zie Figuur 9.

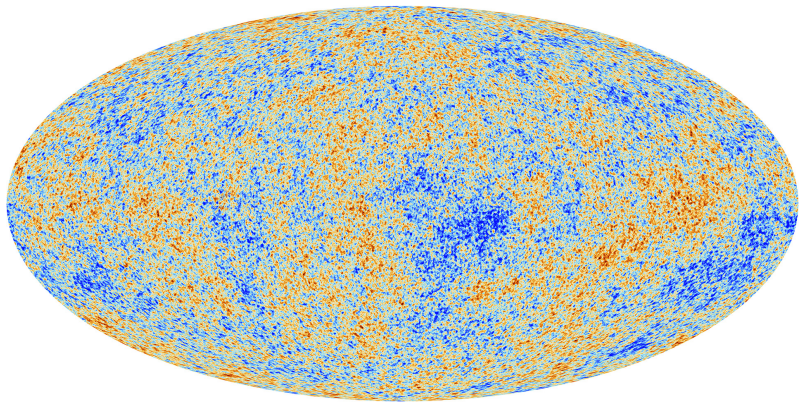

Figuur 9: De kosmische achtergrond straling, zoals gemeten door de Planck satelliet, na verwijdering van objecten op de voorgrond en artefacten. De afwijkingen van het gemiddelde liggen tussen de $-500\,\mu K$ (donker blauw) en $500\,\mu K$ (donker rood).

De temperatuur was nagenoeg constant in het vroege universum. De kleine variaties in de temperatuur van de kosmische achtergrond straling kunnen goed beschreven worden met behulp van een zogenaamd Gaussisch stochastisch veld. Cosmologen en theoretisch natuurkundigen zijn geïntereseerd in afwijkingen van deze variaties in de temperatuur van de kosmische achtergrond straling van de voorspelling door een Gaussisch stochastisch veld. Deze afwijkingen zouden een unieke bron van informatie over het vroege universum zijn en geven mogelijk inzicht in de fundamentele natuurwetten.

Topologie

Topologie geeft ons methoden om de afwijkingen te detecteren. Topologie is de tak van wiskunde die gaat over de eigenschappen van ruimten die behouden blijven onder continue deformaties, zoals buigen en strekken, maar niet scheuren.

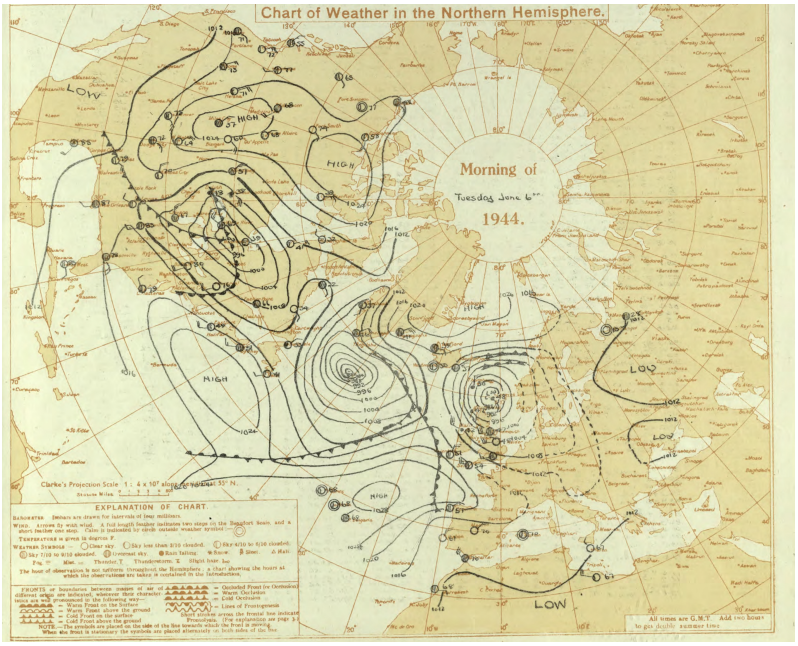

Figuur 10: De weerkaart voor D-Day met isobaren. Met dank aan the Meteorological office, Air ministry, Verenigd Koninkrijk .

Dit vergt enige uitleg. Wij zullen ons concentreren op oppervlakten van gelijke temperatuur in het vroege universum. Deze oppervlakken kunnen verge-

leken worden met de isobaren, waarmee we bekend zijn vanwege het weerbericht.

Een oppervlak van gelijke temperatuur kan meerdere samenhangscomponenten hebben. Dit is te vergelijken met het bestaan van meerdere hogedrukgebieden, elk omgeven door lijnen van gelijke druk. Het aantal samenhangscomponenten is een topologische invariant, omdat deze behouden is onder continue deformaties.

Een andere topologische invariant is de Euler karakteristiek χ. De Euler karakteristiek van een oppervlak met een enkele samenhangscomponent wordt gegeven door

$$\chi = 2 - 2g,$$

waar g het aantal gaten is. Wij hebben de Euler karakteristiek geïllustreerd in Figuur 11. De Euler karakteristiek van een oppervlak met meerdere samenhangscomponenten is de som van de Euler karateristieken van de individuele samenhangscomponenten.

De Euler karakteristiek kan berekend worden door gebruik te maken van de stelling van Gauss-Bonnet. De stelling van Gauss-Bonnet vertelt ons dat de integraal van de Gauss kromming, een lokale meetkundige grootheid, de Euler karakteristiek geeft. Deze stelling is opmerkelijk omdat het een relatie geeft tussen een lokale (meetkundige) grootheid en een globale (topologische) grootheid.

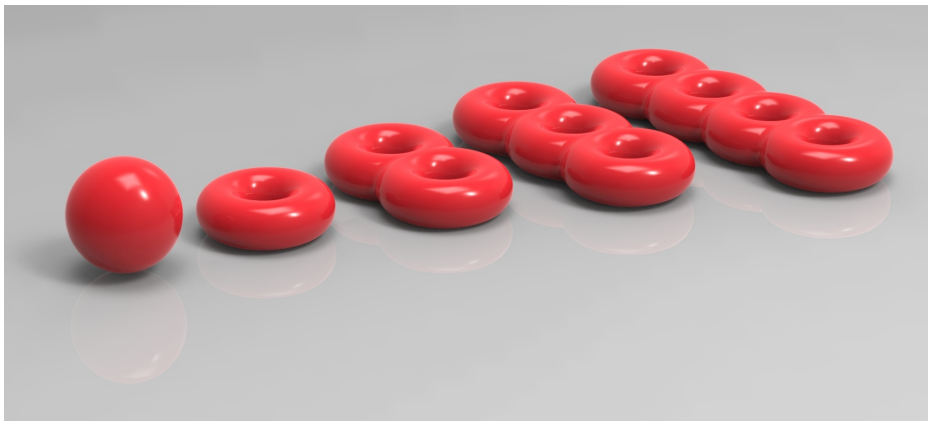

Figuur 11: Oppervlakken met nul, een, twee, drie en vier gaten en daarom Euler karakteristiek 2, 0, -2, -4 en -6., respectievelijk.

Numerieke resultaten

De topologische invarianten van oppervlakken van gelijke temperatuur in het universum helpen de kleine variaties in de temperatuur te karakteriseren. Hierdoor is het in de nabij toekomst wellicht mogelijk om afwijkingen van de voorspellingen gedaan door een Gaussisch stochastisch veld te detecteren.

De noodzaak van numerieke methoden

In dit proefschrift bewijzen wij dat de stelling van Gauss-Bonnet uniek is. Hiermee bedoelen wij dat de Euler karakteristiek de enige topologische invariant is die gevonden kan worden door lokale meetkundige grootheden te integreren. Dit betekent dat de numerieke studies echt noodzakelijk zijn om inzicht te verschaffen in de topologie van een Gaussisch stochastisch veld, en dus in de temperatuurverdeling in het vroege universum. Sterker nog, wij laten zien dat er zelfs geen nauwkeurige afschattingen van het aantal samenhangscomponenten mogelijk zijn.

Appendix: Computational Geometric Learning

The European Union-project: Computational Geometric Learning

The research presented in this thesis has been conducted in the context of the 7th Framework Programme for Research of the European Commission, under FET-Open grant number 255827.

FET-Open grant number 255827 was awarded to a project named Computational Geometric Learning. The main motivation given in the proposal was:
'At the heart of this project is the insight that most data are structured, although this intrinsic geometric structure is often not easy to capture. The long-term vision is to have efficient and reliable methods for geometric data analysis that find and exploit hidden structure and by that lead to fast and robust geometric data processing in high dimensions. In this project, we aim at laying the foundations of a new field computational geometric learning that provides efficient and reliable methods for geometric data analysis.'

Partners

The partners of the Computational Geometric Learning project were:

- Friedrich-Schiller-Universität Jena
- Eidgenössische Technische Hochschule Zürich
- Freie Universität Berlin
- Technische Universität Dortmund
- Institut national de recherche en informatique et en automatique
- National and Kapodistrian University of Athens

- Tel Aviv University
- Rijksuniversiteit Groningen

Work Packages

The project was subdivided into several work packages:

1. Geometric inference and approximation
2. Fundamental data structures and algorithms for high-dimensions
3. Modelling high-dimensional geometric structures in science and engineering

The Rijksuniversiteit Groningen participated in work packages 1 and 3.

Our focus within work package 1 was the approximation of embedded surfaces and manifolds. This is the topic of the first part of this thesis. Chapter 2 considers surfaces and Chapter 3 treats triangulations of manifolds.

Within work package 3 the Rijksuniversiteit Groningen focussed on the topology of geometric patterns in the large scale structure of the universe. The study of these patterns is almost exclusively numerical in nature. In the second part of this thesis we show that analytic results cannot be expected and thus these numerical results are necessary.

Appendix: Publications

The following parts of this thesis have been published or have been accepted for publication in journals or conference proceedings:

Section 2.2 is published as:
M.H.M.J.Wintraecken and G.Vegter. On the Optimal Triangulation of Convex Hypersurfaces, Whose Vertices Lie in Ambient Space. *Mathematics in Computer Science, Online, 2014*

Sections 3.1- 3.3 and 3.5- 3.9 have been accepted for publication at Geometriae Dedicata, a conference version has been accepted for *SOCG2015*, both as:
R.H. Dyer, G.Vegter and M.H.M.J.Wintraecken. Riemannian Simplices and Triangulations.

Chapter 5 has appeared as:
M.H.M.J.Wintraecken and G.Vegter. A geometrical take on invariants of low-dimensional manifolds found by integration. *Topology and its Applications, 160: 2175 - 2182, 2013*

Workshop contributions have been given at EUROCG13 and EUROCG14.

Acknowledgements

Many people contributed to this thesis, either directly or indirectly, which I hope to reflect below. However, I am well aware that my list is not all inclusive nor can it do justice in all cases.

First of all I would like to thank Gert Vegter and Rien van de Weijgaert for making this thesis possible, your encouragement in writing and your efforts to turn me into an independent researcher. Gert, you are perhaps the most optimistic person I've ever met, and I appreciate you greatly for it. Rien, your general interest and knowledge makes you as close to a 'uomo universale' as modern man can be, which I greatly admire.

I am greatly indebted to Ramsay Dyer for an intensive collaboration that is reflected in the third chapter of this thesis, but certainly is not limited to that part of the thesis.

I thank Bernard Jones for his encouragement and discussions on all things ranging from the history of science to Ricci flows.

The efforts of the members of the assessment committee, Henk Broer, Jean-Marie Morvan and John Sullivan are greatly appreciated.

I am truly grateful to the European taxpayer for paying my wages, via FET-Open grant number 255827 (CGL-Computational Geometry Learning).

I further thank the following people for their direct involvement:
Niels Bos for his graphics and design work, discussions and supporting me as a paranimf,
Vladimír Krajňák for supporting me as a paranimf,
Dror Atariah and Günther Rote for hospitality and discussions which let to great improvements to the second chapter of this thesis,
Jaap Top for always being available to bounce an idea on, to proofread short texts and offer advice,
Alef Sterk for proofreading many an introduction,
Erik van den Ban for discussion and suggestions on Chapter 5,
Pratyush Pranav for his collaboration on a number of projects, that are not part of this thesis,

Aernout van Enter for discussions, pointing out [Sim79], and proofreading the section on Gaussian random fields,
Shmuel Weinberger for pointing out [KKNO73],
Robert Adler for sharing his vast knowledge of the literature on Gaussian random fields,
Marius Crainic for illuminating [Gil84],
Sietse Ringers, whose help with LaTeX and computers in general is greatly appreciated,
Hans Duistermaat, without whom I most probably would not have started,
Bas Heijne and Peter Dickinson for discussions,
Johan Hidding and Patrick Bos for collaboration and discussions,
Jean-Daniel Boissonnat for hospitality,
Arijit Ghosh, for discussions in particular with respect to Chapter 3,
Stefan von Deylen for pointing out the work of Sander [San12] and giving insight into his thesis work,
David Cohen-Steiner for pointing out [DS91],
Miriam Dür for her involvement in my thesis,
Joep van den Beuken for proofreading the summary,
Arthemy Kiselev for use of his knowledge of Russian,
Kerstin Bunte and Andrey Krutov for sharing templates for a thesis,
a number of anonymous reviewers for their helpful comments,
Herbert Edelsbrunner, Wojciech Hellwing, Michael Kerber, Changbom Park and Monique Teillaud for collaboration on various projects not reflected in this thesis,
all collaborators in the CGL-project,
the family of the late Floris Takens for the books they gave,
the support staff in the Bernoulliborg.

During my stay in Groningen I was fortunate to be involved in the theses of David de Laat, Job Feldbrugge, Keimpe Nevenzeel, Matti van Engelen, Mirjam Soeten and Sanne Jonker, which was interesting and enjoyable.

Apart from a number of people already mentioned, I would also like to thank Adriána Szilágyiová, Afzal Soomro, Amit Chattopadhyay, Ane Anema, Anne Tuijp, Anneroos Everts, Bolor Jargalsaikhan, Burcu Beygu, Dayal Strub, Dirk van Kekem, Eduardo Ruiz Duarte, Esra Russell, Fatma Şengüler-Çiftçi, Florian Kerber, Harsh Vinjamoor, Hildeberto Jardon, Jakob Bosma, Jakob van Bethlehem, Julia Sponsel, Lei Zhao, Mahdi Shafiee Kamalabad, Mohammad Zaman, Mónika Józsa, Nikolay Martynchuk, Nynke Niezink, Pariya Behrouzi, Remko Klein, Reza Mohammadi, Steven Rieder, Sunayana Gosh, Susan Klooster, Tali Spiegel, Tim Evink, Tim van der Beek, Wouter Lueks, Xia Liu, Alice Hannah, Anne Franzen, Bas Fagginger-Auer, Chris Wever, George Downward, Hedwig van Driel, Jasper van Heugten, Joost de Graaf, Lianne van Swieten, Martijn Mink, Miranda Marsman, Miriam Loois, Niels Keizer, Ninke Gahrmann, Ralph

van Gelderen, Rob van den Hengel, Sabine van Dijk, Sander Wolters for their friendship.

I also want to express my gratitude to Hans Kämper, whose lessons were a source of solace.

Finally, I would like to thank my sister Kathelijne, parents Karin and John Wintraecken and late grandmother Netty Beuten for everything.

Bibliography

[ABN+10] J.A. Adler, O. Bobrowski, M.S. Norman, E. Subag, and S. Weinberger. Persistent homology for random fields and complexes. *Borrowing Strength: Theory powering applications*, 6:124–143, 2010. 243

[Abr51] A.A. Abrahamov. On the topological invariants of Riemannian spaces obtained by integration of tensor fields. *Doklady Akademii Nauk*, 81:125–128, 1951. 247

[Abr97] P. Abrahamsen. A review of gaussian random fields and correlation funcitons, 1997. 202

[ACDL00] N. Amenta, S. Choi, T. K. Dey, and N. Leekha. A simple algorithm for homeomorphic surface reconstruction. In *Proceedings of the Sixteenth Annual Symposium on Computational Geometry*, SCG '00, pages 213–222, New York, NY, USA, 2000. ACM. 63

[Adl81] R.J. Adler. *The geometry of random fields*. John Wiley and sons, 1981. 202, 242, 262, 267, 275, 276

[Ara12] M. A. Aragon-Calvo. The MIP Ensemble Simulation: Local Ensemble Statistics in the Cosmic Web. *ArXiv e-prints*, October 2012. 201

[AT07] R.J. Adler and J.E. Taylor. *Random Fields and Geometry*. Monographs in Mathematics. Springer, 2007. 202, 204, 208, 237, 239, 242, 267, 275, 278

[Ata14] D. Atariah. *Parameterizations in the Configuration Space and Approximations of Related Surfaces*. PhD thesis, Freie Universität Berlin, 2014. 5, 22, 41, 53, 54

[BBKS86] F.M. Bardeen, J.R. Bond, N. Kaiser, and A.S. Szalay. The statistics of peaks of Gaussian random fields. *The astrophysical Journal*, 304:15–61, 1986. 202, 208, 242, 262, 267, 271, 272, 275, 276

[BCSM+06] Jean-Daniel Boissonnat, David Cohen-Steiner, Bernard Mourrain, Günter Rote, and Gert Vegter. Meshing of surfaces. In Jean-Daniel Boissonnat and Monique Teillaud, editors, *Effective Computational Geometry for Curves and Surfaces*, pages 181–229. Springer-Verlag, Mathematics and Visualization, 2006. 6

[BDG13a] J.-D. Boissonnat, R. Dyer, and A. Ghosh. Delaunay triangulation of manifolds. Research Report RR-8389, INRIA, 2013. (also: arXiv:1311.0117). 10, 61, 68, 121, 138, 140, 142

[BDG13b] J.-D. Boissonnat, R. Dyer, and A. Ghosh. The stability of Delaunay triangulations. Research Report RR-8276, INRIA, 2013. (to appear in Int. J. Comp. Geom. & Appl. special issue for SoCG 2012). 10, 106

[Ber87a] M. Berger. *Geometry I*. Universitext. Springer-Verlag, 1987. 145

[Ber87b] M. Berger. *Geometry II*. Universitext. Springer-Verlag, 1987. 79

[Ber03] M. Berger. *A Panoramic View of Riemannian Geometry*. Springer-Verlag, 2003. 58, 59, 62

[BF81] R. Bhatia and S. Friedland. Variation of Grassman powers and spectra. *Linear Algebra and Applications*, 40:1–18, 1981. 115

[BG88] M. Berger and B. Gostiaux. *Differential Geometry: Manifolds, Curves and Surfaces*. Number 115 in Graduate Texts in Mathematics. Springer-Verlag, 1988. 237, 238

[BG09] Y. Baryshnikov and R. Ghrist. Target enumeration via Euler characteristic integrals. *SIAM Journal on Applied Mathematics*, 70:825–844, 2009. 241, 243

[BG14] J.-D. Boissonnat and A. Ghosh. Manifold reconstruction using tangential Delaunay complexes. *Discrete and Computational Geometry*, 51(1):221–267, 2014. 10, 64

[Bha97] R. Bhatia. *Matrix Analysis*. Number 169 in Graduate Texts in Mathematics. Springer-Verlag, 1997. 115

[BHH+03] C. L. Bennett, M. Halpern, G. Hinshaw, N. Jarosik, A. Kogut, M. Limon, S. S. Meyer, L. Page, D. N. Spergel, G. S. Tucker, E. Wollack, E. L. Wright, C. Barnes, M. R. Greason, R. S. Hill, E. Komatsu, M. R. Nolta, N. Odegard, H. V. Peiris, L. Verde, and J. L. Weiland. First-Year Wilkinson Microwave Anisotropy Probe (WMAP) Observations: Preliminary Maps and Basic Results. *The Astrophysical Journal Supplement*, 148:1–27, September 2003. 191, 195

[BK81] P. Buser and H. Karcher. *Gromov's almost flat manifolds*, volume 81 of *Astérique*. Société mathématique de France, 1981. 62, 67, 73, 75, 107, 110, 125, 131, 132, 133, 134, 135

[BKP96] J. R. Bond, L. Kofman, and D. Pogosyan. How filaments of galaxies are woven into the cosmic web. *Nature*, 380:603–606, April 1996. 194, 200

[BO05] J.-D. Boissonnat and S. Oudot. Provably good sampling and meshing of surfaces. *Graphical Models*, 67(5):405–451, 2005. 5, 63

[Bra04] R.H. Brandenberger. Lectures on the theory of cosmological perturbations. In *The Early Universe and Observational Cosmology*, volume 646 of *Lecture Notes in Physics*, pages 127–167. Springer, 2004. 187, 193

[Bro08] E.M. Bronstein. Approximation of convex sets by polytopes. *Journal of Mathematical Sciences*, 153(6):727–762, 2008. 20

[BSW+09] M. Boylan-Kolchin, V. Springel, S. D. M. White, A. Jenkins, and G. Lemson. Resolving cosmic structure formation with the Millennium-II Simulation. *Monthly Notices of the Royal Astronomical Society*, 398:1150–1164, September 2009. 196, 197, 200

[BvDP12] E. G. P. Bos, R. van de Weygaert, K. Dolag, and V. Pettorino. The darkness that shaped the void: dark energy and cosmic voids. *Monthly Notices of the Royal Astronomical Society*, 426:440–461, October 2012. 201

[Cai34] S. S. Cairns. On the triangulation of regular loci. *Annals of Mathematics. Second Series*, 35(3):579–587, 1934. 9, 63

[Car29] E. Cartan. Groupes simples clos et ouverts et géométrie riemanienne. *Journal Mathématiques Pures et Appliquées*, 8:1–33, 1929. 8, 62

[Car03] S.M. Carroll. *Spacetime and Geometry*. Addison Wesley, 2003. 187

[CDR05] S.-W. Cheng, T. K. Dey, and E. A. Ramos. Manifold reconstruction from point samples. In *SODA*, pages 1018–1027, 2005. 10, 64

[CDS13] S.-W. Cheng, T.K. Dey, and J.R. Shewchuk. *Delaunay Mesh Generation*. Computer and information science series. CRC Press, 2013. 10

[CG06] Frédéric Cazals and Joachim Giesen. Delaunay triangulation based surface reconstruction. In Jean-Daniel Boissonnat and Monique Teillaud, editors, *Effective Computational Geometry for Curves and Surfaces*, pages 231–276. Springer-Verlag, Mathematics and Visualization, 2006. 6

[Cha06] I. Chavel. *Riemannian Geometry: A Modern Introduction*. Number 98 in Cambridge studies in advanced mathematics. Cambridge University Press, 2006. 62, 70, 75, 107

[Che44] S.S. Chern. A simple intrinsic proof of the gaussbonnet formula for closed riemannian manifolds. *Annals of Mathematics*, 45(4):747–752, 1944. 238

[Che52] S.S. Chern. On the kinematic formula in the euclidean space of n dimensions. *American Journal of Mathematics*, 74:227–236, 1952. 240

[Che70] J. Cheeger. Finiteness theorems for Riemannian manifolds. *Am. J. Math*, 92(1):61–74, 1970. 75

[Che00] B-Y Chen. Riemannian submanifolds. In *Handbook of differential geometry, Vol. I*, pages 187–418. North-Holland, Amsterdam, 2000. 58

[Chr92] G. Christakos. *Random Field models in Earth sciences*. Academic Press, 1992. 202, 205, 207, 208

[Cla06] K.L. Clarkson. Building triangulations using ϵ-nets. *Proceedings of the thirty-eighth annual ACM symposium on Theory of computing*, 2006. 5, 22, 54

[Cox98] H.S.M. Coxeter. *Non-Euclidean geometry*. The mathematical association of America, 6 edition, 1998. 79

[CPJ+03] M. Colless, B. A. Peterson, C. Jackson, J. A. Peacock, S. Cole, P. Norberg, I. K. Baldry, C. M. Baugh, J. Bland-Hawthorn, T. Bridges, R. Cannon, C. Collins, W. Couch, N. Cross, G. Dalton, R. De Propris, S. P. Driver, G. Efstathiou, R. S. Ellis, C. S. Frenk, K. Glazebrook, O. Lahav, I. Lewis, S. Lumsden, S. Maddox, D. Madgwick, W. Sutherland, and K. Taylor. The 2dF Galaxy Redshift Survey: Final Data Release. *ArXiv Astrophysics e-prints*, June 2003. 194, 201

[CR75] G. Chincarini and H. J. Rood. Size of the Coma cluster. *Nature*, 257:294, September 1975. 199

[CSX07] L. Chen, P. Sun, and J. Xu. Optimal anisotropic meshes for minimizing interpolation errors in l_p-norm. *Mathematics of computation*, 76(257):179–204, 2007. 5, 21

[CvJF14] M. Cautun, R. van de Weygaert, B. J. T. Jones, and C. S. Frenk. Evolution of the cosmic web. *Monthly Notices of the Royal Astronomical Society*, 441:2923–2973, July 2014. 199

[DC76] M.P. Do Carmo. *Differential Geometry of Curves and Surfaces*. Prentice-Hall, 1976. 48, 240, 270

[DD95] P. Desnogues and O. Devillers. A locally optimal triangulation of the hyperbolic paraboloid. In *Canadian Conference on Computational Geometry, Quebec, Canada*, pages 49–54, Aug 1995. 5

[Dek94] A. Dekel. Dynamics of Cosmic Flows. *Annual Review of Astronomy and Astrophysics*, 32:371–418, 1994. 201

[Del34] B. Delaunay. Sur la sphère vide. *Izv. Akad. Nauk SSSR, Otdelenie Matematicheskii i Estestvennyka Nauk*, 7:793–800, 1934. 64

[Dey07] T.K. Dey. *Curve and Surface Reconstruction: Algorithms with Mathematical Analysis*. Number 23 in Cambridge monographs on applied and computational mathematics. Cambridge University Press, 2007. 10

[DFN90] B.A. Dubrovin, A.T. Fomenko, and S.P. Novikov. *Modern Geometry methods and Applications: Part III Introduction to Homology Theory*. Graduate texts in Mathematics. Springer, 1990. 210

[dGH86] V. de Lapparent, M. J. Geller, and J. P. Huchra. A slice of the universe. *Astrophysical Journal, Part 2 - Letters to the Editor*, 302:L1–L5, March 1986. 194, 200

[DK04] J.J. Duistermaat and J.A.C. Kolk. *Multidimensional Real Analysis I: Differentiation*. Number 86 in Cambridge Studies in Advanced Mathematics. Cambridge University Press, 2004. 278

[dL11] D. de Laat. Upper bounds on the optimal meshing error of manifolds in higher codimension. Master's thesis, Rijksuniversiteit Groningen, 2011. 5, 21

[DR94] A. Dekel and M. J. Rees. Omega from velocities in voids. *Astrophysical Journal, Part 2 - Letters*, 422:L1–L4, February 1994. 201

[DS91] E.F. D'Azevedo and R.B. Simpson. On optimal triangular meshes for minimizing the gradient error. *Numerische Mathematik*, 59:321–348, 1991. 5, 312

[DZM08] R. Dyer, H. Zhang, and T. Möller. Surface sampling and the intrinsic Voronoi diagram. *Computer Graphics Forum (Special Issue of Symp. Geometry Processing)*, 27(5):1393–1402, 2008. 60, 63

[EH10] H. Edelsbrunner and J. L. Harer. *Computational Topology: An Introduction*. American Mathematical Soc., 2010. 210, 228

[Ein15] A. Einstein. Feldgleichungen der gravitation. *Sitzungsberichte der Königlich Preussische Akademie der Wissenschaften*, 2:844–847, 1915. 188

[EJS80] J. Einasto, M. Joeveer, and E. Saar. Structure of superclusters and supercluster formation. *Monthly Notices of the Royal Astronomical Society*, 193:353–375, November 1980. 199

[ES97] H. Edelsbrunner and N. R. Shah. Triangulating topological spaces. *Int. J. Comput. Geometry Appl.*, 7(4):365–378, 1997. 64

[Fed59] H. Federer. Curvature measures. *Transactions of the America mathematical Society*, 93:418–491, 1959. 28, 245

[Fed96] H. Federer. *Geometric Measure Theory*. Classics in Mathematics. Springer, 1996. 245

[Fix09] D. J. Fixsen. The Temperature of the Cosmic Microwave Background. *The Astrophysical Journal*, 707:916–920, December 2009. 191

[Fom87] A.T. Fomenko. *Differential Geometry and Topology*. Contemporary Soviet Mathematics. Consultants Bureau, New York and London, 1987. 248, 253, 256

[Fré48] M. Fréchet. Les éléments aléatoires de nature quelconque dans un espace distancié. *Annales de l'Institut Henri Poincaré*, 10:215–310, 1948. 8, 62

[Fri22] A. Friedmann. Uber die krümmung des raumes. *Zeitschrift für Physik*, 10:377–386, 1922. 189

[Fri24] A. Friedmann. Uber die möglichkeit einer welt mit konstanter negativer krümmung des raumes. *Zeitschrift für Physik*, 21:326–332, 1924. 189

[Fri82] S. Friedland. Variation of tensor powers and spectra. *Linear and Multilinear algebra*, 12:81–98, 1982. 61, 115

[Fri99a] A. Friedmann. On the curvature of space. *General Relativity and Gravitation*, 31:1991–2000, 1999. 189

[Fri99b] A. Friedmann. On the possibility of a world with constant negative curvature of space. *General Relativity and Gravitation*, 31:2001–2008, 1999. 189

[FT48] L. Fejes Tóth. Approximation by polygons and polyhedra. *Bull. Amer. Math. Soc.*, 54:431–438, 1948. 5

[FT53] L. Fejes Tóth. *Lagerungen in der Ebene, auf der Kugel und im Raum*. Berlin, Göttingen, Heidelberg: Springer, 1953. 5, 13, 14, 21, 37, 38, 40, 54

[FTH08] J. A. Frieman, M. S. Turner, and D. Huterer. Dark Energy and the Accelerating Universe. *Annual Review of Astronomy and Astrophysics*, 46:385–432, September 2008. 191

[FvEvdW+15] J.L. Feldbrugge, M.J. van Engelen, R. van de Weygaert, P. Pranav, G. Vegter, and M. Wintraecken. Submitted. *Monthly Notices of the Royal Astronomical Society*, 2015. 242

[Gho10] S. Ghosh. *Geometric Approximation of curves and singularities of secant maps*. PhD thesis, Rijksuniversiteit Groningen, 2010. 5

[Gil84] P.B. Gilkey. *Invariance Theory, The Heat Equation, And the Atiyah-Singer Index Theorem*. Mathematics Lecture Series. Publich or Perish, inc., 1984. 247, 312

[Gol05] R. Goldman. Curvature formulas for implicit curves and surfaces. *Computer aided Geometric Design*, 22:632–658, 2005. 268

[GPP12] C. Gay, C. Pichon, and D. Pogosyan. Non-Gaussian statistics of critical sets in 2D and 3D: Peaks, voids, saddles, genus, and skeleton. *Physical Review D*, 85(2):023011, January 2012. 243, 262, 277

[GPV07] Sunayana Ghosh, Sylvain Petitjean, and Gert Vegter. Approximation by conic splines. *Mathematics in Computer Science*, 1(1):39–69, 2007. 5

[Gru93a] P.M. Gruber. Asymptotic estimates for best and stepwise approximation of convex bodies I. *Forum Mathematicum*, 5:281–297, 1993. 5, 19, 26, 32

[Gru93b] P.M. Gruber. Asymptotic estimates for best and stepwise approximation of convex bodies II. *Forum Mathematicum*, 5:521–538, 1993. 5, 19, 26, 32

[GSG+14] L. Guzzo, M. Scodeggio, B. Garilli, B. R. Granett, A. Fritz, U. Abbas, C. Adami, S. Arnouts, J. Bel, M. Bolzonella, D. Bottini, E. Branchini, A. Cappi, J. Coupon, O. Cucciati, I. Davidzon, G. De Lucia, S. de la Torre, P. Franzetti, M. Fumana, P. Hudelot, O. Ilbert, A. Iovino, J. Krywult, V. Le Brun, O. Le Fèvre, D. Maccagni, K. Małek, F. Marulli, H. J. McCracken, L. Paioro, J. A. Peacock, M. Polletta, A. Pollo, H. Schlagenhaufer, L. A. M. Tasca, R. Tojeiro, D. Vergani, G. Zamorani, A. Zanichelli, A. Burden, C. Di Porto, A. Marchetti, C. Marinoni, Y. Mellier, L. Moscardini, R. C. Nichol, W. J. Percival, S. Phleps, and M. Wolk. The VIMOS Public Extragalactic Redshift Survey (VIPERS). An unprecedented view of galaxies and large-scale structure at 0.5 ¡ z ¡ 1.2. *Astronomy & Astrophysics*, 566:A108, June 2014. 194, 201

[GT78] S. A. Gregory and L. A. Thompson. The Coma/A1367 supercluster and its environs. *Astrophysical Journal*, 222:784–799, June 1978. 199

[Gut81] A. H. Guth. Inflationary universe: A possible solution to the horizon and flatness problems. *Physical Review D*, 23:347–356, January 1981. 193

[GVL96] G. H. Golub and C. F. Van Loan. *Matrix computations*, volume 3. JHU Press, 1996. 133

[Hat01] A. Hatcher. *Algebraic Topology*. Cambridge University Press, 2001. 210

[HGIW86] A.S.J. Hamilton, J.R. Gott III, and D. Weinberg. The topology of the large-scale structure of the universe. *The astrophysical Journal*, 309:1–12, 1986. 242, 262, 263, 266, 267, 275

[Hir76] M.W. Hirsch. *Differential Topology*. Springer-Verlag: New York, Heidelberg, Berlin, 1976. 222, 248

[HJS+05] J. Huchra, T. Jarrett, M. Skrutskie, R. Cutri, S. Schneider, L. Macri, R. Steining, J. Mader, N. Martimbeau, and T. George. The 2MASS Redshift Survey and Low Galactic Latitude Large-Scale Structure. In A. P. Fairall and P. A. Woudt, editors, *Nearby Large-Scale Structures and the Zone of Avoidance*, volume 329 of *Astronomical Society of the Pacific Conference Series*, page 135, June 2005. 194, 201

[Hör90] L. Hörmander. *The Analysis of Linear Partial Differential Operators I*. Number 256 in Grundlehren der mathematischen Wissenschaften. Springer Verlag, second edition, 1990. 273

[HPW06] K. Hildebrandt, K. Polthier, and M. Wardetzsky. On the convergence of metric and geometric properties of polyhedral surfaces. *Geometriae Dedicata*, 123:89–112, 2006. 46

[HSW14] N. Hamaus, P. M. Sutter, and B. D. Wandelt. Universal Density Profile for Cosmic Voids. *Physical Review Letters*, 112(25):251302, June 2014. 201

[Hub29] E. Hubble. A Relation between Distance and Radial Velocity among Extra-Galactic Nebulae. *Proceedings of the National Academy of Science*, 15:168–173, March 1929. 190

[Ick84] V. Icke. Voids and filaments. *Monthly Notices of the Royal Astronomical Society*, 206:1P–3P, January 1984. 201

[IR08] I.C.F. Ipsen and R. Rehman. Perturbation bounds for determinants and characteristic polynomials. *Society for Industrial and Applied Mathematics' Journal on Matrix Analysis and Applications*, 30(2):762–776, 2008. 115

[Jon97] B.J.T. Jones. Statistics and random functions in astrophysics. In C.H. Lineweaver, J.G. Bartlett, A. Blanchard, M. Signore, and J. Silk, editors, *The Cosmic Microwave Background*, pages 67 – 110, 1997. 202

[Jon15] B.J.T. Jones. *Precision Cosmology*. Cambridge university press, To be published 2015. 202

[Kam93] G.K. Kamenev. The efficiency of hausdorff algorithms for approximating connvex bodies by polytopes. *Computational Mathematics and Mathematical Physics*, 33:709–716, 1993. 22

[Kar77] H. Karcher. Riemannian center of mass and mollifier smoothing. *Communications on Pure and Applied Mathematics*, 30:509–541, 1977. 8, 62, 70, 71, 73, 83, 84, 86, 87, 95, 120

[Kar89] H. Karcher. Riemannian comparison constructions. In S.S. Chern, editor, *Global Differential Geometry*, pages 170–222. The mathematical association of America, 1989. 78

[Kau76] H. Kaul. Schranken für die christoffelsymbole. *Manuscripta mathematica*, 19:261–273, 1976. 62

[Ken90] W.S. Kendall. Probability, convexity, and harmonic maps with small image I: Uniqueness and fine existence. *Procedings of the London Mathematical society*, s3-61 (Issue 2):371–406, 1990. 8, 62, 83, 84

[KKNO73] U. Karras, M. Kreck, W.D. Neumann, and E. Ossa. *Cutting and Pasting of Manifolds; SK-Groups*, volume 1 of *Mathematics Lecture Series*. Publish or Perish, Boston, 1973. 259, 312

[Kno13] J. Knoblauch. *Grundlagen der Differentialgeometrie*. Druck und verlag von B.G. Teubner: Leipzig, 1913. 268

[KOSS81] R. P. Kirshner, A. Oemler, Jr., P. L. Schechter, and S. A. Shectman. A million cubic megaparsec void in Bootes. *Astrophysical Journal, Part 2 - Letters to the Editor*, 248:L57–L60, September 1981. 200

[KOSS87] R. P. Kirshner, A. Oemler, Jr., P. L. Schechter, and S. A. Shectman. A survey of the Bootes void. *Astrophysical Journal*, 314:493–506, March 1987. 200

[Lei99] G. Leibon. *Random Delaunay triangulations, the Thurston-Andreev theorem, and metric uniformization*. PhD thesis, UCSD, 1999. arXiv:math/0011016v1. 60, 63

[Lem27] G. Lemaître. Un univers homogène de masse constante et de rayon croissant, rendant compte de la vitesse radiale des nébuleuses extra-galactiques. *Annales de la Société Scientifique de Bruxelles*, 47A:49–59, 1927. 189, 190

[Lem13] G. Lemaître. Republication of: A homogeneous universe of constant mass and increasing radius accounting for the radial velocity of extra-galactic nebulae. *General Relativity and Gravitation*, 45:1635–1646, 2013. 189, 190

[Lin82] A. D. Linde. A new inflationary universe scenario: A possible solution of the horizon, flatness, homogeneity, isotropy and primordial monopole problems. *Physics Letters B*, 108:389–393, February 1982. 193

[Lud94] M. Ludwig. Asymptotic approximation of convex curves. *Archiv der Mathematik*, 63:377–384, 1994. 5

[Lud98] M. Ludwig. Asymptotic approximation of convex curves: the hausdorff metric case. *Archiv der Mathematik*, 70:331–336, 1998. 5

[LW10] G. Lavaux and B. D. Wandelt. Precision cosmology with voids: definition, methods, dynamics. *Monthly Notices of the Royal Astronomical Society*, 403:1392–1408, April 2010. 201

[Mas77] W.S. Masssey. *Algebraic Topology: An Introduction*. Springer-Verlag: New York, Heidelberg, Berlin, 1977. 248

[MFB92] V.F. Mukhanov, H.A. Feldman, and R.H. Brandenberger. Theory of cosmological perturbations. *Physics Reports*, 215(56):203 – 333, 1992. 193

[Mil65a] J. Milnor. *Lectures on the h-cobordism theorem*. Princton Mathematical notes. Princeton university press, 1965. 253

[Mil65b] J. Milnor. *Topology from the differentiable viewpoint*. The University Press of Virginia, 1965. 278

[Mil73] J.W. Milnor. *MorseTheory*. Number 51 in Annals of Mathematics Studies. Princeton University Press, Princeton, New Jersey, 1973. 210, 219, 221, 222, 236

[Möb27] A.F. Möbius. *Der barycentrische Calcul, ein neues Hülfsmittel zur analytischen Behandlung der Geometrie: dargestelllt und insbesondere auf die Bildung neuer Classen von Aufgaben und die Entwicklung mehrerer Eigenschaften der Kegelschnitte angewendet*. Leipzig, Verlag von Johann Ambrosius Barth, 1827. 8

[Mor08] J.-M. Morvan. *Generalized Curvatures*. Number 2 in Geometry and Computing. Springer-Verlag, 2008. 237, 240

[MS74] J.W. Milnor and J.D. Stasheff. *Characteristic Classes*. Number 76 in Annals of Mathematics Studies. Princeton University Press and University of Tokyo Press, Princeton, New Jersey, 1974. 247, 261

[MT02] J. M. Morvan and B. Thibert. On the approximation of a smooth surface with a triangulated mesh. *Comput. Geom. Theory Appl.*, 23(3):337–352, November 2002. 46

[MTW73] C.W. Misner, K.S. Thorne, and J.A. Wheeler. *Gravitation*. W.H. Freeman and company, 1973. 187, 188

[Mun68] J. R. Munkres. *Elementary differential topology*. Princton University press, second edition, 1968. 9, 63, 126, 147

[Mun84] J.R. Munkres. *Elements of Algebraic Topology*. Addison-Wesley Publishing Company, 1984. 210

[Mun00] J.R. Munkres. *Topology*. Prentice-Hall, 2000. 30

[MW90] H. Martel and I. Wasserman. Simulation of cosmological voids in Lambda greater than 0 Friedmann models. *Astrophysical Journal*, 348:1–25, January 1990. 201

[Nas56] John Nash. The imbedding problem for riemannian manifolds. *The Annals of Mathematics*, 63(1):pp. 20–63, 1956. 7, 20

[Nev13] K. Nevenzeel. Triangulating the darkness; topological dark energy differentiation. Master's thesis, Kapteyn Astronomical Institute, 2013. 243

[O'N06] B O'Neill. *Elementary Differential Geometry*. Elsevier, 2006. 47, 48, 50, 244, 245, 270, 274

[OR09] E. Outerelo and J. M. Ruiz. *Mapping degree theory*, volume 108. American Mathematical Soc., 2009. 128

[PAA+14a] Planck Collaboration, P. A. R. Ade, N. Aghanim, M. I. R. Alves, C. Armitage-Caplan, M. Arnaud, M. Ashdown, F. Atrio-Barandela, J. Aumont, H. Aussel, and et al. Planck 2013 results. I. Overview of products and scientific results. *Astronomy and Astrophysics*, 571:A1, November 2014. 191, 192, 195

[PAA+14b] Planck Collaboration, P. A. R. Ade, N. Aghanim, C. Armitage-Caplan, M. Arnaud, M. Ashdown, F. Atrio-Barandela, J. Aumont, C. Baccigalupi, A. J. Banday, and et al. Planck 2013 results. XVI. Cosmological parameters. *Astronomy and Astrophysics*, 571:A16, November 2014. 189

[PAG+99] S. Perlmutter, G. Aldering, G. Goldhaber, R. A. Knop, P. Nugent, P. G. Castro, S. Deustua, S. Fabbro, A. Goobar, D. E. Groom, I. M. Hook, A. G. Kim, M. Y. Kim, J. C. Lee, N. J. Nunes, R. Pain, C. R. Pennypacker, R. Quimby, C. Lidman, R. S. Ellis, M. Irwin, R. G. McMahon, P. Ruiz-Lapuente, N. Walton, B. Schaefer, B. J. Boyle, A. V. Filippenko, T. Matheson, A. S. Fruchter, N. Panagia, H. J. M. Newberg, W. J. Couch, and T. S. C. Project. Measurements of Ω and Λ from 42 High-Redshift Supernovae. *The Astrophysical Journal*, 517:565–586, June 1999. 191

[Pee80] P. J. E. Peebles. *The large-scale structure of the universe*. Princeton Series in Physics. Princeton, N.J., Princeton University Press, 1980. 187, 194

[Pet84] S. Peters. Cheeger's finiteness theorem for diffeomorphism classes of Riemannian manifolds. *J. Reine Angew. Math.*, 394:77–82, 1984. 62, 75

[PEvdW+15] P. Pranav, H. Edelsbrunner, M.A.M. van de Weijgaert, M. Kerber, B.J.T. Jones, G. Vegter, and M.H.M.J. Wintraecken. On the betti of the universe and her persistence. *To be submitted*, 2015. 243

[PKH+00] H. Pottmann, R. Krasauskas, B. Hamann, K. Joy, and W. Seibold. On piecewise linear approximation of quadratic functions. *Journal for Geometry and Graphics*, 4(1):9–31, 2000. 5, 22, 41, 53

[PL07a] D. Park and J. Lee. Void Ellipticity Distribution as a Probe of Cosmology. *Physical Review Letters*, 98(8):081301, February 2007. 201

[PL07b] D. Park and J. Lee. Void-Supercluster Alignments. *Astrophysical Journal*, 665:96–101, August 2007. 201

[PPC+13] C. Park, P. Pranav, P. Chingangbam, R. van de Weygaert, B. Jones, G. Vegter, I. Kim, J. Hidding, and W. A. Hellwing. Betti Numbers of Gaussian Fields. *Journal of Korean Astronomical Society*, 46:125–131, June 2013. 242, 243, 277

[PUP02] A. Papoulis and S. Unnikrishna Pillai. *Probability Random Variable and Stochastic Processes*. McGraw-Hill Series In Systems Science. McGraw-Hill, 2002. 202, 206, 208

[PW65] A. A. Penzias and R. W. Wilson. A Measurement of Excess Antenna Temperature at 4080 Mc/s. *Astrophysical Journal*, 142:419–421, July 1965. 191

[RFC+98] A. G. Riess, A. V. Filippenko, P. Challis, A. Clocchiatti, A. Diercks, P. M. Garnavich, R. L. Gilliland, C. J. Hogan, S. Jha, R. P. Kirshner, B. Leibundgut, M. M. Phillips, D. Reiss, B. P. Schmidt, R. A. Schommer, R. C. Smith, J. Spyromilio, C. Stubbs, N. B. Suntzeff, and J. Tonry. Observational Evidence from Supernovae for an Accelerating Universe and a Cosmological Constant. *The Astronomical Journal*, 116:1009–1038, September 1998. 191

[RM96] B. S. Ryden and A. L. Melott. Voids in Real Space and in Redshift Space. *Astrophysical Journal*, 470:160, October 1996. 201

[Rob35] H. P. Robertson. Kinematics and World-Structure. *Astrophysical Journal*, 82:284, November 1935. 189

[Rob36a] H. P. Robertson. Kinematics and World-Structure II. *Astrophysical Journal*, 83:187, April 1936. 189

[Rob36b] H. P. Robertson. Kinematics and World-Structure III. *Astrophysical Journal*, 83:257, May 1936. 189

[Rog64] C.A. Rogers. *Packing and Covering*. Cambridge: University Press, 1964. 19

[RS72] C.P. Rourke and B.J. Sanderson. *Introduction to piecewise-linear topology*. Number 69 in Ergebnisse der mathematik und ihrer grenzgebiete. Springer-Verlag, 1972. 221

[Rus10] R.M. Rustamov. Barycentric coordinates on surfaces. *Eurographics Symposium on Geometry Processing*, 29(5), 2010. 8, 60, 62, 121

[Rv07] E. Romano-Díaz and R. van de Weygaert. Delaunay Tessellation Field Estimator analysis of the PSCz local Universe: density field and cosmic flow. *Monthly Notices of the Royal Astronomical Society*, 382:2–28, November 2007. 201

[San76] L.A. Santaló. *Intergral geometry and Geometric Probability*. Number 1 in Encyclopedia of Mathematics and its applications. Eddison-Wesley publishing company, 1976. 240

[San12] Oliver Sander. Geodesic finite elements on simplicial grids. *International Journal for Numerical Methods in Engineering*, 92(12):999–1025, 2012. 8, 60, 62, 70, 84, 312

[San13] Oliver Sander. Geodesic finite elements of higher order, 2013. 8, 73, 84

[SBK+92] G. F. Smoot, C. L. Bennett, A. Kogut, E. L. Wright, J. Aymon, N. W. Boggess, E. S. Cheng, G. de Amici, S. Gulkis, M. G. Hauser, G. Hinshaw, P. D. Jackson, M. Janssen, E. Kaita, T. Kelsall, P. Keegstra, C. Lineweaver, K. Loewenstein, P. Lubin, J. Mather, S. S. Meyer, S. H. Moseley, T. Murdock, L. Rokke, R. F. Silverberg, L. Tenorio, R. Weiss, and D. T. Wilkinson. Structure in the COBE differential microwave radiometer first-year maps. *Astrophysical Journal, Part 2 - Letters*, 396:L1–L5, September 1992. 191, 195

[Sch81] R. Schneider. Zur optimalen approximation konvexer hyperflächen durch polyeder. *Mathematische Annalen*, 256:289–301, 1981. 5, 18, 19, 32, 38, 54

[Sch91] P. Schapira. Operations on constructible functions. *Journal of Pure and Applied Algebra*, 72:83–93, 1991. 241

[Sch95] P. Schapira. Tomography of constructible functions. In *proceedings of 11th International Symposium on Applied Algebra*, pages 427–435. Algebraic Algorithms and Error-Correcting Codes, 1995. 241

[Sim79] B. Simon. *Functional Integration and Quantum physics*. Pure and applied mathematics. Acadenic press, 1979. 206, 312

[SLWW12] P. M. Sutter, G. Lavaux, B. D. Wandelt, and D. H. Weinberg. A First Application of the Alcock-Paczynski Test to Stacked Cosmic Voids. *Astrophysical Journal*, 761:187, December 2012. 201

[Spi75a] M. Spivak. *A comprehensive introduction to differential geometry: Volume III*. Publish or Perish, 1975. 20, 47, 244, 268

[Spi75b] M. Spivak. *A comprehensive introduction to differential geometry: Volume IV*. Publish or Perish, 1975. 20

[Spi75c] M. Spivak. *A comprehensive introduction to differential geometry: Volume V*. Publish or Perish, 1975. 20, 238, 244, 247

[Spi99] M. Spivak. *A comprehensive introduction to differential geometry: Volume II*. Publish or Perish, 1999. 47, 48, 246, 270

[Sti93] J. Stillwell. *Classical Topology and Combinatorial Group Theory*. Graduate Texts in Mathematics. Springer, 1993. 248

[Sv04] R. K. Sheth and R. van de Weygaert. A hierarchy of voids: much ado about nothing. *Monthly Notices of the Royal Astronomical Society*, 350:517–538, May 2004. 201

[SWJ+05] V. Springel, S. D. M. White, A. Jenkins, C. S. Frenk, N. Yoshida, L. Gao, J. Navarro, R. Thacker, D. Croton, J. Helly, J. A. Peacock, S. Cole, P. Thomas, H. Couchman, A. Evrard, J. Colberg, and F. Pearce. Simulations of the formation, evolution and clustering of galaxies and quasars. *Nature*, 435:629–636, June 2005. 196

[TBS+04] M. Tegmark, M. R. Blanton, M. A. Strauss, F. Hoyle, D. Schlegel, R. Scoccimarro, M. S. Vogeley, D. H. Weinberg, I. Zehavi, A. Berlind, T. Budavari, A. Connolly, D. J. Eisenstein, D. Finkbeiner, J. A. Frieman, J. E. Gunn, A. J. S. Hamilton, L. Hui, B. Jain, D. Johnston, S. Kent, H. Lin, R. Nakajima, R. C. Nichol, J. P. Ostriker, A. Pope, R. Scranton, U. Seljak, R. K. Sheth, A. Stebbins, A. S. Szalay, I. Szapudi, L. Verde, Y. Xu, J. Annis, N. A. Bahcall, J. Brinkmann, S. Burles, F. J. Castander, I. Csabai, J. Loveday, M. Doi, M. Fukugita, J. R. Gott, III, G. Hennessy, D. W. Hogg, Ž. Ivezić, G. R. Knapp, D. Q. Lamb, B. C. Lee, R. H. Lupton, T. A. McKay, P. Kunszt, J. A. Munn, L. O'Connell, J. Peoples, J. R. Pier, M. Richmond, C. Rockosi, D. P. Schneider, C. Stoughton, D. L. Tucker, D. E. Vanden Berk, B. Yanny, D. G. York, and SDSS Collaboration. The Three-Dimensional Power Spectrum of Galaxies from the Sloan Digital Sky Survey. *Astrophysical Journal*, 606:702–740, May 2004. 194, 201

[TCHP14] R. B. Tully, H. Courtois, Y. Hoffman, and D. Pomarède. The Laniakea supercluster of galaxies. *Nature*, 513:71–73, September 2014. 201

[TSK+08] R. B. Tully, E. J. Shaya, I. D. Karachentsev, H. M. Courtois, D. D. Kocevski, L. Rizzi, and A. Peel. Our Peculiar Motion Away from the Local Void. *Astrophysical Journal*, 676:184–205, March 2008. 201

[vDar] S.W. von Deylen. *Numerische Approximation in Riemannschen Mannigfaltigkeiten mithilfe des Karcher'schen Schwerpunktes*. PhD thesis, Freie Universität Berlin, 2014 (to appear). 8, 62

[vdW] M.A.M. van de Weijgaert. Lecture notes; large scale structure formation. 187

[vdWB96] R. van de Weijgaert and E. Bertschinger. Peak and gravity constraints in gaussian primodial density fields: an application of the hoffman- ribak method. *Monthly Notices of the Royal Astronomical Society*, 281:84–118, 1996. 202, 271

[vdWPJ+11] R. van de Weygaert, P. Pranav, B. J. T. Jones, E. G. P. Bos, G. Vegter, H. Edelsbrunner, M. Teillaud, W. A. Hellwing, C. Park, J. Hidding, and M. Wintraecken. Probing Dark Energy with Alpha Shapes and Betti Numbers. *ArXiv e-prints*, October 2011. 242, 243

[vdWVE+11] R. van de Weygaert, G. Vegter, H. Edelsbrunner, B.J.T. Jones, P. Pranav, C. Park, W.A. Hellwing, B. Eldering, N. Kruithof, E.G.P. Bos, J. Hidding, J. Feldbrugge, E. ten Have, M. van Engelen, M. Caroli, and M. Teillaud. Alpha, betti and the megaparsec universe: On the topology of the cosmic web. *Transactions on Computational Science*, 14:60–101, 2011. 242, 243

[vv93] R. van de Weygaert and E. van Kampen. Voids in Gravitational Instability Scenarios - Part One - Global Density and Velocity Fields in an Einstein - De-Sitter Universe. *Monthly Notices of the Royal Astronomical Society*, 263:481, July 1993. 201

[Wal37] A. G. Walker. On milne's theory of world-structure. *Proceedings of the London Mathematical Society*, s2-42(1):90–127, 1937. 189

[Wal84] R.M. Wald. *General Relativity*. University of Chicago Press, 1984. 187, 188

[Wal94] R.M. Wald. *Quantum field theory in curved spacetime and black hole thermodynamics*. University of Chicago Press, 1994. 193

[WB08] R.van de Weygaert and J.R. Bond. Clusters and the theory of the cosmic web. In Manolis Plionis, David Hughes, and Omar Lpez-Cruz, editors, *A Pan-Chromatic View of Clusters of Galaxies and the Large-Scale Structure*, volume 740 of *Lecture Notes in Physics*, pages 335–408. Springer Netherlands, 2008. 187, 194

[Wei08] S. Weinberg. *Cosmology*. Oxford university press, 2008. 187, 191, 192, 206

[Wey39] H. Weyl. On the volume of tubes. *American Journal of Mathematics*, 61(2):461–472, 1939. 239

[Whi40] J. H. C. Whitehead. On C^1-complexes. *Ann. of Math*, 41(4), 1940. 63

[Whi57] H. Whitney. *Geometric Integration Theory*. Princeton University Press, 1957. 63, 121, 128, 147

[Zel70] Y. B. Zel'dovich. Gravitational instability: An approximate theory for large density perturbations. *Astronomy and Astrophysics*, 5:84–89, March 1970. 194, 199